

IMPROVING TREATMENT OUTCOMES IN MODELS OF  
GLIOBLASTOMA CANCER

by

Maïté Verreault  
B.Sc., Université Laval, 2002  
M.Sc., Université Laval, 2004

A thesis submitted in partial fulfillment of  
the requirements for the degree of

DOCTOR OF PHILOSOPHY

in

The Faculty of Graduate Studies  
(Pathology and Laboratory Medicine)

The University of British Columbia  
(Vancouver)

June 2011

## Abstract

**Introduction:** Despite the use of treatments, tumour recurrence in glioblastoma (GBM) patients is inevitable, partly because of the blood-brain barrier and the poor perfusion of the tumour vasculature, which act as two major obstacles to effective drug delivery. In order to address the latter, the capacity of liposomal formulations of irinotecan (Irinophore C<sup>TM</sup>; IrC<sup>TM</sup>), doxorubicin (Caelyx<sup>®</sup>) and vincristine to improve vascular function through normalization of GBM vasculature was assessed. In the following studies, the effect of IrC<sup>TM</sup> on the pharmacokinetics of irinotecan and its therapeutic efficacy in an orthotopic GBM model was compared to administration of the free form of the drug. In addition, siRNA-based therapy was explored as a potential strategy to enhance the efficacy of chemotherapeutics such as irinotecan. In one series of studies, the impact of cationic liposomes used for *in vitro* ILK (Integrin-Linked Kinase)-targeting siRNA delivery was compared to electroporation. Following successful identification of the most efficacious siRNA delivery method, EGFR and Rictor were selected as therapeutic targets because these proteins are involved in two of the most common molecular pathways reported to be dysregulated in GBM. The therapeutic potential of the combined silencing of EGFR and Rictor was assessed in *in vitro* and *in vivo* models of GBM. **Results and conclusion:** It was found that IrC<sup>TM</sup>, Caelyx<sup>®</sup> and liposomal vincristine induce vascular normalization in GBM tumours. It was also demonstrated that IrC<sup>TM</sup> increases exposure of the brain to irinotecan and its active metabolite SN-38 and improves survival of GBM tumour-bearing animals compared to treatment with free irinotecan. *In vitro* siRNA transfection using cationic lipids was found to alter the ILK downregulation time course compared to electroporation and to induce changes in pathway signaling that occurred independently of ILK silencing. Combined silencing of EGFR and Rictor reduced cell migration and increased cell

sensitivity to chemotherapeutics *in vitro*. *In vivo*, dual silencing of EGFR and Rictor led to GBM tumour eradication. In parallel, GBM cell lines expressing red fluorescent proteins were developed as a tool for orthotopic GBM tumour imaging in live animals. These studies demonstrate the potential of siRNA-based therapy targeting EGFR and Rictor to act in combination with optimized chemotherapy agents such as IrC<sup>TM</sup> to improve treatment outcome in GBM.

## Preface

The present thesis includes published material for which multiple co-authors were involved. Below is a description of the contribution of the candidate as well as all co-authors to the work that resulted in the manuscripts presented.

**Chapter 2:** Maite Verreault, Dita Strutt<sup>1</sup>, Dana Masin<sup>2</sup>, Malathi Anantha<sup>3</sup>, Andrew Yung<sup>4</sup>, Piotr Kozlowski<sup>5</sup>, Dawn Waterhouse<sup>6</sup>, Marcel B. Bally<sup>7</sup> and Donald T. Yapp<sup>8</sup>. Vascular normalization in orthotopic glioblastoma following intravenous treatment with lipid-based nanoparticulate formulations of irinotecan (Irinophore C<sup>TM</sup>), doxorubicin (Caelyx®) or vincristine. *BMC Cancer*. 2011; April 8 (11):124. The identification and design of the research program for this chapter was made entirely by the candidate under the supervision of co-author 7. All parts of the research as well as the analysis of the data were done entirely by the candidate. The manuscript was prepared primarily by the candidate with the contribution of co-authors 7 and 8 to the reviewing and editing. Co-authors 1, 2, 3, 4, 5 and 6 were involved in technical support.

**Chapter 3:** Maite Verreault, Dita Strutt<sup>1</sup>, Dana Masin<sup>2</sup>, Malathi Anantha<sup>3</sup>, Dawn Waterhouse<sup>4</sup>, Don T Yapp<sup>5</sup> and Marcel B. Bally<sup>6</sup>. Irinophore C<sup>TM</sup>, a lipid-based nanoparticulate formulation of irinotecan, is more effective than free irinotecan when used to treat an orthotopic glioblastoma model. *Accepted with revisions by Journal of controlled Release in May 2011*. The identification and design of the research program for this chapter was made entirely by the candidate under the supervision of co-author 6. All parts of the research as well as the analysis of the data were done entirely by the candidate. The manuscript was prepared primarily by the candidate with the contribution of co-authors 5 and 6 to the reviewing and editing. Co-authors 1, 2, 3 and 4 were involved in technical support.

**Chapter 4:** Maite Verreault, Dita Strutt<sup>1</sup>, Dana Masin<sup>2</sup>, Dieter Fink<sup>3</sup>, Raji Gill<sup>4</sup> and Marcel B. Bally<sup>5</sup>. Development of Glioblastoma Cell Lines Expressing Red Fluorescence for Non-invasive Live Imaging of Intracranial Tumours. *Anticancer Research*. 2011;31(8):in press. The identification and design of the research program for this chapter was made entirely by the candidate under the supervision of co-author 5. All parts of the research as well as the analysis of the data were done entirely by the candidate. The manuscript was prepared primarily by the candidate with the contribution of co-authors 5 to the reviewing and editing. Co-authors 1, 2, 3 and 4 were involved in technical support.

**Chapter 5:** Maite Verreault and Marcel B. Bally<sup>1</sup>. siRNA Mediated Integrin-Linked Kinase Suppression: Non-specific effects of siRNA/cationic liposome complexes trigger changes in the expression of phosphorylated-AKT and mTOR independently of ILK silencing. *Oligonucleotides*. 2009 Jun;19(2):129-40. The identification and design of the research program for this chapter was made by the candidate under the supervision of co-author 1. All parts of the research as well as the analysis of the data were done entirely by the candidate. The manuscript was prepared primarily by the candidate with the contribution of co-author 1 to the reviewing and editing.

**Chapter 6:** Maite Verreault, Amelia Stegeman<sup>1</sup>, Corinna Warburton<sup>2</sup>, Dita Strutt<sup>3</sup>, Dana Masin<sup>4</sup> and Marcel B Bally<sup>5</sup>. Combined RNAi mediated suppression of Rictor and EGFR inhibits tumour growth in an orthotopic glioblastoma tumour model. *Submitted for publication in April 2011*. The identification and design of the research program for this chapter was made by the candidate under the supervision of co-author 5. All parts of the research as well as the analysis of the data were done entirely by the candidate. The manuscript was prepared primarily by the candidate with the contribution of co-author 5 to the reviewing and editing. Co-authors 1, 2, 3 and 4 were involved in technical support.

**Study Protocol approval:**

The UBC Animal Care Committee reviewed and approved the certificate # A07-0423 for intracranial tumour cell inoculation, Maestro imaging and MRI scanning.

# Table of contents

Abstract.....	ii
Preface.....	iv
Table of contents.....	vii
List of tables.....	ix
List of figures.....	x
Lists of abbreviations (in alphabetical order).....	xii
Acknowledgements.....	xvii
Dedication.....	xviii
Chapter 1: Introduction.....	1
1.1 Overview.....	1
1.2 Research hypothesis and specific objectives.....	2
1.3 Glioblastoma and other astrocytic brain tumours: incidence and pathology.....	5
1.4 Glioblastoma: diagnosis, standard of care, treatments and challenges.....	6
1.5 Targeted therapy for malignant glioma.....	12
1.6 Clinical application of antisense oligonucleotide and siRNA.....	22
1.7 Delivery strategies for targeted therapeutics in GBM.....	25
1.8 Focus of the present thesis.....	34
Chapter 2: Vascular normalization in orthotopic glioblastoma following intravenous treatment with lipid-based nanoparticulate formulations of irinotecan (Irinophore C <sup>TM</sup> ), doxorubicin (Caelyx <sup>®</sup> ) or vincristine.....	36
2.1 Introduction.....	36
2.2 Materials and methods.....	38
2.3 Results.....	44
2.4 Discussion.....	63
2.5 Acknowledgements.....	70
Chapter 3: Irinophore C <sup>TM</sup> , a lipid-based nanoparticulate formulation of irinotecan, is more effective than free irinotecan when used to treat an orthotopic glioblastoma model.....	71
3.1 Introduction.....	71
3.2 Materials and methods.....	72
3.3 Results.....	78
3.4 Discussion.....	89
3.5 Conclusion.....	94
3.6 Acknowledgements.....	95
Chapter 4: Development of glioblastoma cell lines expressing red fluorescence for non-invasive live imaging of intracranial tumours.....	96
4.1 Introduction.....	96
4.2 Materials and methods.....	98
4.3 Results and discussion.....	101
4.4 Conclusion.....	116
4.5 Acknowledgements.....	118
Chapter 5: siRNA-mediated Integrin-Linked Kinase suppression: nonspecific effects of siRNA/cationic liposome complexes trigger changes in the expression of phosphorylated-AKT and mTOR independently of ILK silencing.....	119
5.1 Introduction.....	119
5.2 Materials and methods.....	122
5.3 Results.....	125

5.4 Discussion .....	140
5.5 Acknowledgements .....	144
Chapter 6: Combined RNAi mediated suppression of Rictor and EGFR inhibits tumour growth in an orthotopic glioblastoma tumour model .....	145
6.1 Introduction .....	145
6.2 Materials and methods .....	148
6.3 Results .....	154
6.3 Discussion .....	171
6.4 Acknowledgements .....	176
Chapter 7: Discussion and conclusions .....	177
7.1 Summary .....	177
7.2 Defining the optimal siRNA delivery system for GBM therapy .....	181
7.3 The consequences of vascular normalization are dependent on tumour dynamics .....	183
7.4 Development of mKate2-expressing U118MG GBM line for non-invasive imaging .....	189
7.5 Conclusion .....	190
Bibliography .....	192

## List of tables

Table 1: WHO classification of astrocytic tumours.....	6
Table 2: Protein targets that have been inhibited by means of non-viral gene silencing agents in orthotopic GBM pre-clinical studies or clinical trials (CTr), or by SMI in GBM clinical trials phase II/III (definition of abbreviations is given on page xii-xvi).....	19
Table 3: Formulation specifications of Irinophore C <sup>TM</sup> , liposomal vincristine and Caelyx <sup>®</sup> .....	31
Table 4: Plasma and brain irinotecan and SN-38 AUC <sub>0-24hrs</sub> values (µg•hr/mL) following i.v. injection of 25mg/kg irinotecan or IrC <sup>TM</sup> in healthy Rag2M mice.....	79
Table 5: Plasma and brain lactone/carboxylate (wt:wt) ratios (L/C) for irinotecan and SN-38 following i.v. injection of 25mg/kg IrC <sup>TM</sup> or irinotecan in healthy Rag2M mice.....	83
Table 6: Repeated dose (Q7Dx3) tolerability study of IrC <sup>TM</sup> and free drug (irinotecan) in healthy Rag2M mice.....	84
Table 7: Antitumour efficacy of Irinophore C <sup>TM</sup> and free irinotecan in orthotopic U251MG tumour-bearing Rag2M mice.....	87
Table 8: Tumour area and fraction of Ki67 positive cells in brain sections isolated from untreated, IrC <sup>TM</sup> and irinotecan treated mice at indicated time points. ....	89

## List of figures

Figure 1: a) H&E staining and b) electron micrograph of a brain section showing astrocytes and other brain cell types. ....	6
Figure 2: Micro- and macroscopic view of a GBM tumour. ....	7
Figure 3: Electron micrograph showing the structure of brain capillaries from normal and tumour tissue .....	11
Figure 4: Gene targets in pre-clinical (no colour) and clinical studies phase I (yellow), II (orange) and III (purple) for gene silencing strategies (ASOs, Ribozymes and RNAi) in cancer therapy. ....	14
Figure 5: Mechanisms of action of three gene silencing strategies: antisense oligonucleotides, ribozymes and short interfering RNA.....	15
Figure 6: Immunoblot obtained from U251MG cell protein lysate.....	22
Figure 7: Biological barriers preventing therapeutic agent access to the targeted GBM cancer cells from systemic administration to intracellular or intranuclear delivery .....	29
Figure 8: Irinophore C <sup>TM</sup> , Caelyx <sup>®</sup> and liposomal vincristine significantly inhibit tumour growth, decrease proliferation and increase tumour perfusion in subcutaneous GBM tumours. ....	45
Figure 9: Orthotopic GBM tumours treated with Irinophore C <sup>TM</sup> , Caelyx <sup>®</sup> and liposomal vincristine are significantly smaller than untreated controls. ....	48
Figure 10: Irinophore C <sup>TM</sup> , Caelyx <sup>®</sup> and liposomal vincristine treatments are associated with vascular normalization of the tumour vasculature in subcutaneous GBM tumours. ....	51
Figure 11: Irinophore C <sup>TM</sup> , Caelyx <sup>®</sup> and liposomal vincristine treatments are associated with vascular normalization of the tumour vasculature in orthotopic GBM tumours. ....	54
Figure 12: Irinophore C <sup>TM</sup> reduced K <sub>trans</sub> measures compared to values obtained from control orthotopic tumours.....	56
Figure 13: d-HMVEC and HBMEC were plated under proliferative conditions or non-proliferative conditions.....	58
Figure 14: Proliferating HMVEC cells are more sensitive to SN-38, docetaxel, paclitaxel, doxorubicin and vincristine than non-proliferating cells.....	61
Figure 15: Proliferating HBMEC cells are more sensitive to SN-38, docetaxel, paclitaxel, doxorubicin and vincristine than non-proliferating cells.....	62
Figure 16: Proposed role of vessel normalization in the response of tumors to antiangiogenic therapy.....	66
Figure 17: Irinotecan levels in the blood and brain are greater following administration of IrC <sup>TM</sup> than following administration of free irinotecan. ....	80
Figure 18: Irinophore C <sup>TM</sup> exhibits significant activity in an orthotopic GBM model.....	86
Figure 19: IrC <sup>TM</sup> -treated tumours revealed a transient increase in cell proliferation after treatment. ....	88
Figure 20: Selection and characterization of mKate2 transfected U251MG cells expressing low, medium, high and very high levels of the fluorescent protein.....	103
Figure 21: Characterization of mCherry transfected U251MG cells expressing low, medium and high levels of the fluorescent protein.....	105
Figure 22: The neurosphere forming fraction and CD24/CD44 phenotype of transduced lines is comparable to the parental line.....	108
Figure 23: Parental, mKate2 (low) and mCherry (medium) expressing U251MG cells grow when implanted orthotopically in Rag2M mice. ....	110
Figure 24: The relationship between fluorescence signal (scaled count/second) and cell number <i>in vitro</i> is linear for $\geq 100$ cells.....	111

Figure 25: The <i>in vitro</i> and <i>in vivo</i> sensitivity of mKate2 (low) to chemotherapeutic drugs is comparable to that seen for the parental line. ....	114
Figure 26: The use of albino NOD.CB17-SCID mice allows for weekly imaging of orthotopic tumour progression. ....	116
Figure 27: Delivery of CY5-siRNA using Lipofectamine 2000 or nucleofection.....	128
Figure 28: A flow cytometry analysis of the cell cycle distribution following ILK targeted siRNA transfection.....	131
Figure 29: Quantification of ILK downregulation 72hrs after ILK siRNA delivery using cationic lipids or nucleofection.....	133
Figure 30: Quantification of ILK downregulation over time following ILK siRNA delivery using cationic lipids or nucleofection.....	134
Figure 31: Quantification of p473-AKT suppression 72hrs and over time following ILK siRNA delivery using cationic lipids or nucleofection.....	137
Figure 32: The impact of cationic lipids on protein levels following siRNA delivery using nucleofection.....	140
Figure 33: Co-transfection of siRNA sequences specific to Rictor and EGFR results in downregulation of their respective proteins in the U251MG GBM line and Rictor silencing correlates with decreases in p(473)-AKT levels. ....	156
Figure 34: Co-transfection of siRNA sequences specific to Rictor and EGFR results in downregulation of their respective proteins in U118MG and LN229 GBM lines and Rictor silencing correlates with decreases in p(473)-AKT levels in U118MG line only.....	158
Figure 35: The combination of EGFR and Rictor silencing results in a reduction in cell migration. ....	161
Figure 36: The combination of EGFR and Rictor silencing results in an increase in cell sensitivity to chemotherapeutic drugs.....	163
Figure 37: Un-induced lentiviral shRNA-transduced cells behave similarly to parental cells... ..	166
Figure 38: Induction of lentiviral shRNA-transduced cells results in downregulation of the corresponding proteins <i>in vitro</i> . ....	167
Figure 39: Induction of orthotopically implanted shRNA-transduced cells results in downregulation of corresponding protein <i>in vivo</i> and the combined silencing of Rictor and EGFR results in a complete inhibition of tumour growth.....	170
Figure 40: <i>In vitro</i> cell proliferation rate of GBM cell lines U251MG, U118MG and LN229..	184
Figure 41: Analysis of the effect of Irinophore C <sup>TM</sup> on the tumour micro-environment of U118MG GBM orthotopic model.....	186
Figure 42: Comparisons of <i>in vitro</i> cell proliferation rate, <i>in vitro</i> drug sensitivity, and <i>in vivo</i> tumour growth rate between parental and mKate2-expressing U118MG lines.....	190

## **Lists of abbreviations (in alphabetical order)**

ABC: ATP binding cassette

ASO: antisense oligonucleotide

AUC: area-under-the-curve

$\beta$ -Ctnin:  $\beta$ -Catenin

BBB: blood-brain barrier

Bcl-2: B-cell leukemia/lymphoma 2

BLI: bioluminescence imaging

BTIC: brain tumour initiating cells

C: control

CCAM6: carcinoembryonic antigen-related cell adhesion molecule 6

CCNU: N-(2-chloroethyl)-N'-cyclohexyl-N-nitrosourea

CDK4: cyclin-dependent kinase 4

CDKN2A: cyclin-dependent kinase inhibitor 2A

cDNA: complementary DNA

CED: convection-enhanced delivery

CL: cationic lipid, c-mR: c-met receptor

CNS: central nervous system

C-RS: control reverse sequence

CT: computed tomography

CTr: clinical trial

Cthpsin: cathepsin

CXCR4: chemokine receptor 4

d-HMVEC: dermal human microvascular endothelial cells

(DCE)-MRI: (dynamic contrast enhanced) magnetic resonance imaging

DOTAP: 1,2-dioleoyl-3-trimethylammonium-propane

DSPC: 1,2-distearoyl-*sn*-glycero-phosphocholine

DSPE: distearoylphosphatidylethanolamine

ECM: extra-cellular matrix

EGFR: epidermal growth factor receptor

EpA2/B4: ephrin A2/B4

EPR: enhanced permeability and retention

EZH2: enhancer of zeste homolog 2

FACS: fluorescence-activated cell sorting

FAK: focal adhesion kinase

FBS: fetal bovine serum

FDA: food and drug administration

FGF: fibroblast growth factor

FT: farnesyltransferase

GBM: glioblastoma

Gd-DTPA: gadolinium diethylenetriamine penta-acetic acid

GFAP: glial fibrillary acidic protein

H: human

H&E: hematoxylin and eosin

HBMEC: human brain microvascular endothelial cells

HDAC: histone deacetylase

HIV: human immunodeficiency virus

HPLC: high-performance liquid chromatography

hrs: hours

hTERT: human telomerase reverse transcriptase

i.cr.: intracranial

IDH1: isocitrate dehydrogenase 1

IGF-1R: insulin-like growth factor receptor type I

ILK: integrin-linked kinase

Immunolip.: immunoliposome

i.n.: intra-nasal

i.p.: intraperitoneal injection

IrC<sup>TM</sup>: Irinophore C<sup>TM</sup>

i.t.: intra-tumoural

i.v.: intravenous injection

L/C: lactone/carboxylate ratio

LNP: lipid nanoparticle

LUV: large unilamellar vesicle

M: mouse

mAb: monoclonal antibody

MAPK: mitogen-activated protein kinase

MDM2: mouse double minute 2

MEK: MAPK kinase

MGMT: O-6-methylguanine methyltransferase

MLV: multilamellar vesicle

MMP-9: matrix metalloproteinase 9

mRNA: messenger RNA

mTOR(C2): mammalian target of rapamycin (complex 2)

NF- $\kappa$ B: nuclear factor-  $\kappa$ B

NRP/B: nuclear-restricted protein/brain

OCT: optimal cutting temperature compound

p53: protein 53

p473-AKT: serine 473-phosphorylated AKT

PCV: procarbazine/lomustine/vincristine

PDGF(R): platelet-derived growth factor (receptor)

PDK1/2: phosphoinositide-dependent kinase 1/2

PEG: polyethylene glycol

PEI: polyethylenimine

PET: positron emission tomography

PI: propidium iodide

PKC: protein kinase C

PI3K: phosphoinositide 3'-hydroxykinase

Pltph: pleiotrophin

PTEN: phosphatase and tensin homolog

Q7Dx3: weekly for 3 weeks

R: receptor

RalBP1: ral-binding protein 1

RB1: retinoblastoma protein 1

Rictor: rapamycin insensitive companion of mTOR

RGD: arginine-glycine-aspartic acid

RISC: RNA-induced silencing complex

RNAi: RNA interference

RR2: ribonucleotide reductase R2 subunit

RTK: receptor tyrosine kinase

s.c.: subcutaneous

SEM: standard error of the mean

S/H: scatter factor/hepatocyte growth factor

siRNA: small interfering RNA

shRNA: small hairpin RNA

SMI: small molecule inhibitor

Tmrse: telomerase

TMZ: temozolomide

TRPM-2: testosterone-repressed prostate message-2 or clusterin

UPA(R): urokinase plasminogen activator (receptor)

VEGF(R): vascular endothelial growth factor (receptor)

WHO: World Health Organization

## **Acknowledgements**

I would like to use this space to express my gratitude towards everyone around me who contributed from near or far to this thesis. First, I would like to thank my supervisor Marcel Bally for his constant support, even in the most discouraging or challenging moments and of course, for mentoring and inspiring me throughout the whole process. I would also like to thank my supervisory committee for sharing their advice and expertise. I wouldn't have been able to accomplish all I did without the expertise, skills and support from Experimental Therapeutics actual or ex lab members, in particular Jessica Kalra, Jesse Popov, Catherine Tucker, Don T Yapp, Brent Sutherland, Visia Dragowska, Lincoln Edwards, Malathi Anantha, Corinna Warburton, Hong Yan, Dita Strutt, Dana Masin, Maryam Osooly, Young Joo Yang and Amelia Stegeman. I am grateful for all the love and support from my family: my mother, father, brother, sister-in-law and my close friend Marie, the Lunn family and the Olsen family. Finally, I would like to thank my partner, Daniel Lunn, for love and inspiration and for helping me taking my mind away from my work obsessions.

## **Dedication**

I dedicate this thesis to all the mice that were  
sacrificed for the studies presented here.

# **Chapter 1: Introduction**

## **1.1 Overview**

An estimated 62,930 new cases of primary non-malignant and malignant brain and central nervous system (CNS) tumours were expected to be diagnosed in the United States in 2010 among which an estimated 12,920 people succumbed to the disease [1]. In Canada, 2,600 new cases of brain cancer were diagnosed in 2010 and 1,750 patients with brain cancer died of the disease [2]. Gliomas are tumours that arise from glial cells and represent 32% of CNS tumours in adults and 55% in children [1]. Glioblastoma (GBM) is the most aggressive and the most common (53.8%) tumour among gliomas [1]. The current standard of care for GBM patients begins with maximal safe surgical resection, followed by radiation therapy with concurrent temozolomide (TMZ) or adjuvant TMZ therapy [3]. Despite aggressive therapeutic interventions, the median overall survival of GBM patients remains 14.6 months after diagnosis and the 5-year survival rate is less than 10% [1, 4]. Thus, therapy, particularly in the relapse setting, is given as a palliative option. There are many reasons for our inability to effectively treat this disease. The surgical option is potentially curative, but very often the disease will infiltrate into the surrounding brain tissue and is almost impossible to remove completely. This failure to cure by surgical intervention requires that patients are managed through a multidisciplinary approach integrating radiotherapy, chemotherapy and new forms of targeted therapies, a strategy contemplated in this thesis.

Other contributions to treatment failure in GBM include the location of tumours in a chemically protected and immune privileged site. More specifically, the presence of the blood-brain barrier and the poorly perfused nature of the GBM tumour vasculature act as major obstacles to the delivery of therapeutic molecules to the region of cancer cell growth and progression [5-7]. Even when drug candidates can gain access to tumour cells by penetration

across the blood-brain barrier (BBB), tumour drug resistance may emerge. Drug resistance arises due to multiple factors including: (i) the heterogenous nature of tumours which comprise tumour cells with varying replication rates, (ii) the presence of cells which express drug resistance mechanisms including drug pumps or DNA repair proteins, (iii) cells that possess an aberrant balance between survival and apoptosis factors, (iv) cells that are capable of migrating into regions of the brain where drug access is limited and (v) the presence of dormant tumour cells that are highly invasive and resistant to chemotherapeutic agents and that are capable of replenishing the tumour cell population [8-11]. Research is desperately needed to define strategies that will improve the efficacy of GBM treatment options. This thesis research has concentrated on two central areas: i) improving the capacity of chemotherapeutic drugs to access tumour cell populations and ii) improving the tumour response to anti-cancer drugs through use of gene silencing therapeutics.

## **1.2 Research hypothesis and specific objectives**

The overarching hypothesis for this thesis is that strategies that increase delivery of chemotherapeutic drugs to the brain will improve treatment outcomes in patients with glioblastoma and the efficacy of these drugs will be enhanced by combining them with silencing of signaling pathways known to play a role in the promotion of tumour growth and progression. This general hypothesis is tested through specific research efforts, each defined by more specific hypotheses and well-defined objectives as outlined below:

**Specific Hypothesis 1 (Chapter 2):** Extended exposure to chemotherapeutic drugs will result in an improvement in vascular function in GBM. **Objective 1:** To determine how treatment with liposomal formulations of irinotecan, doxorubicin or vincristine influence the tumour vasculature in subcutaneous and orthotopic GBM models. **Specific objective 1.1:** To assess the impact of treatment with liposomal formulations on subcutaneous GBM tumour size

and delivery of fluorescent dye Hoechst 33342. **Specific objective 1.2:** To assess the impact of treatment with liposomal formulations on orthotopic GBM tumour size and delivery of fluorescent dye Hoechst 33342. **Specific objective 1.3:** To assess the impact of treatment with liposomal formulations on tumour morphology and permeability of GBM vasculature. **Specific objective 1.4:** To assess the impact of extended drug exposure on proliferative and non-proliferative brain and dermal endothelial cells *in vitro*.

**Specific Hypothesis 2 (Chapter 3):** Extended exposure to irinotecan will improve its therapeutic activity in an orthotopic model of GBM. **Objective 2:** To compare the therapeutic activity of Irinophore C<sup>TM</sup>, a liposomal formulation of irinotecan, to the free form of the drug in an orthotopic model of GBM. **Specific objective 2.1:** To measure irinotecan and SN-38 levels in plasma and in the brain after a single dose of Irinophore C<sup>TM</sup> or the free form of the drug. **Specific objective 2.2:** To evaluate the impact of Irinophore C<sup>TM</sup> and the free form of the drug on survival at equivalent and equitoxic doses in orthotopic GBM.

**Specific Hypothesis 3 (Chapter 4):** Non-invasive imaging of intracranial tumours will facilitate therapeutic assessments of agents in orthotopic models of GBM through better-defined, more humane, experimental endpoints. **Objective 3:** To develop and characterize GBM cell lines expressing red fluorescent proteins as a tool for non-invasive imaging of orthotopic tumours. **Specific objective 3.1:** To define a mCherry or mKate2-expressing U251MG cell population that exhibits *in vitro* and *in vivo* growth rates comparable to the parental line. **Specific objective 3.2:** To confirm that the transduction and selection process have preserved the parental line's population heterogeneity in regards to stem-like cell fraction and cell surface markers. **Specific objective 3.3:** To assess whether the mCherry and mKate2-expressing lines can be imaged intracranially. **Specific objective 3.4:** To demonstrate the use of mKate2-expressing U251MG to monitor GBM tumour progression and treatment response.

**Specific Hypothesis 4 (Chapter 5):** Cationic lipids used to facilitate siRNA delivery *in vitro* and *in vivo* will influence transfection efficacy and induce changes in intracellular signaling pathways. **Objective 4:** To determine how cationic lipid-mediated transfection of siRNA targeting Integrin-Linked Kinase (ILK) compares to a transfection method relying on electroporation and to assess subsequent effects on molecular signaling *in vitro*. **Specific objective 4.1:** To compare the efficacy of siRNA delivery *in vitro* between cationic lipids and electroporation-mediated transfection. **Specific objective 4.2:** To compare the level of downregulation as a function of time following delivery of siRNA targeting ILK using cationic lipids or electroporation. **Specific objective 4.3:** To assess the impact of ILK siRNA transfection on p(473)-AKT levels. **Specific objective 4.4:** To assess the impact of cationic lipids used to transfect non-specific or ILK-targeting siRNA on AKT/mTOR pathway.

**Specific Hypothesis 5 (Chapter 6):** Rictor and EGFR silencing in GBM models (*in vitro* and *in vivo*) will combine to achieve therapeutic effects which will be further enhanced when silencing is achieved in combination with chemotherapeutic agents designed for use in treatment of GBM. **Objective 5:** To assess the therapeutic potential of the RNAi-mediated combined silencing of EGFR and Rictor alone and in combination in GBM models. **Specific objective 5.1:** To evaluate the impact of the combined silencing of EGFR and Rictor on cell proliferation, migration and sensitivity to chemotherapeutic drugs *in vitro*. **Specific objective 5.2:** To develop shRNA-expressing U251MG GBM lines targeting EGFR and/or Rictor and to confirm that the transduction and selection process did not alter the *in vitro* characteristics of this cell line. **Specific objective 5.3:** To evaluate the impact of the combined silencing of EGFR and Rictor when shRNA-expressing lines are implanted orthotopically.

In the following sections, background information is provided to help those reviewing this thesis to understand the broader issues involved in the treatment of GBM, the use of conventional chemotherapeutics for treating GBM as well as the role that targeted therapeutics

will play in the future treatment of patients diagnosed with GBM. Particular emphasis has been placed on use of gene silencing as an approach to achieve target specific effects. The use of siRNA to correct one or more specific defects within cancer cells is a powerful tool to determine whether an overexpressed or defective protein plays a role in a brain cancer cell's ability to proliferate, survive, promote angiogenesis and/or metastasize. This strategy has tremendous appeal since siRNA could transition seamlessly into a therapeutic agent used to achieve better treatment outcomes for selected GBM patient population.

### **1.3 Glioblastoma and other astrocytic brain tumours: incidence and pathology**

The most common (80%) form of malignant primary brain tumour originates from the neuroglial cells and is referred to as glioma [1]. Glioma patients generally present with headache, vomiting, occasional transient or partial blindness due to raised intracranial pressure, and local or general brain dysfunction possibly leading to altered behaviour or seizures [12, 13]. Despite heavy treatment, the median overall survival remains 14.6 months after diagnosis [14].

Tumours originating from astrocytes constitute 76% of the cases of gliomas, and glioblastoma (GBM) is the most common malignant form of astrocytic glioma (53.8%) [1]. In addition to more than 10 billion neurons, astrocytes (from Greek *astron*: star) constitute substantial cell population present in the gray matter of the cerebral cortex. They are involved in structural support and regulation of the intercellular environment and the blood-brain barrier (BBB) (Figure 1). The other types of neuroglial cells of the cerebral cortex that play an important role in the maintenance of the structure and the integrity of the brain micro-environment include: 1) the oligodendrocytes (from Greek *oligos*, small; *dendron*, tree) involved in the process of myelination, 2) the microglia involved in phagocytosis in response to central nervous system (CNS) damage, and 3) the ependymal cells forming the epithelium of the brain

ventricles [15]. Astrocytic tumours are classified according to the World Health Organization (WHO) system (Table 1).

**Figure 1: a) H&E staining and b) electron micrograph of a brain section showing astrocytes and other brain cell types.**

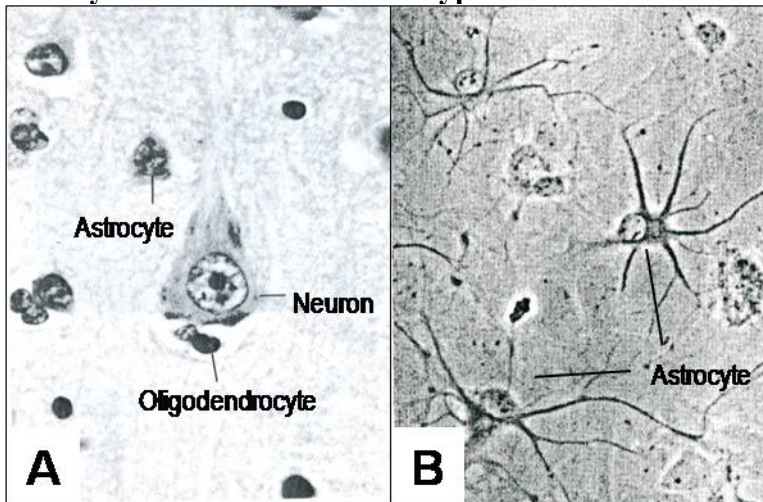


Figure 1: Adapted from [15]

**Table 1: WHO classification of astrocytic tumours**

Tumour type	WHO malignancy grade	Histological characteristics	Mutations commonly found
Low grade astrocytoma: Pilocytic astrocytoma Pleomorphic xanthoastrocytoma Subependymal giant cell astrocytoma	I I I-III I	Well-differentiated (resemble astrocytes) and express GFAP, slow-growing lesions, well-circumscribed	P53
Diffuse astrocytoma: Fibrillary Protoplasmic Gemistocytic	II II II II	Well-differentiated and express GFAP, diffuse and infiltrating lesions	P53, MDM2, IDH1/2
Anaplastic astrocytoma Glioblastoma Giant cell glioblastoma Gliosarcoma	III IV IV IV	Pleomorphic cells, mainly undifferentiated and loss of GFAP, highly cellular, high levels of mitosis, necrosis	P53, MDM2, CDK4/6, RB1, PTEN, EGFR, p16, CDKN2A, NRP/B

Table 1: References - [13, 16, 17]. Definition of abbreviations is given on page xii-xvi.

## 1.4 Glioblastoma: diagnosis, standard of care, treatments and challenges

Diagnosis and grading of a brain tumour begins with brain imaging. Several imaging technologies are available to determine the tumour location and biological activity, and to assess

the tumour response to the treatment [12]. The most common techniques include Computed Tomography (CT), Magnetic Resonance Imaging (MRI) and Positron Emission Tomography (PET). A CT scan allows for tumour localization and the assessment of tumour morphology. MRI provides a higher resolution image of the tumour that can be used for better localization of the tumour and surrounding structures, diagnosis, presurgical planning and stereotaxic biopsy. PET imaging is used for the metabolic and functional assessment of the tumour, and this information can be used for grading and assessing tumour response to the treatment. Diagnosis of glioma is confirmed by histopathological analysis of the tumour biopsy. GBM lesions exhibit a mixed infiltrative and expansive growth pattern, in contrast to low grade astrocytoma which will tend to be purely expansive [18]. Infiltration typically follows white matter tracts such as the corpus callosum and the internal capsule (Figure 2). The lesions present a high density of small and pleomorphic tumour cells that are characterized by large and elongated nuclei, frequent mitotic figures, endothelial cell proliferation and necrosis that can be surrounded by dense accumulations of tumour cells (palisading necrosis) [16, 18]. The information obtained from tumour imaging and histopathology is used to guide treatment decision for each individual.

**Figure 2: Micro- and macroscopic view of a GBM tumour.**

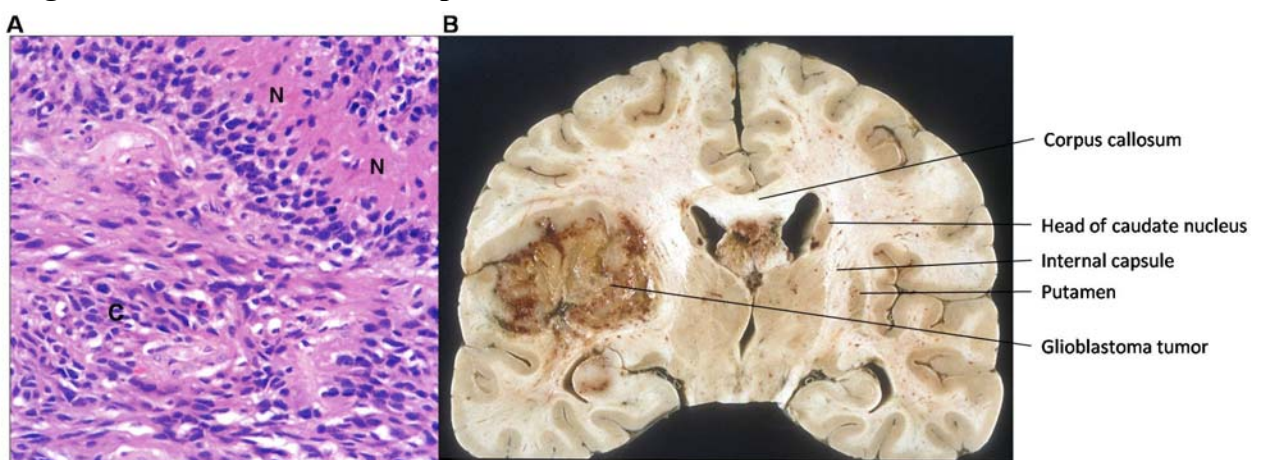


*Figure 2: a) H&E staining of a GBM tumour showing high cellular density (C) and (N) necrosis.*

*b) Brain showing the location of the internal capsule and a GBM tumour - adapted from [19, 20]*

The current standard of care for GBM patients consists of maximal safe surgical resection, followed by radiation therapy with temozolomide (TMZ; Temodar), and adjuvant TMZ therapy [3]. TMZ is an alkylating agent, triggering cell death by the addition of DNA damaging alkyl groups on guanine bases [21]. The inclusion of TMZ in GBM standard of care improved the 2-year survival times by 26% compared to historical values, however, the 5-year survival of GBM patients still remains at less than 30% [1, 4]. An important predictive factor in response to TMZ is the level of methylation of the O-6-methylguanine methyltransferase (MGMT) promoter region found in the tumour. Promoter methylation of the MGMT gene prevents the expression of the MGMT enzyme capable of removing alkyl groups [22]. GBM tumours carrying a non-methylated promoter (40-55% of cases [23, 24]) respond poorly to TMZ and there is currently no alternative treatment for these patients. It is important to note that all three GBM cell lines (U251MG, U118MG and LN229) used in the research chapters have a methylated MGMT promoter [25, 26].

Before the introduction of TMZ as the standard of care for GBM patients, nitrosoureas were the foundation of GBM treatment for more than 30 years [27]. Among them, the alkylating agent Carmustine (1,3-bis (2-chloroethyl)-1-nitrosourea) was used in conjunction with radiotherapy [28-30]. Severe pulmonary toxicity and limited efficacy of the drug due to insufficient drug delivery motivated the development of Carmustine wafers (Gliadel). Administration of Carmustine using biodegradable polymer wafers provides a controlled release of the drug in the brain micro-environment while minimizing systemic toxicity [31]. However, recent trials showed that the system provides no additional benefit compared to TMZ [32]. A combination regimen consisting of the nitrosourea Lomustine (N-(2-chloroethyl)-N'-cyclohexyl-N-nitrosourea; CCNU), the alkylating agent Procarbazine and the microtubules destabilizer Vincristine (PCV) has also been used extensively for the treatment of GBM [33]. Yet, high incidence of hematological toxicities and inferior response rates in comparison to TMZ [27, 33]

avored the establishment of TMZ as the current standard of care. The topoisomerase I inhibitor irinotecan (CPT-11; Camptosar) is a FDA-approved drug for colorectal cancer. Promising results for GBM patients in phase II trials were demonstrated with this compound, especially when used in combination with other agents such as TMZ or Carmustine [34-37], and it may soon be integrated among the Food and Drug Administration (FDA)-approved options for GBM patients. This compound is now recommended by the National Comprehensive Cancer Network for use in combination with bevacizumab for GBM treatment [38]. As noted already, this thesis explores the use of a novel lipid-based nanopharmaceutical formulation of irinotecan for use in treatment of an orthotopic model of GBM. Chapters 2 and 3 clearly demonstrate the superiority of this formulation when compared to the parent drug.

More recently, targeted agents have been developed and showed some activity in GBM patients. Among them, a monoclonal antibody raised against the vascular endothelial growth factor (VEGF), Bevacizumab (Avastin), was recently approved by the FDA for the treatment of recurrent GBM as several clinical trials demonstrated its efficacy as a single agent to prolong the survival of patients [34, 39]. The epidermal growth factor receptor (EGFR) inhibitors gefitinib (Iressa) and erlotinib (Tarceva) have shown some efficacy in the treatment of malignant glioma [40, 41], but response rates have been variable and unpredictable [27]. Imatinib Mesylate (Gleevec) was developed to specifically inhibit Bcr-Abl signal transduction in chronic myeloid leukemia, and was later shown to also inhibit c-Kit and platelet-derived growth factor receptor (PDGFR) activity. The latter finding supported clinical testing of Imatinib for GBM treatment, and similarly to the EGFR inhibitors, response rates were variable but promising [42, 43]. Other targeted therapy compounds currently evaluated for use in GBM treatment are described in section 1.5.

One of the major challenges of GBM chemotherapy is the achievement of adequate drug concentration within the tumour itself and this can largely be attributed to the presence of the

BBB [3]. Unlike capillaries elsewhere in the body, endothelial cells of brain capillaries have tight junctions that are highly resistant to the passage of ions or small molecules and do not exhibit trans-endothelial transport [44]. Moreover, the astrocytes and pericytes play an important role in regulating this barrier through molecular cross-talk involving adhesion and tight-junction molecules, the integrins and other extracellular matrix molecules (reviewed in [45]) (Figure 3a). The BBB in GBM tumours exhibits more frequent fenestrations, a loss of tight intercellular junctions and less developed astrocytic pericapillary sheath, all factors contributing to increasing its permeability [46] (Figure 3b-d). However, this compromised BBB still acts as an obstacle for many drugs [6]. Therefore, the main limitation for drug choice in the treatment of GBM is the capacity of the compound to penetrate the BBB. Two main mechanisms by which a synthetic drug molecule can cross the BBB are: 1) by transmembrane diffusion or 2) through transporters [47]. Most drugs used for management of GBM (e.g. temozolomide, carmustine) are small and lipophilic molecules that cross the BBB by transmembrane diffusion. This mechanism is a non-saturable process that depends on molecular diffusion through cell membranes. Factors influencing this process include a good balance between liposolubility (penetration through cell membrane) and hydrosolubility (to improve drug circulation and presentation to the BBB) which are influenced by chemical structure, size and charge [47]. The capacity to escape the ATP-Binding Cassette (ABC) transporters, such as the P-glycoprotein [48] responsible for brain-to-blood efflux, is also important. Saturable transport systems can be used to improve the pharmacokinetic profile of a substance and to target uptake into specific regions of the CNS [47]. Analogs of transporter ligands have been developed for various CNS pathologies [49]. Alternatively, influx transporters can be targeted in a “Trojan-horse” like strategy (i.e. molecules that do not cross the BBB are coupled to ligand molecules that do) but unfortunately, these chemical modifications often results in a decrease in ligand uptake or routing of the hybrid compound to lysosome compartments for degradation [47].

**Figure 3: Electron micrograph showing the structure of brain capillaries from normal and tumour tissue**

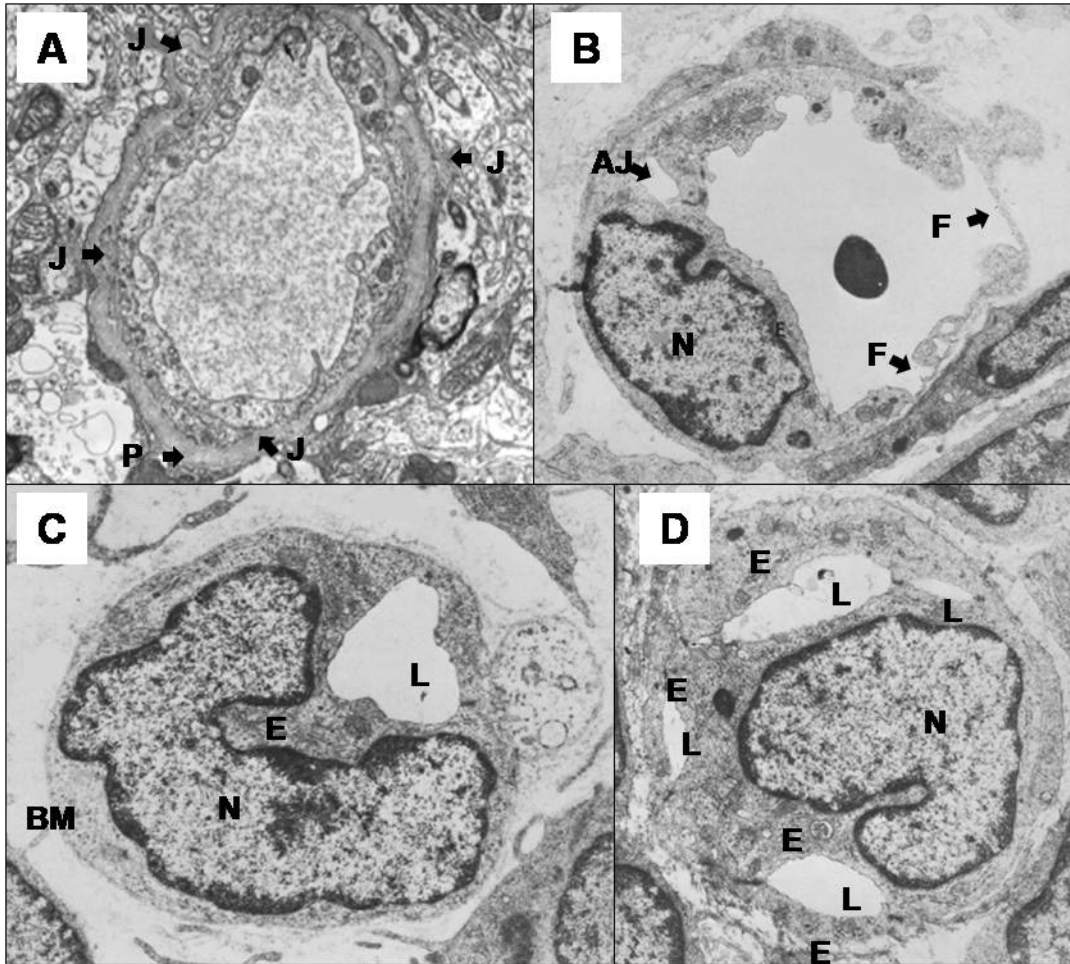


*Figure 3: a) This normal brain capillary is made of two endothelial cells bound together with tight junctions (J) forming a thin and regular layer around the lumen. Processes of pericytes (P) can be seen embedded in the basement membrane. b, c, d) Capillaries from astrocytoma tumours are lined by immature endothelial cells (E) of irregular thickness, hyperplastic nuclei (N), discontinuous basement membrane (BM) and a decreased presence of pericytes or astrocytic processes. Abnormal intercellular junctions (AJ), fenestrations (F) and irregular slit-like lumen (L) can be seen in these micrographs. Adapted from [50, 51].*

In the case where therapeutic agents capable of crossing the BBB, such as TMZ or irinotecan, are available and do exhibit considerable anticancer activity, the most significant problem for GBM cancer patients is repopulation of malignant cells following treatment, causing

inevitable relapse [1, 14]. In light of this problem, the value of combining standard chemotherapy with targeted agents that increase tumour drug sensitivity is now being recognized [52]. The goal of this effort is to target survival and/or proliferation-promoting proteins which are over-expressed, or have up-regulated activity, in cancer cells. Moreover, many trials have indicated that groups of cancer patients treated similarly on the basis of a histopathology classification (e.g. glioblastoma, low grade astrocytoma, etc.) exhibit very different responses to the same treatment [27], implying that various gene expression patterns underlying the disease phenotype may play a more important role in treatment outcomes. This observation highlights the necessity of developing tumour-targeted gene therapy treatments that would be personalized for the specific molecular lesions present in a patient's tumour.

## **1.5 Targeted therapy for malignant glioma**

<sup>1</sup>Cancer is believed to be a genetic disease, arising as a result of genetic mutations that endow the cell with many specific functional capabilities [53] such as cell proliferation, survival, invasion and metastasis (Figure 4) [54, 55]. Recent advances in molecular genetics have enabled the development of methods to specifically target gene expression (small interfering RNA; siRNA, antisense oligonucleotides; ASO, or ribozymes, Figure 5) or the activity of proteins (small molecule inhibitors; SMI). Our current understanding of cancer biology has made it clear that gene targeting therapies will provide an effective strategy to treat cancer. In the next paragraphs, I will summarize the approaches used in targeted therapy for the treatment of malignant glioma. The targets and potential therapeutic effects will be discussed based on the six essential alterations in cell physiology that dictate malignant growth as described elsewhere [54, 55]: (I) self-sufficiency in growth signals and (II) insensitivity to growth inhibitory signals;

---

<sup>1</sup>Sections 1.5-1.7 were adapted from a previously published review: Gene Silencing in the Development of Personalized Cancer Treatment: The Targets, the Agents and the Delivery Systems. Verreault M, Webb MS, Ramsay EC, Bally MB. *Current Gene Therapy*. 2006 Aug;6(4):505-33.

(III) evasion of programmed cell death; (IV) sustained angiogenesis; (V) tissue invasion and metastasis and (VI) limitless replicative potential. It is interesting to note that Hanahan *et al* have recently defined two additional hallmarks of malignancy (reprogramming of energy metabolism and evading immune destruction) [55], but these emerging hallmarks will not be discussed further in the context of this thesis. Table 2 presents a list of genes or associated protein targets that have been inhibited by means of non-viral gene silencing agents in orthotopic GBM pre-clinical or clinical studies, or by SMI or monoclonal antibodies (mAb) in GBM clinical trials phase II/III. It is interesting to note that very few of these studies have assessed the efficacy of the targeted therapy agent in combination with standard chemotherapy or radiation. Figure 4 shows a summary of all gene targets that were silenced by administration of non-viral gene silencing agents in preclinical or clinical evaluations of all types of cancers.

**Figure 4: Gene targets in pre-clinical (no colour) and clinical studies phase I (yellow), II (orange) and III (purple) for gene silencing strategies (ASOs, Ribozymes and RNAi) in cancer therapy.**

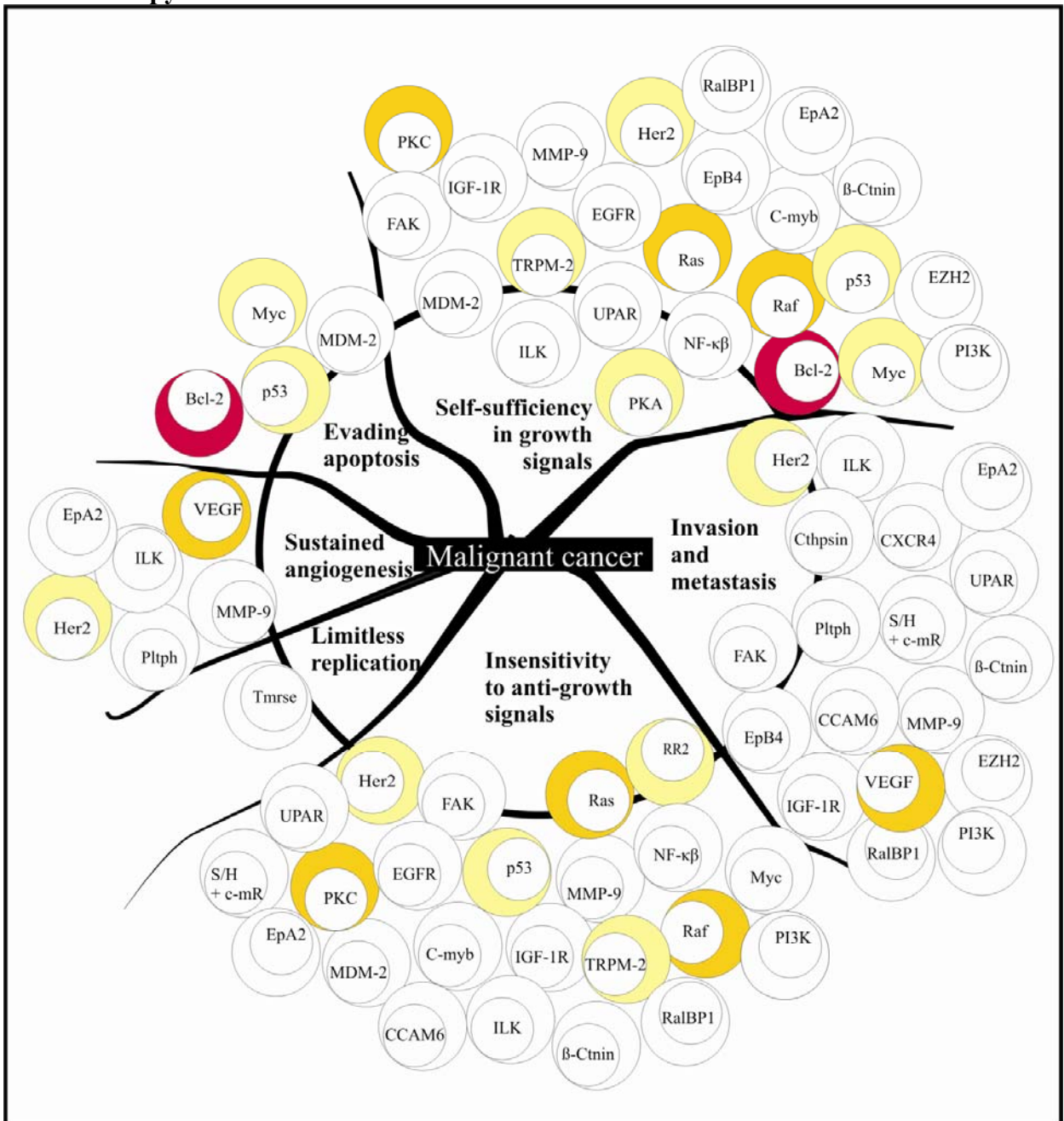


*Figure 4: Targets are classified according to their role in the six essential alterations in cell physiology that dictate malignant growth, as described elsewhere [54]. Definition of abbreviations is given in page xii-xvi. From [56].*

**Figure 5: Mechanisms of action of three gene silencing strategies: antisense oligonucleotides, ribozymes and short interfering RNA**

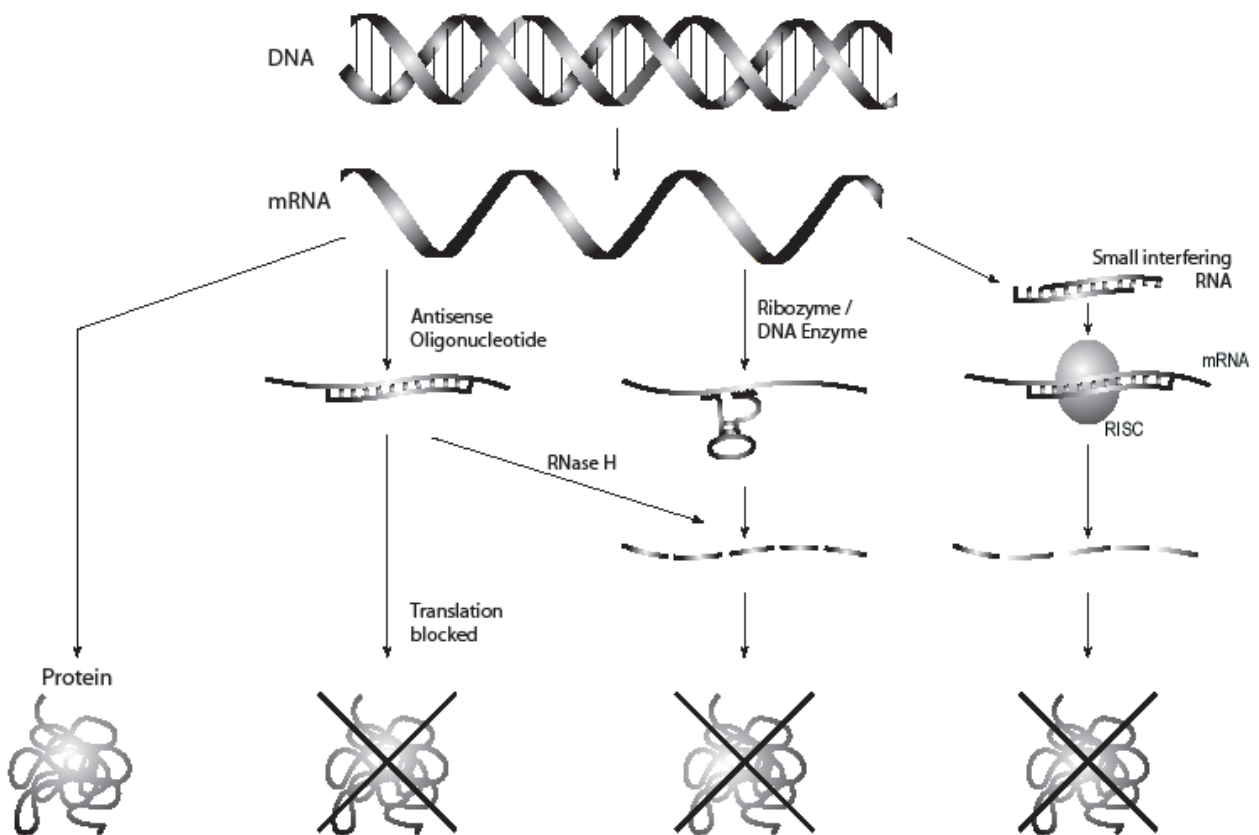


Figure 5: Antisense oligonucleotides are unmodified or chemically modified single-stranded DNA or RNA molecules 13-25 nucleotides long that are specifically designed to hybridize to corresponding mRNA by Watson-Crick binding [57]. The binding to target mRNA results in prevention of gene translation through various mechanisms such as cleavage of the target mRNA by RNase H, steric disruption of ribosome assembly, modulation of RNA splicing or modulation of polyadenylation [57-59]. Catalytic RNA enzymes, named ribozymes, are naturally occurring RNA-based enzymes that bind to and catalyze cleavage of RNA molecules in a sequence-specific manner [60]. siRNAs was first discovered in 1991 [61, 62] and consists of 21-25 base pair RNA sequences specific to a target mRNA. SiRNAs induce the enzymatic degradation of the target mRNA through incorporation into a multi-subunit RNA-induced silencing complex (RISC) [63]. From [56].

### 1.5.1 Self-sufficiency in growth signals and insensitivity to growth inhibitory signals

Tumour cells generate many of their own growth signals, thereby reducing their dependence on stimulation from the normal tissue microenvironment [54, 55]. Molecular strategies for achieving autonomy involve: I) alterations in extracellular growth signals, II) alterations in transducers of those signals, III) alterations in components enabling or preventing the cell to enter cell cycle [54]. For example, protein overexpression of the Epidermal Growth Factor Receptor (EGFR), involved in growth signal transduction, was reported in 60% of GBM cases; EGFR gene amplification was reported in 40% of cases; EGFR truncated transcript encoding for a constitutive activity of the receptor was reported in 20% of cases and mutations of EGFR extracellular domain was reported in 15% of cases [64, 65]. These mutations are quite often combined in the same tumour cell, leading to overactivation of EGFR pathways [66, 67]. Antisense oligonucleotide (ASO) [68] and RNAi [69] mediated inhibition of EGFR has been shown to induce a strong reduction in tumour growth and increased the survival of orthotopic GBM tumour bearing mice. However, the inhibition of EGFR using SMI in clinical phase II trials was not representative of this success. As discussed earlier, erlotinib [41, 70] or gefitinib [40, 71] SMI showed variable activity in GBM patients although better efficacy was seen when used in combination with TMZ. The constitutive activation of the PI3K/AKT pathway associated with the mutation of phosphatase and tensin homolog (PTEN; 60% of GBM cases) has also received considerable attention as it is generally associated with aggressive disease and poor prognosis [72, 73]. The mammalian target of rapamycin (mTOR) was identified as a major downstream effector in this pathway [74]. Phase II clinical trials using the mTOR SMI Temsirolimus (CCI-779) induced disease stabilization and an increase in survival in some GBM patients of phase II clinical trials [75, 76]. Chapter 6 of this thesis will be presenting the therapeutic potential of combined silencing of Rictor, a member of the mTOR complex 2, and EGFR in GBM *in vitro* and *in vivo* models.

### **1.5.2 Evasion of programmed cell death**

The ability of tumour cell populations to expand in number is determined not only by the rate of cell proliferation but also by the rate of cell death. Acquired resistance toward programmed cell death, apoptosis, is a hallmark of most and perhaps all types of cancer [54, 55], causing the tumour to resist conditions that would normally kill cells. In this context, Bcl-2 targeted therapy has attracted the most attention with studies both in pre-clinical cancer models and patients (ASO Oblimersen, SMI AT-101). Although the potential of Bcl-2 targeting has not yet been demonstrated in GBM patients, one report showed that siRNA-mediated inhibition of Bcl-2 can increase the efficacy of taxol in a pre-clinical orthotopic model of GBM [77].

### **1.5.3 Sustained angiogenesis**

Strong evidence indicates that the growth of GBM depends on angiogenesis [78, 79]. However, experimental models of GBM have shown that the resulting vessels are poorly organized and poorly functional, and it is believed that high levels of angiogenesis in GBM are associated with increased hypoxia and interstitial fluid pressure that contribute to the disease malignancy and resistance to treatments [80, 81]. This aspect of GBM vasculature will be discussed further in chapter 3. Members of the VEGF family have emerged as prime mediators of angiogenesis in GBM [78]. As already noted, several clinical trials have demonstrated the efficacy of Avastin (Bevacizumab), a monoclonal antibody (mAb) against VEGF as a single agent and in combination with TMZ or irinotecan to prolong the survival of patients [34, 39, 82]. Avastin was recently approved by the FDA for the treatment of recurrent GBM and is showing promising efficacy in clinical trials for newly diagnosed GBM patients [83]. Many other VEGF or VEGFR inhibitors are currently being tested in the clinic [79].

### **1.5.4 Tissue invasion and metastasis**

Proteins responsible for tissue invasion and metastatic behaviour are often effectors allowing the cell to grow in the absence of extra-cellular (ECM) adhesion signals. The most

obvious example is the integrin family, which is involved in ECM anchorage independent growth of tumour cells, and provides the traction necessary for cell motility and invasion (reviewed in [84]). An integrin SMI, cilengitide, has shown some promising activity in GBM clinical trial phase I/II in combination with TMZ [85], and is now moving to phase III [86]. In addition, enzymes that are involved in the degradation of the ECM will allow cancer cells to invade surrounding brain tissue. Matrix-metalloproteinases (MMPs) were shown to play a central role in the proteolysis necessary for this process [87]. Intratumoural administration of a shRNA against MMP-9 inhibited tumour growth in an orthotopic GBM mouse model [88]. To date, no MMP inhibitors have made their way to a phase II clinical trial for GBM treatment. Moreover, the clinical evaluation of MMP inhibitors as single agents in cancers other than GBM has not been associated with significant anti-tumour responses [89, 90] and they will most likely show better efficacy in a combination setting.

### **1.5.5 Limitless replicative potential**

Some studies suggest that at a given point during the course of tumour progression, evolving premalignant cell populations acquire the capacity to breach the mortality barrier [54, 55]; they become capable of unlimited replicative cycles. Overexpression of telomerase reverse transcriptase (hTERT), a unique ribonucleoprotein enzyme responsible for adding telomeric repeats onto 3' ends of chromosomes [91], could play an important role in the development of cellular immortality and oncogenesis. Telomerase activity has been detected in 89% of GBM cases and correlates with tumour grade [92], whereas low expression of hTERT was shown to be associated with a better prognosis [93]. Pre-clinical investigation of hTERT targeted therapy illustrates that downregulation of this gene results in tumour regression and increased survival in orthotopic GBM murine models [94, 95].

**Table 2: Protein targets that have been inhibited by means of non-viral gene silencing agents in orthotopic GBM pre-clinical studies or clinical trials (CTr), or by SMI in GBM clinical trials phase II/III (definition of abbreviations is given on page xii-xvi)**

Target	Experimental design	Agent	Benefit	Ref
<b>Self-sufficiency in growth signals and insensitivity to growth inhibitory signals</b>				
EGFR	I.cr. U87 line in mice	shRNA in PEGylated immunolip. (h-Insuline R and m-Transferrin R) i.v.	Tumour growth inhibition and increased survival	[69]
	I.cr U87 line in mice	ASO plasmid in PEGylated immunolip. (h-Insuline R and m-Transferrin R) i.v.	Tumour growth inhibition and increased survival	[68]
	Phase II CTr	SMI erlotinib (Tarceva®), gefitinib (Iressa®) i.v.	Minimal as single-agent. Some efficacy with TMZ	[41, 70, 71]
PKC family	Phase II CTr	ASO i.v. (Aprinocarsen)	Minimal benefit	[96]
	Phase II/III CTr	SMI Enzastaurin	Minimal benefit	[97, 98]
UPA/UP AR	4910 line i.cr. In mice	shRNA i.p.	Tumour growth inhibition and increased survival	[99]
mTOR	Phase II CTr	SMI Temsirolimus i.v	Disease stabilization and increased survival	[75, 76]
GF	Phase II CTr	SMI Suramin i.v	No benefit with radiotherapy	[100]
FT	Phase II CTr	SMI Tipifarnib i.v	No benefit	[101, 102]
HDAC	Phase II CTr	SMI Vorinostat i.v	Modest activity	[103]
PDGF R	Phase II CTr	SMI Imatinib (Gleevec®) i.v.	Variable response	[42, 43]
<b>Evasion of programmed cell death</b>				
Bcl-2	U251 line i.cr. in mice	siRNA cDNA i.p.	Enhanced efficacy of taxol on tumour growth inhibition	[77]
<b>Sustained angiogenesis</b>				
VEGF	Phase II/III CTr	Bevacizumab (Avastin)	Active, with and w/o irinotecan or TMZ and FDA-approved for recurrent disease	[34, 39, 82]
FGF	Phase II CTr	Thalidomide i.v.	Minimal benefit as a single agent, some benefit with carmustine or irinotecan	[104-106]
Pleiotro-phin	U87 line i.cr. in mice	PEI-siRNA i.t.	Tumour growth inhibition	[107]
<b>Tissue invasion and metastasis</b>				
Cathepsin B	SNB19 line i.cr. in mice	shRNA i.t.	Tumour growth inhibition	[108]
MMPs	SNB19 line i.cr. in mice	shRNA i.t.	Tumour growth inhibition	[88]
Integrins	Phase I/II CTr	SMI Cilengitide i.v.	Some activity with TMZ	[85]

**Table 2 (cont'd): Protein targets that have been inhibited by means of non-viral gene silencing agents in orthotopic GBM pre-clinical studies or clinical trials (CTr), or by SMI in GBM clinical trials phase II/III (definition of abbreviations is given in page xii-xv)**

Target	Experimental design	Agent	Benefit	Ref
<b>Limitless replication</b>				
hTERT	SNB-19 and LN-18 lines i.cr. in mice	ASO in cat. Lip.	Tumour growth inhibition. More active when combined with IFN- $\gamma$ injections	[94]
	U373 line i.cr. in mice	ASO i.t.	Increased survival	[95]
	U251MG i.cr. in rats	GRN183 ASO i.n.	Tumour growth inhibition and increased survival	[109]
<b>Unclear pathological function</b>				
Tenascin-C	Phase I CTr	Long RNA molecule i.t.	Increased survival	[110, 111]

### 1.5.6 Targeting multiple pathways

As mentioned above, hallmarks of cancer cell malignancy include upregulation or dysregulation of multiple pathways, with deregulations increasing in number as the cancer progresses. In contrast to this observation, the vast majority of clinical trials to date have focused on a single agent that targets a single molecular aberration. It is expected that a therapeutic modality targeting one of these dysregulated pathways will only result in modest benefits to patients in terms of disease-free survival time. Cellular proliferation, growth and death are regulated by an intricate network of cellular functions, and it is very likely that disturbances in the balance between these pathways will lead to the activation of compensating mechanisms in normal cells as well as cancer cells. While it is well understood that a combination of chemotherapeutic agents inclusive of drugs with differing mechanisms of action is generally more efficacious than single agent chemotherapy in the treatment of aggressive cancers, clinicians and scientists are now beginning to realize the benefits of combining agents targeting different biological pathways in order to effectively silence as many cancer phenotypes as possible.

An example of the benefit of combining two SMIs targeting complementary pathways in GBM was reported by our group [112]. In these studies, the aberrant downstream signaling associated with the EGFR mutation commonly found in GBM [113] was targeted using the SMI of the mitogen-activated protein kinase (MAPK)/MAPK kinase (MEK) pathway, U0126, which prevents MAPK phosphorylation [114, 115], or the Raf-1 inhibitor GW5074, which prevents MEK activation [116]. Both inhibitors were used in combination with gene silencing strategies targeting the Integrin-Linked Kinase (ILK). ILK was previously suggested to be involved in the constitutive activation of AKT [117, 118] associated with the deletion of PTEN found in 15-70% of GBM tumours [119-121]. The Ras/MAPK and PI3K/AKT pathways have both shown to be implicated in GBM progression [122], and it was anticipated that therapies that target both of these cell signaling pathways could lead to an effective treatment option.

The SMIs GW5074 or U0126 in combination with the transfection of ILK ASO using cationic liposomes (Lipofectamine 2000<sup>TM</sup>) were found to act synergistically in SF188 and U251MG GBM lines and to increase cell death as compared to the use of the agents alone. Moreover, the combination reduced colony formation in soft-agar when compared to treatments with the single agents. Interestingly, the use of U0126 in ILK ASO transfected U251MG cells further reduced the level of ILK as compared to ILK ASO treatment alone, an observation that I subsequently confirmed with ILK siRNA using the nucleofection transfection system (Amaxa) (Figure 6). It was suggested that U0126 may potentiate ASO or siRNA transfection efficiency, or that a synergistic effect between U0126 and ILK ASO on ILK expression levels could explain this effect. I also believe that a reduction in proliferation rate induced by U0126 may have contributed to further downregulation of ILK by reducing the dilution of the silencing agent that occurs during cell division. Regardless, it was concluded that enhanced ILK suppression helps to explain the synergistic interactions reported in the *in vitro* assays, and that this combination

may be more effective in GBM than any of the agents given as monotherapy. My contribution to this work was the initial spark that led me to the research story presented in this thesis.

**Figure 6: Immunoblot obtained from U251MG cell protein lysate.**

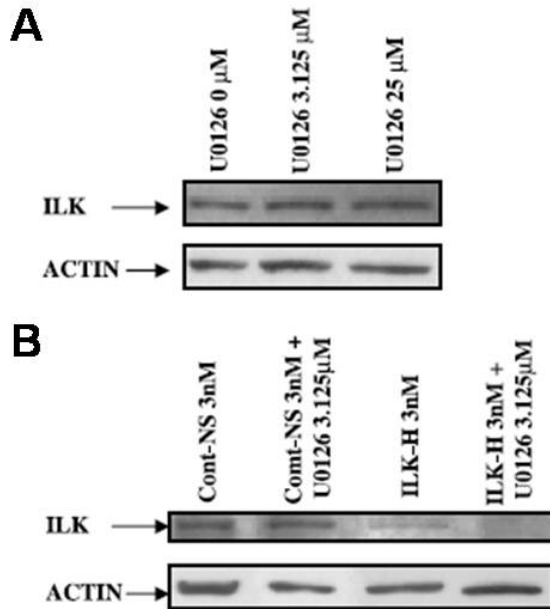


Figure 6: a): U251MG cells were treated with either 3.125 or 25  $\mu\text{mol/L}$  of U0126 MEK inhibitor and harvested 48hr later. b): U251MG cells were transiently transfected with ILK siRNA (ILK-H) alone and in combination with U0126 at a molar ratio of 1:1,190. ILK and  $\beta$ -actin were probed by immunoblotting and  $\beta$ -actin served as a loading control. Increased ILK silencing can be seen when U0126 is added to ILK-H transfected cells (b), although no effect on ILK levels were observed with U0126 treatment alone (a). From [112].

## 1.6 Clinical application of antisense oligonucleotide and siRNA

The idea of targeting gene expression at the level of transcription or translation has been mirrored by the emergence of gene therapy as a strategy to specifically silence the activity of any defective or overactive gene without the limiting step of SMI availability [123]. Since tumour cells have a different pattern of gene expression in comparison with normal cells, gene silencing can theoretically be used to specifically target tumour-associated genes or mutated genes without

altering gene expression of normal cells [124]. The most commonly used strategies employed to achieve gene silencing involve administration of ASOs or siRNAs that can inhibit the expression of specific proteins (Figure 5). However, the therapeutic value of this technology is proving difficult to establish, in part because of the lack of pharmaceutically viable products that can be administered orally, intravenously or intraperitoneally, and that can deliver the gene silencing agent to the target tumour cell populations in sufficient quantity to achieve target knockdown.

Since the first report describing inhibition of gene expression with exogenous nucleic acids by use of a single-stranded DNA in Rous sarcoma virus [125], ASOs have been widely tested in mammalian cells [126], and *in vivo* tumour models [127]. One of the original clinical trials using ASOs as a treatment against cancer was reported in 1993 [128]. To date, only two ASOs have received or are in process of receiving FDA approval: Vitravene™ for use in cytomegalovirus retinitis (blocks translation of the virus' immediate-early transcriptional gene unit), and OGX-011 (Custirsen; against secretory clusterin) for metastatic prostate cancer. At the moment, no ASO has been approved for use in the treatment of brain cancer. Rigorous criteria for the design of target-specific ASO and their control sequences have been outlined previously [129]. In spite of these efforts, ASO technology has faced several technical challenges including *in vivo* stability, binding affinity to target mRNA, delivery to the target cells, and non-antisense effects of ASOs [57]. Human clinical trials and many pre-clinical studies have highlighted several non-specific toxicities attributable to the chemical structure of ASOs, including thrombotic diseases, hypotension and immune activation [130]. This immunostimulatory activity is strongly dependent on the presence of unmethylated CG dinucleotides in certain base contexts, so-called CpG motifs [57], and is a consequence of the induction of natural killer cell production and interferon response normally used to eliminate CpG-containing bacterial DNA [131]. The immune consequences of ASO use can be avoided by the selection of CpG-free sequences or by the use of oligonucleotide backbones that do not induce immune stimulation

[132, 133]. It is worth noting that CpG oligonucleotides, which are deliberately designed to stimulate an immune response, are being tested and could also provide various potential clinical applications for treating cancer [134, 135]. The immune stimulatory activity of certain ASOs could be a means to provide multiple mechanisms of action that work in conjunction to achieve optimal therapeutic effects. It has long been thought that targeted therapeutics based on ASO technology will have the most significant impact on cancer treatment in combination with approved anticancer agents [136]. However, due to the lack of success in the clinical application of ASOs, the attention has now turned to siRNAs as an alternative gene silencing strategy.

Almost 10 years after their therapeutic potential was first reported, siRNAs are still regarded as the most potent, robust, and easy-to-use inhibitor activated through a natural process. Some findings suggest that RNAi-mediated mechanisms can also control gene expression at the post-transcriptional level and can operate in both nuclear and cytoplasmic compartments through DNA methylation, heterochromatin formation or DNA elimination [137]. Several pre-clinical studies have been conducted delivering synthetic siRNAs to silence genes that are believed to be responsible for cancer development. However, siRNA technology is facing the same stability and delivery issues encountered with ASOs. The first human clinical trials were conducted using siRNAs against VEGF or against human immunodeficiency virus (HIV) RNAs [138]. However, in both studies, siRNAs were delivered locally, thereby making it easier to achieve therapeutically relevant concentrations without dealing with the problems of systemic delivery and stability [139].

State-of-art reviews regarding siRNAs activity *in vivo* and *in vitro* have recently been published [140-142]. Some reports showing a non-specific activation of the interferon response induced by siRNAs in cultured cells raised concerns about their safety for *in vivo* use [143, 144]. However, subsequent studies demonstrated that this response is sequence and concentration - dependent and that better designs for siRNA therapeutics can prevent non-specific immune

activation [145-147]. Interestingly, the lack of interferon response was even noted when CpG motifs were included in the sequence [147], in contrast to what was observed for ASOs [57]. The issue of off-target effects associated with siRNAs has also been the subject of intensive study over the past several years. Transcriptional profiling studies have revealed that siRNA duplexes can potentially silence genes other than the intended target, and it was found that these genes were carrying complimentary regions to one of the siRNA strand [123, 148]. It was more recently found that chemical modifications into the seven nucleotides critical for siRNA specificity, termed the “seed region” [123, 149], can substantially reduce off-targeting [150].

## **1.7 Delivery strategies for targeted therapeutics in GBM**

Despite the fact that we are still learning to navigate the technology of RNAi in order to achieve optimal benefits with minimal side-effects, the high specificity and potency of siRNAs, together with the unlimited possibility of designs for siRNAs against any genes, make this technology an attractive option for targeted therapy. Above all, the main challenge for use of siRNAs in GBM is to define a viable option for safe and effective delivery to the tumour. Once this is achieved, RNAi will be regarded as the most powerful tool for designing personalized treatment strategies. Some of the strategies that have been developed and explored pre-clinically for gene silencing agent delivery to brain tumours are discussed below, with references to successful achievements in the clinic for chemotherapeutic agent delivery.

### **1.7.1 Bypassing the blood-brain barrier**

As discussed in section 1.4, the BBB constitutes one of the main barriers to the development of new therapeutics for GBM treatment. Hence, a great deal of research has been focused on defining strategies aimed at bypassing the BBB and increasing delivery of therapeutics. One of these strategies consists of a direct intratumoural (i.t.) injection, and has been successfully used in pre-clinical brain tumour models for delivery of gene silencing agents

[88, 94, 108, 151], and in the clinic for chemotherapeutic agents [152, 153]. The only clinical trial testing the efficacy of RNAi in GBM was done by local delivery of a 146 nucleotides long RNA molecule (ATN-RNA) targeting Tenascin-C mRNA [110, 111]. Although its role in GBM pathology is still unclear, the expression of the ECM glycoprotein Tenascin-C was found to correlate with tumour grade [154]. Treatment with ATN-RNA was associated with increased survival in GBM patients and these results constitute the first demonstration of a potential clinical application for RNAi in the treatment of GBM. Convection-enhanced delivery (CED) is another technique tested in the clinic for local delivery, and consists of placing catheters into the surgical cavity after the resection procedure and delivery of antineoplastic agents through the catheters using positive pressure (0.5 to 15.0µl/min). This technique was shown to increase the anti-tumour efficacy of paclitaxel [155] and the recombinant protein Cintredekin besudotox [156] in GBM patients. CED was also used to deliver siRNAs to the CNS of non-human primates, and resulted in a durable and specific silencing of the selected target [157]. Carmustine wafers (Gliadel) are currently used in the clinic and represent a good example of local delivery. In this system, Carmustine is incorporated in a hydrophobic matrix made of a polyanhydride polymer that protects the agent from hydrolysis [158, 159]. After tumour resection, the wafer discs are implanted at the surface of the resection cavity and the drug is slowly released for a period of three weeks [160]. Although wafers have shown some promising efficacy when combined with temozolomide [161], it is not indicated for patients with infiltrative or multifocal tumours. It is believed that local administration does not allow access to infiltrative cancer cells that are a predominant hallmark of GBM, and this is especially true for macromolecules such as ASOs or siRNAs.

In order to overcome the limitations of direct i.t. administration of agents, other routes of administration have been explored, including systemic administration (intraperitoneal (i.p.) and intravenous (i.v.)), some of which integrating the use of delivery systems (Table 2). Challenges

and opportunities for these strategies will be discussed in the following section. Interestingly, the intranasal (i.n.) route of delivery was recently shown to promote a rapid and efficient delivery of molecules that do not cross the BBB to the brain [162]. The i.n. technique allows for a noninvasive bypass of the BBB via the nasal mucosa, through the olfactory and trigeminal nerves, directly to the brain and cerebrospinal fluid [163]. The ASO GRN163 specific to hTERT was successfully delivered to pre-clinical orthotopic tumours using this technique [109]. The i.n. technique was also used in a phase I/II clinical trial to administer perillyl alcohol, a Ras inhibitor, and results suggested some antitumour activity without any toxicity in GBM patients [164]. These studies, together with other pre-clinical reports [163, 165-167], suggest that the i.n. route of administration may be of great therapeutic value for treatment of brain tumours and could be part of the solution to the issue of polynucleotide therapeutics delivery. It should be noted, however, that material delivery in tissues other than the brain (liver, kidney, heart, muscles) was also detected following i.n. administration [163], suggesting the need for combining this administration route with delivery systems that would improve specificity to the tumour. The currently accepted mechanisms of transport following intranasal administration are the intraneuronal transport following endocytosis or an extracellular diffusion along the nerves [162]. Thus it is clear that the size limitation imposed by these routes may restrict the possible delivery systems that could be used.

### **1.7.2 Limitation to systemic administration**

Strategies used to administer agents through systemic administration include simple infusion as well as more sophisticated delivery systems designed to promote intracellular delivery. In this context, the success of gene silencing therapy for cancer depends in large part on stable and tumour-specific delivery, which can be achieved only if therapeutic molecules can survive as active agents as they cross various biological barriers. These barriers are illustrated in Figure 7. As described earlier, the BBB consists of endothelial cells, pericytes, astrocytes

endothelial and neuronal cells that are organized in such way to confer a unique selective permeability to the CNS vascular network [168], restricting the passive transport of most therapeutic molecules [6] (Figure 3a). Some success in delivering molecules across the BBB has been made with long circulating carrier systems (see section 1.7.4) that can take advantage of the fact that tumour-associated BBB consists of poorly formed vascular endothelium that is more permeable to circulating macromolecules than the normal BBB [169] (Figure 3b-d). Strategies to open the BBB have also been explored and include osmotic disruption [170], the use of vasomodulators to increase permeability [171], or the use potassium channel agonists to increase the formation of transport vesicles [172].

Although it has been shown that siRNAs are more stable in cells than a single-stranded antisense molecule [173], naked RNA sequences injected *in vivo* are rapidly eliminated and have a short duration of effect [60]. Pre-clinical studies suggest that this can be overcome by use of multiple i.v. or i.p. injections of naked siRNAs [174], and can lead to successful downregulation of the target in intracranial tumour [77]. However, other studies reported very little accumulation of siRNA in the brain following i.v. administration, and preferential accumulation was observed in the liver and the kidneys [175-177]. Other reports show that a high-pressure delivery technique could increase delivery of siRNAs given i.v. [178-180] or i.p [147], but no evidence of delivery to the brain was shown [178]. Moreover, this technique is not relevant to human therapies as it involves high pressure and massive volume delivery schemes to generate transiently high local intravascular pressure [63, 181]. It is now widely recognized that if siRNAs are to be used in the clinic for GBM patients, they will have to be formulated with a delivery system strategy in order to increase the agent's half-life and tumour specific delivery.

**Figure 7: Biological barriers preventing therapeutic agent access to the targeted GBM cancer cells from systemic administration to intracellular or intranuclear delivery**

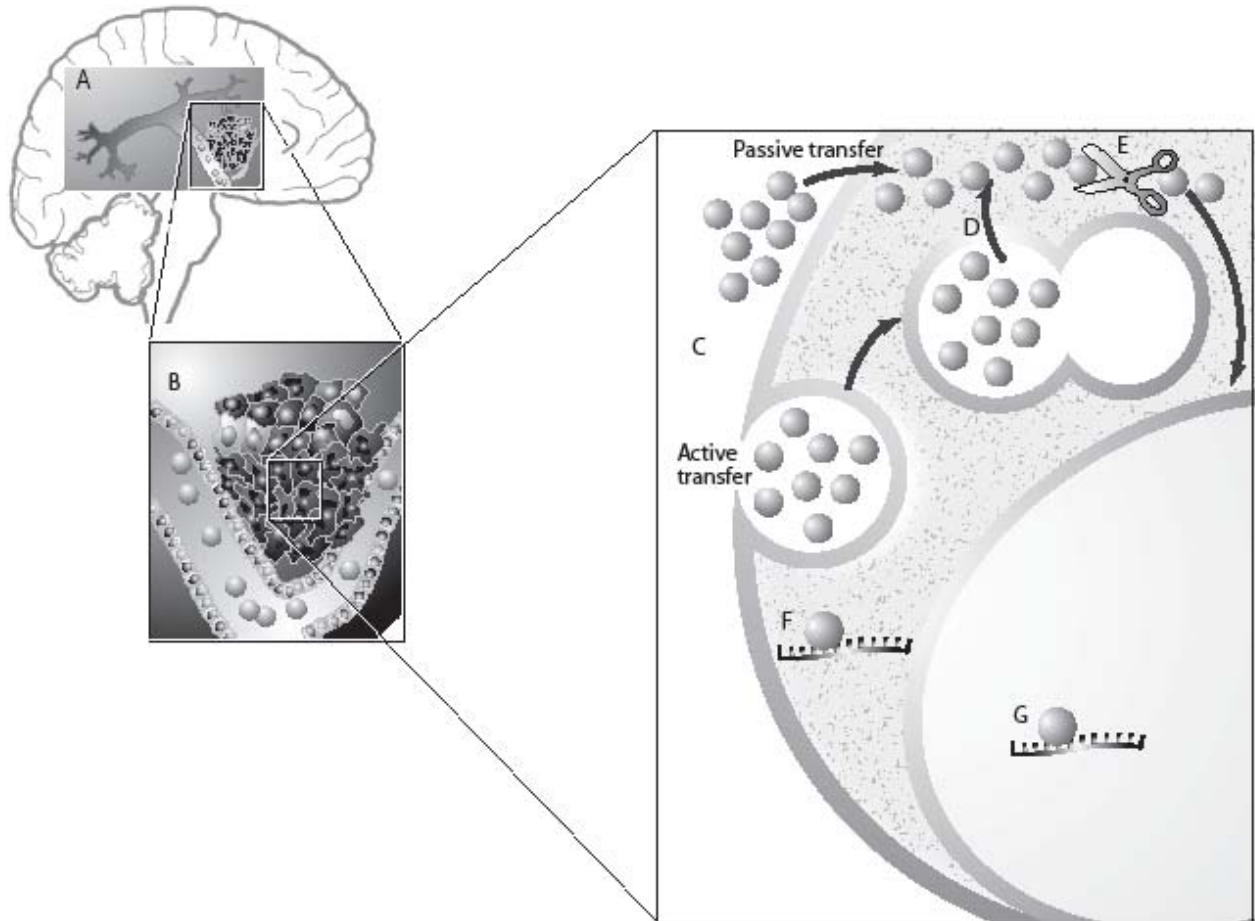


*Figure 7: Grey circles represent DNA or RNA therapeutic molecules delivered with the help of a liposomal nanoparticle delivery system. Barriers limiting access and activity of gene silencing nucleic acid in GBM tumours are: a) Degradation in the blood or uptake by the liver; b) Passage from the circulation across the blood-brain barrier and into the extravascular space within the tumour; c) Passage into cytoplasm of target cells; d) If associated with a carrier system or internalized via endocytosis, the agent needs to be released from the carrier and/or the endosomes; e) Nucleases in tumour cell's cytoplasm; f-g) Binding to target mRNA. Adapted from [56].*

### 1.7.3 Liposomal nanoparticle delivery systems

Studies over the last few decades have established that liposomal nanoparticle (LNP) formulations of selected antineoplastic agents can be more effective than a drug administered in its free form, due to their capacity to increase drug circulation time. Further, increased tumour delivery is observed due to the increased permeability of blood vessels in the tumour environment; a process referred to as the “enhanced permeability and retention effect” (EPR) [182]. Conventional LNPs, which consist of bilayer lipid vesicles, are prepared with phospholipids (e.g. phosphatidylcholine or phosphatidylglycerol) [183]. The incorporation of cholesterol in these formulations influences the mechanical strength and permeability of LNP membranes [184]. Stealth LNP can also be made by coating the LNP surface with the hydrophilic polymer polyethylene glycol (PEG), which provides a barrier against interactions with molecular and cellular components in the plasma compartment [183] and can engender remarkable increases in plasma longevity of the carrier [185]. The FDA-approved and commercially available doxorubicin LNP formulation (Caelyx® or Doxil®) is an example of a PEG-coated formulation [186] (Table 3), and was used in some of the studies presented in Chapter 2.

The agent to be incorporated in the LNP is either encapsulated during the hydration stage (passive loading), or remotely loaded using one of many different active loading strategies [187]. An example of the latter consists of trapping drugs that behave like weak bases into pre-formed LNPs using a transmembrane pH gradient. This strategy was developed on the principle that the neutral and hydrophobic form of the drug is capable of crossing the lipid membrane, but will then be converted into a charged and hydrophilic form at the lower pH inside the LNP. The charged form of the drug is no longer as membrane permeable and thus is trapped within the liposome [187]. The liposomal formulation of vincristine used in studies presented in Chapter 2 was prepared using this strategy [188] (Table 3). The third liposomal formulation used in the

studies presented in this thesis, Irinophore C<sup>TM</sup> (IrC<sup>TM</sup>) [189], relies on the divalent metal ionophore A23187 to transport passively encapsulated copper from the interior of the liposome in exchange for two protons, thus creating and stabilizing the pH gradient. This pH gradient, again, drives drug encapsulation (Table 3). What is interesting about the IrC<sup>TM</sup> preparation is the fact that the retained copper influences drug retention such that the combination of copper and the transmembrane pH gradient provide significant improvements in drug retention. It is not clear how copper influences drug retention, but it may involve complexation of copper and the encapsulated drug or copper-membrane interactions that change membrane permeability [189-191].

**Table 3: Formulation specifications of Irinophore C<sup>TM</sup>, liposomal vincristine and Caelyx<sup>®</sup>**

Agent	Drug	Lipid composition	Drug loading strategy	Ref.
Irinophore C <sup>TM</sup>	Irinotecan	DSPC/Cholesterol (55:45 molar ratio)	A23187/Cu <sup>2+</sup> -induced pH-gradient and intraliposomal drug retention by formation of Cu <sup>2+</sup> /irinotecan complexes	[189-191]
Liposomal vincristine	Vincristine	DSPC/Cholesterol (55:45 molar ratio)	Citric acid-induced pH-gradient	[188, 192]
Caelyx <sup>®</sup>	Doxorubicin-HCl	HSPC/Cholesterol/ <sup>2000</sup> PEG-DSPE (95.8:31.9:31.9 weight ratio)	Ammonium ion induced pH-gradient and intraliposomal drug precipitation by formation of (Dox-NH <sub>3</sub> ) <sub>2</sub> SO <sub>4</sub>	[186]

Liposomal formulations have shown some success in the delivery of drugs to brain tumours. Liposomal doxorubicin (Caelyx<sup>®</sup> or Doxil<sup>®</sup>) was reported to be less toxic in the clinic than the unencapsulated form [193-195]; when used to treat malignant glioma, stabilization of the disease (reduction of tumour volume of < 50% or a < 25% increase in tumour volume for more than 8 weeks) was observed [196, 197]. An orthotopic GBM pre-clinical study showed anti-vascular activity of doxorubicin when encapsulated in LNPs, and these effects were not observed with the free form of the drug or in normal brain tissue [198]. Other pre-clinical studies showed that liposomal formulations of irinotecan are more efficacious than the unencapsulated form in brain tumours [199, 200] and in colorectal and adenocarcinoma tumours

[189, 201, 202]. Interestingly, very little effort has been made in the development of SMI that could be administered in LNPs. It appears that if the expertise and knowledge that was gained over the last decades in the field of lipid-based delivery systems was directed towards improving SMI delivery to brain tumours, potential therapeutic success could have already been achieved.

In developing lipid-based delivery systems for gene silencing agents, the goal is to design a system that simultaneously achieves high efficiency (defined by delivery and release of the agent to the disease site), prolonged effects and low toxicity [203]. Small cationic LNPs can interact with negatively charged DNA or RNA, leading to the formation of complexes with a prolonged half-life in the circulation [204] and capable of promoting cellular internalization [183]. Some cationic LNP formulations are commercially available for *in vitro* use (e.g. Lipofectamine 2000<sup>TM</sup> used in the studies presented in Chapter 5). A report showed that hTERT-targeted ASO delivery using cationic LNPs resulted in increased survival of intracranial tumour bearing mice [95]. Numerous other studies have been done using i.v. or i.p. injections of siRNAs [205-207] or ASOs [208] complexed with cationic LNPs in cancer models other than brain tumour. These techniques led to good silencing efficiency with no significant signs of toxicity. It is important to mention that some studies have demonstrated immune system activation induced by common cationic lipids following systemic administration [209-211]. Furthermore, another limitation to the therapeutic use of positively charged complexes is that they are cleared rapidly following intravenous administration [212] as they bind to proteins in the plasma and form aggregates which are eliminated by non-target cells [213]. Since neutralized complexes have proven to be less efficient, cationic complexes possessing hydrophilic steric barriers, achieved through the use of surface grafted polymers like polyethylene glycol (PEG), have been pursued to address the problem of plasma protein binding and rapid elimination [214]. PEG-immunoliposomes (made by adding antibodies at the surface of LNPs) are able to efficiently deliver ASO [68] and siRNAs [69] to orthotopic brain tumours following systemic

administration. Stable nucleic-acid-lipid particles (SNALP) consist of lipid bilayer particles prepared with a mixture of cationic and fusogenic lipids, and have been shown to exhibit the stability, small size, low surface charge and low toxicity required for *in vivo* administration [215], and to promote efficient siRNA cellular uptake [216]. The lipid particles are coated with PEG molecules which dissociates from the SNALP rapidly after administration, thus transforming the carrier into a transfection-competent entity [217]. SNALP-formulated siRNA have shown improved circulation time and increased downregulation efficacy in mice and nonhuman primates liver [215, 218, 219], and recent modifications to the lipid composition have triggered a substantial 10-fold improvement in activity *in vivo* [220]. Alternatives to cationic lipids complexed with therapeutic polynucleotides are also being explored to overcome the limitations observed with current formulations. In particular, reductions in *in vivo* toxicity and targeting efficiency for a certain cell population are a main focus. I have discussed these options in a review that was published in Current Gene Therapy [56].

It has become clear that delivery systems, whether they are lipid-based, polymer-based or antibody-conjugated, can have a significant benefit in enhancing stability of drugs, facilitating delivery to tumour sites and perhaps delivery to the intracellular compartments containing the molecular targets. Moreover, the reduced toxicity profile associated with many liposomal drug formulations compared to the free form of the drug [192, 194] could be used to administer higher doses that would lead to increased drug delivery to brain tumours. To date, the full potential of this technology has not been explored in GBM and I consider this to be a significant opportunity for development of targeted therapeutic approaches that consider the use of multiple therapeutics all designed to inhibit phenotypes of GBM that contribute to its aggressive behaviour.

## 1.8 Focus of the present thesis

The research presented in this thesis was done under the overarching hypothesis that strategies that increase delivery of chemotherapeutic drugs to the brain will improve treatment outcomes in patients with glioblastoma and the efficacy of these drugs will be enhanced by combining them with silencing of signaling pathways known to play a role in the promotion of tumour growth and progression. This hypothesis was tested through the six specific research hypotheses and objectives outlined in section 1.2.

The impact of IrC<sup>TM</sup>, Caelyx® and liposomal vincristine on the tumour vasculature was first assessed in subcutaneous and orthotopic models of GBM (Chapter 2). It was found that all three formulations significantly inhibit GBM tumour growth. Most importantly, the results obtained suggest that the liposomal formulations induce a normalization of the architecture of tumour vasculature. This strategy may prove valuable to increase the delivery of molecules capable of crossing a normal blood-brain barrier, such as temozolomide.

The impact of IrC<sup>TM</sup> administration on irinotecan delivery to the brain and its efficacy was then compared to the administration of the free form of the drug (Chapter 3). Results obtained showed that the delivery of irinotecan and its active metabolite SN-38 to the brain is improved following administration of IrC<sup>TM</sup> compared to irinotecan. A repeated dose toxicology study in tumour-free rodents showed that IrC<sup>TM</sup> was much better tolerated than the free drug. Further, at equivalent and equitoxic doses, the therapeutic efficacy of IrC<sup>TM</sup> was greater than that of irinotecan.

To be able to follow the progression of orthotopic GBM tumours in live animals, GBM cell lines expressing red fluorescent proteins were developed as a tool for tumour imaging in live animals (Chapter 4). It is demonstrated that the fluorescent signal expressed by the resulting

mKate2 or mCherry expressing tumour cells implanted intracranially can be monitored in live animals by multi-spectral imaging.

In order to characterize how cationic lipids used for siRNA transfection techniques can influence delivery and molecular signaling, the impact of the commonly employed Lipofectamine 2000<sup>TM</sup> on the extent of the target downregulation, the kinetics of silencing and the downstream consequences of the downregulation was assessed using a siRNA sequence specific to ILK. These results were compared to results obtained following electroporation-mediated transfection (Chapter 5). Results indicate that cationic lipid formulation used for siRNA delivery can induce non-specific side effects exerted on the mTOR/AKT pathways; effects that occur independently of ILK silencing.

Finally, the therapeutic potential of the combined silencing of EGFR and Rictor was assessed *in vitro* and *in vivo* by means of RNA interference (Chapter 6). It was found that the dual silencing resulted in a reduction of cell migration and an increase in sensitivity to chemotherapeutic drugs *in vitro*. Unexpectedly, the combined silencing of EGFR and Rictor *in vivo* resulted in a complete inhibition of tumourigenicity, thus preventing completion of further studies assessing the activity of chemotherapeutic drugs in combination with EGFR and Rictor dual silencing. Despite the fact that the synergy between the dual silencing and chemotherapeutic drugs could not be studied *in vivo*, it was concluded based on the *in vitro* data that the proposed targeted therapy would be expected to increase chemotherapeutic drug efficacy. Most importantly, the fact that dual silencing completely inhibited tumourigenicity suggests that such treatment could impede chemo and radiation resistant -tumour cells from replenishing the tumour after treatment.

## **Chapter 2: Vascular normalization in orthotopic glioblastoma following intravenous treatment with lipid-based nanoparticulate formulations of irinotecan (Irinophore C<sup>TM</sup>), doxorubicin (Caelyx<sup>®</sup>) or vincristine.**

### **2.1 Introduction**

<sup>2</sup>Glioblastoma (GBM) tumours are largely refractory to systemic treatments; the median survival time for patients with GBM is 14.6 months and the 2-year survival rate is less than 30%. Chemotherapy for GBM is compromised in part by the blood-brain barrier limiting drug access to the malignant cells. In addition, pre-clinical models showed that GBM tumours are poorly perfused [80, 81] due to factors such as reduced blood flow rates, elevated hematocrit and interstitial fluid pressure, and an increase in geometric resistance [221-224], all of which impede drug delivery to the tumour tissue. Strategies which improve vascular function in GBM tumours should improve the delivery of other drugs capable of crossing the blood brain barrier and this should be associated with an increase in therapeutic activity.

Our laboratory has previously characterized and described the effects of a liposomal formulation of irinotecan (Irinophore C<sup>TM</sup>; IrC<sup>TM</sup>) [190, 225]. Encapsulation of irinotecan into liposomes improved the pharmacokinetic profile of the drug and its active metabolite, SN-38. More specifically, administration of IrC<sup>TM</sup> resulted in a 1000-fold increase in the area-under-the-curve of plasma irinotecan concentration when compared to free drug (Camptosar). In addition, following IrC<sup>TM</sup> injection, the plasma levels of SN-38 were maintained at concentrations that were up to 40-fold higher than that achieved following injection of free drug [190]. Following IrC<sup>TM</sup> treatment, the s.c. (subcutaneous) colorectal tumours (HT-29) exhibited more functional

---

<sup>2</sup>This chapter was previously published: M. Verreault, D. Strutt, D. Masin, M. Anantha, A. Yung, P. Kozlowski, D. Waterhouse, M.B. Bally and D.T. Yapp. 2010. Vascular normalization in orthotopic glioblastoma following intravenous treatment with lipid-based nanoparticulate formulations of irinotecan (Irinophore C<sup>TM</sup>), doxorubicin (Caelyx<sup>®</sup>) or vincristine. BMC Cancer. 2011; April 8(11):124.

tumour blood vessels, reduced hypoxia, and increased tumour perfusion. Importantly, these changes in tumour vasculature were associated with increased tumour uptake of doxorubicin and 5-FU given intravenously [225]. The latter data were consistent with the idea that the tumour vasculature in the treated tumours acquires a more “normal-like” function; an effect of anti-angiogenic therapies described as ‘normalization’ [226, 227].

The primary goal of the studies reported here was to determine whether IrC<sup>TM</sup> is efficacious in models of GBM, and whether treatment with this drug formulation would also result in normalization of GBM vasculature. The effects of IrC<sup>TM</sup> on the growth rates and vascular function of the HT-29 colorectal cancer model was attributed to significant increases in the drug circulation lifetime and plasma concentration when encapsulated in liposomes [190, 225]. We further reasoned that liposomal formulations of other drugs with known activity against proliferating endothelial cells should have preferential cytotoxicity towards angiogenic tumour vessels and could potentially also ‘normalize’ the chaotic and erratic vasculature of tumours. Thus, part of these studies assessed the effects of liposomal vincristine [192] and doxorubicin (Caelyx<sup>®</sup>) on tumour vasculature. Vincristine has previously been shown to be active against proliferating endothelial cells [228]. Liposomal formulations of doxorubicin have also been shown to have direct effects on tumour associated vasculature [198, 229, 230].

The data reported here assess the effects of IrC<sup>TM</sup>, Caelyx<sup>®</sup> (a commercially available and FDA-approved liposomal formulation of doxorubicin), and liposomal vincristine on tumour vasculature in subcutaneous and orthotopic models of GBM. The results indicate that IrC<sup>TM</sup> was the most active formulation when using treatment endpoints based on changes in tumour size as well as tumour vascular morphology and function in GBM grown subcutaneously and orthotopically. The effects were consistent with the idea that following treatment, there was normalization of tumour vasculature. In the subcutaneous tumours, vascular ‘normalization’ was associated with increased tumour uptake of Hoechst 33342, while in the orthotopic glioma

tumours, treatment-induced vascular ‘normalization’ was associated with decreased tumour uptake of Hoechst 33342.

## **2.2 Materials and methods**

### **2.2.1 Cell culture**

Adult dermal human microvascular endothelial cells (d-HMVEC; Cambrex Bio Science, Walkersville, MD, USA), Human brain microvascular endothelial cells (HBMEC; ScienCell Research Laboratories, San Diego, CA, USA) and U251MG glioblastoma cells (American Type Culture Collection, Manassas, VA, USA) were characterized and authenticated by the cell banks using immunofluorescent methods and used for a maximum of eight passages for the endothelial cells and fifteen passages for U251MG. Stock cells lines were maintained in the absence of penicillin and streptomycin and screened for mycoplasma prior to preparing a stock of cells that were frozen for use in experiments. D-HMVEC cells were maintained in Endothelial Cell Basal Medium-2 (Clonetics®, Lonza, Basel, Switzerland) supplemented with 5ng/mL Fibroblast Growth Factor, 20ng/mL Vascular Endothelial Growth Factor, 10ng/mL Epidermal Growth Factor (Clonetics®, Lonza), 10 unit/mL Heparin (Pharmaceutical Partners of Canada) 1% L-glutamine, 1% penicillin/streptomycin (Stem Cell Technologies, Vancouver, BC, Canada) and 10% Fetal Bovine Serum (FBS; Hyclone, Logan, UT), and plated in 1% gelatin (Sigma, Oakville, ON, Canada) pre-coated dish. HBMEC cells were maintained in Endothelial Cell Medium supplemented with Endothelial Cell Growth Supplement (ScienCell Research Laboratories) containing 5µg/mL Insulin, 10ng/mL Epidermal Growth Factor, 2ng/mL Fibroblast Growth Factor, 2ng/mL Insulin-like Growth Factor-1, 2ng/mL Vascular Endothelial Growth Factor, 1µg/mL hydrocortisone, 5% FBS and 1% penicillin/streptomycin, and plated in 15µg/mL fibronectin (Sigma) pre-coated dish. U251MG cells were maintained in DMEM medium supplemented with 1% L-glutamine, 1% penicillin/streptomycin (Stem Cell

Technologies, Vancouver, BC, Canada) and 10% FBS (Hyclone, Logan, UT). All cell lines were cultured at 37°C in a humidified atmosphere containing 5% CO<sub>2</sub>, and used during their exponential growth phase unless otherwise stated.

### **2.2.2 GBM animal model s.c. and orthotopic**

All protocols involving work with live animals were reviewed and approved by the University of British Columbia Animal Care Committee (certificate of approval # A07-0423). For the subcutaneous GBM model, U251MG cells ( $5 \times 10^6$ ) were implanted subcutaneously into the backs of Rag2M mice (7-10 weeks old females, n=9). To generate orthotopic GBM tumours, animals were anesthetized by injection of 120mg/kg i.p. ketamine (Ketalean®, Bimeda-MTC, Cambridge, ON, Canada), 10mg/kg i.p. xylazine (Rompun®, Bayer inc., Toronto, ON, Canada), and 0.5mg/kg s.c. acepromazine (Atravet®, Wyeth, Guelph, ON, Canada), and were given 1mg/kg s.c. Metacam® analgesic (Boehringer Ingelheim, Burlington, ON, Canada). U251MG ( $7.5 \times 10^4$ ) cells were implanted into the right caudate nucleus-putamen (ML -1.5 mm; AP +1mm; DV -3.5mm) of mice (n=5-6) using a stereotaxic injection frame (Stoelting Company, Wood Dale, IL). Animals were treated with 25mg/kg IrC<sup>TM</sup>, 15mg/kg doxorubicin liposome (Caelyx®, Schering-Plough, QC, Canada), 2mg/kg liposomal vincristine i.v. on day 21, 28 and 35 after inoculation. Dosing of Caelyx® and liposomal vincristine resulted in less than 5% body weight loss, while IrC<sup>TM</sup> treatment did not cause any change in body weight. Previous tests in our laboratory have shown that the maximum tolerated single doses for IrC<sup>TM</sup>, Caelyx® and liposomal vincristine are >120mg/kg, 17mg/kg and 3mg/kg, respectively. IrC<sup>TM</sup> [189] and liposomal vincristine [188] were prepared as described previously. S.c. tumour size was measured throughout the study by caliper and tumour weights were extrapolated from the measurements using the following formula:  $mg = (\text{tumour width}^2 \times \text{tumour length})/2$  [231]. Mice were injected with Hoechst 33342 (1.2 mg/mouse i.v.; Sigma) twelve (s.c. model) or twenty (orthotopic model) minutes prior to sacrifice on day 42. This timing was chosen based on

previous studies [225] and tests aimed at determining the optimal timing for Hoechst 33342 injection without saturation of the tissue and before any decrease in Hoechst 33342 staining could be observed due to possible metabolic elimination. All animals were terminated by CO<sub>2</sub> asphyxiation and s.c. tumours or brains were harvested and cryopreserved in OCT (Sakura Finetek, CA) on dry ice and stored at -80°C.

### **2.2.3 Hoechst 33342, Ki67, CD31, collagen IV, NG2 and nuclei density staining and quantification**

Optimal Cutting Temperature compound (OCT)-preserved s.c. tumours were cryosectioned using a Leica CM1850 Cryostat (Leica, ON, Canada) and 10µm sections were collected in the middle of each tumour. OCT preserved brains were cryosectioned and 10µm sections were collected from the Bregma +1.0 location. Sections were fixed in a 1:1 mixture of acetone:methanol for 15 minutes at room temperature, then blocked with blocking buffer (Odyssey blocking buffer, Rockland, PA, USA) for 1 hour at room temperature. Sections were stained with rat anti-mouse CD31 antibody (1:100 dilution, PharMingen #550274, BD Biosciences), rabbit anti-human Ki-67 (Invitrogen #18-0191z; 1:100), rabbit anti-Collagen IV antibody (1:400, Abcam # ab19808, Cambridge, MA, USA) and mouse anti-NG2 chondroitin sulfate proteoglycan antibody (1:100, Millipore # MAB5384, Billerica, MA, USA). Primary antibodies were incubated on sections overnight at 4°C. Secondary antibodies (Alexa 488 goat anti-rat #A11006, Alexa 546 goat anti-rabbit #A-11035 and Alexa 633 goat anti-mouse #A-21126, 1:200, Invitrogen) were incubated for 1hr at room temperature. Nuclei were stained with Draq5 (Biostatus, Leicestershire, UK; 1:200) for 30min at 37°C. Slides were mounted with PBS and imaged for Alexa 488 (L5 filter), Hoechst (A4 filter), Alexa 546 (Cy3 filter), Cy5 (Cy5 filter) and Draq5 (Cy5 filter) using a robotic fluorescence microscope (Leica DM6000B, Leica, ON, Canada) and a composite colour image of these markers was produced (Surveyor software, Objective Imaging Ltd.). Thresholds for each marker were set using Photoshop; the threshold

level was set using a scale from 1 to 255 units, and was defined at 2 units higher than the minimal level necessary to obtain a negative signal for non-specific staining, and was kept the same for all sections. Acquired images were quantified for positive pixels or colocalization (double-positive pixels) using an in-house segmentation algorithm, normalized to the number of pixels in the tumour area and expressed as positive fraction (positive pixels divided by non-necrotic tumour area; MATLAB, The Mathworks, Natick, MA, USA). Non-necrotic tumour areas were defined by cropping out necrotic and non-tumour tissue on the basis of positive Ki-67 and Draq5 co-stained sections and were quantified using the same in-house algorithm. Colocalization was considered positive when two positive pixels from one stain of interest were located within a 3 pixel radius from one pixel of the other stain of interest. Of note, one cancer cell nucleus measures between 3 and 6 pixels. Blood vessel diameter was defined by taking 10 measurements/tumour section in a 15 x 15 cm box at 200% magnification using Photoshop, and was expressed in pixels. For differential analysis between the tumour's center and periphery, the boundary between the tumour center and periphery area was established at 20% of tumour diameter distance from tumour margin. Another set of sections was stained with hematoxylin and eosin (H&E) for histopathology analysis. The fraction of collagen IV-free blood vessels was defined as Collagen IV negative/CD31 positive pixels over total CD31 pixels. The fraction of NG2-free blood vessels was defined as NG2 negative/CD31 positive pixels over total CD31 pixels. The amount of basement membrane empty sleeves was defined as CD31 negative pixels/collagen IV positive pixels divided by the total non-necrotic tumour area.

#### **2.2.4 Magnetic resonance imaging and $K_{\text{trans}}$ measurement in U251MG orthotopic tumours**

All magnetic resonance experiments were carried out using a 7.0 Tesla Magnetic Resonance (MR) scanner (Bruker, Ettlingen Germany). A Bruker (Ettlingen, Germany) volume coil (inner diameter of 7cm) and rectangular surface coil (1.7x1.4cm) was used for signal transmission and reception respectively. The coil was tuned to the hydrogen proton frequency

(300.3MHz). The  $K_{trans}$  values were obtained from serial images acquired to monitor changes in the concentration of the MR-visible contrast agent gadolinium diethylenetriamine penta-acetic acid (Gd-DTPA; Bayer Schering Pharma) within each pixel, during the initial uptake and subsequent washout of the agent in the tumour. The MRI scans follow the protocol reported by Lyng et al. [232]; briefly, mice were anaesthetized with isoflurane (5% induction, 2% maintenance), a catheter inserted into the lateral tail vein and the animal was placed supine with its head above the surface coil. A proton-density weighted scan was first acquired to serve as a baseline for conversion of pixel intensity to absolute concentration values of the contrast agent. A volume equivalent to 10uL per gram body weight of the contrast agent (0.03 M Gd-DTPA in saline) was injected via the tail vein catheter in a period of 10-15 seconds. The contrast series consisted of a 3D RF-spoiled Fast Low Angle Shot (FLASH) sequence with timing and resolution parameters as follows: echo time/repetition time=2.8/9.2 ms, Field of view=1.92x1.92x1.6cm, Matrix size=128x128x16cm, acquisition time per image=9.45 seconds. Twenty baseline scans were acquired before contrast agent injection and 250 scans were acquired afterwards, resulting in a total acquisition time of 43 minutes. The concentration-time curve for each pixel was fit to a two-compartment Kety model [233] which describes the pharmacokinetics of the contrast agent using three parameters:  $v_e$  (volume of extracellular extravascular space),  $K_{trans}$  (volume transfer constant between the vasculature and tissue compartment) and  $V_p$  (fractional volume of the vascular compartment).

### **2.2.5 *In vitro* endothelial cell exposure and nuclei count**

For proliferative conditions, Dermal Human MicroVascular Endothelial Cells (d-HMVEC; 600 cells/well) and Human Brain Microvascular Endothelial Cells (HBMEC; 5000 cells/well) were plated in black 96-well plates (Optilux™, BD Biosciences, Mississauga, ON, Canada) and drugs were added the day after. For non-proliferative conditions, d-HMVEC cells (5000 cells/well) and HBMEC (50000 cells/well) were plated in black 96 well plates and drugs

were added four days after. Irinotecan (Sandoz, QC, Canada), SN-38 (LKT Laboratories, MN, USA), vincristine (Novopharm, ON, Canada), docetaxel, paclitaxel (Taxol®; Bristol Myers Squibb Canada, QC, Canada) and doxorubicin (Adriamycin<sup>TM/MC</sup>, Pfizer, QC, Canada) were added in concentrations ranging from 1 to 100,000pM on cells and replaced daily for 7 days. At the end of drug treatment, cells were fixed with 3.5% paraformaldehyde (Electron Microscopy Sciences, PA, USA) for 15 minutes at -20°C, permeabilized with 0.1% Triton (Perkin-Elmer, MA) in PBS for 10 minutes at room temperature, blocked for 1hr at 4°C (Odyssey blocking buffer, Rockland, PA, USA) and incubated overnight with Ki67 antibody (Invitrogen #18-0191z; 1:100 dilution in blocking buffer). Cells were then incubated with Anti-rabbit Alexa 488 secondary antibody (Molecular Probe #A11034, Invitrogen; 1:200 in blocking buffer) for 1hr at room temperature. Nuclei were stained with Draq5 dye (Biostatus, Leicestershire, UK; 1:200 in PBS) for 30 min at 37°C. Twenty fluorescent photographs/well (Alexa 488 excitation: 495nm, emission: 519nm; Draq5 excitation: 697nm, emission: 646nm) were taken at 10x magnification using an InCell Analyzer 1000 (Amersham Bioscience) and the total nuclei count (Draq5 stained nuclei) as well as Ki67 expressing nuclei count (Draq5 and Alexa 488 double stained nuclei) were quantified using InCell Developer Toolbox software (Amersham Bioscience, GE Healthcare, Baie d'Urfe, QC, Canada). Dose-response curves generated from total nuclei count were used to calculate drug concentrations causing a decrease in endothelial cell nuclei count by 20% (fraction affected:  $F_a = 0.2$ ), 50% ( $F_a = 0.5$ ), 75% ( $F_a = 0.75$ ) and 90% ( $F_a = 0.9$ ) and compared for both proliferative and non-proliferative cells. All data points represent the average of 3 independent experiments in triplicate +/- S.E.M.

### **2.2.6 Statistical analysis**

All statistical data was collected using GraphPad Prism (San Diego, CA). Because all treatment drugs were chosen based on previous rationale justifying their inclusion in the study, the experimental design should not be regarded as a screening assay and statistical analysis was

done using the single comparison non-parametric two-tailed Mann Whitney test and no correction was made for multiple comparisons. All data are expressed +/- S.E.M.

## 2.3 Results

### 2.3.1 Irinophore C<sup>TM</sup>, Caelyx<sup>®</sup> and liposomal vincristine inhibit tumour growth and increase Hoechst 33342 delivery in subcutaneous GBM tumours

Rag2M mice bearing s.c. U251MG tumours (n=9) were treated i.v. (once weekly for 3 weeks) with 25mg/kg IrC<sup>TM</sup>, 15mg/kg Caelyx<sup>®</sup> or 2mg/kg liposomal vincristine. Tumour growth was monitored during the entire treatment period, and tumours were harvested 7 days after the last treatment. As noted in Figure 8a, the three drugs inhibited tumour growth significantly compared to untreated control (p<0.05-0.001). At the end of the study (day 42), the weight of treated tumours ranged from 34 to 80 mg compared to an average of 502 mg for untreated control animals. A representative tumour section (H&E) derived from each treatment group is also provided in Figure 8a. The total non-necrotic tumour area (excluding necrotic and non-tumour area) measured in number of image pixels for each treated group is summarized in Figure 8b. The measurements of area of viable tumour tissue correlated with the tumour weight measurement and was significantly reduced for all treatment groups (compared to untreated tumours; p<0.0001). The proliferation marker Ki67 was used to estimate the fraction of viable cells undergoing active proliferation within the tumour (positive Ki67 staining divided by total viable tissue, expressed as Ki67 positive fraction). Liposomal vincristine had no apparent effect on the Ki67 staining compared to control tumours. Treatment with IrC<sup>TM</sup> caused a 2-fold decrease in Ki67 staining (p<0.01). In contrast, a significant (p<0.01) increase in Ki67 staining was observed in tumours from animals treated with Caelyx<sup>®</sup> (Figure 8b). It should be noted that Caelyx<sup>®</sup> treatment was also associated with enlarged tumour cell nuclei (see arrow heads in inset H&E image Figure 8a) and this may suggest that the treatment promoted cell cycle arrest [234]. This observation is in accordance with previously published findings on the effects of

doxorubicin on cell cycle [235-237] and the fact that cellular Ki67 antigen has been shown to accumulate in some type of cell cycle arrest [238]. Finally, a decrease in number of cell nuclei per tumour area (nuclei density) with a concomitant increase in connective tissue was observed by examination of the H&E stained sections in tumours from mice treated with IrC<sup>TM</sup>.

**Figure 8: Irinophore C<sup>TM</sup>, Caelyx<sup>®</sup> and liposomal vincristine significantly inhibit tumour growth, decrease proliferation and increase tumour perfusion in subcutaneous GBM tumours.**

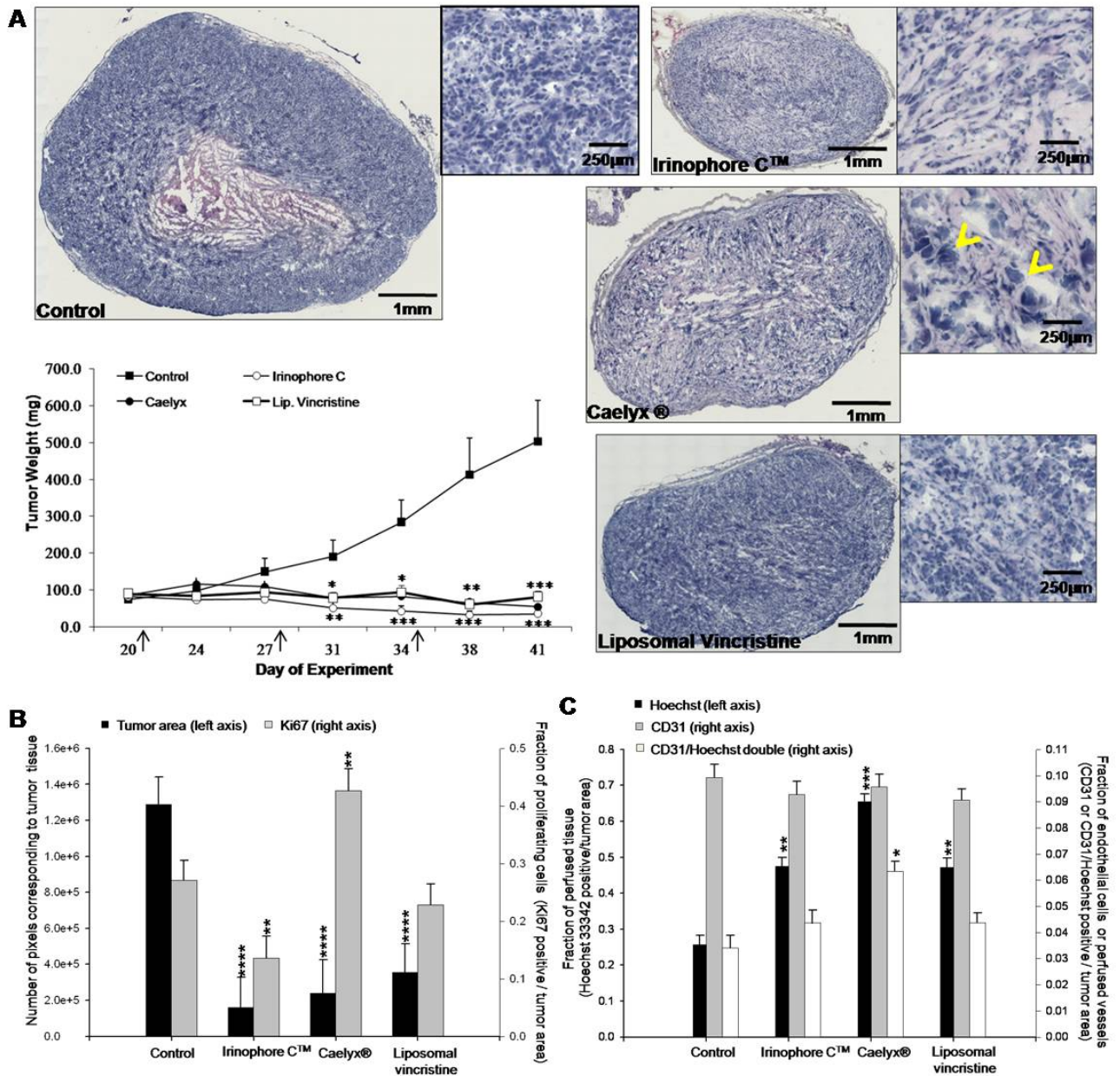


Figure 8: a) Representative H&E sections of tumours from each treatment group show the efficacy of the treatments in controlling tumour growth. Arrow heads indicate enlarged nuclei

associated with Caelyx<sup>®</sup> treatment. Tumour weights were calculated on the basis of caliper measurements (see material and methods); arrows indicate the treatment days. The IrC<sup>TM</sup> statistical significance is indicated by bottom stars, while Caelyx<sup>®</sup> and liposomal vincristine statistical significances are indicated by top stars such as \**p*-value ≤ 0.05; \*\**p*-value ≤ 0.01; \*\*\**p*-value ≤ 0.001. b) The area of viable tissue in tumour sections following treatment was expressed in number of pixels and correlated well with tumour volumes (■, left axis). The fraction of viable, actively proliferating cells (■, right axis) in the tumours was significantly decreased by IrC<sup>TM</sup>. Ki67 staining was also increased in Caelyx<sup>®</sup>-treated tumours. c) Hoechst perfusion in the tumours was increased significantly by IrC<sup>TM</sup> and Caelyx<sup>®</sup> treatment (■, left axis). The number of endothelial cells per unit area of viable tissue were unchanged by the treatments (■, right axis); however, the fraction of endothelial cells that were perfused (CD31 and Hoechst positive; □, right axis) was increased by treatment with Caelyx<sup>®</sup>. \**p*-value ≤ 0.05; \*\**p*-value ≤ 0.01; \*\*\**p*-value ≤ 0.001.

The effects of the selected liposomal drugs on tumour blood vessels were also evaluated. As summarized in Figure 8c, the CD31 staining (positive CD31 fraction) did not change significantly when comparing tumours from control animals to those from treated animals. Prior to sacrifice, animals were injected with Hoechst 33342 (Hoechst), a marker for tumour perfusion that was previously validated by correlation with  $K_{trans}$  measurements [225]. Total Hoechst staining in viable tissue (positive Hoechst fraction) was increased in the tumours obtained from treated animals ( $p < 0.01-0.001$ ; Figure 8c). CD31 and Hoechst co-staining was measured to provide an indication of changes in functional blood vessels [225]. The results, summarized in Figure 8c, indicate that the number of functional blood vessels increased significantly ( $p < 0.05$ ) in Caelyx<sup>®</sup> treated tumours while there were no significant changes observed in tumours from IrC<sup>TM</sup> and liposomal vincristine treated animals.

### **2.3.2 Irinophore C<sup>TM</sup>, Caelyx<sup>®</sup> and liposomal vincristine inhibit tumour growth and decrease Hoechst 33342 delivery in orthotopic GBM tumours**

Rag2M mice (n = 5 or 6) were inoculated with U251MG cells orthotopically (see Methods) and 21 days later the animals were treated i.v. (weekly for 3 weeks) with 25mg/kg IrC<sup>TM</sup>, 15mg/kg Caelyx<sup>®</sup> and 2mg/kg liposomal vincristine. Forty-two days after cell inoculation, animals were sacrificed and their brains harvested. A representative tissue section (Hematoxylin and Eosin; H&E) showing the site of tumour growth (dark blue) within the brain of treated animals is provided for each treatment group in Figure 9a. Inset images have been included to show that following treatments, the tumour nuclear density drops slightly when compared to untreated controls. The average total non-necrotic tumour tissue in the tumour area for each treatment group was quantified to provide a measure of efficacy (Figure 9b). There was a significant reduction in tumour area for all treatment groups when compared to controls ( $p < 0.0001$ ). In contrast to the results obtained with the s.c. glioma model, there was no significant change in Ki67 staining observed following treatment (Figure 9b).

**Figure 9: Orthotopic GBM tumours treated with Irinophore C<sup>TM</sup>, Caelyx<sup>®</sup> and liposomal vincristine are significantly smaller than untreated controls.**

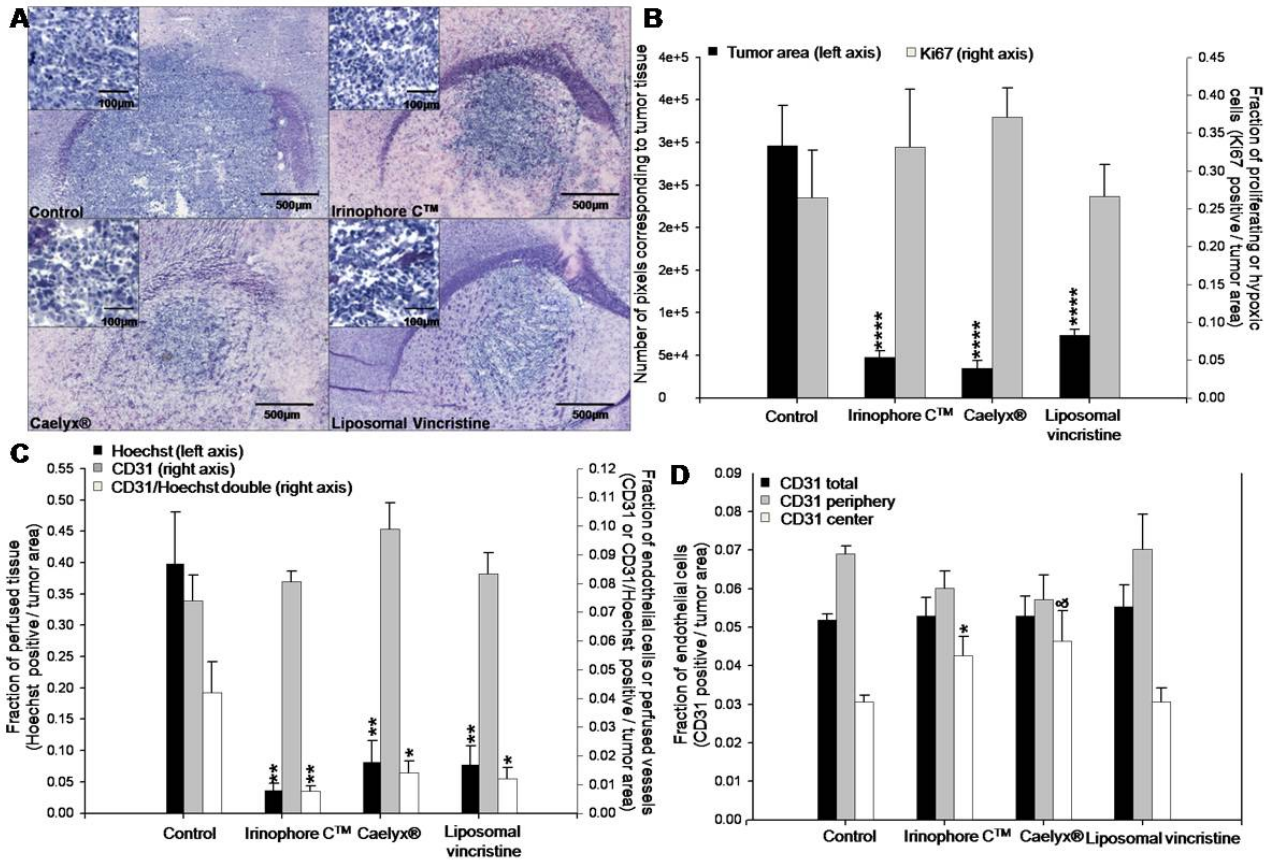


Figure 9: a) Representative H&E section images of brain sections from mice in each treatment group show that the area of tumour tissue (dark blue) from treated animals are smaller than untreated controls. b) Tumour areas were quantified in number of pixels, and used as a measure of treatment induced reduction of the tumour mass (■, left axis). No significant changes in proliferative activity (□, right axis) were observed. c) Hoechst 33342 staining was reduced significantly following treatments with either of the three liposomal agents (■, left axis). The total number of endothelial cells per unit area of viable tissue (□, right axis) was unchanged across all groups, but the fraction of endothelial cells that was co-stained with Hoechst was significantly reduced (□, right axis). d) The density of endothelial cells (positive CD31 pixels divided by periphery or center tumour area pixels) in the center of tumours treated with IrC<sup>TM</sup> was significantly higher compared to control tumours (□). No changes in endothelial cell density

were seen in the total tumour area (■) or the periphery of tumours (▣). \* $p$ -value  $\leq 0.05$ ; \*\* $p$ -value  $\leq 0.01$ ; \*\*\* $p$ -value  $\leq 0.001$ . Non-significant trends are indicated such as  $p$ -value = 0.067.

Prior to sacrifice, animals were also injected with Hoechst 33342. In tumours from untreated control mice, Hoechst staining was significantly greater in tumour tissue compared to matched regions of normal brain tissue (0.398 +/-0.083 and 0.023+/-0.015 pixels/unit area, respectively;  $p < 0.01$ ). This staining pattern has been described elsewhere [239, 240] and is consistent with the fact that Hoechst 33342 does not cross the blood-brain barrier. Interestingly, the data summarized in Figure 9c show that Hoechst staining in the orthotopic tumour tissue from animals treated with the liposomal drugs was significantly reduced ( $p < 0.01$ ) when compared to tumours from control animals. The decrease in Hoechst staining in orthotopic tumours from treated animals was in marked contrast to treatment-induced increases in Hoechst staining noted for tumours derived from the same cell line (U251MG) and grown subcutaneously (Figure 8c).

No significant changes in overall CD31 staining (pixels/unit area) (Figure 9c) were noted in the orthotopic tumours obtained from treated animals (compared to controls). However, CD31/Hoechst co-staining was significantly reduced ( $p < 0.01-0.05$ ) in tumours from treated animals when compared to control animals (Figure 9c). Moreover, treatment of orthotopic tumour bearing animals with IrC<sup>TM</sup> was associated with a significant ( $p < 0.05$ ) increase in CD31 staining in the center of tumours when compared to untreated tumours (Figure 9d;  $p < 0.05$ ).

### **2.3.3 Assessing vascular normalization in GBM tumours from animals treated with Irinophore C<sup>TM</sup>, Caelyx<sup>®</sup> or liposomal vincristine**

Several structural determinants, described as indicators of vascular normalization [241-243], were assessed in the orthotopic and s.c. GBM tumour models following treatment and these data were compared to tumours from untreated control animals. The parameters evaluated

included: (i) the extent of discontinuous basement membrane (collagen IV-free CD31 pixels) in the tumour tissue, (ii) the fraction of pericyte-uncovered blood vessels (NG2-free CD31 pixels) in the tumour tissue and (iii) the blood vessel diameter. Furthermore, the proportion of empty basement membrane sleeves (CD31-free collagen IV pixels) was evaluated as an indication of regression of pre-existing blood vessels [226]. Treatment-induced changes in these factors are summarized in Figure 3 (s.c. tumours) and 4 (orthotopic tumours).

In s.c. GBM tumours, the fraction of NG2-free blood vessels was reduced by 25% in tumours from animals treated with IrC<sup>TM</sup> ( $p < 0.05$ ; Figure 10a). Decreases in NG2-free blood vessels were also noted in tumours from animals treated with Caelyx<sup>®</sup> ( $p = 0.071$ ) or liposomal vincristine ( $p = 0.121$ ); but the effects were not considered significant. The number of collagen IV-free blood vessels was decreased in s.c. tumours from animals treated with IrC<sup>TM</sup> or Caelyx<sup>®</sup> (41-75% decrease;  $p < 0.05-0.001$ ; Figure 10a). Blood vessel diameter was also reduced (32%-51%;  $p < 0.001$ ) in s.c. tumours from all treatments groups. Finally, the number of empty basement membrane sleeves in tumours from IrC<sup>TM</sup> and Caelyx<sup>®</sup> treated animals was increased 3.4- to 3.8-fold following treatment ( $p < 0.0001$ ). A similar effect was noted for tumours from animals treated with liposomal vincristine, but the effect was not considered significant ( $p = 0.054$ ). Representative immunofluorescence micrographs highlighting the effects of IrC<sup>TM</sup> treatment on the tumour vasculature of s.c. U251MG tumours (Figure 10c) compared to untreated tumour (Figure 10b) are provided to support the results summarized in Figure 10a.

**Figure 10: Irinophore C<sup>TM</sup>, Caelyx<sup>®</sup> and liposomal vincristine treatments are associated with vascular normalization of the tumour vasculature in subcutaneous GBM tumours.**

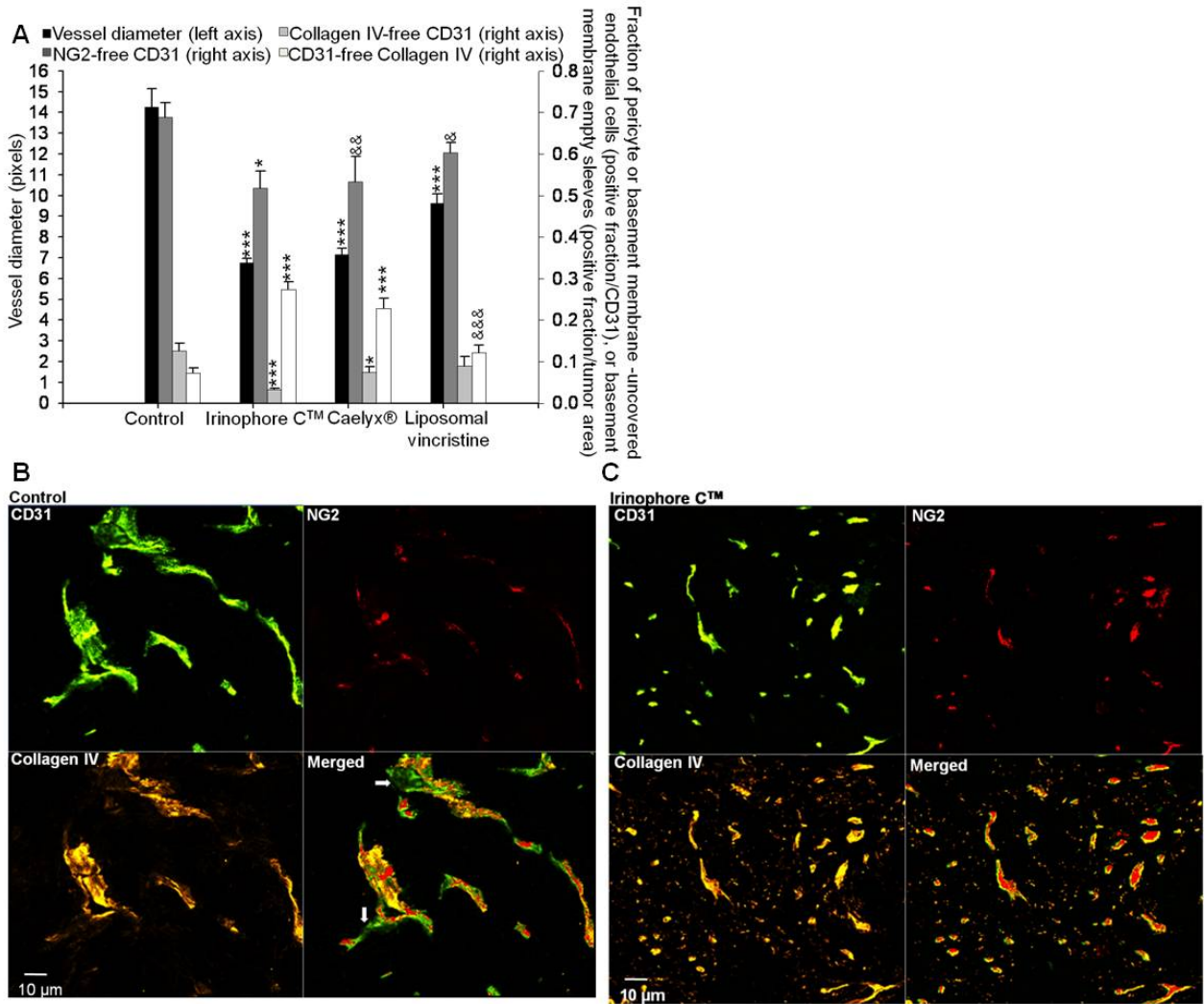


Figure 10: a) The diameters of tumour blood vessels were reduced significantly by all three treatments compared to control tumours (■, left axis). The fraction of NG2-free CD31 pixels (■, right axis), collagen IV-free CD31 pixels (■, right axis) were reduced in IrC<sup>TM</sup> treated tumours indicating that fewer immature vessels are present following treatments. The proportion of empty basement membranes (CD31 free-collagen IV staining; □, right axis) in the viable tissue was also reduced by all liposomal treatments. b and c) Representative and merged images of CD31, Collagen IV and NG2 staining for control tumours (b) and tumours from IrC<sup>TM</sup> treated mice (c). Basement membrane (collagen IV; yellow)-uncovered blood vessels (CD31; green) can be seen in control tumor section (arrows). A reduction in blood vessel diameter and an increase in

*basement membrane coverage of blood vessels following treatment can be seen. Following IrC<sup>TM</sup> treatment, more pericytes are present (NG2; red) and more endothelial cells are associated with the pericytes (merged image, green and red). Treatment with IrC<sup>TM</sup> also results in an increase in empty basement membrane sleeves (i.e. CD31 free-collagen IV; yellow). The entire image represents non-necrotic and viable tissue. \*p-value ≤ 0.05; \*\*p-value ≤ 0.01; \*\*\*p-value ≤ 0.001; \*\*\*\*p-value ≤ 0.0001. Non-significant trends are indicated such as &p-value = 0.121; &&p-value = 0.071; &&&p-value = 0.054.*

Similar results were obtained when evaluating the orthotopic U251MG tumours obtained from treated animals compared to controls. In addition, histological assessments of brain tissue surrounding the tumour allowed comparisons between vessels in the tumour vs. normal brain tissue. The fraction of collagen IV-free blood vessels in normal brain (0.049±0.015) was 69% lower (p<0.05) than that observed in tumour tissue from control untreated animals (0.160±0.033), indicating that the organization of the basement membrane architecture is decreased in the tumour compared to normal tissue. Tumours from animals treated with IrC<sup>TM</sup> showed a significant 71% (p<0.05) decrease in the fraction of collagen IV-free blood vessels when compared to tumours from control animals (Figure 11a). A similar effect was observed in tumours from animals treated with Caelyx<sup>®</sup>, but the effect was not considered significant (p=0.064). In normal brain tissue, blood vessel diameters were 54% smaller (4.9±0.5 pixels; p<0.0011) than blood vessel diameters observed in orthotopic tumour tissue obtained from untreated animals (10.9±0.6 pixels). Orthotopic tumours from animals treated with IrC<sup>TM</sup> or Caelyx<sup>®</sup> exhibited a reduction in blood vessels diameters of 39% (p<0.01; Figure 11a) when compared to control tumours. In contrast to results obtained with the s.c. tumours of treated animals, the level of empty basement membrane sleeves (Collagen IV-free CD31 staining) in the orthotopic tumours did not change following treatment (Figure 11a). It should be noted that the level of empty basement membrane sleeves in the normal brain tissue (0.035±0.009) was

found to be similar to that measured in orthotopic tumour tissue from untreated animals (0.047 $\pm$ 0.009). Treatments did not induce significant changes in fraction of NG2-free blood vessels (Figure 11a). The fraction of NG2-free vessels in the normal brain could not be evaluated as NG2 proteoglycan was found at the surface of polydendrocytes, a subpopulation of glial cells found in the brain [244]. Representative immunofluorescence micrographs illustrating the effects of IrC<sup>TM</sup> treatment on the orthotopic tumour vasculature are provided in Figure 11b. Normal brain tissue sections are shown in Figure 11c for comparison.

**Figure 11: Irinophore C<sup>TM</sup>, Caelyx<sup>®</sup> and liposomal vincristine treatments are associated with vascular normalization of the tumour vasculature in orthotopic GBM tumours.**

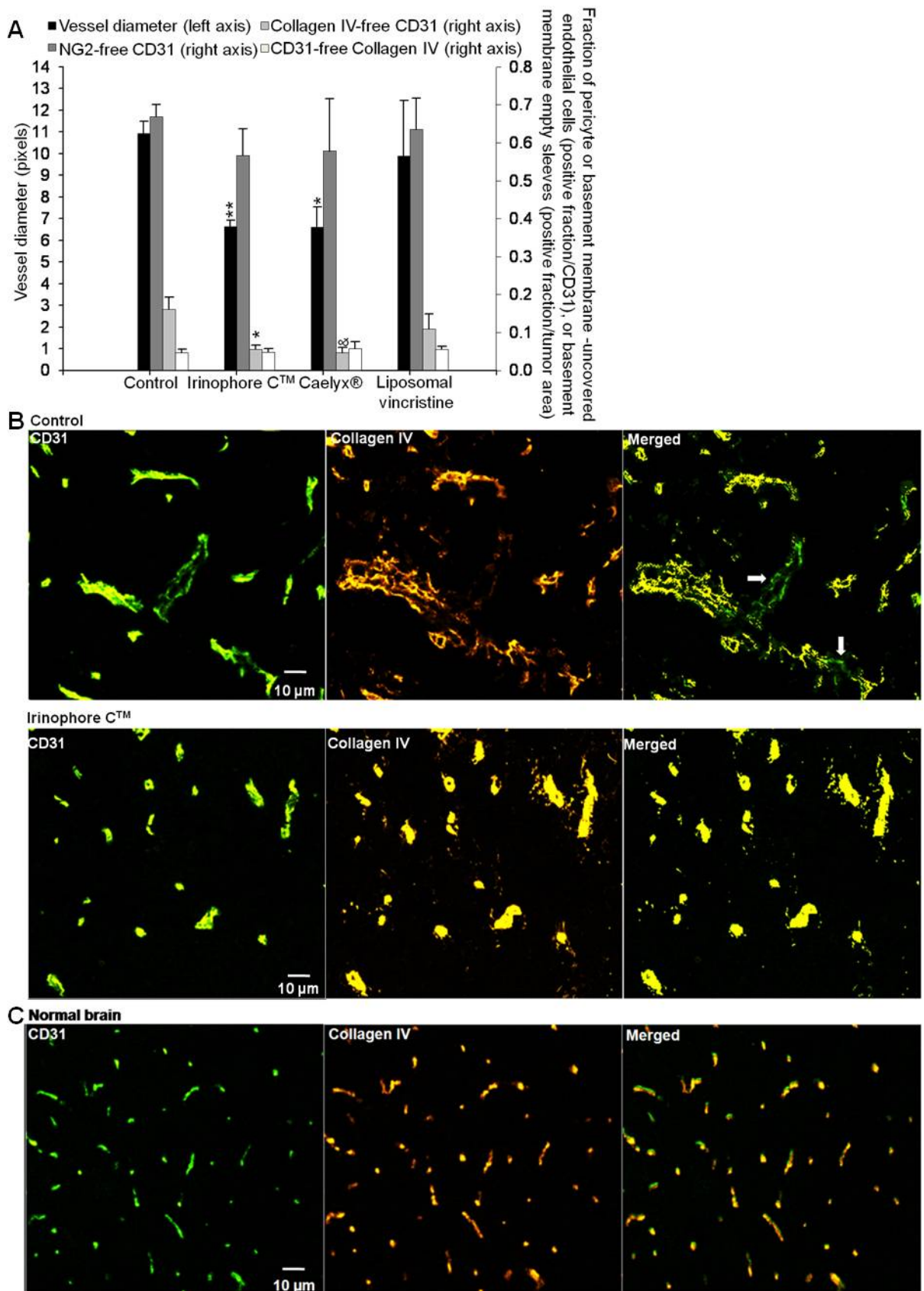


Figure 11: a) Vessel diameters (■, left axis) and the fraction of collagen IV-free CD31 pixels (■, right axis) in orthotopic GBM tumours were reduced by IrC<sup>TM</sup> and Caelyx<sup>®</sup>. However, no changes were seen in the fraction of NG2-free CD31 positive endothelial cells (■, right axis) or Collagen IV-free CD31 positive endothelial cells (□, right axis). b) Representative images from untreated and IrC<sup>TM</sup> treated tumours; similar images for normal brain tissue are shown for comparison. (c) Blood vessel diameters (CD31; green) are reduced by IrC<sup>TM</sup> treatment. The fraction of basement membrane (collagen IV; yellow)-uncovered vessels (CD31; green) (see arrows in control tumor section) is reduced by treatment with IrC<sup>TM</sup>. The entire image represents non-necrotic and viable tissue. \**p*-value ≤ 0.05; \*\**p*-value ≤ 0.01; Non-significant trends are indicated such as &*p*-value = 0.064.

#### 2.3.4 Magnetic resonance imaging–measured changes in vascular permeability/flow ( $K_{trans}$ )

The results summarized thus far are consistent with the idea that following treatment of animals bearing GBM tumours with lipid-based nanopharmaceutical formulations of vincristine, doxorubicin and irinotecan, there is a “normalization” of blood vessel structure. When considering these effects along with the antitumour activity, the greatest effects were observed following treatment with IrC<sup>TM</sup>. In order to confirm the idea of an IrC<sup>TM</sup>-induced vascular normalization, non-invasive magnetic resonance imaging was used to assess  $K_{trans}$ , a volume transfer constant of a solute between the blood vessels and extra-cellular tissue compartment, in orthotopic tumours grown in untreated and IrC<sup>TM</sup> treated mice. The median values of  $K_{trans}$  for the tumours within the control and treated groups have been summarized Figure 12. The results demonstrate that the median  $K_{trans}$  value in untreated tumours was ~7 times greater than in treated tumours (0.0232 and 0.0034 ml/g/min, respectively, *p*<0.05). It should be noted that the values for  $K_{trans}$  in tumours from untreated animals were more variable when compared to the tumours from treated mice (s.e.m ±0.010 and ±0.0003, respectively).

**Figure 12: Irinophore C<sup>TM</sup> reduced  $K_{trans}$  measures compared to values obtained from control orthotopic tumours.**

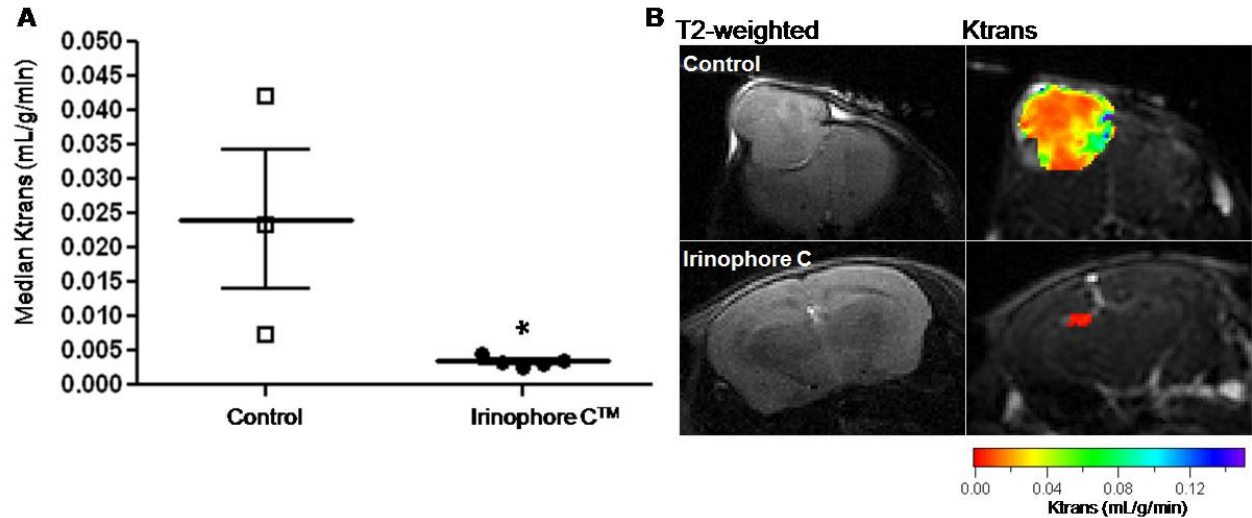


Figure 12: a) Individual and median (thick line)  $K_{trans}$  values for untreated and IrC<sup>TM</sup>-treated orthotopic tumours with standard error of the mean (thin line). \* $p$ -value  $\leq 0.05$ . b) Representative images obtained from a control or IrC<sup>TM</sup>-treated animal showing  $K_{trans}$  values throughout the tumor. T2-weighted images are provided as an anatomical reference.

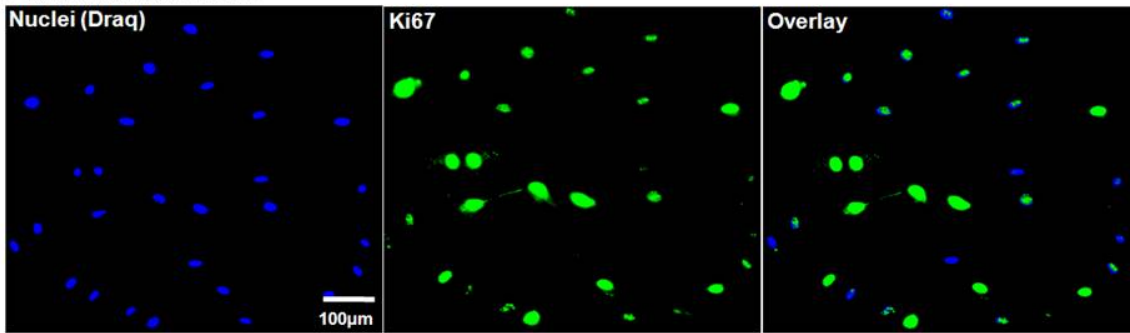
### 2.3.5 *In vitro* studies on endothelial cells mimicking the extended drug exposure achieved when using liposomal drug delivery formulations

In an attempt to better understand the effects of liposomal formulations used here on tumour vasculature, an *in vitro* endothelial cell assay was used to assess the impact of extended drug exposure. It is well established that these liposomal formulations engender significant increases in plasma drug concentrations over extended time periods following intravenous administration [190, 192]. Thus, an extended drug exposure protocol was used to assess the effects of drugs in a model representative of the endothelial cells forming vessels in the subcutaneous or brain microenvironment. Dermal Human MicroVascular Endothelial Cells (d-HMVEC) and Human Brain Microvascular Endothelial Cells (HBMEC) were cultured under proliferative or non-proliferative conditions and exposed to the indicated drugs for 7 days. As illustrated in Figure 13a, the total nuclei count and the number of nuclei expressing the Ki67

proliferation marker were quantified using high content screening (Incell analyzer 1000) to discriminate between cytotoxic (reduction in total number of nuclei) and cell proliferation inhibitory effects (reduction in Ki67 expressing fraction). Under proliferative conditions, the nuclei count for the endothelial cell lines used increased up to 3-fold over the 7 day time period. The Ki67 expressing nuclei fraction ranged from 42 to 68% over this time frame (Figure 13a and b). Under non-proliferative conditions, the nuclei count for cell lines (d-HMVEC and HBMEC) remained unchanged from day 1 to day 7, and the Ki67 expressing nuclei fraction ranged from 7 to 31% (Figure 13a and b).

**Figure 13: d-HMVEC and HBMEC were plated under proliferative conditions or non-proliferative conditions.**

**A Proliferative conditions**



**Non-proliferative conditions**



**B**

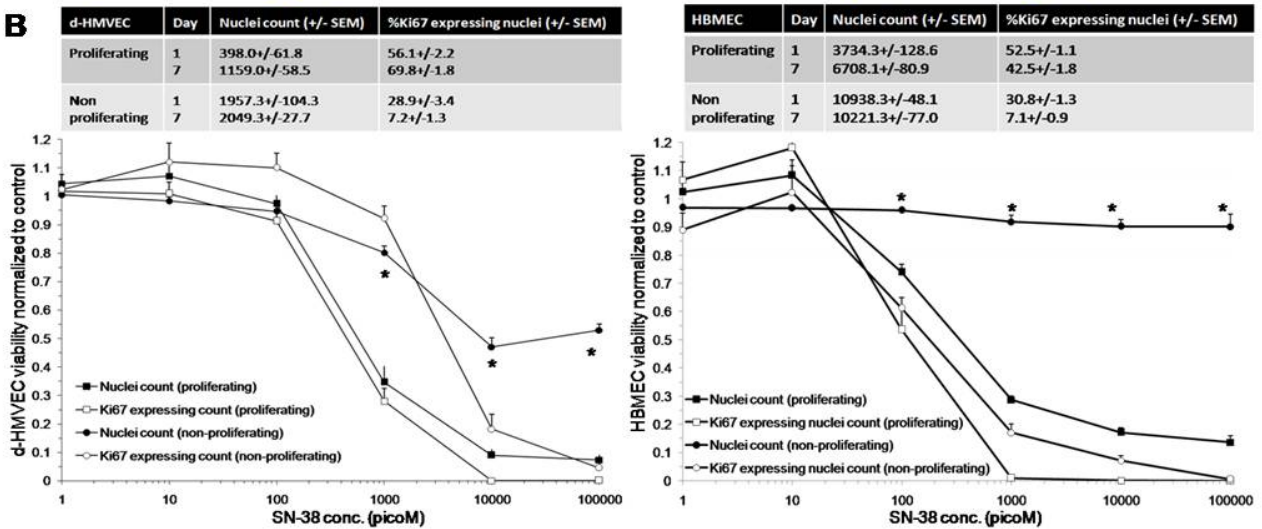


Figure 13: a) Representative composite colour images of d-HMVEC cells are shown; Draq (blue; nuclei), and Ki67 (green). Under proliferative conditions, the number of nuclei and Ki67 positive staining are similar; whereas under non-proliferative conditions, the number of nuclei with positive Ki67 staining is much lower. b) Total nuclei count and Ki67 expressing nuclei fraction of untreated cells for both cell lines under proliferative and non-proliferative conditions on day 1 and day 7 after plating (3 independent experiments; 3-21 replicates per experiment).

*Cells were exposed for 144hrs to increasing drug concentrations (1-100,000 picoM). Total nuclei count as well as nuclei expressing Ki67 expressing counts were normalized to counts obtained from control untreated cells. Representative data for d-HMVEC and HBMEC exposed to SN-38 is shown (3 independent experiments; 3 replicates per experiment +/-SEM). \*p-value < 0.0001 between total nuclei count of proliferative and non-proliferative cells.*

The activity of the drugs against the cells maintained under the two conditions was compared to assess the selectivity of the drugs for proliferating endothelial cells compared to non-proliferating endothelial cells. For all drugs used in this study, the dose-response curves for Ki67 expressing nuclei of proliferating cells matched the ones for the total nuclei count, suggesting that the drugs tested were cytotoxic rather than anti-proliferative. Representative dose-response curves for d-HMVECs and HBMECs exposed to SN-38, the active metabolite of irinotecan, under proliferative and non-proliferative conditions are shown in Figure 13b. The data indicate that SN-38 is significantly more active against proliferating endothelial cells than non-proliferating cells. In an effort to highlight differences in drug activity under proliferating and non-proliferating conditions, drug concentrations decreasing d-HMVEC total nuclei count by 20% (fraction affected:  $F_a = 0.2$ ), 50% ( $F_a = 0.5$ ), 75% ( $F_a = 0.75$ ) and 90% ( $F_a = 0.9$ ) were calculated from the dose-response curves and compared for both proliferative and non-proliferative cells (Figure 14). For example, results obtained at  $F_a=0.75$  indicate that the greatest differential effects were observed when using SN-38 and vincristine, where the drug dose required to achieve a 75% decrease in nuclei count under proliferative conditions were at least 100- and 90.9-times lower, respectively, than the drug dose required to achieve the same effect level under non-proliferation conditions. These effects were much greater than those seen using the positive control compounds docetaxel and paclitaxel. In contrast, there was little or no difference in the concentrations of irinotecan or doxorubicin required to achieve an  $F_a$  of 0.75 under proliferating and non-proliferating conditions. Similar results were obtained when using

HBMECs (Figure 15). It should be noted that the drug doses required to achieve an Fa value of 0.5 for SN-38 and vincristine was 45 to 5000 times greater for U251MG glioblastoma cells when compared to the proliferating endothelial cells, and the increased specificity for proliferating endothelial cells has been noted previously for paclitaxel and SN-38 when compared against human colorectal and breast cancer cells [245, 246].

**Figure 14: Proliferating HMVEC cells are more sensitive to SN-38, docetaxel, paclitaxel, doxorubicin and vincristine than non-proliferating cells.**

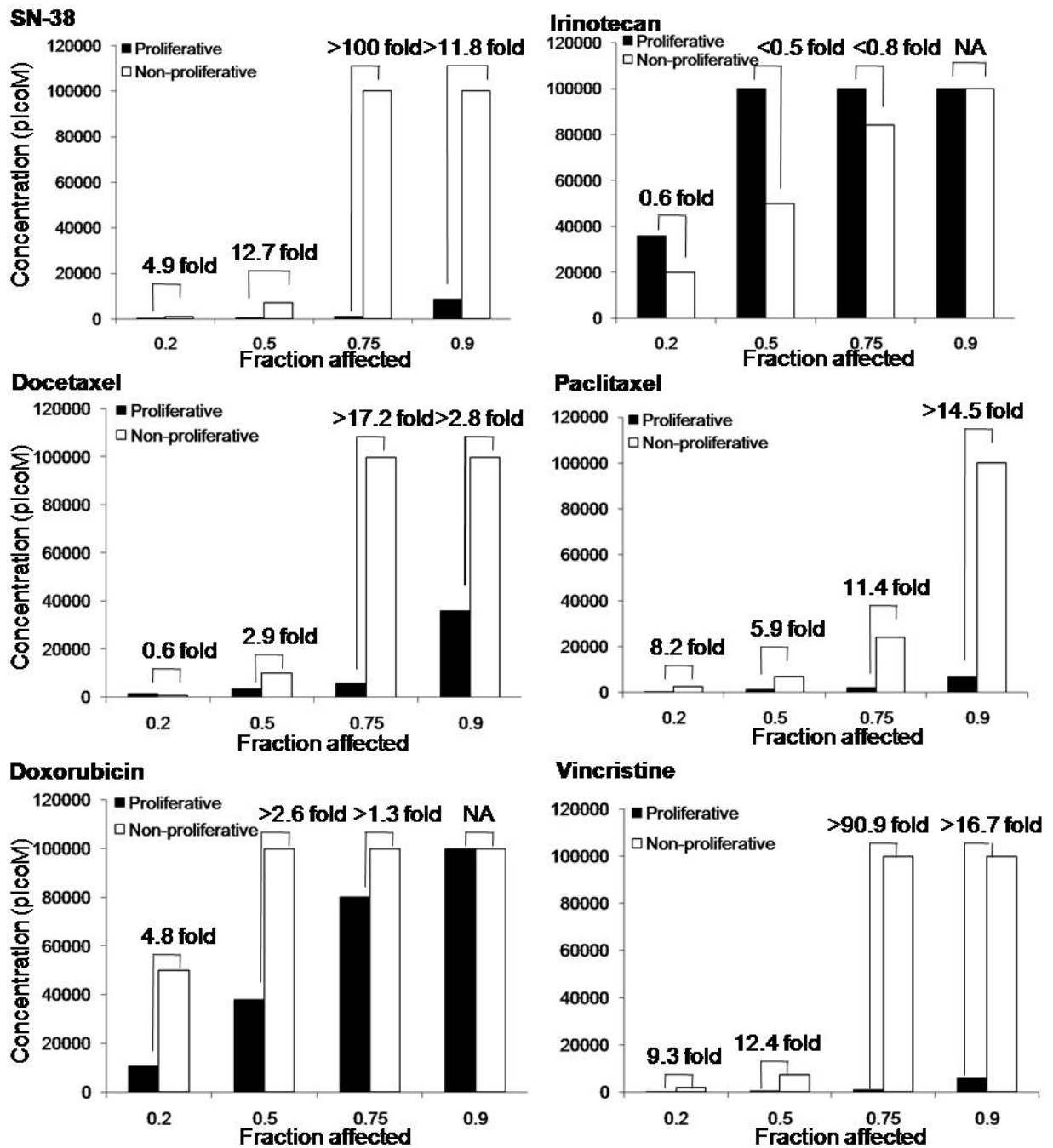


*Figure 14: Concentrations at which a Fa of 0.2-0.9 was observed in d-HMVEC total nuclei count for both proliferative and non-proliferative conditions. The fold difference in drug concentration required to achieve the specified Fa is indicated above each pair of columns.*

**Figure 15: Proliferating HBMEC cells are more sensitive to SN-38, docetaxel, paclitaxel, doxorubicin and vincristine than non-proliferating cells.**

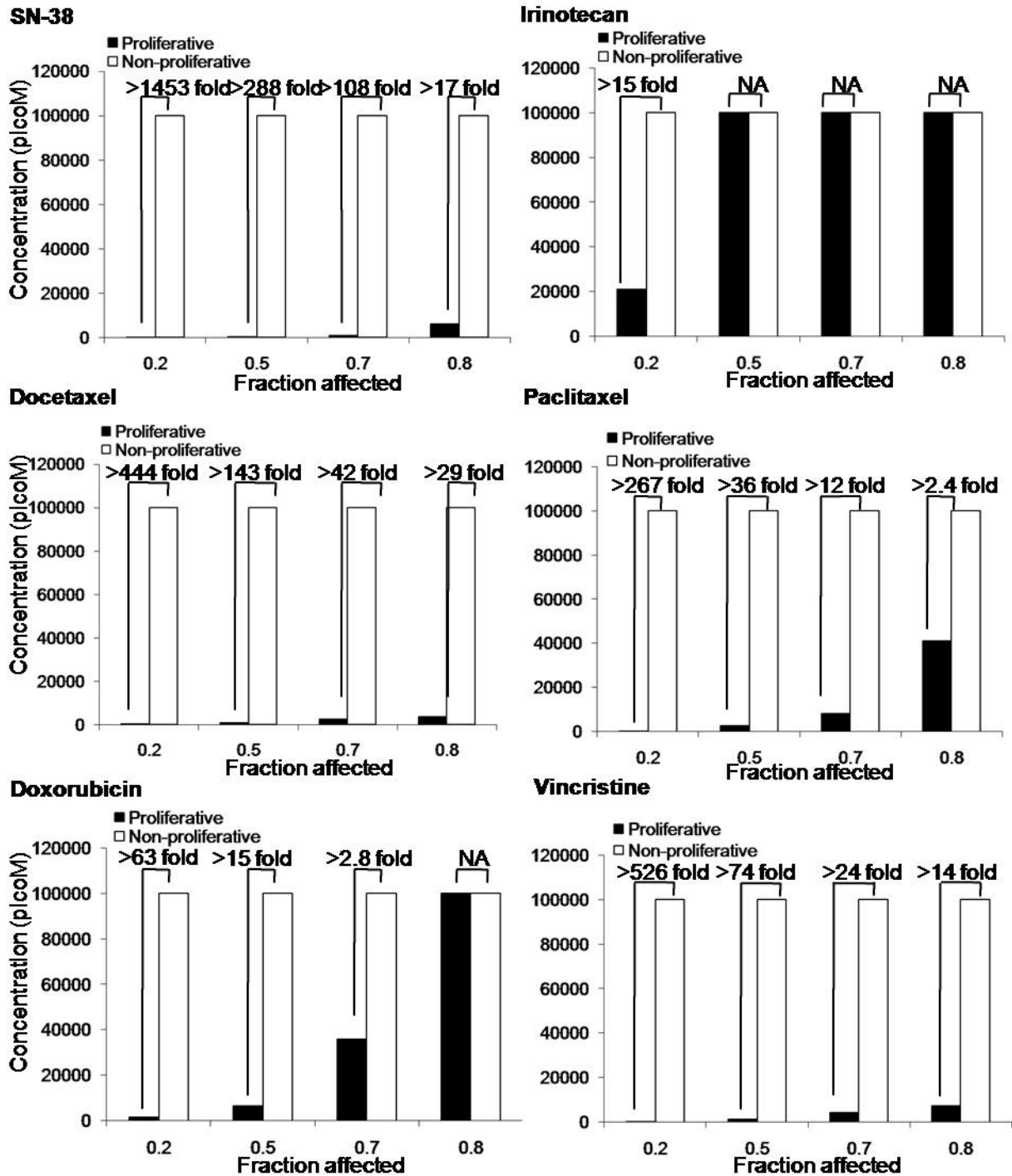


*Figure 15: Concentrations at which a Fa of 0.2-0.9 was observed in HBMEC total nuclei count for both proliferative and non-proliferative conditions. The fold difference in drug concentration required to achieve the specified Fa is indicated above each pair of columns.*

## 2.4 Discussion

Studies over the last few decades have established that liposomal formulations of selected antineoplastic agents can be more effective than the same drug administered in free form. Liposomal formulations of anticancer drugs are known to have long circulation half-lives *in vivo*, and release the drug slowly over time [190, 192]. Thus, the pharmacological properties of a drug given in its free form (e.g. via bolus injection or slow infusion) is changed dramatically by encapsulation in liposomes. As a result, one might anticipate that the use of liposomal drugs will expose tumours to drugs for extended periods of time when compared to treatment with the free drug. This, of course, is well established in the literature and has been explained on the basis of the enhanced permeability and retention (EPR) effect known to promote accumulation of intravenously administered liposomal drug formulations in tumours [182]. What is often not considered in studies with liposomal formulations is that these formulations constantly release the associated drug while in the circulation compartment, thereby extending the presence of the drug in the plasma compartment. This study tries to address whether part of the treatment benefits could be attributed to direct effects of the free drug (available in the blood compartment) on tumour vascular endothelial cells. The fact that these drug formulations are active against proliferating vasculature was anticipated, but not demonstrated to date. Liposomes drug formulations are known to accumulate and release drugs in close proximity to tumour blood vessels [198, 230]. More intriguing, however, is the possibility that exposing the tumour vasculature to low concentrations of drug for extended periods may produce effects that are comparable to the vascular normalization effects described in the context of anti-angiogenic therapy [226, 227] as discussed below.

In the present study, it is demonstrated that IrC<sup>TM</sup>, Caelyx<sup>®</sup> and liposomal vincristine are effective against GBM grown subcutaneously or orthotopically (in the brain). The tumour masses in treated animals were significantly smaller compared to control ( $p < 0.01$ ; Figure 8 and

9), indicating that the liposomal drugs used in this study are potent against GBM, regardless of the site of tumour growth. Analysis of the tumour tissue, and in particular the vascular morphology, also indicates that treatments affected the tumour vasculature to various degrees. Overall, IrC<sup>TM</sup> impacted the vasculature to a greater extent than the other formulations, and generated tumours with blood vessels that were morphologically more mature. In the subcutaneous model, IrC<sup>TM</sup> restored the basement membrane architecture, increased the pericyte coverage and reduced blood vessel diameters. The data suggest a restoration of the vessel architecture to a more normal state. In the more clinically relevant orthotopic model, IrC<sup>TM</sup> treatment restored the basement membrane architecture and reduced blood vessel diameters of the tumour vasculature, again suggesting a restoration of the vessel architecture to a more normal state. IrC<sup>TM</sup> treatment also increased the quantity of vessel staining in the center of tumours, suggesting a more homogeneous distribution of blood across the entire tumour. Further, IrC<sup>TM</sup> reduced  $K_{trans}$  values calculated from Dynamic Contrast Enhanced (DCE) -MRI studies significantly. Based on changes in vessel morphological appearance, the drop in  $K_{trans}$  values was interpreted as a decrease in vessel permeability [247] and is consistent with the suggestion that IrC<sup>TM</sup> treatment improved vascular function in the tumour. The larger variability in  $K_{trans}$  values determined in tumours from control animals reflects the random nature of chaotic and leaky blood vessels in individual tumours [248]. It had already been established in s.c. tumours that Hoechst 33342 could be used as a marker for tumour vessel function by validation with  $K_{trans}$  measurements [225], but this had not been done for the orthotopic GBM tumour described here. It is shown here that the observed reduction in Hoechst 33342 staining after treatment while total CD31 staining remained constant correlates with a reduction in  $K_{trans}$  measures. Taken together, these observations strongly suggest an improvement in vascular function. The tumour blood vessels in tumours from animals treated with IrC<sup>TM</sup> behave more like vessels in the normal brain where the blood-brain barrier is intact.

The concept of ‘blood vessel normalization’ was first postulated in the 70s [249] and more recently, the clinical potential of vascular normalization has been described [226, 227]. As with most solid tumours, the microvasculature of gliomas is characterized by tortuous and fenestrated vessels with diameters that are larger than normal [250] and discontinuous basement membrane which rarely encloses pericytes [50] (Figure 16). In glioma [241, 242, 251], antiangiogenic therapies can stop the growth of tumour vessels, prune immature and inefficient tumour vessels and normalize surviving vasculature by increasing the fraction of pericyte-covered vessels, restoring the abnormally thick and irregular basement membrane and reducing the high vascular permeability of these vessels [226, 227] (Figure 16). In glioblastoma patients, a “vascular normalization index” was defined by changes in vascular permeability ( $K_{trans}$  values), microvessel volume and circulating collagen IV. It was found that this index was closely associated with overall survival and progression-free survival in response to Cediranib, a pan-VEGFR inhibitor [251]. Pre-clinically, the delivery of temozolomide in an intracerebral model of glioma increased after treatment with the angiogenesis inhibitor SU5416. This drug restored capillary architecture and decreased interstitial fluid pressure [252]. Such studies offer strong evidence that the tumour vasculature in GBM is a valid target, and that therapies which ‘normalize’ tumour vasculature may improve the delivery of a second drug at some point in the treatment regimen.

**Figure 16: Proposed role of vessel normalization in the response of tumors to antiangiogenic therapy.**

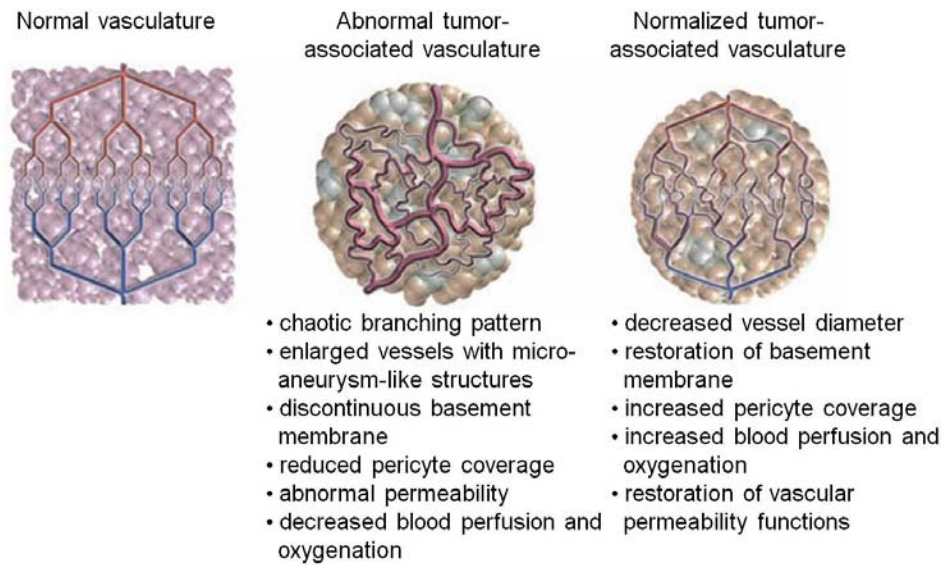


*Figure 16: Tumor vasculature is structurally and functionally abnormal. It is proposed that vascular normalization improves both the structure and the function of tumor vessels. Adapted from [248].*

The studies described here, together with an earlier publication [225], offer strong evidence that liposomal formulations of selected drugs, and especially IrC<sup>TM</sup>, induce a normalization of the tumour vasculature. In this study, collagen IV and NG2 were used as markers for basement membrane and pericytes, respectively. However, there is no consensus in the field for a definitive marker of these parameters. Other markers used to evaluate basement membranes include nidogen or laminin, and desmin or  $\alpha$ -smooth muscle actin for pericytes [226, 243]. These caveats notwithstanding, the morphological changes observed were associated with changes in Hoechst 33342 uptake in the tumour and when using this parameter, remarkably different results were obtained depending on the site of tumour growth (subcutaneous vs orthotopic). In the subcutaneous model, the liposomal treatments increased the amount of Hoechst 33342 staining in the tumour tissue (Figure 8c), while in the orthotopic tumours Hoechst 33342 staining was reduced (Figure 9c). As noted above, treatment effects were similar if blood

vessel morphology parameters were used as a measured endpoint. While initially surprising, the Hoechst 33342 uptake data may actually be consistent with restoration of the blood-brain barrier, which is more impermeable to Hoechst 33342. It is well established that Hoechst 33342 is a p-glycoprotein substrate [253]. It does not accumulate in normal brain tissue because it cannot cross the blood brain barrier, but it is present in untreated orthotopic brain tumours which exhibit leakier blood vessels. This idea was further confirmed by  $K_{\text{trans}}$  measurements, which strongly suggested a vasculature normalization induced by IrC<sup>TM</sup>. This interpretation suggests that Hoechst 33342 is not an appropriate marker for tumour *perfusion* in orthotopic glioma models, as it was previously used in a s.c. tumour model [225]. It does, however, function as a *permeability* marker for perfused tumour associated blood vessels, which is reduced upon normalization. The impact of vascular normalization on tumour perfusion in orthotopic GBM tumours could not be assessed in the present study because MRI  $K_{\text{trans}}$  data and Hoechst 33342 staining data are not direct measures of perfusion in the brain tumour. However, data obtained in the subcutaneous model suggest that treatment with liposomal drugs does not reduce tumour perfusion, as measured by CD31/Hoechst 33342 double staining, and may even increase it, as suggested by data obtained from Caelyx®-treated s.c. tumours. Studies to measure the delivery of a second drug that can cross the BBB in liposomal drug-treated tumours are underway and will provide an indication of the impact of vascular normalization on vessel perfusion in the orthotopic model.

The idea that liposomal formulations of anti-cancer drugs, in addition to having a direct cytotoxic effect on the tumour cells, may also act through anti-angiogenic mechanisms is intriguing. It seems reasonable to suggest that the extended drug release characteristics associated with the liposomal drug formulations used in this study [190, 192] may have effects on blood vessels in a manner similar to metronomic dosing schedules – i.e. frequent, low dose administration of drugs with no prolonged drug-free breaks [254]. Metronomic dosing is now

acknowledged to act specifically on the proliferating endothelial cells of tumour blood vessels [255] and was more recently shown to improve tumour perfusion and to decrease hypoxia in a pancreatic tumour model [256]. To examine this hypothesis, an *in vitro* assay was used to evaluate the activity of irinotecan, doxorubicin and vincristine (the drugs encapsulated by liposome examined in this study) against proliferating endothelial cells. The assay was adapted from one developed by Bocci et al. to examine the effects of metronomic drug exposure against endothelial cells [246]. Previous reports suggest that docetaxel and paclitaxel have potent activity against endothelial cells in an *in vitro* metronomic dosing regimen [245, 246, 257], so these drugs were included in the assay as positive controls. The effects of SN-38 were also evaluated in the assay because SN-38 is a more active metabolite of irinotecan generated by tissue and plasma carboxylesterases *in vivo* [258, 259]. Further it has already been established that following treatment with IrC<sup>TM</sup>, high levels of SN-38 are maintained in the plasma compartment for extended time periods [190]. SN-38 levels may play an important role in the anti-cancer activity of IrC<sup>TM</sup>.

The *in vitro* metronomic dosing assay presented in Figures 14 and 15 suggested that vincristine and SN-38, like the taxanes (docetaxel or paclitaxel), are highly active against proliferating endothelial cells (Figure 13a-b). In contrast, free irinotecan has little specificity for proliferating endothelial cells over non-proliferating cells *in vitro*. The data for free vincristine corroborate the effects on tumour vasculature seen with the liposomal form of the drug used here, while the results obtained with free irinotecan, which is not specific for proliferating endothelial cells, is actually contradictory. IrC<sup>TM</sup> was the most active of the three liposomal formulations used. The results in Figures 14 and 15 would strongly suggest that the activity of IrC<sup>TM</sup> may be explained by the high plasma levels of SN-38 generated following administration of IrC<sup>TM</sup> [189, 190]. Thus it can be concluded from the studies presented here that the active

metabolite of irinotecan, SN-38, may be the agent promoting vascular normalization in the models used here.

Interestingly, the *in vitro* assay suggests that doxorubicin should have little specificity on proliferating endothelial cells, yet i.v. administration of Caelyx<sup>®</sup> resulted in effects on the tumour vasculature that were comparable to those seen following administration of IrC<sup>™</sup>. The reasons for this are unclear at present but may be related to disruptions in the production of hypoxia-induced VEGF caused by doxorubicin [260]. Previous studies completed using the rat intracranial 9L tumour model treated with a formulation of doxorubicin comparable to that used here [198] showed the presence of vascular breakdown and hemorrhage 48 hours after treatment. In contrast, the results summarized here were obtained using tumours harvested one week after the final treatment; thus the data here may reflect late effects on tumour vasculature. Further, 9L is a gliosarcoma cell line which exhibits a slower doubling time (34.9hrs [261]) than the U251MG glioblastoma cell line (20.9hrs) used in this study. The resulting 9L tumours are also histologically distinct [261] when compared to the U251MG model. These differences will likely impact how tumours respond to agents capable of promoting vascular normalization. Studies assessing how vascular functions change in relationship to tumour growth rate are currently being completed.

In aggregate, data from this study indicate that liposomal formulations of irinotecan, doxorubicin and vincristine exert anti-angiogenic effects, as measured by endpoints assessing increases in mature blood vessels and improved vascular function. The normalization of tumour vessels appears to be transient in nature [248] but may create a window where blood flow is improved, leading to an opportunity to improve drug delivery for other drugs. The fact that all three formulations were therapeutically active in the orthotopic model suggests that vascular normalization did not prevent the drugs from accessing tumour cells, despite the fact that our interpretation of data obtained from Hoechst 33342 suggests a reduction in vessel permeability.

Data that will be presented in chapter 3 show that once irinotecan is released from the lipid carrier, the drug and its active metabolite SN-38 are capable of crossing a normal blood-brain barrier [262]. Vincristine was also shown to be able to cross a normal blood-brain barrier [263]. Thus, it can be speculated that vascular normalization would increase the delivery of drug that has dissociated from the liposome across the tumour vasculature, allowing higher levels of drug to diffuse into a greater volume of tumour tissue. Studies assessing the consequences of liposomal drug-induced vascular normalization on the delivery of a second drug capable of crossing the blood-brain barrier will provide important information regarding the impact of tumour vessel permeability on drug delivery. In the case of GBM, an obvious choice of such a drug is temozolomide. Pre-clinical studies to assess the impact of IrC<sup>TM</sup> treatments on the delivery of temozolomide are currently on-going.

## **2.5 Acknowledgements**

The research described in this original paper was supported by grant funding from the Canadian Institutes of Health Research, the Cancer Research Society, Inc. and the National Cancer Institute of Canada (now the Canadian Cancer Society Research Institute). DTY was supported by Rethink Breast Cancer. The authors would like to acknowledge the staff and management personnel of the Animal Research Center at the BC Cancer Agency.

## **Chapter 3: Irinophore C<sup>TM</sup>, a lipid-based nanoparticulate formulation of irinotecan, is more effective than free irinotecan when used to treat an orthotopic glioblastoma model**

### **3.1 Introduction**

<sup>3</sup>As discussed in the introduction of this thesis, recurrence after treatment is typical in patients with GBM [4]. However, some progress is being made in defining better treatment options for GBM patients. The chemotherapeutic agent temozolomide (TMZ) offers modest therapeutic benefits when used as a single agent and is proving to be more useful when combined with other therapies. TMZ administered with concurrent radiation, for example, improves median free survival time by about 2.5 months and increases 2 year survival times from 10.9% to 27.2% [4, 14] when compared to radiation alone. However, even with this combination, a majority of patients relapse.

Other combination treatment strategies are now being evaluated as potential treatments for patients with recurrent GBM. One such approach assessed bevacizumab, a VEGF specific monoclonal antibody, in combination with irinotecan and demonstrated meaningful improvements in progression free survival and 2 year survival times [34]. The responses were sufficient for the FDA to support accelerated approval for bevacizumab for recurrent GBM patients [264] and the National Comprehensive Cancer Network now recommends this combination for GBM treatment [38]. Despite clinical evidence demonstrating the activity of irinotecan alone or in combination with other drugs [34-37, 265], the role of irinotecan in the management of GBM patients remains unclear. Questions regarding its use arose from clinical observations suggesting that administration of high doses of irinotecan can induce a cholinergic

---

<sup>3</sup>This chapter was submitted for publication in March 2011: M. Verreault, D. Strutt, D. Masin, M. Anantha, D. Waterhouse, D.T. Yapp and M.B. Bally. Irinophore C<sup>TM</sup>, a lipid-based nanoparticulate formulation of irinotecan, is more effective than free irinotecan when used to treat an orthotopic glioblastoma model. *Accepted with revisions by Journal of Controlled Release in May 2011.*

syndrome and is associated with other adverse side-effects including vomiting, diarrhea, diaphoresis and cramping abdominal pain. These toxicities limit dosing of this drug in patients who already have a poor health status [266].

Our research has established that Irinophore C<sup>TM</sup> (IrC<sup>TM</sup>), a lipid-based nanoparticulate formulation of irinotecan, exhibits improved anti-tumour efficacy (compared to irinotecan) in a panel of human tumours grown subcutaneously [189, 190]. Improved outcomes are due, in part, to formulation-mediated increases in plasma and tumour levels of the active (lactone) form of irinotecan [18] as well as maintaining significant plasma levels of SN-38 for extended time periods. SN-38 is an active metabolite of irinotecan and is 100- to 1000-fold more potent than the parent drug [259]. Moreover, as demonstrated in chapter 2, the formulation improves tumour vascular function, an effect that is expected to improve delivery and efficacy of other anti-cancer drugs. The study summarized here was designed to establish the therapeutic potential of IrC<sup>TM</sup> as a single agent for treatment of GBM. The activity of IrC<sup>TM</sup> against a model of orthotopic GBM was compared to free irinotecan. The data show that the delivery of irinotecan, and its active metabolite SN-38, to the brain is improved following administration of IrC<sup>TM</sup> compared to irinotecan. A repeated dose toxicology study in tumour-free rodents shows that IrC<sup>TM</sup> is much better tolerated than the free drug. Further, at equivalent and equitoxic doses, the therapeutic efficacy of IrC<sup>TM</sup> was better than that of irinotecan. The results of these studies are important to support future studies evaluating the role of IrC<sup>TM</sup> in improving treatment outcomes in a combination setting with TMZ.

## **3.2 Materials and methods**

### **3.2.1 Irinophore C<sup>TM</sup> formulation**

Briefly, 1,2-distearoyl-*sn*-glycero-phosphocholine and cholesterol (DSPC/Cholesterol; 55:45 mol%) (Avanti Polar Lipids, Alabaster, AL, USA) large unilamellar vesicles (LUVs) were

prepared as previously described [189]. Lipids were dissolved in chloroform at the required molar ratio, labeled with the non-exchangeable, non-metabolizable lipid marker  $^3\text{H-CHE}$  (PerkinElmer Life Sciences, Boston, MA, USA), and dried to a thin film under a stream of nitrogen gas. Subsequently, the lipid was placed in a high vacuum for  $\geq 3$  h to remove any residual solvent. The lipid films were hydrated at  $65^\circ\text{C}$  following addition of a 300 mM copper sulfate solution. Hydration included five cycles of freeze-and-thaw (5 minutes each, freezing in liquid nitrogen and thawing at  $65^\circ\text{C}$ ) [267]. The multilamellar vesicle (MLV) suspensions were then extruded 10 times through stacked polycarbonate filters of  $0.1\mu\text{m}$  pore size at  $65^\circ\text{C}$  (Extruder<sup>TM</sup>, Northern Lipids, Vancouver, BC, Canada). The resultant LUVs typically possessed mean vesicular diameters in the range  $110\text{ nm} \pm 30\text{ nm}$  as determined using Phase Analysis Light Scattering (PALS) methods (ZetaPALS, Brookhaven Instruments Corp., Holtsville, NY, USA). The LUVs' external buffer was exchanged using Sephadex G-50 size exclusion chromatography with SHE buffer (300 mM sucrose, 20 mM HEPES, 15 mM EDTA; pH7.5).

The divalent metal ionophore A23187 (calcimycin; Sigma, Oakville, ON, Canada; 1 mg/mL solution in 100% ethanol) was added to liposomes ( $0.5\mu\text{g}/\text{mg}$  lipid) and incubated at  $60^\circ\text{C}$  for 30 minutes. Subsequently, irinotecan hydrochloride trihydrate (Camptosar<sup>®</sup>, Pharmacia; BC Cancer Agency Pharmacy, Vancouver, BC, Canada) was added to liposomes at  $50^\circ\text{C}$  such that the final drug-to-lipid ratio was 0.2:1 (mol drug: mol total lipid). Drug uptake was determined after thirty minutes of incubation by separating encapsulated drug from free drug using a Sephadex G-50 column equilibrated with PBS buffer. Fractions containing the liposomes were analyzed in order to confirm drug-to-lipid ratio. Lipid concentrations ( $^3\text{H-CHE}$ ) were measured using liquid scintillation counting (Packard 1900TR Liquid Scintillation Analyzer). Irinotecan concentration was determined by measuring absorbance at 370 nm. Briefly, a portion of the sample collected from the column was adjusted to a final volume of  $100\mu\text{L}$  with PBS.

Subsequently, 900 $\mu$ L Triton X-100 1% was added and the samples were heated in a water bath at  $> 90^{\circ}\text{C}$  until the cloud point of the detergent was observed. The samples were then cooled to room temperature and the absorbance was determined against a freshly prepared irinotecan standard curve (Hewlett Packard UV-Vis spectrophotometer, model 8453). For efficacy studies, IrC<sup>TM</sup> was concentrated using Amicon Ultra-15 centrifugal Filter Tubes (3000 x g for 30 minutes; Millipore, Billerica, MA, USA) to achieve the desired concentration such that the drug dose (mg/kg) could be administered in a volume of 200  $\mu$ L. The concentrations of lipid and irinotecan present in the injected samples were confirmed as described above.

### **3.2.2 Animal husbandry**

Animal studies were conducted in accordance with the Canadian Council on Animal Care's Guidelines, and the University of British Columbia's Animal Care Committee (IACC) approved the animal care protocols. Mice were housed under standard conditions in an SPF facility with enrichment and had access to food and water *ad libitum*. All animals were observed at least once per day for morbidity, more if deemed necessary during the pre-treatment and treatment periods. Animals were terminated (CO<sub>2</sub> asphyxiation) if signs of morbidity reached predetermined levels as outlined in a standard operating procedure assessing animal health status. A necropsy was performed on these animals to assess changes in gross tissue pathology.

### **3.2.3 Pharmacokinetic study**

Irinotecan or IrC<sup>TM</sup> was injected i.v. (200 $\mu$ L bolus administration) in Rag2M mice (7-10 weeks old females, 5-6/Gr.) at a drug dose of 25mg/kg. At defined time points, mice were terminated by CO<sub>2</sub> asphyxiation and blood was collected by cardiac puncture, centrifuged at 2500 rpm for 15 minutes and plasma was stored at  $-80^{\circ}\text{C}$ . Brains were harvested and stored at  $-80^{\circ}\text{C}$  until analysis. Irinotecan (lactone and carboxylate forms together) and SN-38 (lactone and carboxylate forms together) levels in the brain and plasma were analyzed by High-Performance Liquid Chromatography (HPLC) as described previously [190]. Briefly HPLC separation of

irinotecan and SN-38 lactone and carboxylate forms was performed using a 250 x 4.6mm Symmetryshield™ RP18 5µM Column and Symmetryshield™ RP18 guard column (Waters, Mississauga, ON, Canada). Gradient elution was used with mobile phase A composed of 75mM ammonium acetate and 7.5mM tetrabutylammonium bromide adjusted to pH 6.4 with glacial acetic acid (Fisher Scientific, Nepean, ON, Canada) and mobile phase B was acetonitrile. Gradient profile was as follows: Time = 0 min: 78% A : 22% B, Time = 10 min: 64% A : 36% B, Time = 16 min: 78% A : 22% B, Time = 20 min: 78% A : 22% B. A 10 µL sample was injected onto the column (column temp. = 40°C) and eluted at a flow rate of 1mL/min. Irinotecan and SN-38 forms were detected using a Waters 2475 multi-wavelength fluorescence detector (Waters, Mississauga, ON, Canada) set with time program events of  $\lambda_{ex}=370\text{nm}$ ;  $\lambda_{em}=425\text{ nm}$  between times 0 – 12.5 min for irinotecan forms, and  $\lambda_{ex}=370\text{ nm}$ ;  $\lambda_{em}=535\text{ nm}$  between times 12.5 – 20 min for SN-38 forms. Prior to injection, all samples were maintained at 4°C to reduce conversion between lactone and carboxylate forms. Standard curves of irinotecan and SN-38 lactone form were prepared by serial dilutions in a 2:1:1 sodium acetate (100mM pH 4.0):Methanol:Acetonitrile buffer. For the carboxylate form of irinotecan and SN-38, serial dilutions were prepared in a 2:1:1 sodium borate (100mM pH 9.0):MeOH:ACN buffer. The limit of quantification for irinotecan and SN-38 lactone and carboxylate forms was 1 and 10ng/mL, respectively. Irinotecan pharmacokinetic parameters were calculated using the non-compartmental analysis function of WinNonLin software version 5.0.1 (Pharsight, Mountain View, CA, USA). In order to account for the amount of drug measured in tissue samples that was due to drug in the plasma compartment within the brain, a plasma volume correction was applied and was based on previously reported studies estimating the plasma volume within the brain at 11µL/gram tissue [268]. Area-under-the-curve (AUC) values were calculated using GraphPad Prism (San Diego, CA, USA) software.

### **3.2.4 Repeated dose toxicology study**

Mice (n=3/group) were individually weighed and injected with IrC<sup>TM</sup> or irinotecan weekly for three weeks (Q7D x3). The mice were monitored continually for acute signs of toxicity for the first six hours after intravenous administration of the drugs, and on a daily basis thereafter. Body weights and overall body conditioning score for individual mice were measured three times weekly. If body weight loss (BWL) was less than 15% of initial and overall health status was maintained (as judged by body weight loss, hydration levels, behavioural observations, signs of weakness and levels of activity as outlined within a health monitoring assessment standard operating procedure), mice received further treatments. Mice were monitored for health status for 14 days following the last drug dose.

### **3.2.5 Orthotopic GBM animal model**

U251MG glioblastoma cell line was purchased from American Type Culture Collection (Manassas, VA, USA). The cell line was used for a maximum of fifteen passages. U251MG were maintained in DMEM medium supplemented with 1% L-glutamine, 1% penicillin/streptomycin (Stem Cell Technologies, Vancouver, BC, Canada) and 10% FBS (Hyclone, Logan, UT, USA) and cultured at 37°C in a humidified atmosphere containing 5% CO<sub>2</sub>. Animals were anesthetized by injection of 120mg/kg i.p. ketamine (Ketalean®, Bimeda-MTC, Cambridge, ON, Canada), 10mg/kg i.p. xylazine (Rompun®, Bayer inc., Toronto, ON, Canada), and 0.5mg/kg s.c. acepromazine (Atravet®, Wyeth, Guelph, ON, Canada), and were given 1mg/kg s.c. Metacam® analgesic (Boehringer Ingelheim, Burlington, ON, Canada). U251MG cells ( $7.5 \times 10^4$ ) were implanted into the right caudate nucleus-putamen (ML -1.5 mm; AP +1mm; DV -3.5mm) of Rag2M mice (7-10 weeks old females, 6-8/Gr.) brains using a stereotaxic injection frame (Stoelting Company, Wood Dale, IL, USA). Animals were treated i.v. with 25mg/kg or 50mg/kg IrC<sup>TM</sup> or irinotecan (Sandoz, QC, Canada) on day 21, 28 and 35 after inoculation, or IrC<sup>TM</sup> 100mg/kg on day 21, 35 and 42. The latter schedule was selected

because the 100mg/kg IrC™ dose, although well tolerated in tumour free mice, exhibited unexpected toxicities in orthotopic GBM tumour-bearing animals. Therefore, these animals were allowed to recover for two weeks before being given the subsequent doses of IrC™ (100mg/kg) on day 35 and 42. These subsequent doses were well tolerated. The results were measured on the basis of animal survival times. However, death cannot be ethically used as an end point. Therefore mice were euthanized when their health status was considered to be poor enough to warrant euthanasia. A standard operating procedure, approved by the Institutional Animal Care Committee, was used to provide comprehensive assessments of body weight, hydration, behavioural changes, appearance and activity levels. On the basis of this assessment methodology, animals would be euthanized when their health status score was 10 and the time of death was recorded as one day after the animals were terminated. All animals were terminated by CO<sub>2</sub> asphyxiation.

### **3.2.6 Ki67 and Draq5 nuclei staining and quantification**

U251MG tumour-bearing mice were left untreated, or treated with irinotecan at 50mg/kg or IrC™ at 25mg/kg on day 21, 28 and 35 and terminated on day 42, 50 or 70 (n=3-4/gr.). All animals were terminated by CO<sub>2</sub> asphyxiation and brains were harvested and cryopreserved in OCT (Sakura Finetek, CA, USA) on dry ice and stored at -80°C. OCT preserved brains were cryosectioned and 10µm sections were collected from the Bregma +1.0 location. Sections were fixed in a 1:1 mixture of acetone:methanol for 15 minutes at room temperature, then blocked with blocking buffer (Odyssey blocking buffer, Rockland, PA, USA) for 1 hour at room temperature. Sections were incubated with rabbit anti-human Ki-67 (Invitrogen #18-0191z; 1:100) overnight at 4°C. Alexa 546 goat anti-rabbit #A-11035 secondary antibody (1:200, Invitrogen) was incubated for 1hr at room temperature. Nuclei were stained with Draq5 (Biostatus, Leicestershire, UK; 1:200) for 30min at 37°C. Slides were mounted with PBS and imaged for Alexa 546 (Cy3 filter) and Draq5 (Cy5 filter) using a robotic fluorescence

microscope (Leica DM6000B, Leica, ON, Canada). The threshold for Ki67 marker was set using Photoshop, using a scale from 1 to 255 units, and was defined at 2 units higher than the minimal level necessary to obtain a negative signal for non-specific staining. The threshold level was kept the same for all sections. Acquired images were quantified for positive pixels using an in-house segmentation algorithm, normalized to the number of pixels in the non-necrotic tumour area and expressed as positive fraction (positive pixels divided by non-necrotic tumour area; MATLAB, The Mathworks, Natick, MA, USA). Non-necrotic tumour areas were defined by cropping out non-tumour tissue or non-tumour and necrotic tissue, respectively, on the basis of Draq5 stained sections and were quantified using the same in-house algorithm.

### **3.2.7 Statistical analysis**

Statistical analysis for survival curves was determined using a log rank test as assessed by SPSS 17.0 (SPSS Inc, Chicago, IL, USA). All other statistical analyses were completed using GraphPad Prism (San Diego, CA, USA). For single comparisons, statistical analyses were completed using the parametric two-tailed Student T-Test. For multiple comparisons, analyses were completed using a one-way ANOVA test with Tukey post-tests. All data are expressed as the mean +/- S.E.M.

## **3.3 Results**

### **3.3.1 Irinotecan levels in the blood and brain are greater following administration of IrC™ than following administration of free irinotecan**

Rag2M mice were injected with irinotecan (25mg/kg), administered as free drug or IrC™. The free drug formulation used in these studies was the clinical product Camptosar®; a drug product that contains 20 mg irinotecan; 45 mg sorbitol; and 0.9 mg lactic acid per mL. At various time points, blood and brain tissue were collected and processed as described in the Methods for analysis of irinotecan and SN-38 (lactone and carboxylate forms). The results,

summarized in Figure 17, demonstrate a 330- to 1200-fold increase in the plasma concentrations of irinotecan following injection of IrC<sup>TM</sup> when compared to mice injected with free drug (p<0.0001; Figure 17a). The carrier-mediated increase in irinotecan plasma levels is emphasized by a 760-fold increase in mean plasma area-under-the-curve within 0-24hrs period (AUC<sub>0-24hrs</sub>) of the lactone form of irinotecan following administration of IrC<sup>TM</sup> (Table 4). These data are consistent with previously published data where a 1000-fold increase in plasma irinotecan lactone AUC<sub>0-24hrs</sub> was observed following IrC<sup>TM</sup> administration compared to irinotecan at a drug dose of 50mg/kg given i.v. in BALB/c mice [190]. There was a 7- to 26-fold increase in SN-38 (lactone) concentrations in the plasma following injection of IrC<sup>TM</sup> when compared to the plasma SN-38 concentrations achieved following administration of the free drug (p<0.01 to p<0.0001, depending on time point; Figure 17c). The mean AUC<sub>0-24hrs</sub> for SN-38 (lactone) was increased 30-fold following IrC<sup>TM</sup> injection when compared to the free drug (Table 4).

**Table 4: Plasma and brain irinotecan and SN-38 AUC<sub>0-24hrs</sub> values (µg•hr/mL) following i.v. injection of 25mg/kg irinotecan or IrC<sup>TM</sup> in healthy Rag2M mice.**

Compartment	Compound	AUC <sub>0-24hrs</sub> (µg•hr/mL) Irinotecan treatment	AUC <sub>0-24hr</sub> (µg•hr/mL) IrC <sup>TM</sup> treatment
Plasma	Irinotecan	7.47	5672.55
	SN-38	4.90	145.27
Brain	Irinotecan	11.81	14.83
	SN-38	0.05	1.85

**Figure 17: Irinotecan levels in the blood and brain are greater following administration of IrC™ than following administration of free irinotecan.**

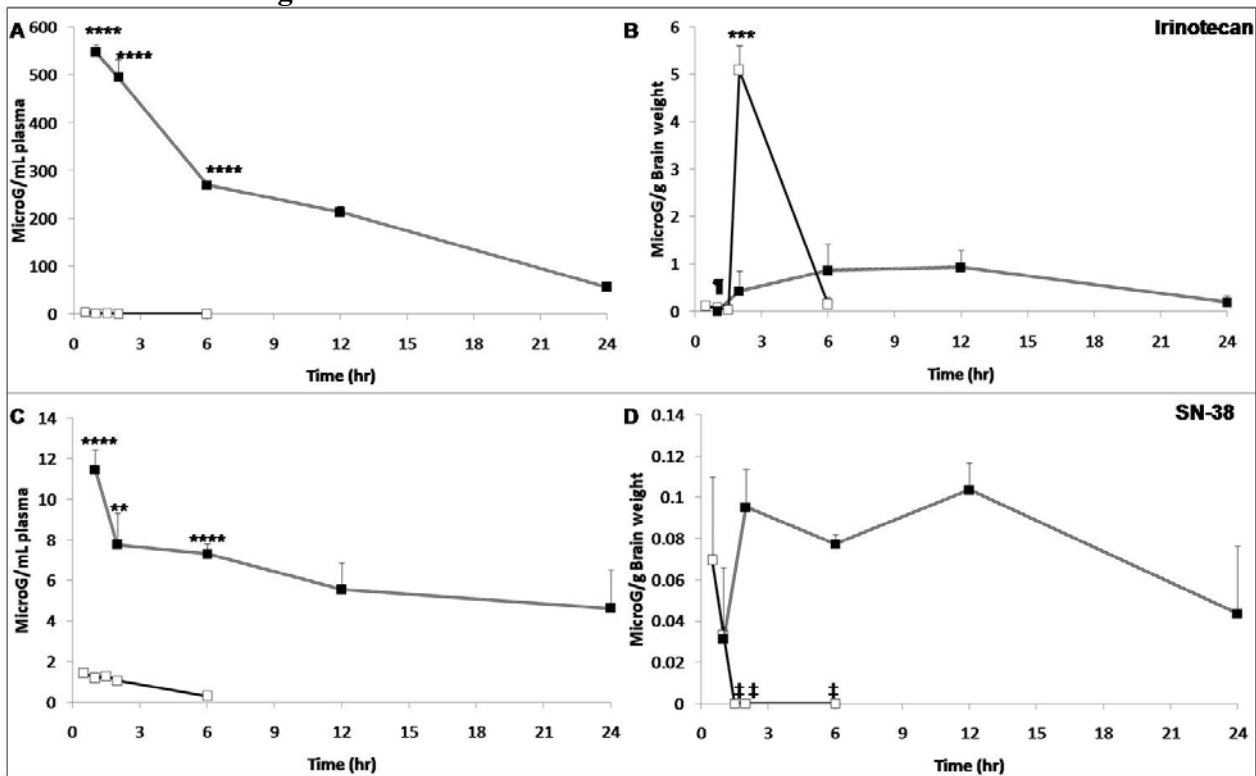


Figure 17: Irinotecan (□) or IrC™ (■) at 25mg/kg were given i.v. in healthy Rag2M mice. Mice were sacrificed at indicated time points. a) Plasma and b) brain levels of irinotecan in lactone (active) configuration were measured by HPLC. c) Plasma and d) brain levels of lactone SN-38 were also measured by HPLC. Statistical significances are indicated such as \**p*-value ≤ 0.05; \*\**p*-value ≤ 0.01; \*\*\**p*-value ≤ 0.001; \*\*\*\**p*-value ≤ 0.0001 compared to irinotecan injection. ‡: values were below detection limits (applicable to irinotecan treatment only). ¶: values were ≤0 after plasma volume correction was applied (applicable to IrC™ treatment only).

Irinotecan is known to cross the blood brain barrier (BBB) [269], and is active in treatment of brain cancers [37]. A primary objective of the studies summarized here was to determine whether the delivery of irinotecan across the blood brain barrier is enhanced when the drug is delivered as IrC™ compared to free drug (Campotosar®) administered at an equivalent drug dose. It is important to note that there is no evidence to suggest that the lipid based formulation (~100nm DSPC/Cholesterol liposomes) used to prepare IrC™ is capable of crossing the BBB in

healthy tissue, thus it is assumed that irinotecan or SN-38 accumulation in brain tissue comes from drug released from the carrier while in the circulation. Figures 17b and d summarize the data obtained when measuring irinotecan (Figure 17b) and SN-38 (Figure 17d) in brains of mice given an i.v. injection of IrC<sup>TM</sup> or free drug (25mg/kg). Drug present in the plasma compartment of the brain was accounted for by applying a correction factor (11 $\mu$ L of plasma/gram of tissue) determined for brain [268]. Following free drug administration, the maximum level of irinotecan measured in the brain was 5.1 $\mu$ g/g tissue (2hrs post-administration) and this value decreased 35-fold to 0.14 $\mu$ g/g tissue 6hrs after drug administration (Figure 17b). Interestingly, the level of irinotecan measured 2hrs post IrC<sup>TM</sup> injection was 12-fold lower ( $p < 0.001$ ) than that observed following administration of the free drug; a result that is consistent with the fact that the majority of drug in the plasma compartment is carrier-associated and that the carrier itself is unable to cross the BBB. The level of irinotecan measured in the brain measured at the 12hrs after IrC<sup>TM</sup> administration was 0.93 $\mu$ g/g tissue. At the 24hr time point, 0.19 $\mu$ g of irinotecan per gram of tissue was still detected in brains of the IrC<sup>TM</sup> injected mice. When considering the 24hr time course, it is notable that the mean AUC<sub>0-24hrs</sub> for irinotecan was comparable in animals given the free drug or IrC<sup>TM</sup> (Table 4). The maximum SN-38 concentration measured in the brain of mice given free drug was 0.07 $\mu$ g/g tissue (30 minutes post-injection; Figure 17d). By 1.5hrs, the SN-38 levels were below the detection limit of the assay used. In contrast, following administration of IrC<sup>TM</sup>, the SN-38 levels in the brain were 0.10 $\mu$ g/g tissue 6hrs post-injection and the SN-38 levels in the brain were maintained at levels above 0.04 $\mu$ g/g tissue for at least 24hrs after drug administration. The mean AUC<sub>0-24hrs</sub> for SN-38 in brain tissue was 37-fold greater in animals treated with IrC<sup>TM</sup> when compared to those animals given free drug (Table 4).

The studies summarized above compared irinotecan and SN-38 levels in the plasma and brain of healthy mice following administration of IrC<sup>TM</sup> or the free drug. The analytical methods used (see Methods) measured both the closed ring active lactone form of the drug as well as the

inactive open ring carboxylate form. The ratio of lactone to carboxylate form (L/C ratio) provides a measure of drug stability following administration, and these ratios have been summarized in Table 5. One hour post-injection of IrC<sup>TM</sup>, the average L/C ratio (wt:wt) in the plasma was ~160 times higher ( $p < 0.0001$ ) when compared to the L/C ratio (wt:wt) in the plasma following free drug administration. Depending on the time point selected, the L/C ratio (wt:wt) ranged from 0.62 to 0.80 in the plasma of mice given free drug (i.e. more than half the drug measured was in the inactive form), consistent with the rapid conversion of the lactone to the carboxylate form that occurs when the drug is at neutral pH. In contrast, for animals dosed with IrC<sup>TM</sup>, the L/C ratio (wt:wt) ranged from a high of 116 (at 2hrs) to a low of 69 (at 24hrs), indicating that the majority of drug in the plasma of mice given IrC<sup>TM</sup> was in the active form. This is consistent with the idea that the drug is maintained in the lipid-based carrier formulation at a low pH which preserves the drug in its lactone form. One hour following IrC<sup>TM</sup> administration, the L/C ratio (wt:wt) of SN-38 in the plasma was ~8 times higher ( $p < 0.001$ ) than that observed for mice given free drug (Table 5). This was an unexpected finding considering that the SN-38 forms when irinotecan dissociates from the carrier and one would expect that following dissociation, the conversion to the inactive carboxylate form would be comparable to that seen in mice given the free drug. It is interesting to note that, while the lactone forms of both irinotecan and SN-38 were favorably maintained in the plasma of mice given IrC<sup>TM</sup>, this was not observed in the brain. Even though the L/C (wt:wt) ratios in the brain were comparable (Table 5), it should be noted that the levels of the lactone or carboxylate forms of SN-38 in the brains of mice given free drug were below detection limits after the 1hr time point. The L/C ratio (wt:wt) for SN-38 in the brain of mice given IrC<sup>TM</sup> ranged from 1.3 to 1.7 for the 2, 6 and 24hr time points and were similar to the L/C ratio (wt:wt) observed at the 1hr time point following injection of free drug (Table 5).

**Table 5: Plasma and brain lactone/carboxylate (wt:wt) ratios (L/C) for irinotecan and SN-38 following i.v. injection of 25mg/kg IrC<sup>TM</sup> or irinotecan in healthy Rag2M mice.**

Time point	L/C <sub>Plasma.CPT-11</sub>		L/C <sub>Plasma.SN-38</sub>		L/C <sub>Brain.CPT-11</sub>		L/C <sub>Brain.SN-38</sub>	
	Irinotecan (25mg/kg)	IrC <sup>TM</sup> (25mg/kg)	Irinotecan (25mg/kg)	IrC <sup>TM</sup> (25mg/kg)	Irinotecan (25mg/kg)	IrC <sup>TM</sup> (25mg/kg)	Irinotecan (25mg/kg)	IrC <sup>TM</sup> (25mg/kg)
1hr	0.64+/-0.07	101.46+/-10.9 ****	1.72+/-0.22	14.25+/-2.09 ***	0.64+/-0.20	0 ¶	1.31+/-0.76	0.51+/-0.09
2hrs	0.62+/-0.02	115.8+/-14.6 ****	2.50+/-0.08	9.82+/-1.20 ***	16.08+/-0.69	1.09+/-1.09 ****	0 ¶	1.59+/-0.28
6hrs	0.80+/-0.50	86.83+/-10.13 ****	1.60+/-0.04	12.37+/-1.26 ****	1.02+/-1.02	3.30+/-2.01	0 ‡	1.27+/-0.05
12hrs	N/D	68.9+/-5.5	N/D	10.42+/-2.40	N/D	3.49+/-0.80	N/D	1.67+/-0.20

Table 5: \*\*\**p*-value  $\leq 0.001$ ; \*\*\*\**p*-value  $\leq 0.0001$  compared to free drug at matched time point. ‡: Values were below detection limits. ¶: values were  $\leq 0$  after plasma volume correction was applied. N/D: irinotecan levels following irinotecan administration were not measured at the 12hrs time point.

### 3.3.2 Irinophore C<sup>TM</sup> exhibits significant activity in an orthotopic GBM model

In order to assess the activity of IrC<sup>TM</sup> in an orthotopic model of brain cancer, it was important to establish how well the drug was tolerated when compared to animals given free drug. A limited (n=3) dose range finding study was completed in tumour-free Rag2M mice. The results of this assessment have been summarized in Table 6. When the free drug was administered to mice (using a slow injection method to minimize acute reactions), visible shaking of the animal followed by recovery was noted at doses of 60, 75 and 90mg/kg. At the higher dose, animals needed to be terminated due to poor health status after the second and third doses. There was no change in weight in these animals, but necropsy information suggested GI tract dysfunction when the animals dosed at 60, 75, and 90mg/kg were evaluated. In contrast, IrC<sup>TM</sup> was tolerated at doses up to 120mg/kg and no acute reactions were noted. However, there was a dose dependent decrease in body weight noted after the first and second drug dosing, but not after the last dosing. These animals were also terminated 14 days following the last injection of IrC<sup>TM</sup> and the only gross change noted in some of the animals was enlarged gall bladders. It was concluded, based on the presence or absence of acute reaction following injection and on the

basis of terminal necropsy information, that the therapeutic studies should evaluate free drug efficacy at doses of no greater than 50mg/kg. Although IrC<sup>TM</sup> was well tolerated in tumour free mice at doses of 120mg/kg, the weight loss noted at both 120 and 90mg/kg suggested that efficacy studies should be completed at dose of 100mg/kg or less for IrC<sup>TM</sup>.

**Table 6: Repeated dose (Q7Dx3) tolerability study of IrC<sup>TM</sup> and free drug (irinotecan) in healthy Rag2M mice.**

Treatment	Drug dose (mg/kg)	%BWL	Observations	Necropsy
Irinotecan	50	None	No notation	No notation
	60	None	Shaking 10 minutes post injection then recovery	No notation
	75	None	as above	No notation
	90	None	One mouse died post second injection; once mouse died post third injection	Yellowish fluid in intestines
IrC <sup>TM</sup>	60	None	No notation	No notation
	75	None	No notation	No notation
	90	5.4	Body weight loss on day 5 with recovery thereafter.	No notation
	120	7.4	Body weight loss on day 5 with recovery thereafter.	Two mice with enlarged gall bladders at autopsy.

Orthotopic GBM tumour bearing mice (see Methods) were treated with irinotecan at 25 or 50mg/kg, or IrC<sup>TM</sup> at 25, 50 or 100mg/kg. Results are summarized in Table 7 and Figure 18. The average survival time for saline treated tumour bearing animals was 48.1 days (Table 7). Animals treated on day 21, 28 and 35 with 50mg/kg of free drug exhibited an increase in average survival time of 27%, which was significantly ( $p < 0.05$ ) better than the saline-treated controls, while 25mg/kg free drug did not significantly increase the average survival. In comparison, animals treated with IrC<sup>TM</sup> at 25 and 50mg/kg exhibited increases in average survival of 31% and 49%, respectively ( $p < 0.01-0.001$ ; Table 7). The activity of IrC<sup>TM</sup> given at 25mg/kg was equal to that observed following administration of the free drug at twice the dose (Figure 18a). Further, animals treated with IrC<sup>TM</sup> at 50mg/kg exhibited a statistically significant increase in average survival time of 17% compared to free drug treatment at the same dose ( $p < 0.05$ ; Table 7). These efficacy studies also evaluated the activity of IrC<sup>TM</sup> when administered at 100mg/kg, a dose that

should have been tolerated well based on the findings summarized in Table 6. However, the tumour bearing mice treated with 100mg/kg IrC™ exhibited significant weight loss and a significant change in health status (Figure 18b). This required a change in the dose schedule for those animals treated with IrC™ at this dose, as noted in the Methods. For these treated animals, the increase in average survival achieved was 83% ( $p < 0.001$ ). On day 85, >80% of these animals were still alive while all animals in the other treatment groups were terminated due to progressive disease. The survival curves for all treatment groups (summarized in Figure 18a) were defined by health status assessments (described in the Methods). When the health status assessment resulted in a score of 10 or more, the animals were euthanized. The health status assessment data for the different treatment groups was averaged and these data have been summarized in Figure 18b.

**Figure 18: Irinophore C™ exhibits significant activity in an orthotopic GBM model.**

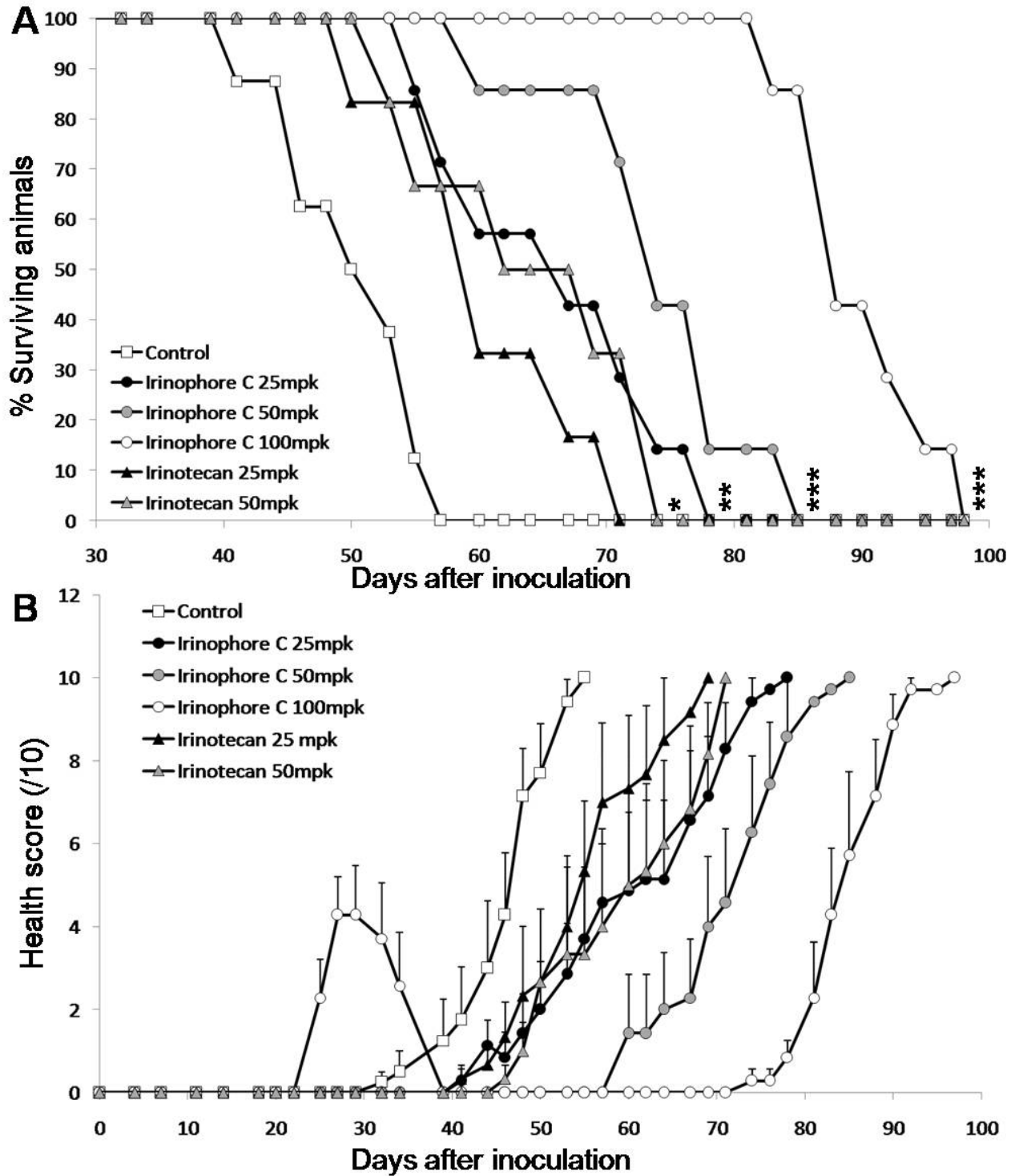


*Figure 18: Orthotopic U251MG GBM tumour-bearing mice were treated with IrC™ at 25, 50 and 100mg/kg or irinotecan at 25 or 50mg/kg. Mice were sacrificed when they showed severe signs of tumour-associated illness (overall health score of 10) and the date of sacrifice was recorded. a) Percentage of surviving animals over time following tumour inoculation and*

treatment with IrC<sup>TM</sup> or irinotecan. \**p*-value ≤ 0.05; \*\**p*-value ≤ 0.01; \*\*\**p*-value ≤ 0.001; \*\*\*\**p*-value ≤ 0.0001 for survival time of treated vs untreated animals. b) Overall health score of control and treated animals over the course of the study. Health scoring takes into consideration the percentage of body weight loss, hydration levels, behavioural observations, signs of weakness and levels of activity.

**Table 7: Antitumour efficacy of Irinophore C<sup>TM</sup> and free irinotecan in orthotopic U251MG tumour-bearing Rag2M mice.**

Treatment	Dose (mg/kg)	Average survival (days+/-s.e.m)	Median survival (days)	Increase in average survival (%)
Untreated	N/A	48.1+/-1.9	49	N/A
Irinotecan	25	58.3+/-3.0	57	21.2
	50	61.3+/-3.7*	59	27.4
IrC <sup>TM</sup>	25	63.1+/-3.2**	60.5	31.1
	50	71.7+/-3.0***#	71	49.1
	100	87.9+/-2.1***	85	82.7

Table 7: \**p*-value ≤ 0.05; \*\**p*-value ≤ 0.01; \*\*\**p*-value ≤ 0.001 compared to control group; #*p*-value ≤ 0.05 compared to matched dose of free drug.

To compare the treatment effects achieved following administration of a 25mg/kg dose of IrC<sup>TM</sup> (Q7D x3) or a 50mg/kg dose of free drug, an assessment of brain tumour histopathology was completed. Brains were harvested on day 42, 55 or 70 after tumour inoculation, sectioned and stained with human-specific Ki67 antibody to assess proliferation and Draq5 nuclei staining to assess tumour size and morphology. Representative brain sections from untreated, IrC<sup>TM</sup> and free drug treated mice obtained 55 or 70 days after tumour cell inoculation are provided in Figure 19. Tumours comprise densely packed Draq5-stained (red) nuclei surrounded by normal brain tissue with sparse nuclei. Ki67-positive proliferating tumour cells are shown in yellow. Analysis of these data for different tumours from the indicated treatment groups has been provided in Table 8. While the tumour area within the brain of irinotecan -treated animals was not statistically different from that of untreated mice on day 55, the tumour area in the brain from IrC<sup>TM</sup> treated mice was 84% (*p*<0.001) and 86% (*p*<0.05) smaller than untreated mice on day 42

and 55, respectively. No differences were observed in proliferation levels (Ki67 positive staining/viable tumour area) of IrC<sup>TM</sup>-treated tumours on day 42 compared to control. However, on day 55 (i.e. 20 days after the last dose of IrC<sup>TM</sup>), the level of Ki67 staining was increased 3.5-fold in the tumours from IrC<sup>TM</sup> treated mice while no changes were observed in free drug treated tumours. Finally, on day 70, the tumour area and Ki67 staining were comparable in the brains from mice treated with IrC<sup>TM</sup> or free drug; a result that is consistent with the survival curves shown in Figure 18a. The tumour area at this time point was similar to that seen on day 55 for untreated controls.

**Figure 19: IrC<sup>TM</sup>-treated tumours revealed a transient increase in cell proliferation after treatment.**

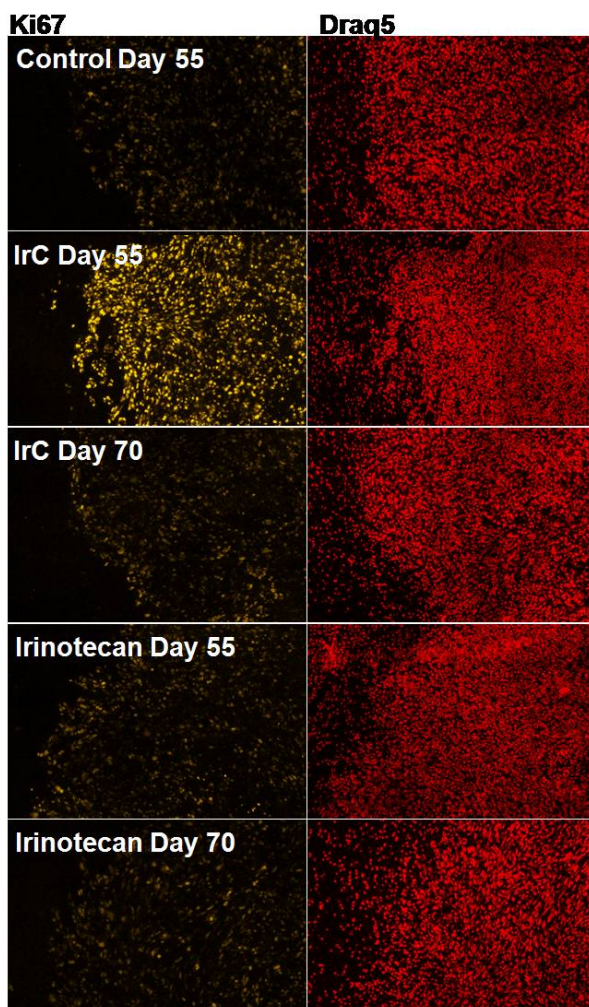


Figure 19: Brains from orthotopic U251MG GBM tumour-bearing mice untreated or treated with IrC™ at 25mg/kg or irinotecan at 50mg/kg were harvested at indicated time points, sectioned and stained for Ki67 proliferative marker and Draq5 nuclei staining as described in the Methods (n=3-4). Representative images showing Ki67 proliferative marker staining (yellow) of untreated mice (control) as well as IrC™ (25mg/kg) or free drug (50mg/kg) treated groups are shown. Corresponding nuclei staining (Draq5; red) images are provided to indicate tumour location (densely packed nuclei on the right surrounded by brain tissue on the left of each image).

**Table 8: Tumour area and fraction of Ki67 positive cells in brain sections isolated from untreated, IrC™ and irinotecan treated mice at indicated time points.**

Treatment	Time point (days)	Tumor area (pixels x 10 <sup>6</sup> )	Ki67 positive fraction (%)
Untreated	42	1.18+/-0.19	6.6+/-1.6
Untreated	55	2.34+/-0.66	6.3+/-2.5
IrC™	42	0.19+/-0.03***	8.3+/-1.9
IrC™	55	0.33+/-0.11*	22.3+/-5.2*
IrC™	70	3.10+/-0.31	4.3+/-0.5
Irinotecan	55	1.66+/-0.25	3.4+/-1.0
Irinotecan	70	3.85+/-0.48	5.1+/-2.0

Table 8: Tumour area was defined by digitally isolating non-tumour tissue from tumour tissue based on Draq5 nuclei staining. Fraction of Ki67 positive cells was defined as Ki67 stained pixels/tumour area pixels x100. \*p-value ≤ 0.05; \*\*\*p-value ≤ 0.001 compared to untreated animals from the same time point.

### 3.4 Discussion

The results presented indicate that following injection of IrC™, there are significantly higher levels of irinotecan and its active metabolite SN-38 in the plasma compartment when compared to mice injected with free drug. Although the mean AUC<sub>0-24hrs</sub> for irinotecan in brain tissue was comparable for animals treated with IrC™ or free drug, exposure of the brain to SN-38 was far greater in mice given IrC™. The data also demonstrated that the plasma L/C ratios

(wt:wt) for irinotecan and SN-38 were significantly higher in animals treated with IrC™ when compared to those animals treated with free drug, suggesting that the IrC™ formulation was able to maintain the drug in its active form for extended time periods. In tumour free mice, IrC™ was much better tolerated than the free drug. However, IrC™ was found to be more toxic in tumour-bearing mice than in tumour free mice. Regardless, the survival times of tumour bearing mice were increased significantly when the mice were treated with IrC™ compared to the free drug. These data support the conclusion that carrier-mediated changes in the pharmacokinetic behaviour and biodistribution of irinotecan and SN-38 increased their therapeutic activity in an orthotopic model of GBM that is somewhat insensitive to irinotecan when given as the free drug. There are three findings that warrant further discussion: (i) the significant increase in toxicity of IrC™ in mice with established orthotopic tumours, (ii) the enhanced Ki67 staining observed 20 days after the end of IrC™ treatment, and iii) the stability of the lactone form of SN-38 in the plasma following IrC™ administration.

In tumour free Rag2M mice, there was a modest (<10%) body weight loss and no substantial changes in overall health status following IrC™ administration (i.v.) at a dose of 120mg/kg (see Table 6). These data are consistent with other toxicity assessments completed with IrC™ in immune competent CD1 mice, which indicated that the formulation is tolerated at doses >250mg/kg (Waterhouse, unpublished observation) when given as a single dose. However, in mice bearing orthotopic GBM tumours, an i.v. dose of 100mg/kg IrC™ induced significant toxicity (see Figure 17b). The increase in toxicity seen in mice bearing orthotopic GBM tumours may be associated with the fact that the blood-brain barrier (BBB) in GBM is poorly functional and exhibits increased permeability [46] compared to normal BBB. Abnormalities in the tumour BBB may promote the enhanced permeability and retention (EPR) effect [182], which would be expected to contribute to an increased accumulation of the IrC™ formulation in the brain when a tumour is present. Thus the initial dose may deposit more drug

than expected (compared with tumour-free brain) and, in turn, cause drug-associated neurotoxicity and an associated change in overall health status. In addition, it was previously reported that irinotecan and SN-38 plasma levels are increased in tumour-bearing mice compared to non-tumour bearing mice following irinotecan injection [270]. This observation was suggested to be due to an increased conversion of irinotecan to SN-38 by carboxylesterases present in the tumour and/or by an impairment of drug clearance mechanisms caused by substances secreted by the tumour. Interestingly, after the tumour-bearing mice recovered from the first dose (a one week delay in treatment), subsequent doses of IrC<sup>TM</sup> at 100mg drug/kg were well tolerated.

We have shown in chapter 2 that the blood vessel structure becomes normalized in both s.c. and orthotopic GBM models following IrC<sup>TM</sup> treatment [271]. In the orthotopic model, this phenomenon is associated with a reduction in the permeability of blood vessels and changes in vascular structure that make the tumour vessels more similar to vascular structure seen in disease-free brain. Normalization of the tumour vasculature following the first dose of IrC<sup>TM</sup> could have reduced the subsequent doses of IrC<sup>TM</sup> reaching the brain and consequently, these second doses would be less toxic. In addition, IrC<sup>TM</sup> treatment in GBM and HT-29 colorectal tumour models was also associated with increases in vessel network (CD31) coverage and tumour oxygenation [225]. From a treatment perspective, the mechanistically unique vascular effects of IrC<sup>TM</sup> will impact tumour behaviour. Studies evaluating the normalization effect induced by anti-angiogenic compounds have established that vascular normalization can increase drug delivery and reduce hypoxia; effects that can potentiate drug efficacy and radiation therapy, respectively [248, 271]. For instance, in a pre-clinical GBM model, the normalization of the capillary architecture and the resulting decrease in interstitial fluid pressure induced by the angiogenesis inhibitor SU5416 increased the delivery of temozolomide [252]. However, it can also be suggested that the improvements in vascular function would promote tumour growth due

to enhanced oxygenation and nutrient delivery. Interestingly, 20 days after the end of IrC<sup>TM</sup> treatment, there was a significant increase in tumour cell proliferation despite the substantial reduction in tumour burden (see Figure 19 and Table 8). No increase in tumour cell proliferation was observed with any of the evaluated time points for mice treated with the free drug. Importantly, this effect on tumour cell proliferation, as measured by Ki67 staining, was transient. No change in Ki67 staining was observed in IrC<sup>TM</sup>-treated tumours 7 days following the last dose of IrC<sup>TM</sup> compared to controls; GBM cell proliferation (as judged by Ki67 staining) in these tumours was similar in control tumours and in tumours from mice treated with IrC<sup>TM</sup>. However, the size of these tumours was significantly reduced. Importantly, enhanced proliferation was also not observed in animals that were terminated 35 days after the last IrC<sup>TM</sup> dose. It can be suggested that, in order to fully take advantage of the vascular normalization induced by IrC<sup>TM</sup>, the drug should be used in combination with other drugs, such as TMZ, that are effective against GBM tumours and are able to cross the BBB. In this context, imaging technologies will be necessary in clinical studies designed to assess IrC<sup>TM</sup>-mediated changes in tumour micro-environment and physiology before, during and after treatment to optimize the benefits of vascular normalization [251, 272].

The idea that a lipid-based formulation of irinotecan could promote tumour vasculature normalization is interesting. The concept of ‘blood vessel normalization’ was first postulated in the 1970s [249] and was more recently studied in the clinic with the emergence of anti-angiogenic compounds [226, 227]. In GBM and most other solid tumours, the tumour microvasculature is characterized by tortuous and fenestrated vessels with diameters that are larger than normal [250] and a discontinuous and thick basement membrane which rarely encloses pericytes [50]. The GBM vasculature was previously described as poorly functional [80, 81, 223, 224], contributing to reducing drug delivery to the tumour tissue [222, 250]. Antiangiogenic therapies have been shown in models of GBM to stop the growth of tumour

vessels and to prune immature and inefficient tumour vessels [241, 242, 251]. The surviving vasculature is then more functional [226, 227]. Jain and others have proposed that vascular normalization could improve tumour oxygenation and drug delivery to the tumour; factors that could improve treatment responses to radiation [242] and chemotherapy [273]. It was previously demonstrated *in vitro* that extended drug exposure increases endothelial cell sensitivity to SN-38 [245]. The increased efficacy of SN-38 against proliferating brain endothelial cells over non-proliferating cells has also been demonstrated in chapter 2 [271]. Therefore, it seems reasonable to suggest that the extended and increased SN-38 exposure following IrC<sup>TM</sup> administration may contribute to the tumour vasculature normalization effect. It should be noted, however, that vascular normalization induced following IrC<sup>TM</sup> administration is different from what has been described for the anti-angiogenic treatments [274]. The latter results in a reduction in microvessel density which is associated, in some cases, with increased hypoxia, invasion and metastasis. As indicated above, tumours in mice treated with IrC<sup>TM</sup> show no changes in microvessel density and exhibit decreases in tumour hypoxia [225, 271].

The data presented suggest that IrC<sup>TM</sup> may exhibit enhanced therapeutic potential because it improves the exposure of the brain to SN-38. It could be argued that the tumour-associated BBB is compromised, allowing the EPR effect to promote delivery of the drug-loaded carriers within the tumour's extravascular spaces. However, it is established that large lipid-based drug formulations cannot cross the BBB. Further, vascular normalization induced by IrC<sup>TM</sup> would limit the delivery of lipid-based formulations, as recently illustrated by Dewhirst's team [275]. It is proposed here that irinotecan and SN-38 in the brain must result from irinotecan that has dissociated from the carrier in the plasma compartment. It can be speculated that the bulk of irinotecan in the plasma compartment of animals injected with IrC<sup>TM</sup> is associated with the carrier and maintained in the lactone form due to the low pH environment within the core of the carrier structure or due to membrane association of the irinotecan [190]. Following irinotecan

release from the carrier, carboxyesterases in the plasma would rapidly convert irinotecan to SN-38. Further, since irinotecan is no longer protected within the low pH environment of the lipid-based formulation, the released drug would also undergo rapid hydrolysis to the inactive carboxylate form of irinotecan. A similar conclusion would be expected for SN-38 that has been generated following esterase-mediated biodegradation of irinotecan, but the results summarized in Table 5 suggest that this is not the case. SN-38 in the plasma compartment is maintained primarily in the lactone form (L/C weight ratios of > 10) following IrC™ administration. In contrast, the L/C ratio (wt:wt) for SN-38 in the plasma of mice injected with free drug was typically ~ 2. It is worth noting that the mean half-life for irinotecan conversion to the carboxylate form after administration in humans is less than 10 minutes, while SN-38 is maintained in its lactone form for extended time periods [276]. Further, it was shown that the rate of lactone to carboxylate conversion for SN-38 and irinotecan is reduced when the drugs are bound to serum albumin in the plasma [277]. Regardless, the preservation of the lactone form of SN-38 is not relevant in the brain compartment, and the increased therapeutic activity of the formulation over that of the free drug is most likely attributable to an increase in exposure time of cancer cells to SN-38 and, as indicated above, the direct (cytotoxic) and indirect (vascular normalization) effects of this drug when the parent drug is given as IrC™.

### **3.5 Conclusion**

IrC™ exerts multiple mechanisms of activity when used to treat tumour bearing animals. As mentioned above, vascular normalization in the tumour is likely due to a direct effect of SN-38 against tumour associated endothelial cells [14]. Vascular normalization would increase the delivery of free drug (i.e. drug that has dissociated from the carrier) across the blood vessel structure. Enhanced delivery of SN-38 achieved following administration of IrC™ would, perhaps, be even greater in regions of the tumour where vascular normalization has occurred.

The effect of the formulation on the tumour micro-environment may provide an opportunity for increasing the delivery and efficacy of a second drug in GBM tumours while also contributing to the therapeutic effects seen with IrC™. It is well established that the anti-proliferative effects of SN-38 increase significantly with exposure time [278, 279]. Hence, the therapeutic activity of irinotecan is increased by the extended exposure of tumour cells to the drugs provided by the drug carrier. This dual mechanism of activity ensures maximal efficacy as judged by the GBM orthotopic model used in this report. The preclinical data generated through this research will be used to support further development of IrC™ for treatment of GBM.

### **3.6 Acknowledgements**

Animal studies were conducted with the support of the excellent staff within the Animal Resource Center at the BC Cancer Agency's Research Centre. The authors would like to thank Dr. Jennifer Flexman for the development of the in-house segmentation algorithm.

# **Chapter 4: Development of glioblastoma cell lines expressing red fluorescence for non-invasive live imaging of intracranial tumours**

## **4.1 Introduction**

Chapter 2 demonstrated important differences in the effect of the liposomal formulations on the vasculature of GBM tumours grown subcutaneously or orthotopically, supporting the fact that studies aimed at exploring the use of a compound for the treatment of GBM in models representative of the clinical reality should be conducted using orthotopic models. Hence, the efficacy study presented in chapter 3 was conducted in an orthotopic model. However, most efficacy studies conducted in brain tumour orthotopic models will use changes in health status as an endpoint. In order to be able to follow the progression of orthotopic GBM tumours in live animals, GBM cell lines expressing red fluorescent proteins were developed in the following study as a tool for tumour imaging in live animals. When this project was initiated, it was expected that a fluorescence-expressing model could be used for all subsequent studies presented in this thesis. However, some challenges were encountered, as will be described, which caused substantial delays in the availability of the model. This chapter is then presented as the development of a model that could be used for future studies on GBM in this laboratory.

<sup>4</sup>Bioluminescent imaging (BLI) is widely used for non-invasive imaging in pre-clinical cancer models [280]. The transduction/transfection of cancer cells with the firefly luciferase gene results in the expression of an enzyme capable of generating visible light by oxidization of its substrate luciferin. This light signal, in turn, can then be detected and used to monitor cancer development, metastasis and/or responses to treatments. It is well established that luciferin is able to cross the blood brain barrier [281-283]. However, in the case of glioblastoma multiforme

---

<sup>4</sup>This chapter was accepted for publication by Anticancer Research in April 2011: M. Verreault, D. Strutt, D. Masin, D. Fink, R. Gill and M.B. Bally. Development of Glioblastoma Cell Lines Expressing Red Fluorescence for Non-invasive Live Imaging of Intracranial Tumours. Anticancer Research. 2011; 31(8): in press.

(GBM), the tumours are generally poorly perfused [7, 80] and hypoxic [284], and these factors can interfere with the distribution and oxidization of luciferin which is typically administered 20-30 minutes prior to BLI [280]. Furthermore, the ability of luciferin to access the tumour cells can also be influenced by blood vessel structure and function within the tumour and the surrounding tissue [285], and treatment-induced changes in vascular perfusion may affect interpretation of BLI images [286]. The use of fluorescent proteins [287] provides an interesting complementary technique to BLI since the fluorescent signal is generated from within the tumour without the need for substrate administration and delivery to tumour cells. The use of red-shifted fluorescent proteins allows for better signal penetration through biological tissue [288] and reduced interference from hemoglobin [289] compared to other fluorescent proteins such as the green fluorescent protein (GFP). Furthermore, recent advances in imaging technologies using multi-spectral detection methods has led to considerable improvements in signal-to-noise ratio and sensitivity of fluorescence imaging [290, 291].

In this study, the development and characterization of U251MG cell lines expressing the red fluorescent proteins mKate2 [289] or mCherry [292] is described. It was found that the transfected population sorted by flow cytometry based on fluorescence intensity behaved differently. Assessing the resulting populations using *in vitro* and *in vivo* assays was necessary to obtain fluorescently labeled cell lines that exhibited growth behaviour and drug sensitivities comparable to that of the parental cell line. U251MG GBM models expressing mKate2 and mCherry were successfully developed using this strategy. To our knowledge, the development of red fluorescent protein expressing-U251MG cells for non-invasive imaging is reported here for the first time.

## 4.2 Materials and methods

### 4.2.1 Cell culture and transduction

U251MG glioblastoma cell lines and HEK 293T embryonic kidney cells (used for lentivirus production only) were purchased from American Type Culture Collection (Manassas, VA). Cell lines were used for a maximum of fifteen passages. All cell lines were maintained in DMEM medium supplemented with 1% L-glutamine, 1% penicillin/streptomycin (Stem Cell Technologies, Vancouver, BC, Canada) and 10% FBS (Hyclone, Logan, UT, USA) and cultured at 37°C in a humidified atmosphere containing 5% CO<sub>2</sub>. The U251MG mKate2 or mCherry expressing cells were generated by lentiviral transduction of U215MG cells with the gene encoding mKate2 [289] or mCherry [292], respectively. The pFUKateW or pFUCHerryW transfer plasmids were generated by inserting the mKate2 gene obtained from the pmKate2-N plasmid (Evrogen) or the mCherry gene obtained from Dr. Alice Mui (Jack Bell Research Center, Vancouver, Canada) into a pFUW vector backbone [293, 294]. Lentivirus particles were generated by incorporating pFUKateW or pFUCHerryW plasmid (10µg) with the envelope plasmid pVSV-G (2.5µg; Clontech) and the packaging plasmid pDeltaR8.91 (7.5µg) [295] in HEK 293T cells using calcium phosphate-mediated transfection (Promega, Madison, WY, USA) in serum and antibiotic-free media. Viral supernatant was harvested, filtered (0.45µm Steriflip® filters, Millipore, Billerica, MA, USA) and placed on 300,000 U251MG cells plated in a 6-well plate (2.5mL supernatant plus 0.5mL fresh serum-free media). Twenty-four hours later, supernatant was replaced by fresh serum and antibiotic containing media, and cells were expanded. Resulting mKate2- or mCherry- expressing U251MG cells were sorted by Becton Dickinson FACS 440 (Fluorescence Activated Cell Sorter) at excitation wavelength of 488 nm and emission wavelength of 590 nm. Cell populations were collected based on their relative fluorescence intensity in relation to the fluorescence intensity of the brightest cells such as: low level of expression (10-20% of maximal fluorescence intensity), medium level of expression (50-

60% of maximal fluorescence intensity), high level of expression (80-90% of maximal fluorescence intensity) and very high level of expression (90-100% of maximal fluorescence intensity). All cell lines were screened for Mycoplasma; after 3 passages in the absence of antibiotics, cell lines were shipped to RADIL (Columbia, MO, USA) where they were tested by PCR assay for all species of mycoplasma known to infect cell cultures.

#### **4.2.2 *In vitro* growth, drug sensitivity and correlation between fluorescence intensity and cell number**

Cells were plated in 96 well plates and MTT reagent (3-(4,5 dimethylthiazol-2-yl)-2,5-diphenyl tetrazolium bromide; Sigma) was added (1.25 mg/mL) at various time points after plating or after drug addition. Three hours after addition of MTT the medium was replaced by DMSO, and plates were read at 570nm using a spectrophotometer. For drug sensitivity assays, irinotecan (Sandoz, QC, Canada) or temozolomide (LKT laboratory) were added 24hrs after plating of the cells, and MTT was added 72hrs after drug addition. To quantify the correlation between fluorescence intensity and cell number, low mKate2 U251MG cells were plated at different cell density (10-100,000 cells) in triplicate in 384 well plates and imaged immediately using the CRi Maestro system. Fluorescence signal was quantified and is expressed as scaled counts/second.

#### **4.2.3 Neurosphere culture and CD24/CD44 phenotypic analysis**

For neurosphere cultures, transduced and parental U251MG cell lines were plated at 20,000 cells/well in ultralow attachment 6 well plates (Stem Cell technologies) with Neurocult NS-A basal medium supplemented with Neurocult proliferation supplement (Stem Cell technologies), Epidermal growth factor (20ng/mL), Fibroblast growth factor (10ng/mL) (Clonetics®, Lonza) and heparin (2µg/mL; Pharmaceutical Partners of Canada) and allowed to grow for 5 days at 37°C. Neurospheres larger than 10 individual cells were counted under a phase contrast microscope.

For CD24/CD44 surface-marker analysis, cells were harvested with 2.5mM EDTA in PBS, washed with cold 0.1% BSA-PBS buffer and incubated on ice with the undiluted antibodies FITC-CD24 (#555427 from Pharmingen) and APC-CD44 antibodies (#559942 from Pharmingen), or with mouse IgG2bk-APC (#555745 from Pharmingen) and with mouse IgG2ak-FITC (#555573 from Pharmingen) for 45 minutes. Cells were then washed with cold 0.1% BSA-PBS buffer and analyzed by FACS. The profile of the JIMT-1 cells (mainly CD44+/CD24+ population [296]) is also shown in Figure 22 as a validation of the antibodies used.

#### **4.2.4 Subcutaneous or orthotopic implantation of mKate2 or mCherry expressing U251MG cell lines**

All protocols involving work with live animals were reviewed and approved by the University of British Columbia Animal Care Committee. For the subcutaneous GBM model, cells ( $5 \times 10^6$ ) were implanted subcutaneously (s.c.) into the backs of Rag2M mice (7-10 weeks old females, n=9). S.c. tumour size was measured throughout the study by caliper and tumour weights were extrapolated from the measurements ( $\text{mg} = (\text{tumour width}^2 \times \text{tumour length})/2$ ). To generate orthotopic GBM tumours,  $7.5 \times 10^4$  cells were implanted into the right caudate nucleus-putamen of Rag2M (5-6/Gr.) or NOD-SCID (4/Gr.) mice using a stereotaxic injection frame (Stoelting Company, Wood Dale, IL, USA). Animals were anesthetized with a Ketamine; Xylazine; ACE mix (120mg/kg i.p.; 10mg/kg i.p.; 0.5mg/kg s.c.) and supplemented with Metacam (1mg/kg s.c.). A burr hole was drilled (Ideal micro-drill<sup>TM</sup> and burr size 0.8mm; Harvard Apparatus, MA, USA) 1.5 mm to the right of midline and 1mm anterior to bregma. The needle of a 10 $\mu$ L Hamilton syringe was slowly inserted through the brain at a depth of 3.5mm and cells were injected at a rate of 1  $\mu$ L/min using an automatic injector (Stoelting Quintessential Injector, Stoelting Company). For the temozolomide (TMZ) efficacy study, mice were injected i.p. with TMZ at a dose of 65mg/kg on Tuesdays and Fridays starting 21 days after tumour cell

inoculation. This treatment schedule was continued for 3 weeks. Mice were imaged while under isoflurane anesthesia using the CRi Maestro system, and fluorescence signals are expressed as scaled counts/second. Prior to scanning, hair was removed from the head using Nair as hair interferes with the imaging method.

All animals were terminated 42 days following tumour cell inoculation using CO<sub>2</sub> asphyxiation and the brains were harvested and cryopreserved in OCT (Sakura Finetek, Torrance, CA, USA) on dry ice and stored at -80C. OCT preserved brains were cryosectioned and 10µm sections were collected from the Bregma +1.0 location. Sections were imaged for mCherry or mKate2 (CY3 filter) using a robotic fluorescence microscope (Leica DM6000B, Leica, ON, Canada), and counterstained with the nuclear dye Hoechst 33342 (1:3000; Sigma; A4 filter). Tumour area was quantified in pixel counts on the acquired images (MATLAB, The Mathworks, Natick, MA, USA) by excluding necrotic and non-tumour areas, and composite colour images were produced (Surveyor software, Objective Imaging Ltd.). Another set of sections was stained with hematoxylin and eosin (H&E) for histopathology analysis.

#### **4.2.5 Statistical analysis**

All statistical data were collected using GraphPad Prism (San Diego, CA, USA). For single comparisons, statistical analysis was done using the single comparison non-parametric two-tailed Mann Whitney test. For multiple comparisons, analysis was done using a one-way ANOVA test with Tukey post-tests. All data are expressed as mean +/- S.E.M.

### **4.3 Results and discussion**

The U251MG cells were transduced with lentivirus to generate a cell population expressing mKate2 fluorescent protein [289]. mKate2-transduced U251MG cells, when viewed under a fluorescence microscope, revealed highly variable fluorescence, as illustrated in the micrograph shown in Figure 20a. Given this variability, mKate2 transduced U251MG cells were

sorted by flow cytometry (FACS) into four populations based on their relative fluorescence intensity. Although U251MG is a stable cell line derived from human glioblastoma multiforme (GBM), it was previously described as heterogeneous [297]. The concept of heterogeneity of a tumour cell population was recognized in earlier studies [298] in regards, for example, to variability in expression of cell surface antigens [299] and metastatic potential [300], and more recently by research highlighting the importance of tumour initiating cells within a tumour cell population [301, 302]. In order to preserve the line's heterogeneity, FACS-based sorting of fluorescence-positive cell populations of various intensity was preferred over clonal selection. Following isolation of the different populations, cells were expanded in culture and the stability of fluorescence expression was confirmed for up to 10 passages by FACS. As illustrated in Figure 20b, FACS analysis of the resulting cell populations after expansion show cells expressing low (10-20% of maximal fluorescence intensity; Low mKate2), medium (50-60% of maximal fluorescence intensity; medium mKate2), high (80-90% of maximal fluorescence intensity; high mKate2) and very high (90-100% of maximal fluorescence intensity; very high mKate2) levels of mKate2 expression. The resulting cell populations were then compared to the parental U251MG cells with the goal of selecting the cell populations which exhibit *in vitro* and *in vivo* growth that was similar to the parental cell line. The results, summarized in Figure 20c and d, demonstrate that very high, high and medium mKate2 expressing cells grew slower, an effect that was particularly evident *in vivo* (Figure 20d). In contrast, the low mKate2 U251MG cell population exhibited a proliferation rate (determined by MTT assay) that was not significantly different from the parental line (Figure 20c). The *in vivo* growth rates of s.c. tumours arising following inoculation of the low mKate2 expressing cell population were also comparable to the parental cell line (Figure 20d). For the mKate2 transduced cell lines, differences in growth rates between the populations with different fluorescence levels may be due to differences in the gene copy numbers transduced into cells.

**Figure 20: Selection and characterization of mKate2 transfected U251MG cells expressing low, medium, high and very high levels of the fluorescent protein.**

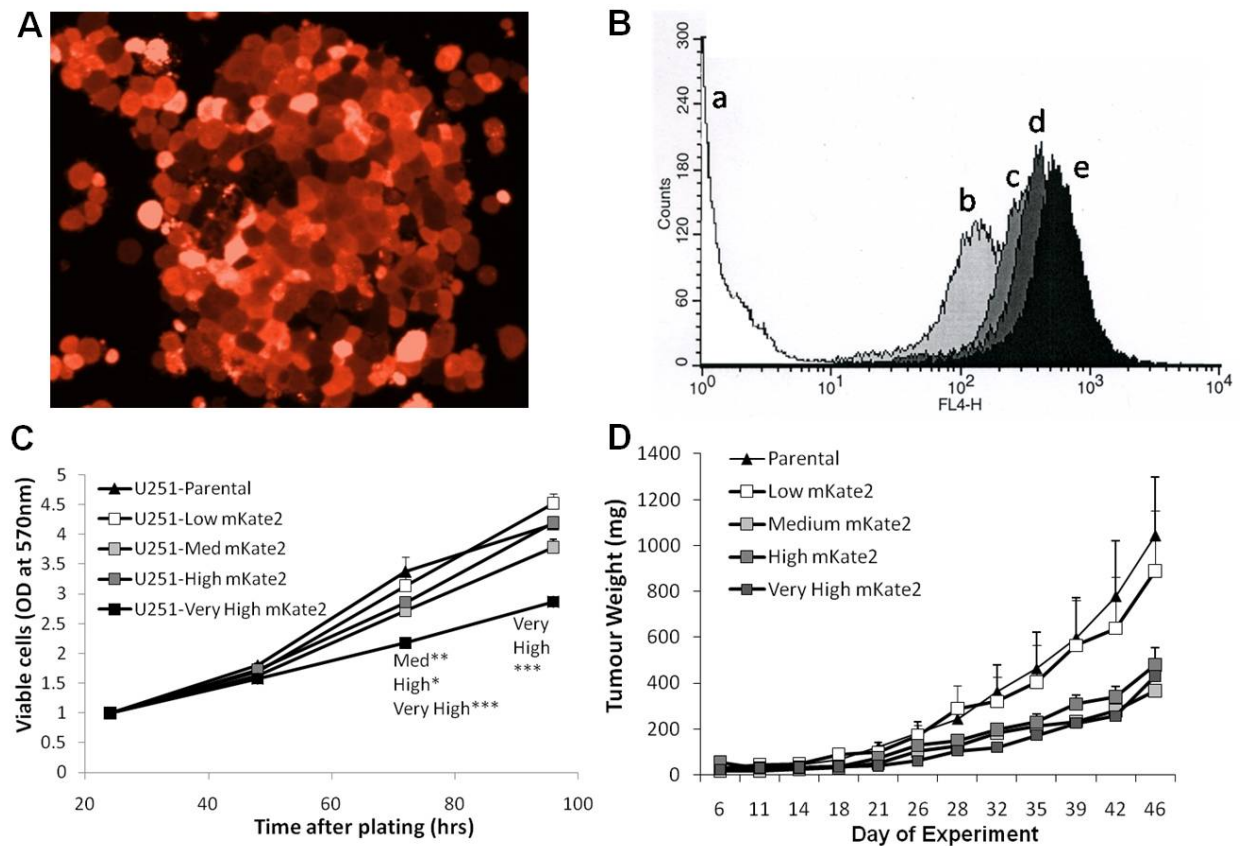


Figure 20: a) Lentivirus transduced, unsorted mKate2-expressing U251MG as observed by fluorescence microscopy; b) mKate2 transfected U251MG cells were sorted by flow cytometry for low (peak b; average signal of 155 fluorescent units), medium (peak c; average signal of 331 fluorescent units), high (peak d; average signal of 389 fluorescent units) or very high (peak e; average signal of 556 fluorescent units) levels of mKate2 expression. Peak a (average signal of 1.5 fluorescent units) represents the parental U251MG cells. c) In vitro U251MG cell proliferation (determined by MTT assay, see Methods) and D) subcutaneous (s.c.) growth of U251MG cells with low (□), medium (□), high (■) and very high (■) levels of mKate2 expression compared to the parental line (▲). For in vitro studies, the error bars represent the standard deviation determined from 3 separate experiments each determined in triplicate. For in vivo

*studies, the error bars represent standard error of the mean determined from 4 animals. \*p-value < 0.05; \*\*p-value < 0.01; \*\*\*p-value < 0.001*

To confirm the correlation between populations' fluorescence intensity and growth rates, mCherry lentivirus transduction of the U251MG cells was also completed and, as described above for the mKate2 expressing cells, the resulting cell population was sorted by flow cytometry into three cell populations expressing low, medium and high levels of mCherry. On the basis of a single time point (96hrs after plating) determined *in vitro*, it was evident that the high mCherry cell line grew slower than the medium, low and un-transduced parental cell populations (Figure 21a). While all three cell lines could be maintained in culture, the growth of tumours following s.c. inoculation of the three cell lines was remarkably different. Both parental and high mCherry cell lines (Figure 21b inset) could generate measureable tumours when inoculated s.c. into Rag2M (~40 mg by day 6; determined by caliper measurements). However, by day 11, the high mCherry expressing tumours had regressed. Eighteen days following cell inoculation of the parental line, tumours were approximately 120 mg, while the high mCherry expressing tumours were no longer detectable. One possible explanation for this may involve the high levels of mCherry protein expression and development of an immune response similar to what has been previously reported for green fluorescent protein (GFP) expressing cells [303]. However, the fact that both the low and medium mCherry expressing cell lines were able to establish solid tumours for more than six weeks following s.c. inoculation (Figure 21b) suggests that mCherry, in itself, is not sufficient to induce immune response capable of causing tumour rejection in these animals. In fact, the medium mCherry U251MG expressing cells exhibited *in vivo* growth rates comparable to that of the parental line (Figure 21b). In contrast to results obtained with mKate2 expressing cells, the low mCherry expressing cells produced much smaller tumours, suggestive of a significantly slower growth rate *in vivo* (Figure 21b). These observations may suggest that, for these transduced cell populations, differences in growth rate

cannot be explained simply on the basis of gene copy number introduced into the parental cells. Regardless of the mechanism(s) influencing the growth rate of the transduced cell lines, the results indicated that U251MG cells expressing mKate2 (low mKate2) or mCherry (medium mCherry) with growth rates comparable to the parental population could be successfully generated.

**Figure 21: Characterization of mCherry transfected U251MG cells expressing low, medium and high levels of the fluorescent protein.**

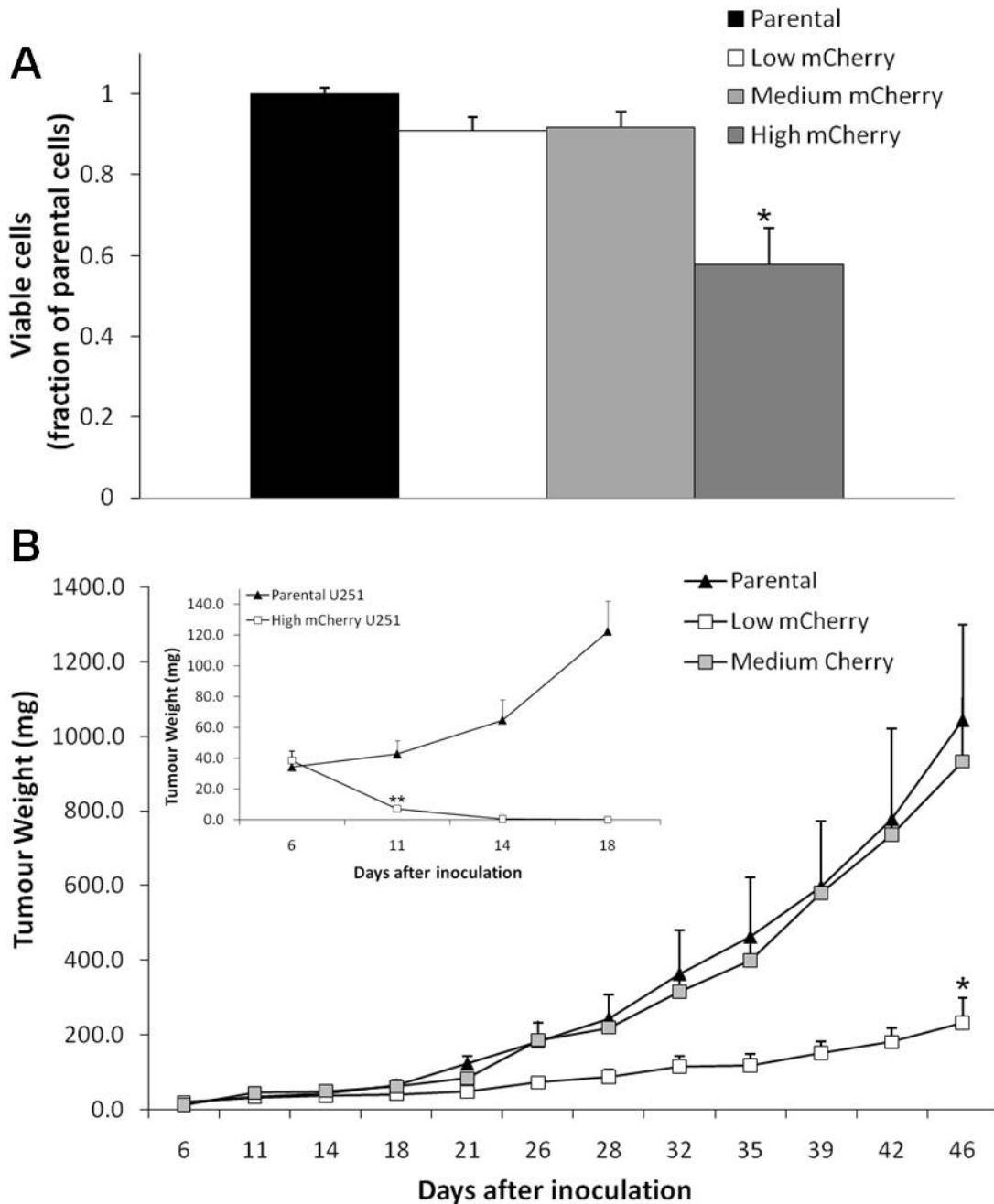


Figure 21: a) The amount of viable cells (determined by MTT assay, see Methods) expressed as a fraction of the parental U251MG cell line obtained 96hrs after plating the indicated cell populations and b) s.c. growth of U251MG cells with low (□) and medium (▣) levels of mCherry expression compared to the parental line (■). Inset) s.c. growth of U251MG cells with high (▣) levels of mCherry expression compared to the parental line (■). For *in vitro* studies, the error bars represent the standard error of the mean determined from 3 separate experiments each determined in triplicate. For *in vivo* studies, the error bars represent standard error of the mean determined from 4 animals. \**p*-value < 0.05; \*\**p*-value < 0.01.

The next step that was taken to characterize the mKate2 and mCherry cell lines involved an evaluation of the cancer stem-like cell fraction and surface marker analysis within transduced cell lines as one approach to determine whether the cell population's inherent heterogeneity was maintained. An analysis of the stem-cell like properties of U251MG based on CD133 expression, self renewing capacity and sphere formation in culture (neurosphere) was completed by other investigators [302] and they provided evidence suggesting that this cell line contains more cancer stem-like cells when compared to other commonly used GBM cell lines. It should be noted that the presence of cancer stem-like cells influences tumour growth and behaviour *in vivo* [301]. To provide an indication of the stem cell-like properties, the current study evaluated neurosphere formation (Figure 22a). The neurosphere generation capacity of the transduced cell populations was comparable to the parental line. More specifically, the number of neurospheres counted in parental, low mKate2 and medium mCherry plated wells were similar. A CD24/CD44 cell surface marker analysis of the transduced cell populations was also determined and compared to that of parental line. CD44 is overexpressed in GBM tumours [304] and was shown to be associated with cancer progression and malignancy [305, 306], whereas low levels of CD24 expression were shown to be associated with a central nervous system stem cell phenotype [307, 308]. The profile of the JIMT-1 cells (mainly CD44+/CD24+ cell populations

[296]) is also shown as a validation of the antibodies used. The parental U251MG line as well as low mKate2 and medium mCherry U251MG lines are CD44+/CD24- (Figure 22b) and no difference was noted between profiles of all three lines. The capacity of the medium, high, very high mKate2 U251MG and low mCherry lines to form neurospheres in culture as well as their CD24/CD44 phenotypes were also evaluated. No difference was found when these cell populations were compared to the parental line. It can thus be concluded that the selection process did not impact the neurosphere forming capacity and expression of CD24/CD44 cell surface markers of the GBM lines.

**Figure 22: The neurosphere forming fraction and CD24/CD44 phenotype of transduced lines is comparable to the parental line.**

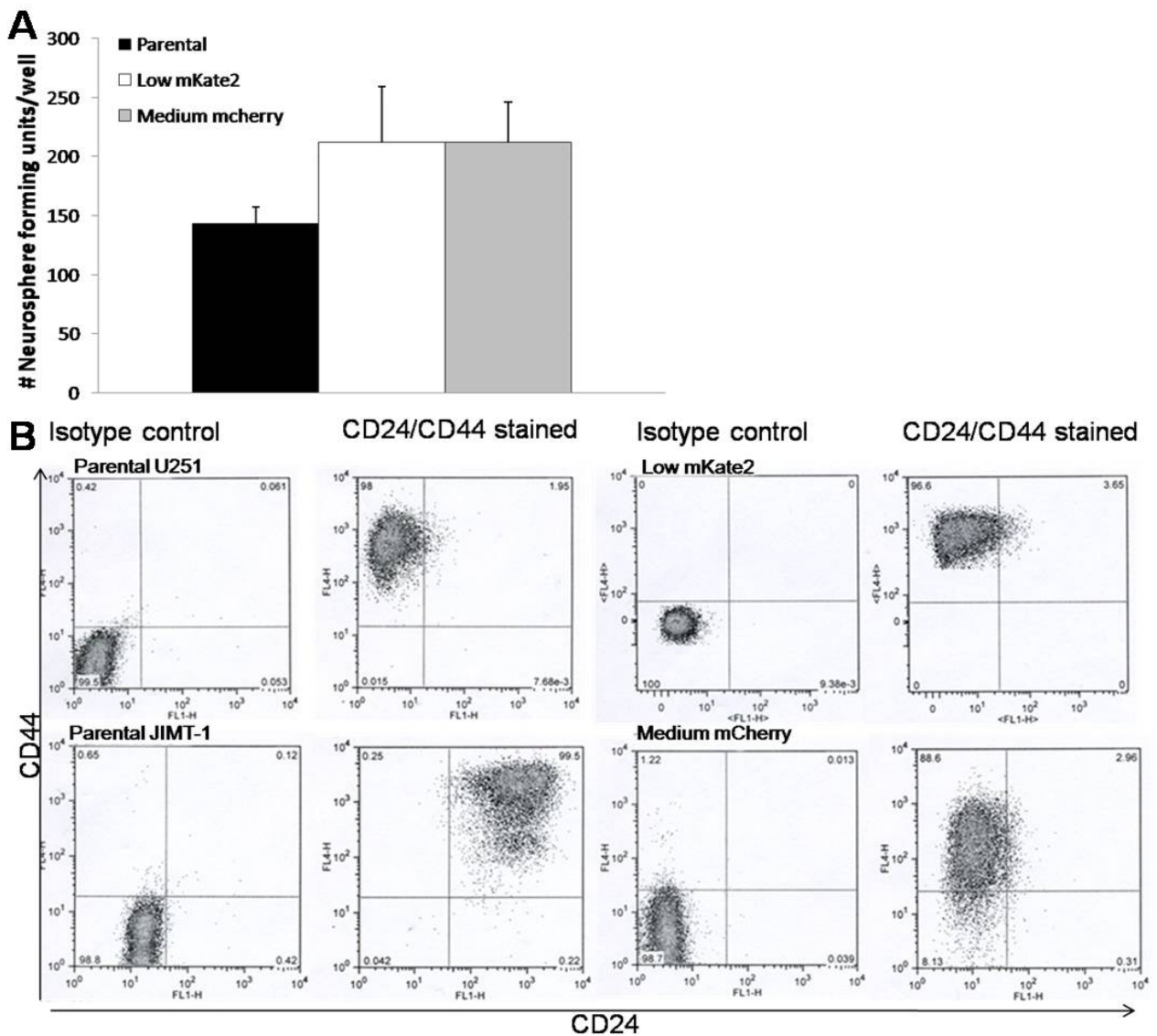
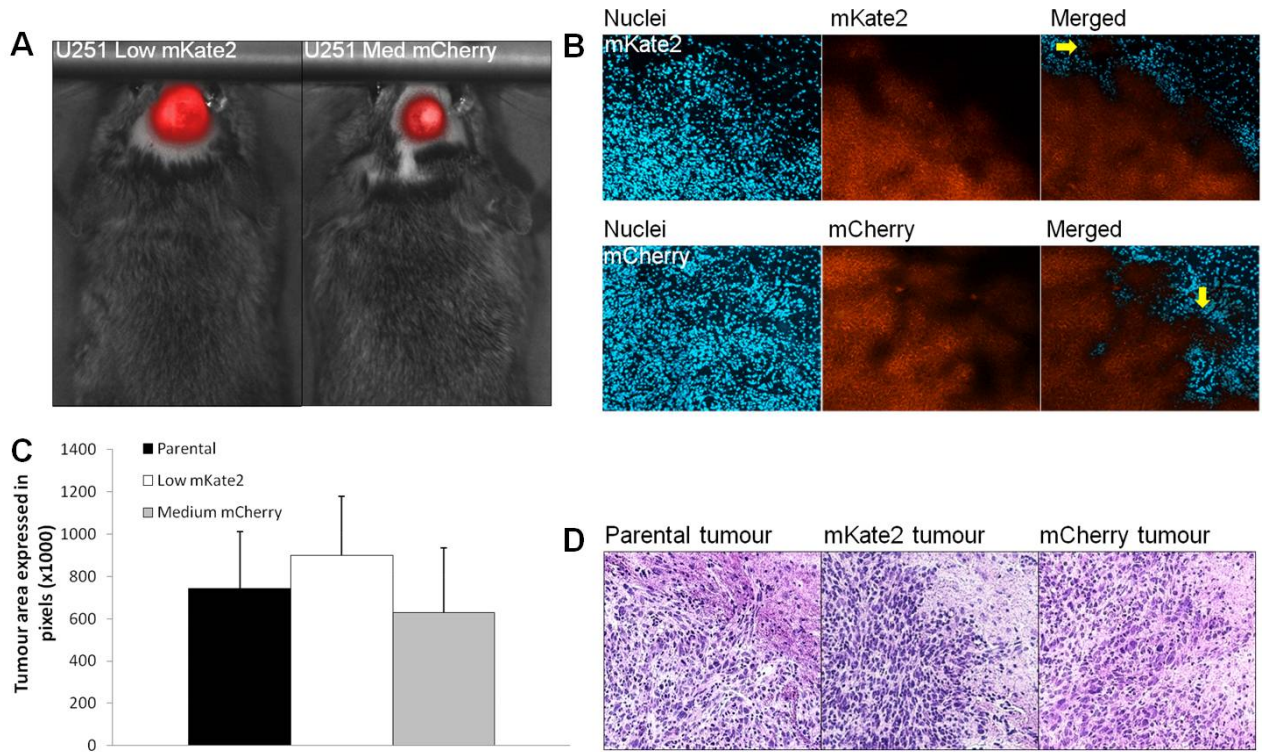


Figure 22: a) A five-day neurosphere culture assay of transduced and parental populations showed no significant differences between populations. Neurosphere forming units derived from parental U251MG cells (■), U251MG cells expressing low levels of mKate2 (□) or medium levels of mCherry (▣). Error bars represent the standard deviation determined from 3 independent experiments. b) CD24-FITC (FL1-H) and CD44-APC (FL4-H) phenotypic analysis of parental, low mKate2 and medium mCherry U251MG lines. JIMT-1 is shown as a validation of the antibodies used in the assay. Graphs on the left show isotype control cells (non-specific

background staining) and on the right, CD24/44 stained cells. Graphs are representative of 3 independent experiments.

To establish the utility of these cell lines for *in vivo* imaging, cells were implanted orthotopically into Rag2M mice (see Methods) and animals were imaged using the Maestro multispectral fluorescent imaging system 42 days after tumour cell inoculation. Representative images of mice bearing low mKate2 or medium mCherry U251MG orthotopic tumours are shown in Figure 23a, which illustrates that the tumours can be easily detected using the Maestro imaging system. Brains from these animals were harvested, sectioned and imaged for the fluorochrome (red) and counterstained with Hoechst 33342 nuclear dye (blue) (Figure 23b). A homogeneous expression of the fluorochromes could be seen across the entire tumour, and the absence of tumour area negative for the fluorochrome suggests that the cell populations did not lose fluorescent protein expression after implantation and expansion *in vivo*. Tumour size was evaluated by pixel counts of viable tumour areas (excluding necrotic and non-tumour areas) from Hoechst 33342 images acquired by robotic microscope scanning of tumour sections (see Methods). Tumour size quantification showed no difference between low mKate2, medium mCherry and parental U251MG tumours (Figure 23c). H&E staining of the tumour sections showed similar histological appearance between the different tumour models (Figure 23d). More specifically, high cellular density could be observed in the tumour (dark purple) and there was evidence of tumour cell invasion from the tumour edges to the surrounding tissue. Importantly, tumour cell invasion from the tumour (red in the merged image) into the surrounding brain tissue (blue in the merged image) was easily detected when the red fluorescent U251MG cells were used (Figure 23b arrows).

**Figure 23: Parental, mKate2 (low) and mCherry (medium) expressing U251MG cells grow when implanted orthotopically in Rag2M mice.**



*Figure 23: a) Representative images, obtained using the Maestro live imaging system, of mice with intracranial mKate2 (low) or mCherry (medium) expressing tumours. b) Brains were harvested at the end of the study on day 42, sectioned and imaged for the respective fluorochrome (red) and counterstained with Hoechst 33342 nuclear dye (blue). Tumour cells invading from the tumour core (red, located at the bottom left corner of each image) into the surrounding brain tissue (blue, located in the top right corner of each image) can be seen (yellow arrows). c) Tumour area was assessed in brains from animals inoculated with mKate2 (low; □) U251 cells, mCherry (medium; ▤) U251 cells and the parental tumours (■). d) H&E sections from parental, mKate2 (low) and mCherry (medium) tumour-bearing animals show high nuclear density in the tumour (dark purple, bottom left corner of each image) and evidence of tumour cell invasion in surrounding brain tissue (top right corner). For in vivo studies, the error bars represent standard error of the mean determined from 4 animals.*

The correlation between fluorescence signal, expressed in scaled count/second, and cell number was then assessed *in vitro* by plating low mKate2 U251MG line in 384 wells plates (Figure 24) and imaging using Maestro. Although the signal emitted by 10 cells was comparable to background value, the signal emitted by 100-100,000 cells was above background level and the relationship between cell number and scaled count/second was linear for cell numbers  $\geq 100$ , with a correlation coefficient of  $5.2 \times 10^{-8}$  scaled count/cell. It is acknowledged that the imaging of cells in culture plates is a limited representation of three-dimensional tumour growth and the signal arising from orthotopic tumours is likely to be partially absorbed by biological tissue. However, the correlation between cell number and fluorescence intensity *in vitro* could be used to estimate the number of cells emitting fluorescent signal arising from a tumour.

**Figure 24: The relationship between fluorescence signal (scaled count/second) and cell number *in vitro* is linear for  $\geq 100$  cells.**

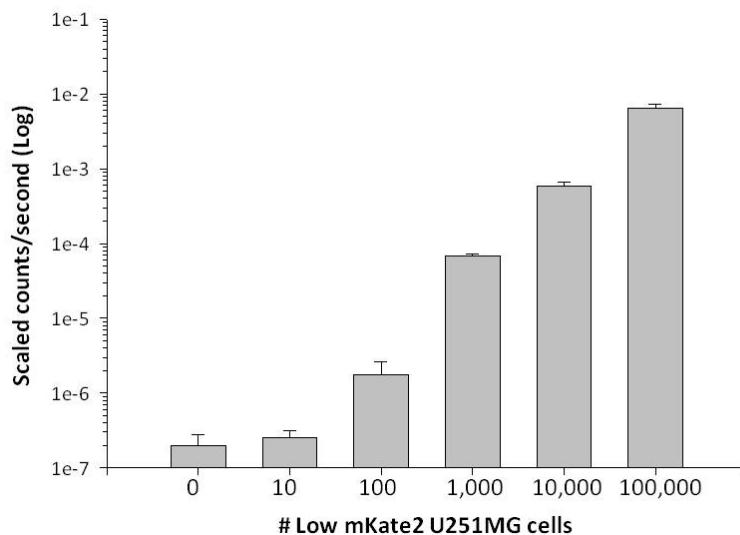


*Figure 24: The low mKate2 U251MG line was plated at different densities (10-100,000 cells) in 384 wells plates and fluorescence signals were measured by Maestro. The error bars represent the standard error of the mean determined from 3 independent experiments.*

The final aspect of the studies summarized here was to establish whether the U251MG mKate2 and mCherry-labeled cells responded to chemotherapeutic drugs in a manner that was

comparable to the parental U251MG cell line. The sensitivity of low mKate2 and medium mCherry U251MG cells to irinotecan and temozolomide (TMZ) *in vitro* were compared to that of the parental line and the results have been summarized in Figure 25a (irinotecan) and 25b (TMZ). Irinotecan activity in GBM patients has been extensively studied [35-37] and this compound is now recommended by the National Comprehensive Cancer Network for use in combination with bevacizumab (Avastin) for GBM treatment [38]. TMZ is standard of care for the treatment of GBM [3]. The irinotecan and TMZ dose-response curves for the selected mKate2 and mCherry cell populations were comparable to those obtained for the parental line (Figure 25a-b).

The effects of treating mice bearing orthotopic U251MG tumours (low mKate2 and parental lines) with TMZ were also assessed and the results of these studies are shown in Figure 25c-f. Hair from the head of the tumour bearing mice had to be removed prior to imaging with Maestro because hair interfered with the imaging method. The Rag2M mice, however, developed pigmentation on skin which was exposed to light after hair removal and this pigmentation interfered with the detection of the fluorescence signal. For this reason, imaging in this mouse strain could only be done once prior to initiation of treatment and at the end. Non-invasive imaging of the mice 42 days after inoculation of low mKate2 U251MG cell lines demonstrated that there was substantial reduction in measurable disease following treatment with TMZ and a substantial increase in measurable disease if the animals were left untreated (Figure 25c). All animals within the groups represented by the images shown in Figure 25c could be analyzed for fluorescent signal intensity, and these data, shown in Figure 25d, demonstrated that following TMZ treatment, there was an 86% decrease in mKate2 fluorescence intensity ( $p < 0.05$ ) when compared to the fluorescence intensity determined prior to treatment initiation. Based on the results summarized in Figure 24, it was estimated that the fluorescence signal emitted from tumours prior to treatment in both groups corresponds to approximately  $73-75 \times 10^3$  cells. Using

this approach, it was estimated TMZ-treated tumours were composed of approximately  $10 \times 10^3$  cells on day 42. When comparing this data to control animals on day 42, a 99.8% reduction in fluorescence intensity was measured ( $p < 0.05$ ; Figure 25d). It was estimated that the fluorescence signal emitted from untreated tumours on day 42 corresponds to approximately  $5 \times 10^6$  cells. The mKate2 fluorescence signal emitted from surviving tumour cells from TMZ-treated tumours (Figure 25e) allowed for an easy and accurate localization of the cells within the brain, which otherwise could not be easily identified using standard nuclei staining techniques, further highlighting the significant advantage of using the red fluorescent U251MG cell line for *in vivo* studies.

Hoechst 33342 was then used to quantify viable tumour area (excluding necrotic and non-tumour areas) in brain sections from parental and mKate2-tumour bearing animals (see Methods), and no significant differences were found between untreated parental and mKate2 tumour sizes (Figure 25f). These results also indicate that there was no difference between tumour sizes when comparing data from TMZ-treated parental or TMZ-treated mKate2 tumours (Figure 25f). Using this approach to assess efficacy, it can be suggested that TMZ treatment was associated with a 97% to 99% reduction ( $p < 0.01$ ) in tumour area for tumours from TMZ-treated mice compared to tumours for untreated mice; a result that was comparable for the parental and low mKate2 U251MG tumour models.

**Figure 25: The *in vitro* and *in vivo* sensitivity of mKate2 (low) to chemotherapeutic drugs is comparable to that seen for the parental line.**

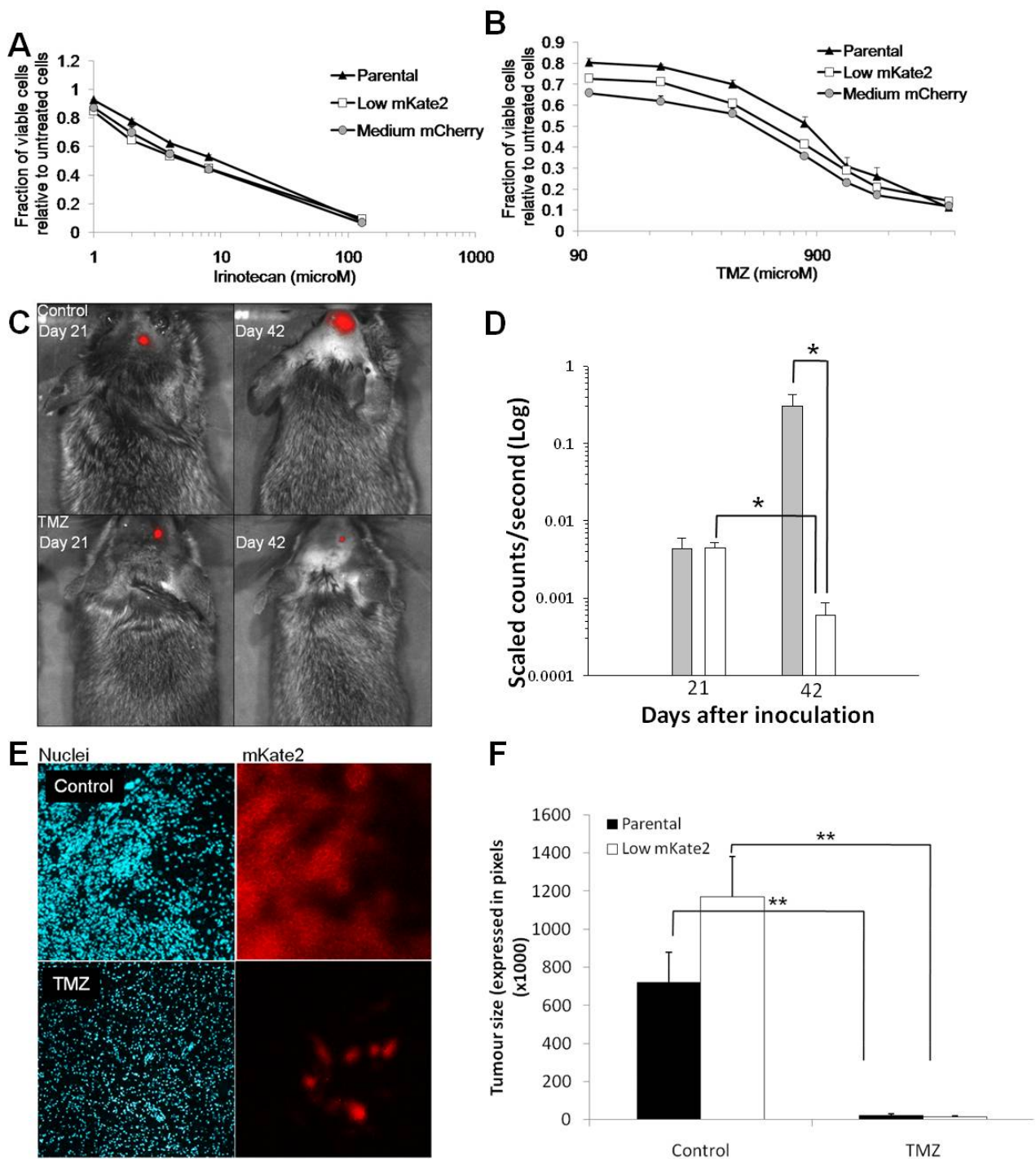


Figure 25: The sensitivity of mKate2 (low; □) and mCherry (medium; ■) expressing U251MG cells to a) irinotecan and b) temozolomide (TMZ) was assessed *in vitro* by MTT assay and compared to the parental line (■). c) The mKate2 (low) U251MG line was implanted

*orthotopically and animals were left untreated or treated with temozolomide. Representative images of mice, obtained using the Maestro live imaging unit, with control and temozolomide treated mKate2 expressing tumour-bearing animals. d) mKate2 fluorescent signal (scaled count/second) was measured prior to treatment initiation (day 21) and at the end of the study (day 42) and showed significant treatment-induced reduction in fluorescence signal intensity. Brains were harvested at the end of study (day 42) and sectioned. e) Brain sections containing mKate2-expressing tumours were imaged for mKate2 protein (red) and counterstained with Hoechst 33342 nuclear dye (blue). f) Tumour area measurement (expressed in pixels) showed no significant difference between parental (■) or mKate2-expressing (□) tumour size when animals were left untreated (control) or treated with TMZ, but treatment induced a significant reduction in tumour size in both models. For in vitro studies, the error bars represent the standard error of the mean determined from 3 separate experiments, each determined in triplicate. For in vivo studies, the error bars represent standard error of the mean determined from 4 animals. \*p-value < 0.05; \*\*p-value < 0.01.*

In order to determine if tumour growth could be monitored over time, it was necessary to consider another mouse strain. NOD.CB17-SCID mouse strain was selected as an alternative to the Rag2M mice. These mice did not develop skin pigmentation following exposure to light. The low mKate2 U251MG line was implanted orthotopically, and mice were imaged weekly. The progression of tumour development was monitored weekly by Maestro imaging. These data have been summarized in Figure 26. Figure 26a provides representative images of mice scanned weekly. Quantification of the fluorescence signal emitted from the brains of these mice (Figure 26b) demonstrates an increase in fluorescence intensity over time. Using the approach outlined in Figure 24, it was estimated that the fluorescence signal emitted from tumours on day 21, 28, 35 and 42 corresponds to approximately  $4.2 \times 10^3$ ,  $2 \times 10^6$ ,  $3.8 \times 10^6$  and  $5.2 \times 10^6$  cells,

respectively. These data would suggest that, in untreated animals, the doubling time of this tumour is 7 to 10 days.

**Figure 26: The use of albino NOD.CB17-SCID mice allows for weekly imaging of orthotopic tumour progression.**

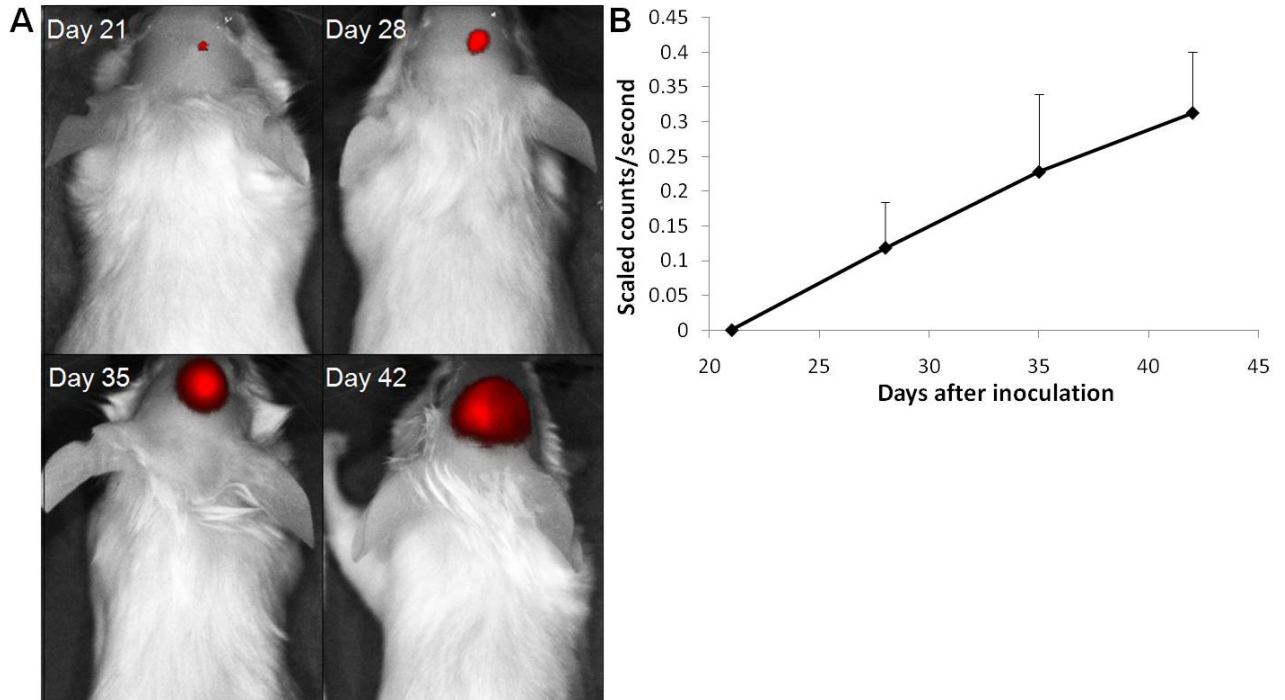


*Figure 26: The mKate2 (low) U251MG line was implanted orthotopically in NOD.CB17-SCID mice and animals were left untreated. mKate2 fluorescent signal (scaled count/second) was measured on day 21, 28, 35 and 42. a) Representative images of mice obtained by weekly scanning using Maestro live imaging unit are shown. b) mKate2 fluorescent signal (scaled count/second) was measured and show a constant progression in signal intensity over time after tumour cell inoculation. The error bars represent standard error of the mean determined from 4 animals.*

#### **4.4 Conclusion**

Cell populations expressing mCherry or mKate2 can be generated and used to establish intracranial tumours that can be imaged non-invasively. Importantly, *in vitro* and *in vivo* studies were needed to assess the behaviour of transduced cell populations in order to identify cell lines

that behaved similarly to the parental cell line. The comparisons described here emphasized on growth rates *in vitro* and *in vivo*, both as orthotopic and s.c. tumours, as well as sensitivity to drugs known to be effective against the parental cell line. It was also shown that the transduced lines retained the capacity of the original population to form neurospheres in culture. Analysis of expression of CD24 and CD44 cell surface markers further confirmed that the CD24/CD44 phenotype of the original population was preserved in the transduced lines. The results suggest that the amount of fluorescent protein generated, which presumably correlates with the number of gene copies transduced into cells, will influence the *in vitro* and *in vivo* growth of selected cell populations, but this parameter is not the only factor involved. It is recommended that investigators evaluate multiple selected populations to identify the subsets that behave comparably to the parental population. Lentiviral transduction has become a common tool in molecular biology. Uses include the development of fluorescence or bioluminescence-expressing cell lines, but these vectors are also used for knock-in [309] or knockdown studies [310]. The data reported here should be considered more generally and suggest that the process of lentivirus transduction and subsequent selection methods may generate cell lines that behave remarkably different from the parental cell line.

Regardless of these caveats, it has been demonstrated that changes in fluorescence signal intensity measured from the brain of animals inoculated with these cells lines can be used to follow tumour progression/regression and treatment efficacy. Based on this lab's experience as well as the experience of other investigators, it is well understood that intracranial tumour models are challenging from an animal ethics perspective. These animals often progress rapidly from an excellent health status to a very poor health status and health monitoring for these studies must be comprehensive in order to minimize the number of animals that succumb to the disease prior to euthanasia. Use of non-invasive imaging should prevent this problem, as tumour development can be monitored prior to any changes in health status and experimental endpoints

can be defined on the basis of tumour size measurements estimated by imaging methods. Importantly, an evaluation of fluorescent cell populations in tissue sections will also allow investigators to track residual tumour cells within the site of injection as well as invading tumour cells which may be more difficult to locate when using classical staining methods. The mKate2-U251MG tumour model is currently being used to assess the therapeutic activity of IrC<sup>TM</sup> in combination with temozolomide.

#### **4.5 Acknowledgements**

The research described in this original paper was supported by grant funding from the Canadian Institutes of Health Research (CIHR). This work would have not been possible without the support of the staff and managers working in the Animal Care Resource Centre at the BC Cancer Agency's Vancouver Research Centre. The authors would like to thank Mrs. Wieslawa Dragowska for technical help and reviewing and editing work and Mrs. Gayle Thornbury for technical help.

## **Chapter 5: siRNA-mediated Integrin-Linked Kinase suppression: nonspecific effects of siRNA/cationic liposome complexes trigger changes in the expression of phosphorylated-AKT and mTOR independently of ILK silencing**

### **5.1 Introduction**

As discussed in the introduction of this thesis, the poor survival rate for GBM patients is associated with the fact that malignant glioma is a highly aggressive and infiltrative disease typically resistant to standard chemotherapeutic agents [311]. It is becoming obvious that conventional treatment approaches (surgery, radiation and/or chemotherapy) for these patients must change if improved treatment outcomes are going to be achieved. Although it is recognized that advances in GBM treatment will continue to rely on current treatment modalities, agents targeting proteins or pathways known to be critical to the progression and infiltration of glioblastoma cells are now being evaluated in patients. These agents, used alone and in combination with established treatments, will hopefully improve treatment outcomes for individuals diagnosed with this devastating cancer.

<sup>5</sup>RNA interference has proven to be one of the most potent, robust and easy-to-use tools to inhibit gene expression [63]. For example, short interfering RNAs (siRNA) are now used routinely to assess the role of selected genes in cell-based assays. Importantly, there is also a great deal of enthusiasm for the development of siRNA sequences as therapeutics. However, there are many challenges that must be overcome if siRNA sequences are to be used therapeutically.

A major problem with the administration of chemically unmodified siRNA concerns rapid degradation, rapid elimination and poor efficacy [60]. In order to overcome these

---

<sup>5</sup>This chapter was previously published: M. Verreault and M.B. Bally. 2009. siRNA Mediated Integrin-Linked Kinase Suppression: Non-specific effects of siRNA/cationic liposome complexes trigger changes in the expression of phosphorylated-AKT and mTOR independently of ILK silencing. *Oligonucleotides*. 2009 Jun;19(2):129-40

limitations, a variety of approaches have been investigated including chemical modification and/or the use of delivery systems. With respect to the latter, lipid-based nanopharmaceuticals have shown some promise in preclinical models [312]. These formulations rely on use of cationic lipids (CL) as components to complex/bind the siRNA [56, 313, 314], albeit the formulations described are as diverse as the cationic lipids being used.

There are many issues that must be addressed if cationic lipids are going to prove to be of value in the development of siRNA therapeutics. It is understood that cationic lipids exhibit activities that can contribute to unacceptable toxicities *in vivo* [209, 315-317] and *in vitro* [318-322]. However, there is also a possibility that charged lipids can contribute non-specifically to beneficial therapeutic effects [323, 324]. This aspect of the technology has not been fully considered and the potential of the cationic lipid to exert an activity that could combine with the effect of the therapeutic siRNA has not been investigated. Such combination effect would only be observed when the therapeutic siRNA is used. It is particularly important to characterize combination effects if the downstream activity of the siRNA targeted gene is involved in cell survival pathways such as the AKT pathway which is activated in many cancers [325].

Our research group has been developing novel therapeutic strategies for patients with glioblastoma multiforme (GBM). The main pathologic characteristics of GBM are unregulated cell proliferation, necrosis and neovascularization; many of which are influenced by the phosphatidylinositol 3-kinase (PI3K) pathway and more specifically by the activity of its downstream target AKT [73, 326-328]. Upon receptor tyrosine kinase (RTK) activation, PI3K induces the attachment of AKT to the plasma membrane, where it subsequently becomes phosphorylated at two key sites, threonine 308 and serine 473, resulting in its full activation [329]. Threonine 308 is phosphorylated by phosphoinositide-dependent kinase (PDK1), whereas the identity of the so-called PDK2 responsible for the phosphorylation of serine 473 of AKT (p473-AKT) is still unclear [330]. Integrin-Linked Kinase (ILK) inhibition studies demonstrated

that this kinase is involved in PTEN regulated signaling and p473-AKT regulation, and has been proposed as a potential PDK2 [112, 118, 331-336]. ILK is a serine/threonine kinase that has been shown to interact with the cytoplasmic domain of the integrin  $\beta$ 1 subunit [337]. It is involved in signal transduction between the integrins and the focal adhesion contacts that coordinate the organization of the actin cytoskeleton [338]. ILK thus promotes resistance to anoikis, which is a specific type of apoptosis caused by detachment of a cell from its supportive matrix [339]. The mammalian Target of Rapamycin (mTOR) is also closely associated with the AKT pathway, being either activated by AKT downstream effectors [340], or contributing to AKT activation [341].

In this chapter, the role of cationic lipids in affecting intracellular signaling associated with siRNA-mediated inhibition of ILK has been investigated. Given the potential that CL could influence cell signaling events enabling cancer cell survival [318-322], it is not unreasonable to suggest that the consequences of ILK siRNA silencing may be influenced by the use of CLs. To test this hypothesis we characterized how a commonly employed cationic lipid used for siRNA transfection impacted 1) the extent of the ILK downregulation, 2) the kinetics of ILK silencing and 3) the downstream consequences of the downregulation. The studies summarized here compared changes in signaling pathways following delivery of ILK targeted siRNA by cationic liposomes (CL, Lipofectamine<sup>TM</sup> 2000) or nucleofection. Nucleofection technology (Amaxa biosystems) has been shown to be highly efficient and relatively free of non-specific effects 48h after transfection [342]. The results presented demonstrate that the CL formulation used for siRNA delivery can induce non-specific side effects exerted on the mTOR/AKT pathways.

## 5.2 Materials and methods

### 5.2.1 Cell culture and transfection

U251MG glioblastoma and PC3 prostate adenocarcinoma cell lines were purchased from American Type Culture Collection (Manassas, VA, USA). U251MG were maintained in DMEM medium supplemented with 1% L-glutamine, 1% penicillin/streptomycin (DMEM, L-glutamine and penicillin/streptomycin from Stem Cell Technologies, Vancouver, British Columbia, Canada) and 10% FBS (Hyclone, Logan, UT, USA). PC3 were maintained in Ham's F12K medium (Gibco, Invitrogen, Carlsbad, CA, USA) supplemented with 1% L-glutamine, 1% penicillin/streptomycin, 10% FBS and 1.5 g/L sodium bicarbonate (Gibco, Invitrogen). Both cell lines were cultured at 37°C in a humidified atmosphere containing 5% CO<sub>2</sub>. For all experiments, cells were used in their exponential growth phase. The cells were transiently transfected with ILK siRNA or reverse ILK siRNA using either CL (Lipofectamine<sup>TM</sup> 2000 reagent; Invitrogen, Frederick, MD, USA; composed of dioleoyl phosphatidylethanolamine (DOPE) and 2, 3-diolexyloxy- N- [2 (Spermine carboxamido) ethyl]- N, N- dimethyl- 1- propanammonium trifluoroacetate (DOSPA)) or nucleofection (Nucleofector Technology; Amaxa biosystems, Gaithersburg, MD). ILK siRNA (0.0625µg-2µg) was mixed with 6µL/mL Lipofectamine 2000 in serum-free medium, and twenty-four hours post-transfection culture medium was replaced by fresh cell medium containing 10% FBS. The Nucleofector Technology was used according to the manufacturer's optimized protocol using 0.0625µg to 2µg siRNA and 100µL of solution T for U251MG cells or V for PC3 cells (Amaxa biosystems; buffer solutions containing potassium and sodium ions, sodium chloride, sodium succinate, manitol, glucose, sodium lactobionate and/or peptides [343]) in combination with device program G16 for U251MG cells or T13 for PC3 cells, and cells were transferred to fresh cell medium containing 10% FBS immediately

after transfection. The cells were harvested using Trypsin (Gibco, Invitrogen, Burlington, Ontario, Canada) 24 to 120hrs after transfection depending on the experiment.

To determine cell doubling time in control and siRNA treated cells, samples were harvested at multiple time points and cell numbers and viability were established by counting cells with a hemocytometer. Trypan blue was used as a dye exclusion marker to assess cell viability. Viable cell concentration was calculated by subtracting the trypan blue positive cells from the total number of cells.

### **5.2.2 RNA interference**

siRNA sequences against the human ILK mRNA (Genbank accession no. GI:3150001) were generated by Qiagen, Inc. (Mississauga, Ontario, Canada) and have been designed and described previously [112, 331]. Briefly, an ILK siRNA sequence that targets the pH domain (ILK-H; sense CCU GAC GAA GCU CAA CGA GAA dTT and antisense UUC UCG UUG AGC UUC GUC AGG dTT) was used as the active silencing sequence, and a non-active reverse ILK siRNA sequence to the pH domain (Rev. Seq.; sense AAG AGC AAC UCG AAG CAG UCC dTT and antisense GGA CUG CUU CGA GUU GCU CUU dTT) was used as the inactive control sequence. Both sequences were verified using NCBI Basic Local Alignment Search Tool (BLAST) to confirm specificity or non-specificity of the active and non-active sequences respectively.

### **5.2.3 Flow cytometric assay and fluorescence microscopy**

A Cy5-tagged ILK-H sequence was used for fluorescence microscopy and flow cytometric assays. Cells were transfected using nucleofection or CL. They were harvested 6h after and analyzed with a FACScalibur flow cytometer (Becton Dickinson, San Jose, CA, USA) for Cy5 fluorescence intensity and viability after propidium iodide staining (PI; 1µg/mL). Events recorded below 138 units on the forward scattered signal channel (FSCH) were excluded from all analyses as they were considered to be due to insignificant debris. Events recorded

above 46 units on the FL4 channel were considered CY5 positive cells. The cells were counterstained with the nuclear stain Hoechst 33342 (1:333 dilution, Sigma), imaged using a fluorescence microscope (40x magnification; Leica DMLB, McBain instruments, Phoenix, AZ, USA) and photographed using the software Openlab (Improvision inc., Lexington, MA, USA). Hoechst and CY5 fluorescence microscopy images were subsequently overlaid and aligned to generate false colour images using Adobe Photoshop (CS).

For cell cycle flow cytometry analysis, cells were harvested 72h after transfection and fixed overnight in 70% ethanol at -20°C and stained with PI containing buffer (PI 50µg/mL; RNase 1mg/mL; Triton X-100 0.1% in PBS) for an hour on ice and analyzed with the flow cytometer. All flow cytometry data and fluorescence microscopy images are representative of at least two independent experiments for which similar results and observations were obtained.

#### **5.2.4 Western blot analysis**

Total protein extracts were isolated from transfected and control cells in lysis buffer (150mM NaCl, 1% NP40, 0.5% sodium deoxycholate, 2.5 mM EDTA, 0.1% SDS, Mini protease inhibitor cocktail tablets from Roche Diagnostics, Mannheim, Germany). Proteins (50µg as determined by Bradford assay) were resolved on 4 to 15% gradient SDS-polyacrylamide pre-cast gels (Bio-Rad, Hercules, CA, USA). Proteins were transferred to nitrocellulose membrane (Pierce, Rockford, IL, USA) and membranes were blocked with Rockland blocking buffer (Gilbertsville, PA, USA) for two hours. The blots were labeled using the following antibodies: anti-ILK (Antibody #3862; rabbit polyclonal; 1:1000 dilution; Cell Signaling Technology, Inc., Danvers, MA, USA), anti-AKT (Antibody #9272; rabbit polyclonal; 1:1000 dilution), anti-phosphorylated AKT-Ser<sup>473</sup> (Antibody #9271; rabbit polyclonal; 1:1000 dilution), anti-PDK1 (Antibody #3062; rabbit polyclonal; 1:1000 dilution), anti-phosphorylated PDK1-Ser<sup>241</sup> (Antibody #3061; rabbit polyclonal; 1:1000 dilution) and anti-mTOR (Antibody #2972; rabbit polyclonal; 1:1000 dilution) and anti-β-actin (AC-15; mouse monoclonal; 1:20000 dilution;

Sigma-Aldrich, Oakville, Ontario, Canada). The secondary antibody used was horseradish peroxidase-conjugated anti-mouse or anti-rabbit IgG (Promega, Madison, WI, USA) at 1:5000 dilution. Proteins were detected by enhanced chemiluminescence (Amersham Pharmacia Biotech, Buckinghamshire, UK) and visualized after exposure to Kodak autoradiography film. Scanning densitometry (Un-Scan-It software; Silk Scientific, Inc., Orem, UT, USA) was done to quantify band intensities by volume/area integration. Densitometry values were normalized to corresponding  $\beta$ -actin or total protein. Each western blot figure is representative of at least three independent experiments and the variability between experiments is indicated by the densitometry results and associated error bars representing the standard error of the mean (SEM). Due to the qualitative nature of western blots technique, no statistical analysis was performed on these values and if individual values were two standard deviations away from the group mean (either below or above), then that value was considered as an extreme value and was excluded from the analysis.

### **5.2.5 Statistical analysis**

All statistical data were collected using GraphPad Prism (San Diego, CA, USA). Parametric analysis was done using standard deviation, mean and n, in an unpaired two-tailed Student T-test.

## **5.3 Results**

### **5.3.1 siRNA delivery efficiency**

A Cy5-tagged siRNA sequence targeting ILK was used to evaluate siRNA delivery to cells in culture. The addition of the Cy5 tag did not interfere with the silencing action of the siRNA and the attached tag has been shown by others to be a representative marker for siRNA cellular delivery [344]. siRNA was delivered to cells using lipofection based or nucleofection approaches. The levels of Cy5 associated with U251MG glioblastoma cells were then assessed

by flow cytometric analysis. Representative results have been summarized in Figure 27a, where cells treated with comparable siRNA levels (2 $\mu$ g Cy5-siRNA) and under conditions where  $\geq 75\%$  viability was achieved (as determined by PI labeling), were scanned 6hrs after siRNA delivery was initiated. More specifically, the viability at 6hrs following treatment for control (mock treated cells) cells, siRNA treated cells by nucleofection and siRNA treated cells by CL was 86%, 78% and 75%, respectively. Seventy-two hours after treatment, there was no difference in cell viability ( $>90\%$  viable) between the control and the transfected populations. The population of Cy5 positive cells was lower (79%) when using the nucleofection method when compared to the lipofection method (94.7%). In addition, as illustrated in Figure 27b where Cy5 fluorescent intensity was measured as a function of the added amount of siRNA, the fluorescence intensity of Cy5 labeled cells was 12 to 30 times greater when siRNA was delivered using lipofection methods as compared to nucleofection method ( $p < 0.0001$ ). siRNA delivery using both techniques was also optimized for PC3 cells to obtain maximal cell viability and delivery. The results are similar to those obtained with the U251MG cell, i.e. siRNA delivery was an order of magnitude greater if lipofection was used as the method to promote siRNA delivery.

The flow cytometry data were confirmed by direct visualization of the targeted cell populations. To visualize Cy5 delivery to U251MG and PC3 cells, fluorescence photographs were obtained 24hrs after transfection and the results have been summarized in Figure 27c-f. The representative photomicrographs suggest that cell (U251MG and PC3)-associated fluorescence was diffuse and homogenously distributed in cell cytoplasm when the siRNA was delivered using nucleofection methods. Following delivery of siRNA by cationic liposomes, the cells exhibited bright fluorescent puncta which were not visible when examining the cells under bright field. This observation suggests that the greater fluorescence intensity observed when using lipofection methods (see Figure 27a) was associated with Cy5-labeled siRNA/CL

complexes, and not intracytoplasmic delivery, at least at the 24hr time point when these cells were evaluated.

**Figure 27: Delivery of CY5-siRNA using Lipofectamine 2000 or nucleofection**

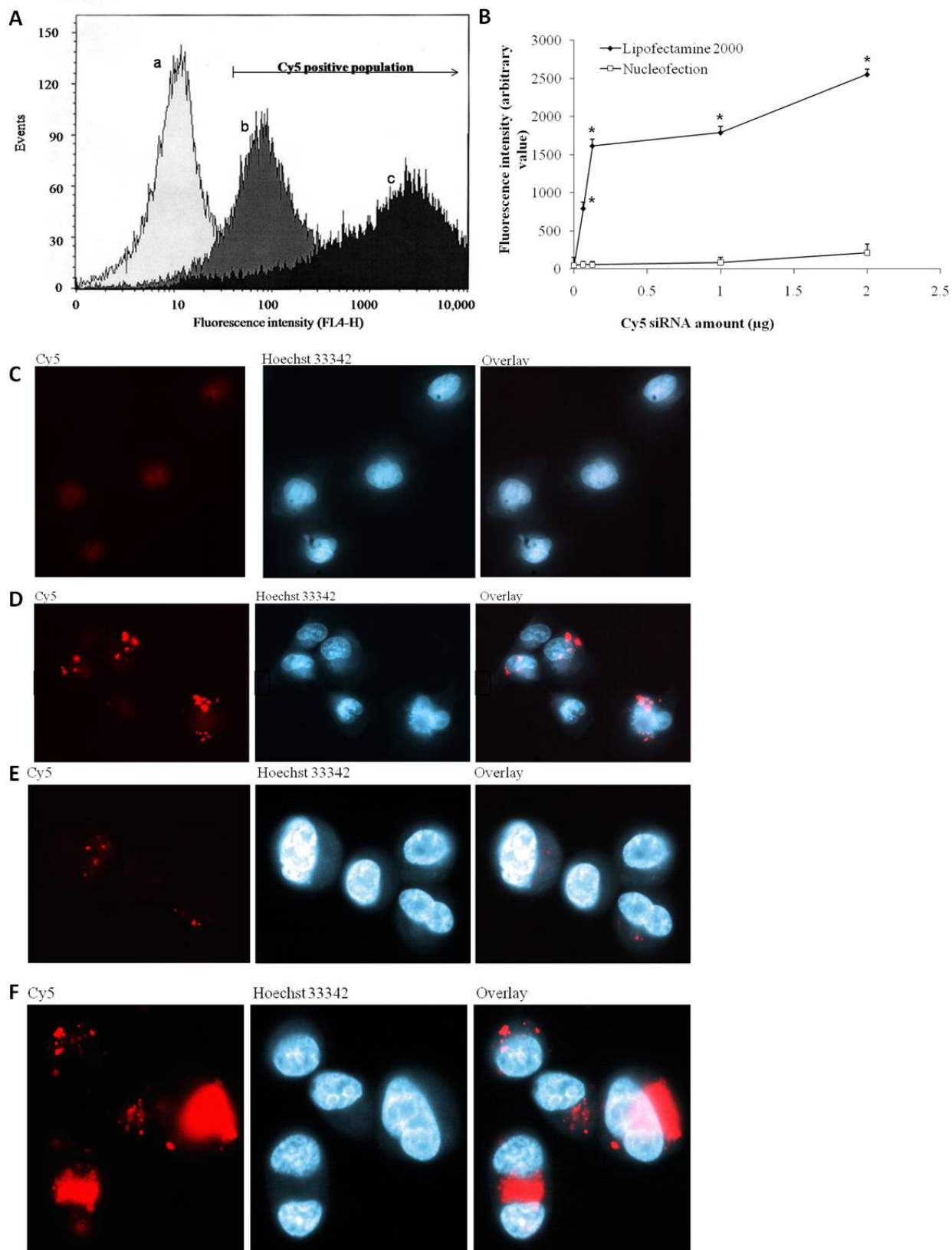


*Figure 27 a): Fluorescence distribution pattern detected by FL4-H channel of Control U251MG cells (peak a), U251MG cells transfected with 2 $\mu\text{g}$  Cy5-siRNA using nucleofection (peak b) or*

*CL (peak c). The arrow represents the threshold for the Cy5-positive population as determined by the end of extreme right tip of the control population. b) Increasing fluorescence correlating with increasing siRNA amounts using nucleofection or CL transfection techniques. Error bars represent the standard deviation obtained following analysis of at least 2 replicas. Representative fluorescence photomicrographs showing U251MG cells 24hrs following delivery of Cy5-labelled siRNA using c) nucleofection or d) CL; and PC3 cells 24hrs following delivery the Cy5-labelled siRNA using e) nucleofection or f) CL. Red is CY5 fluorochrome and blue is the nuclear staining Hoechst 33342. These studies were repeated at least 3 times and the images provided are representative of the individual studies. \*p-value <0.0001*

The impact of siRNA treatment on cell growth was evaluated and the cell (PC3 or U251MG) doubling time was measured by counting cells at various time points after siRNA addition (24-120h). The time required for the cell density to increase from  $2.4 \times 10^5$  cells/mL was used to estimate the doubling time. For example, untreated PC3 cells exhibited a cell doubling time of approximately 29hrs, which is comparable to previously published results [345]. Seventy-two hours after the ILK-specific or the non-active sequence siRNA delivery by nucleofection, the cell doubling time was approximately 31hrs. However, when using CLs alone or when the lipofection method was used for delivery of the reverse sequence, cell doubling time increased to 49hrs. Interestingly, when lipofection was used to deliver the active ILK siRNA, the doubling time was further increased to 60hrs. These data clearly suggest that the transfection method is influencing the behaviour of the cells and the magnitude of this change is dependent on whether the ILK targeted siRNA was used. To exclude the possibility that the effects on cell doubling time were due to delivery method dependent changes in the cell cycle progression, a flow cytometry analysis of the cell cycle distribution was completed. These data have been summarized in Figure 28 a and b and suggest that the cell cycle distribution was not affected by the delivery method used or by the presence of non-active or ILK targeted siRNA. Cell cycle

analysis studies were also performed using treated and control U251MG cells and again, no change in the cell cycle distribution was observed under the conditions used.

**Figure 28: A flow cytometry analysis of the cell cycle distribution following ILK targeted siRNA transfection**

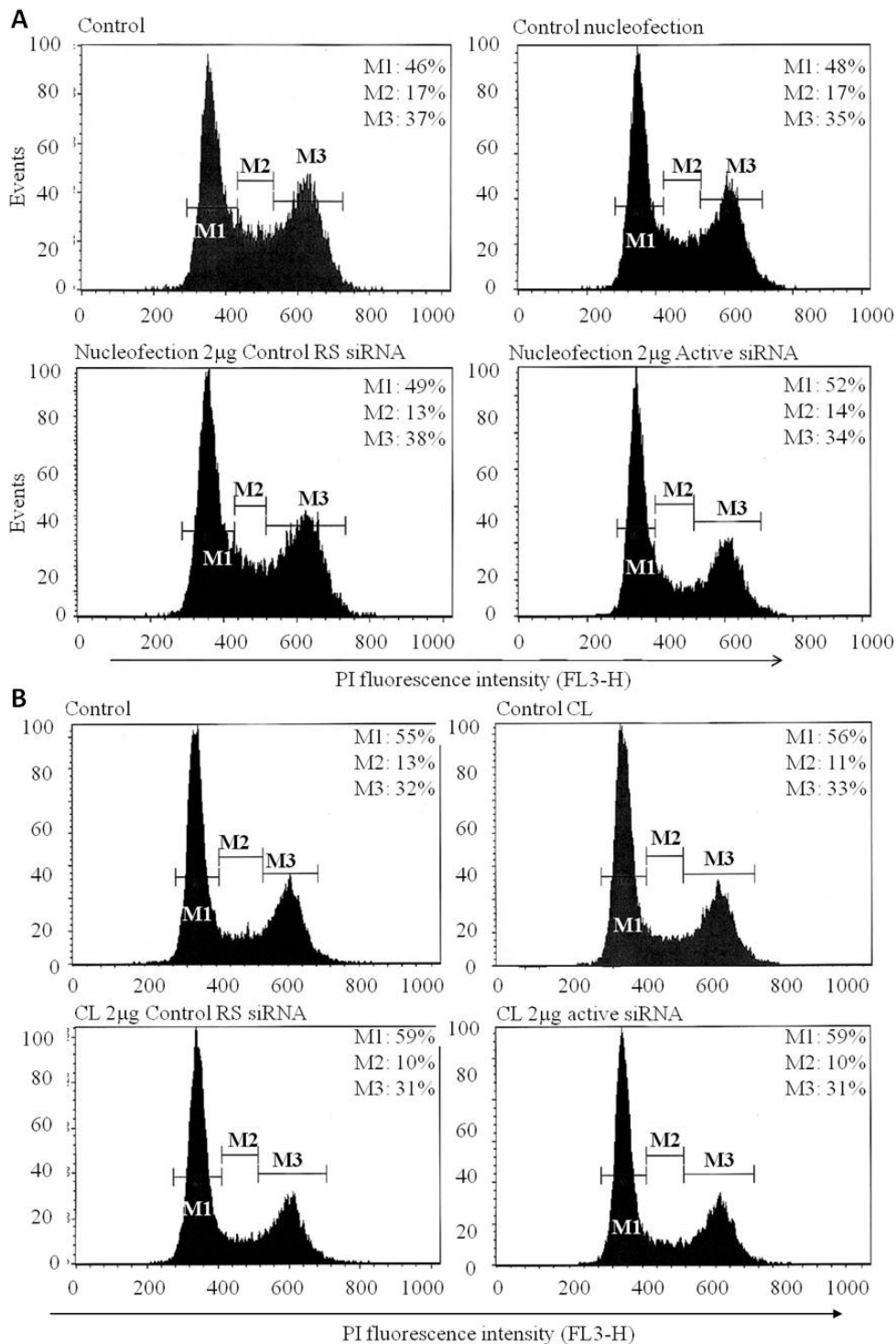


Figure 28 a): Representative flow cytometry analysis of cell cycle distribution of untreated PC3 cells (control), or following nucleofection alone, nucleofection of the control reverse sequence siRNA (Control RS) and nucleofection of ILK siRNA; b): Representative flow cytometry analysis

*of cell cycle distribution of untreated PC3 cells (control), or following treatment CL alone, CL + Control RS and CL + ILK siRNA. These experiments were repeated at least 2 times and the results shown are representative of the different samples.*

### **5.3.2 ILK suppression following ILK siRNA delivery: concentration and time course effects**

The representative western blot results summarized in Figure 29 a and b show the level of ILK in U251MG cells 72hrs after treatment with increasing amounts of ILK siRNA, transfected using nucleofection (Figure 29a) or lipofection (Figure 29b). This time point was selected based on previous studies [112, 331, 332]. The reverse non-active sequence (2 $\mu$ g per well) had no effect on ILK levels. In U251MG cells, ILK siRNA delivery mediated by nucleofection resulted in a 66% (Figure 29a, 2 $\mu$ g per well) decrease in ILK expression relative to controls. Delivery by the lipofection method produced similar decreases in the levels of ILK (55%) (Figure 29b). This level of ILK protein suppression could not be increased by adding higher siRNA doses however the increased siRNA amounts were associated with increased toxicities. A similar study was completed using PC3 cells and 60 to 70% suppression of ILK levels was observed (Figure 29c-d) following delivery using nucleofection or lipofection, respectively. For this cell line, there was no meaningful dose response noted, where 50-60% suppression was observed at doses as low as 0.0625 $\mu$ g.

**Figure 29: Quantification of ILK downregulation 72hrs after ILK siRNA delivery using cationic lipids or nucleofection.**

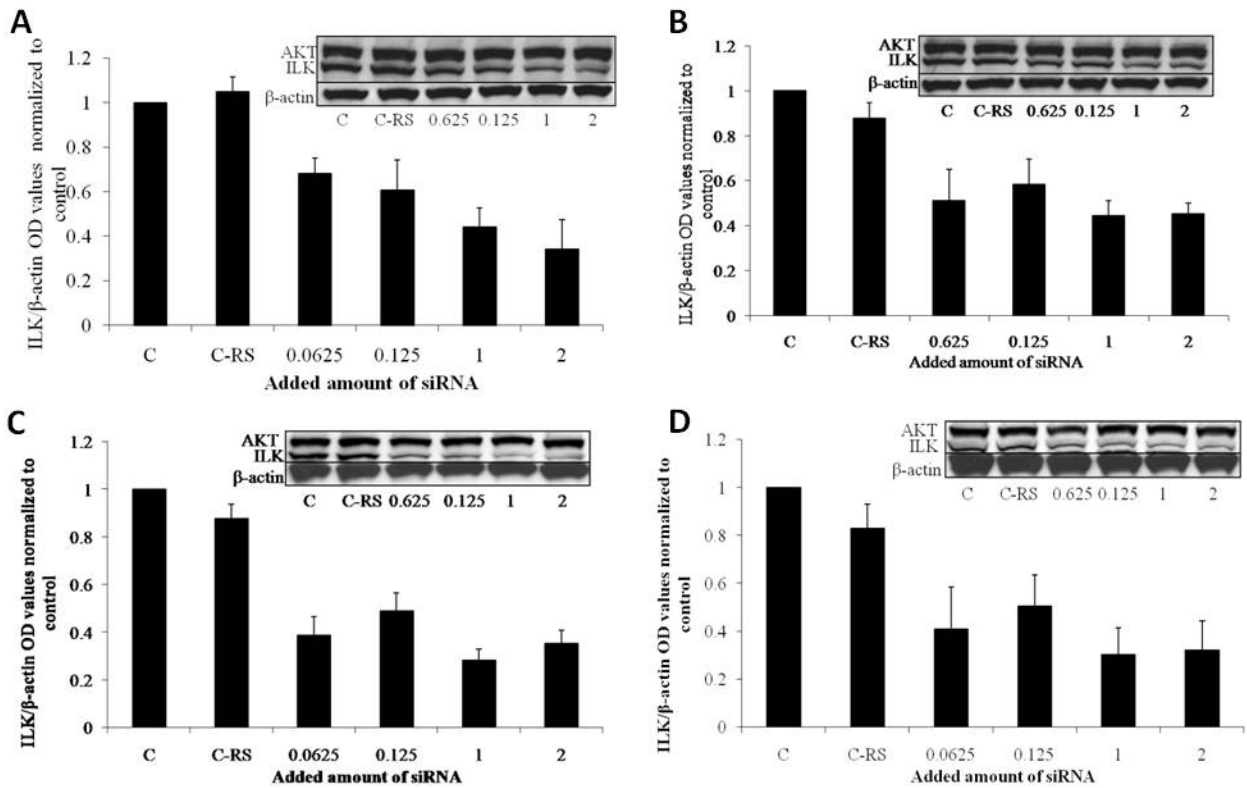


*Figure 29: Histogram representing the average optical density values  $\pm$  SEM (n=3) obtained from immunoblot analysis (ILK, AKT,  $\beta$ -actin) of a-b) U251MG cells and c-d) PC3 cells 72hrs after siRNA delivery using a + c) nucleofection or b + d) CL. The control included 2 $\mu$ g reverse siRNA sequence (C-RS) and the results were compared to ILK decreases associated with increasing amounts (in  $\mu$ g/well) of the ILK siRNA sequence. Ratios of ILK/  $\beta$ -actin optical density values were normalized to the control (untreated) band optical density value. A representative immunoblot has been included in the inset to each panel.*

ILK expression was also assessed at various time points after siRNA delivery (2 $\mu$ g dose) by nucleofection or lipofection. A summary of these studies has been provided in Figure 30. Consistent with what is shown in Figure 29, the non-active siRNA (C-RS) had no effect on ILK levels relative to untreated controls (C) regardless of the time point used. Results for U251MG cells (Figure 30 a and b) indicate that optimal ILK suppression was observed at 96hrs when

siRNA was delivered using nucleofection, where 93% suppression of ILK was noted. The time course of ILK suppression in U251MG cells following ILK siRNA delivery by lipofection suggested that optimal suppression occurred at 120hrs. Overall, the extent of suppression was lower (average of 62% for all time points) when compared to data obtained when siRNA was delivered by nucleofection (average of 73% for all time points). Results obtained in PC3 cells suggested maximum ILK suppression was obtained by 48hrs, regardless of whether the siRNA was delivered by nucleofection (Figure 30c) or lipofection (Figure 30d). The levels achieved at this time point were maintained for the duration of the study (120hrs).

**Figure 30: Quantification of ILK downregulation over time following ILK siRNA delivery using cationic lipids or nucleofection**

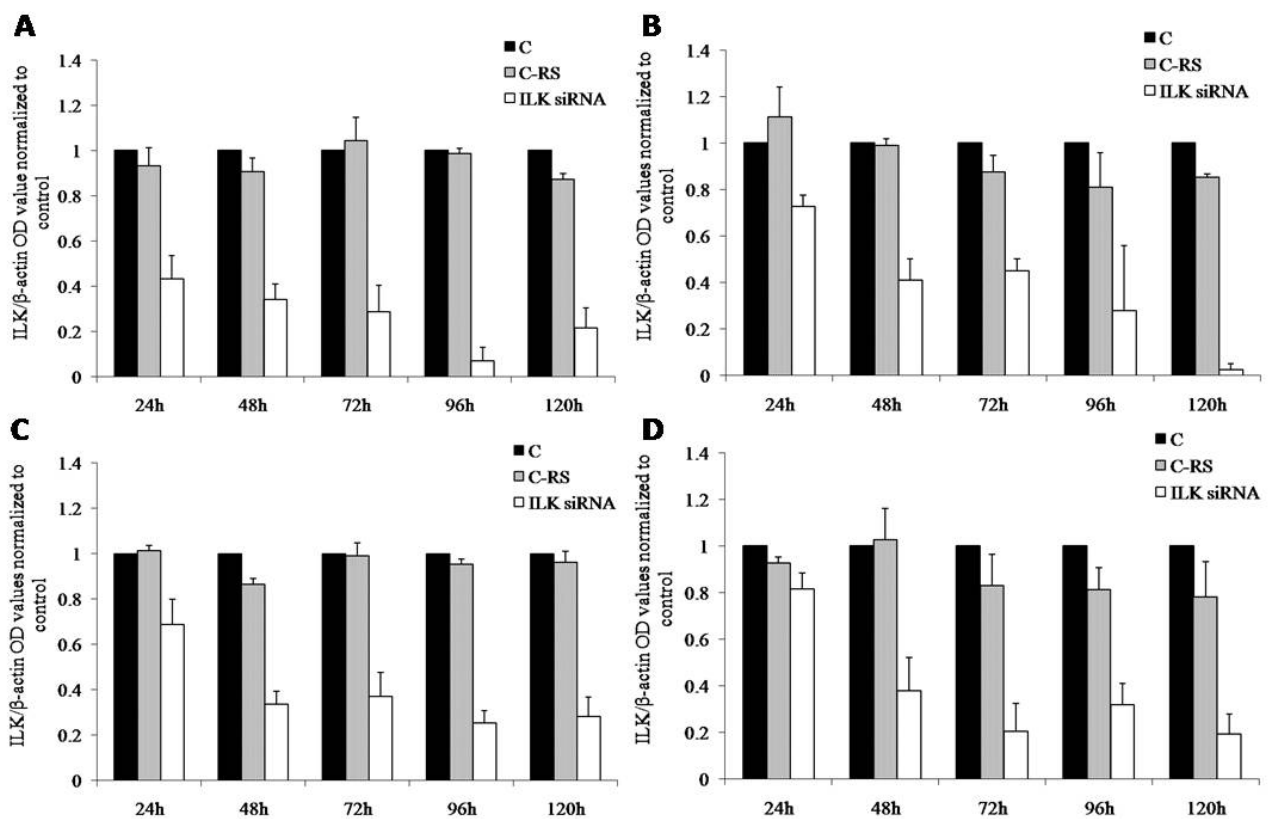


Figure 30: Histogram representing the average optical density values  $\pm$  SEM ( $n=3$ ) obtained from immunoblot analysis (ILK, AKT,  $\beta$ -actin) of a-b) U251MG cells and c-d) PC3 cells where siRNA ( $2\mu\text{g}/\text{well}$ ) was delivered using a + c) nucleofection or b + d) CL. The control included

*2µg/well reverse siRNA sequence (C-RS) and the results were compared to ILK decreases associated with time following addition of the ILK targeted siRNA. Ratios of ILK/ β-actin optical density values were normalized to the control untreated band optical density value.*

### **5.3.3 Suppression of p473-AKT following ILK downregulation**

Inhibition of ILK activity is associated with suppression of p473-AKT [331-333, 336, 346]. Thus phosphorylated levels of AKT were measured following ILK suppression in U251MG (Figure 31a to d) and PC3 (Figure 31 e to h) cells 24 to 120h after ILK siRNA delivery by either nucleofection or lipofection. Albeit surprising, under conditions where 60-90% ILK suppression was achieved in U251MG cells changes in p473-AKT levels were marginal and variable. This was irrespective of siRNA amount or time. It could even be suggested that when lipofection was used as a method to deliver the ILK targeted siRNA to the U251MG cells that there was a measurable increase in p473-AKT, as noted in Figure 31c where the level of p473-AKT was 2-fold higher in cells treated with 2µg of the ILK siRNA. The time course study suggested that p473-AKT levels decreased 48% 120h after ILK siRNA transfection using lipofection (Figure 31d) but the levels of p473-AKT were never decreased by ILK siRNA when delivered using nucleofection (Figure 31c), even though there was substantial and persistent suppression of ILK as noted in Figure 30.

Studies completed in treated PC3 (Figure 31 e to h) were more consistent with those that were expected following ILK silencing and these cells serve as a positive control for ILK suppression-associated decreases in p473-AKT levels [331, 332, 336]. There was approximately a 50% decrease in p473-AKT observed following ILK siRNA delivery by nucleofection (2µg dose, 72h after treatment) (Figure 31e-f). The level of p473-AKT suppression was dose dependent (Figure 31e) and the levels were comparable to control values before the 72h time point and recovered to control values 96h after siRNA was added (31f). When ILK siRNA was delivered using the lipofection method, a 30-50% decrease in p473-AKT in PC3 cells was

maintained for up to 72hrs, returning to control levels by 96hrs. In aggregate, regardless of the method used to deliver the siRNA, p473-AKT levels in the PC3 cells return to control levels even at time points where significant ILK suppression is maintained (see Figure 31 d and e).

**Figure 31: Quantification of p473-AKT suppression 72hrs and over time following ILK siRNA delivery using cationic lipids or nucleofection**

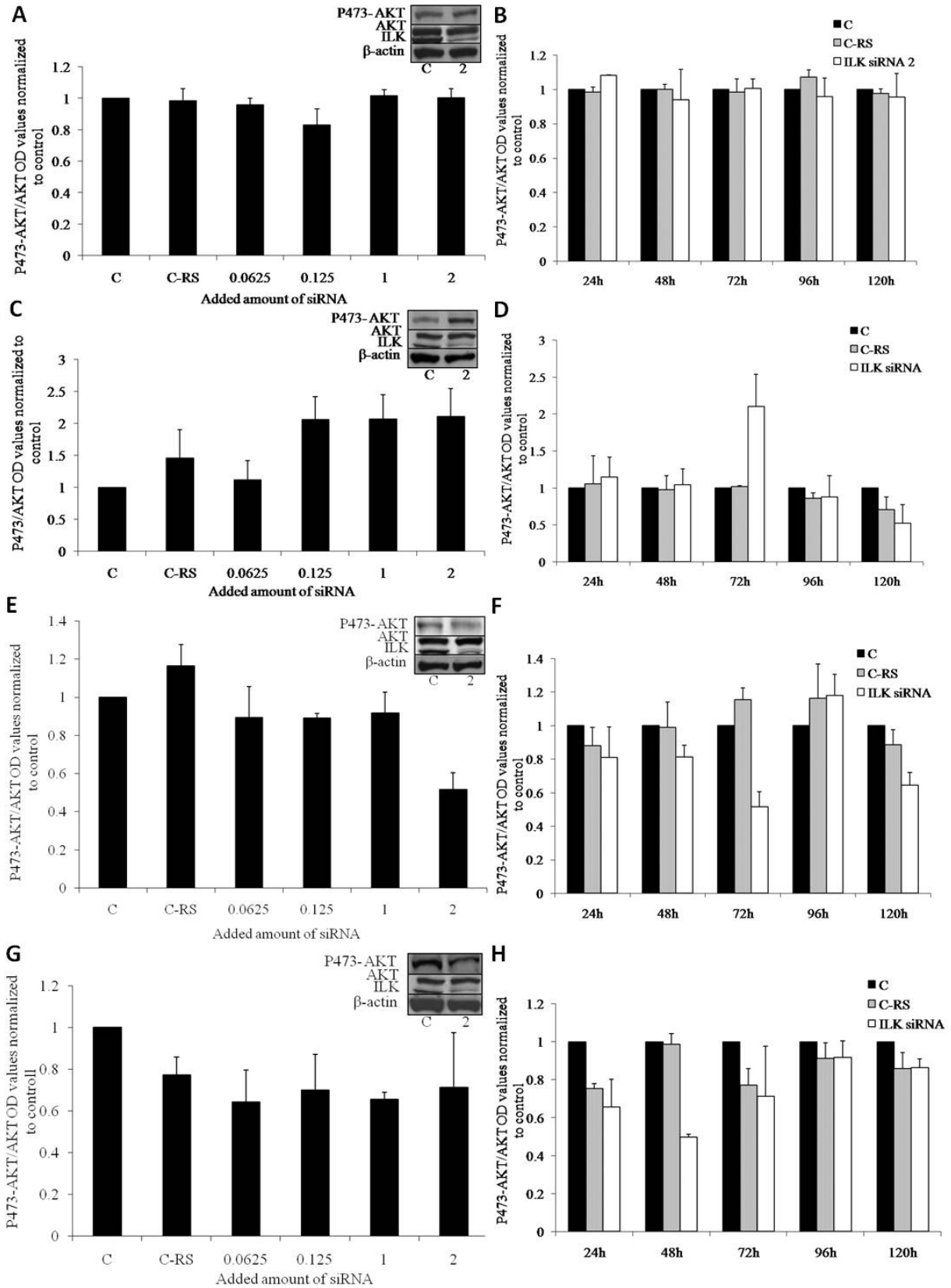


*Figure 31: Histogram representing the average optical density values +/-SEM (n=3) obtained from immunoblot analysis of p473-AKT following treatment of U251MG cells (a to d) and PC3 cells (e to h) with ILK siRNA delivered (2µg/well) using nucleofection methods (a, b, e, and f) or by lipofection methods (c, d, g and h). p473-AKT levels were measured relative to total AKT levels (p473-AKT/AKT ratio) and compared to the control cells (C). The control included 2µg of reverse siRNA sequence (C-RS). a), b), e) and g) evaluated p473-AKT levels following treatment with increasing amounts of ILK targeted siRNA while b), d), f), h) evaluated time course effects following addition of 2µg of ILK targeted siRNA. Representative immunoblots of control untreated cells and cells transfected with 2µg ILK siRNA using the corresponding transfection technique have been included as inset images.*

#### **5.3.4 Effects of cationic liposomes on intracellular pathways influenced by ILK expression**

It is understood that cationic lipids are toxic and recent reports suggest that cationic lipids can broadly influence gene expression [347, 348]. Cationic lipid toxicity can be controlled by using appropriate levels of cationic lipids when preparing siRNA for delivery. However, the influence of cationic lipids on intracellular pathways is more difficult to control and these changes may result in favorable or unfavorable interactions with silencing of a specific target such as ILK. This reasoning led us to ask the question: does the presence of cationic lipids influence the downstream consequences of siRNA mediated silencing of ILK in PC3 and U251MG cells. To address this question, control cells (no nucleofection) or cells treated (using nucleofection) with reverse non-active siRNA sequence or the active ILK siRNA sequence were subsequently exposed to Lipofectamine 2000<sup>TM</sup>. The results have been summarized in Figure 32a-b, where biomarkers linked to the AKT survival pathway (e.g. ILK, AKT, mTOR) were measured 72h after nucleofection in U251MG and PC3 cell lines. This time point was selected because previous studies showed that cells completely recovered from nucleofection associated stress 48h after the procedure [342]. The cationic lipids were added 24h after nucleofection and

were incubated with the cells for 6 hours prior to washing (see Methods). Subsequently the cells were allowed to recover for another 42h before completion of the western blots. Under these conditions, ILK levels in U251MG cells were not influenced by the nucleofection of non-active siRNA, in the presence or absence of added cationic lipids (Figure 32a-b). As expected, when the active ILK siRNA was delivered to U251MG and PC3 cells in absence of cationic lipids, ILK was downregulated (up to 87 and 90% respectively). Interestingly, when ILK siRNA nucleofected cells were exposed to cationic lipids, the level of ILK suppression was enhanced to as much as 95% in U251MG cells. The level of p473-AKT was not changed by the presence of ILK siRNA in PC3 and U251MG cells, but was decreased by 35% when PC3 cells were exposed to cationic lipids. Importantly, this effect of the cationic lipids on p473-AKT was not observed in the non-active siRNA transfected PC3 cells exposed to cationic lipids. The levels of the total AKT were not changed in any of the treatment groups in the absence of CL, however in the presence of CL there were small (10-23%) decreases in AKT levels in both cell lines. PDK1 and its phosphorylated form (serine 241) were also assessed as this protein is responsible for the phosphorylation of AKT at the threonine 308 site, but this marker was not affected by the presence of any siRNA sequence or by exposure to cationic lipids. Importantly, it should be noted that mTOR levels were decreased by up to 61% in U251MG cells treated with non-active siRNA and exposed to cationic lipids, and up to 36% in U251MG cells transfected with ILK siRNA and exposed to cationic lipids. In addition, in control PC3 cells exposed to the cationic lipids the, mTOR levels were decreased by 30%. Interestingly, in PC3 cells in presence of both the reverse sequence and the ILK active siRNA sequences, the levels of mTOR were decreased by 42 and 36% respectively. The presence of cationic lipids appeared to have no additional impact on the mTOR level in these cells.

**Figure 32: The impact of cationic lipids on protein levels following siRNA delivery using nucleofection**

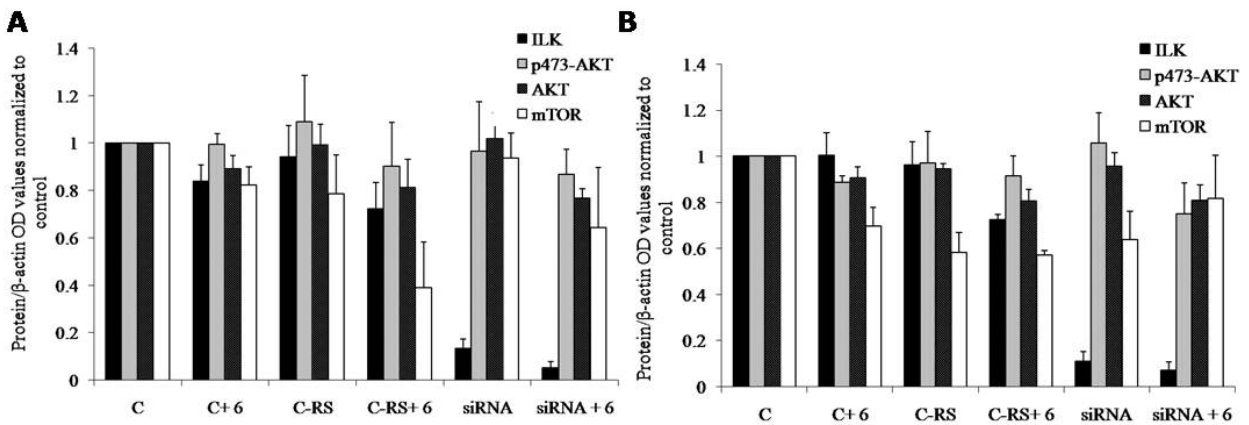


Figure 32: Histogram representing the average optical density values  $\pm$  SEM ( $n=3$ ) obtained from immunoblot analysis (ILK, p473-AKT, AKT, mTOR,  $\beta$ -actin) of a) U251MG cells and b) PC3 cells 72hrs after nucleofection of control reverse siRNA sequence (C-RS;  $2\mu\text{g}$ ) or active ILK siRNA sequence (siRNA;  $2\mu\text{g}$ ). Control cells (C) were not transfected and values of ILK, p473-AKT, AKT, mTOR,  $\beta$ -actin were measured relative to these control cells. To assess the effects of CL on ILK siRNA treatment, cells (24hrs after nucleofection) were exposed for 6hrs to CL ( $6\mu\text{L}/\text{mL}$ ) and allowed to recover for 42hrs before preparing the cells for Western Blot analysis. Ratios of the indicated protein over  $\beta$ -actin optical density values were normalized to the control untreated band optical density value.

## 5.4 Discussion

It has been suggested that cationic lipids can, when added to cells, significantly alter gene expression under conditions where measurements of cell viability indicate that the cells are as viable as control cells. Therefore it is not unreasonable to suggest that cationic lipids may mediate changes in gene expression that combine with effects that are associated with silencing of ILK, a therapeutic target that can influence cell survival. This drug combination effect, which may be beneficial or detrimental, would not necessarily be observed in cells treated with control sequences that do not interfere with target gene expression. In order to address this possibility,

the effect of ILK siRNA was characterized in a well established PTEN negative GBM cell line (U251MG cells) following delivery by nucleofection or cationic liposomes. As a positive control, the studies were also completed in PC3 prostate cancer cells where the effects of ILK targeted siRNA have been more fully characterized [331, 332, 336]. A primary objective of these studies was to compare delivery of siRNA sequences targeting ILK using two different transfection methods (nucleofection versus cationic liposomes). Experiments were designed to provide time course information on levels of ILK and phosphorylated-AKT.

Perhaps not unexpectedly, the delivery of ILK targeted siRNA was significantly greater when using cationic liposomes (see Figures 29-30) but greater delivery was not associated with improved activity. The homogenous distribution of siRNA following nucleofection mediated delivery (Figure 28) has been observed previously [349] and it can be argued that under these conditions, the siRNAs are better able to elicit gene silencing effects through formation of the RISC complex [63]. In contrast, the bulk of cell-associated siRNA observed following delivery by cationic lipids is likely bound to cationic lipid structures and not freely available within the cell [350-352]. Overall, higher levels of ILK downregulation were achieved when using nucleofection methods even where the extent of siRNA delivery was 12 to 30 fold lower than that which could be achieved when using cationic lipids. However, the results clearly indicate that enhanced delivery is not associated with enhanced silencing of the targeted gene (Figures 29-30). Although the maximum level of suppression was comparable for both delivery techniques, this suppression occurred at a later time point when the siRNA sequence was delivered using lipofection (see Figure 30). This delay may be due to the time needed for the CL associated siRNA to dissociate from the lipid and/or lipid structures following intracellular localization.

The results clearly indicate that greater levels of siRNA can be delivered to target cells and this is consistent with the belief that the cationic structures generated when mixing siRNA

with cationic liposomes have an affinity for cells. In this regard the CL serve two purposes: i) to complex the anionic siRNA and ii) to facilitate cell association and subsequent siRNA delivery. However there is a third factor that needs to be considered as it is well established that cationic lipids have cytotoxic effects *in vivo* [209, 315-317] and *in vitro* [318-322]. Surprisingly little is known about the impact of CL based delivery systems on cells, yet previous studies assessing gene expression in target cells exposed to CL would suggest that the effects are not insignificant, even under conditions where cytotoxicity is minimal. For example, a small gene expression study (160 genes) completed by Omid et al. suggests that these effects could exacerbate, attenuate or even mask the desired effects of the gene-based therapeutics [347]. When cells were treated with Oligofectamine, there were changes in 16% of the genes assessed including many genes influencing apoptosis. Further it has been reported that the cationic lipid DOTAP can cause ERK pathway activation through action on PI3 kinase pathway [348]. In this chapter, we explored the effects of cationic lipids at the molecular level related to the targeted protein ILK and demonstrated that Lipofectamine 2000 can affect p473-AKT levels as well as mTOR transcription levels. These effects appear to occur independently of ILK mediated silencing.

Interestingly, our results suggest that prolonged ILK silencing was not associated with prolonged reductions in phosphorylation of AKT at the Serine 473. To our knowledge, this report is the first that has focused on signaling consequences associated with ILK siRNA mediated suppression through an extended time course. This was initially done to ascertain the combined effects of cationic lipids with ILK targeted siRNA, but the results clearly suggest that regardless of the transfection method, suppression of phosphorylation of AKT at the Serine 473 site is transient relative to ILK silencing. ILK has been shown in various cell lines, including U251MG [112, 346] and PC3 [331, 332, 336], to be responsible for phosphorylation of AKT at Serine 473 site. Therefore ILK knockdown would be expected to induce a decrease in phosphorylation of AKT. However, the results shown demonstrate a transient suppression of

phosphorylation of AKT under conditions where there is prolonged silencing of ILK. This must be the result of activation of one or more compensating pathways that eventually result in re-phosphorylation of AKT. A recent paper demonstrated the direct action of mTOR complexed with the 200kDa Rapamycin-Insensitive Companion of mTOR (Rictor) [353] in the phosphorylation of AKT at the Serine 473 site [341] and it can be speculated that mTOR/Rictor may be involved in re-phosphorylation of AKT following silencing of ILK. In fact, studies led by collaborators have recently demonstrated that depletion of ILK and Rictor in breast and prostate cancer cells results in inhibition of phosphorylation of AKT at serine 473 site [336]. The role of Rictor in phosphorylation of AKT in GBM cells will be addressed in chapter 6. Interestingly, siRNA-mediated depletion of Rictor, but not mTOR, inhibited the amount of p473-AKT able to co-immunoprecipitate with ILK in a complex. The latter results are of particular interest in the context of the data presented here which suggest that one of the non-specific effects of cationic lipids when used in combination with siRNA targeting ILK is a significant increase in mTOR expression (Figure 32). This clearly demonstrates a combination effect that results when ILK silencing occurs in the presence of cationic lipids. In light of these results, it is clear that the effects of cationic lipids on the expression or phosphorylation of proteins involved in AKT pathway have to be considered when developing therapeutic strategies targeting this particular pathway. For *in vivo* delivery, we and others recognize that siRNA carriers will remain the best strategy to avoid the degradation of siRNA sequences, to maintain long circulation lifetimes, and to foster enhanced delivery to the target sites as well as the target cell population [56, 313, 314]. However, it appears essential to assess the role of charged lipids in contributing to novel anti-cancer formulations [323].

## **5.5 Acknowledgements**

The research described in this original paper has been supported by grant funding from the Canadian Institutes of Health Research (CIHR) and the National Cancer Institute of Canada (NCIC). MV was a recipient of a PhD scholarship granted by Les Fonds de la Recherche en Santé du Québec (FRSQ) while doing this research. The authors also thank Dr. Emmanuel Ho and Mrs. Wieslawa Dragowska for reviewing work and helpful discussions.

# **Chapter 6: Combined RNAi mediated suppression of Rictor and EGFR inhibits tumour growth in an orthotopic glioblastoma tumour model**

## **6.1 Introduction**

<sup>6</sup>The design of targeted therapy for achieving optimal therapeutic effects is complex. Cancer cell proliferation, growth and death are regulated by intricate networks of signaling pathways, and it is very likely that inhibiting any one specific pathway will activate compensating mechanisms. It is expected that the full potential of targeted therapy will only be realized by targeting multiple biological pathways in order to effectively impede cancer progression and recurrence [354]. Several important factors must be considered in the design of combination treatments involving agents targeting multiple pathways. First, the targeted therapeutic agents used cannot adversely affect outcomes achieved with existing treatments (e.g. radiation therapy or conventional cytotoxic agents). Second, the targeted therapeutic agents must be used selectively in patients with tumours shown to express the targeted proteins or pathways. Finally, this approach will only be valuable for the treatment of GBM if the targeted agents are highly selective and capable of crossing the blood-brain barrier. In this study, the therapeutic potential of simultaneous silencing of the epidermal growth factor receptor (EGFR) and Rictor was assessed *in vitro* and *in vivo* and the rationale for selecting these proteins as therapeutic targets has been outlined below.

One of the most commonly reported molecular defects in GBM is the phosphatase and tensin homolog (PTEN), a negative regulator of the PI3K/AKT pathway. PTEN is mutated in 25-60% of GBM tumours [64, 355] and constitutive activation of the PI3K/AKT pathway, due to PTEN mutation, is associated with increased proliferation rate, invasion, metastasis and poor

---

<sup>6</sup>This chapter was submitted for publication in April 2011: M. Verreault, A. Stegeman, C. Warburton, D. Strutt, D. Masin and M.B. Bally. Combined RNAi mediated suppression of Rictor and EGFR inhibits tumour growth in an orthotopic glioblastoma tumour model. Submitted.

prognosis [72, 73, 356]. Moreover, Molina et al. [357] recently demonstrated, using *in vivo* orthotopic models of GBM, a strong correlation between AKT activation and GBM tumourigenicity and invasiveness. Thus, tremendous efforts have been made to define strategies that inhibit the aberrant PI3K/AKT signaling for treatment of GBM [358]. The activation of AKT through phosphorylation is known to activate mTOR (mammalian target of rapamycin), which regulates a variety of functions associated with tumour pathogenesis [74, 359]. mTOR functions in two distinct multi-component protein complexes, both of which can influence AKT signaling. Inhibition of mTOR Complex 1 (mTORC1) can activate AKT; an effect attributed to Ribosomal S6 Kinase 1 (S6K1) -mediated feedback mechanisms [359-363]. Alternatively, mTOR Complex 2 (mTORC2) can activate AKT through direct phosphorylation at its Serine 473 site (p(ser473)AKT) [341, 353]. All known mTORC2 functions require the presence of the protein Rictor [364] and silencing of Rictor was reported to decrease AKT phosphorylation (ser473) in GBM cells [365]. This latter study also reported elevated levels of Rictor protein in human GBM tumour tissue and cell lines when compared to normal brain tissue [365].

Epidermal Growth Factor Receptor (EGFR) overexpression or overactivation is also commonly observed in GBM tumours (40-70% of the patients) [66]. EGFR overexpression has been correlated with treatment resistance [366], as well as poor survival and poor prognosis [367]. Further, it has been demonstrated that the expression of a specific mutant form of EGFR (EGFRvIII) promotes tumour formation and growth (reviewed in [368]). The oncogenic properties of EGFRvIII overexpression are believed to be a consequence of the constitutive activation of downstream pathways such as PI3K/AKT [369]. This mutant form of EGFR lacks the Endothelial Growth Factor (EGF) binding site, thereby exhibiting reduced internalization rate promoting continuous signaling in the absence of growth factors [370]. EGFR is therefore considered by many as an appropriate therapeutic target in GBM [69, 371].

Despite strong preclinical rationale indicating that targeting of EGFR and mTOR should provide therapeutic benefit in patients with GBM, pharmacological compounds against these targets have already been tested clinically in GBM patients and the results of these studies suggested only modest benefits. More specifically, mTOR small molecule inhibitors (e.g. temsirolimus [75], everolimus [372]) have shown no evidence of therapeutic activity in recurrent GBM disease (reviewed in [364]). Use of the EGFR tyrosine kinase inhibitor gefitinib showed no measurable responses, [40] while treatment with the EGFR inhibitor erlotinib resulted in a 6-11% objective response rate (partial or complete response), albeit these were not linked to EGFR overexpression [41, 373]. Perhaps even more disappointingly, clinical studies evaluating combinations of mTOR and EGFR inhibitors in patients with recurrent glioma demonstrated limited responses and these were not sustained [372, 374]. Thus there is a great deal of preclinical evidence supporting the use of drugs targeting mTOR and EGFR (alone and in combination) but the benefits are not yet being realized in patients.

It is suggested here that strategies targeting Rictor may provide significant anti-cancer benefits, and that Rictor silencing strategies, when combined with EGFR inhibition, will result in optimal therapeutic effects. To validate this concept, RNA interference (RNAi) methods were used to study the effects of combined silencing of Rictor and EGFR. An *in vitro* assessment of the approach was evaluated using siRNA transfection in a panel of three EGFR overexpressing GBM lines, including two PTEN mutant lines (U251MG and U118MG) and one PTEN-wild type line (LN229) [375-378]. The results suggest that siRNA mediated co-silencing of EGFR and Rictor inhibits tumour cell migration in U251MG and LN229. In all three lines, the combined silencing strategy increased sensitivity to conventional chemotherapeutic agents known to be active in patients with GBM. *In vivo* validation of the co-targeting strategy was done using doxycyclin-inducible shRNA-expressing GBM lines implanted orthotopically. The results demonstrate that silencing of EGFR or Rictor alone had no significant effect on tumour

growth in the orthotopic U251MG GBM model, but the dual silencing of EGFR and Rictor *in vivo* results in eradication of the tumour.

## **6.2 Materials and methods**

### **6.2.1 Cell culture and siRNA transfection**

U251MG, U118MG, LN229 glioblastoma and 293T embryonic cell lines were purchased from American Type Culture Collection (Manassas, VA, USA). All cell lines were maintained in DMEM medium supplemented with 1% L-glutamine, 1% penicillin/streptomycin (DMEM, L-glutamine and penicillin/streptomycin from Stem Cell Technologies, Vancouver, British Columbia, Canada) and 10% FBS (Hyclone, Logan, UT, USA). U251MG, U118MG and LN229 cells were transiently transfected with EGFR or Rictor siRNA, alone or in combination, using a nucleofector unit (Nucleofector Technology; Amaxa Biosystems, Gaithersburg, MD, USA) according to the manufacturer's instructions. The optimized protocol used 2µg siRNA and 100µL of solution T for U251MG cells or R for U118MG and LN229 cells (Amaxa Biosystems) in combination with device program G16 for U251MG cells, T20 for U118MG and X9 for LN229 cells. After transfection, cells were transferred to fresh cell medium supplemented with 5ng/mL FGF and 10ng/mL EGF (Clonetics®, Lonza), in tissue culture dishes or plated in 96 well plates for migration or drug sensitivity assays. Cells in tissue culture dishes were harvested using Trypsin (Gibco, Invitrogen, Burlington, Ontario, Canada) 96hrs after transfection for cell cycle and western blot analysis.

siRNA sequences against the human EGFR mRNA (Genbank accession #AY588246) and Rictor mRNA (Genbank accession #AY515854) as well as two scrambled siRNA negative control sequences (Low Duplex #1 and Low Duplex #2) with equivalent GC content were generated by Invitrogen. EGFR siRNA sequence (CCU AUG CCU UAG CAG UCU UAU

CUA A) and Rictor siRNA sequence (CCU AAU GAA UAU GGC UGC AUC CUU U) were verified using NCBI Basic Local Alignment Search Tool (BLAST) to confirm specificity.

### **6.2.2 Scratch-wound healing and drug sensitivity assay**

For the scratch-wound healing assay, cells were grown to 100% confluency in 96 well plates (96hrs after plating of  $1.5\text{-}2 \times 10^4$  cells depending on cell line). A scratch was made with a pipet tip and cells were cultured for an additional 24hrs. Cells were then fixed with 3.5% paraformaldehyde (v/v) in PBS, then stained with eosin (Polyscientific, Bayshore, NY, USA) and photographed on bright field microscope at 5x magnification. Photographs were visualized on Photoshop and scored according to the following criteria: 1: no opening, dense layer of cells and scratch is not visible; 2: no opening but lower cell density along the scratch; 3: scratch  $\leq 0.20\text{mm}$ ; 4: scratch  $0.20\text{-}0.40\text{mm}$ ; 5: scratch  $0.45\text{-}0.75\text{mm}$ ; 6: scratch  $0.80\text{-}1.1\text{mm}$ ; 7: scratch  $>1.1\text{mm}$ . The data shown represent the average of a blind scoring from three independent experiments with 8 replicates each. For drug sensitivity assays, cells were plated in 96 well plates ( $2\text{-}5 \times 10^3$  cells depending on cell line). Twenty-four hours following cell plating, irinotecan (Sandoz, QC, Canada), vincristine (Novopharm, ON, Canada), and temozolomide (LKT laboratories inc., St-Paul, MN, USA) were added and 72hrs after drug addition, MTT reagent (3-(4,5 dimethylthiazol-2-yl)-2,5-diphenyl tetrazolium bromide; Sigma) was added ( $1.25\text{mg/mL}$ ). The plates were incubated for 3hrs and the MTT-containing medium was removed and replaced with DMSO. The amount of the blue formazan compound is reflective of the number of living cells and was determined using spectrophotometry ( $570\text{nm}$ ).

### **6.2.3 Immunohistochemistry and flow cytometry**

Transfected cells were plated in chamber slides and cultured for 96hrs. Subsequently, the cells were fixed with PBS 3.5% (v/v) paraformaldehyde (Electron Microscopy Sciences, PA, USA) for 15 minutes at  $-20^\circ\text{C}$ , blocked for 1hr at  $4^\circ\text{C}$  (Odyssey blocking buffer, Rockland, PA, USA) and incubated overnight with rabbit anti-human p(473)-AKT antibody (Cell Signaling

Technology, Antibody #9271; rabbit polyclonal; 1:100 dilution). Cells were then incubated with Texas Red®-X phalloidin for 30min at room temperature and with anti-rabbit 488 secondary antibody (Molecular Probe #A11034, Invitrogen; 1:200 in blocking buffer) for 1hr at room temperature. Nuclei were stained with Draq5 for 30min at 37°C. Slides were washed with PBS and imaged for Draq5 (Cy5 filter), Texas Red (TX filter) and Alexa 488 (L5 filter) using a fluorescence microscope (Leica DM6000B, Leica, ON, Canada). A composite colour image of these markers was produced (Surveyor software, Objective Imaging Ltd). All fluorescence microscopy images are representative of three independent experiments. For flow cytometry analysis, cells were harvested 96hrs after transfection and fixed overnight in 70% ethanol at -20°C and stained with propidium iodide (PI) -containing buffer (PI 50µg/mL; RNase 1mg/mL; Triton X-100 0.1% in PBS) for an hour on ice and analyzed by flow cytometry.

#### **6.2.4 Western blot analysis**

Western immunoblots were obtained from total protein extracts as described in chapter 5 [379]. The blots were labeled using the following primary antibodies (from Cell Signaling Technology unless otherwise indicated): anti-AKT (Antibody #9272; rabbit polyclonal; 1:1000 dilution), anti-phosphorylated AKT-Ser473 (Antibody #9271; rabbit polyclonal; 1:1000 dilution), anti-Rictor (Antibody #2140; rabbit polyclonal; 1:1000 dilution), anti-EGFR (Antibody #2232; rabbit polyclonal; 1:1000 dilution) and anti-β-actin (AC-15; mouse monoclonal; 1:20 000 dilution; Sigma-Aldrich, Oakville, Ontario, Canada). The secondary antibody used was horseradish peroxidase-conjugated anti-mouse or anti-rabbit IgG (Promega, Madison, WI, USA) diluted 1:5000. Scanning densitometry (Un-Scan-It software; Silk Scientific, Inc., Orem, UT, USA) was used to quantify band intensities by volume/area integration. Densitometry values were normalized to the corresponding β-actin band, and total AKT in the case of p(473)-AKT. Each western blot figure is representative of three independent experiments and the numbers

below each band or shown in histograms represent the average of optical densities +/- SEM of all three experiments.

### **6.2.5 shRNA lentivirus production and U251MG transduction**

Inducible short hairpin RNA constructs (TRIPZ shRNAmir) targeting EGFR (CCC TCC CAG TGC CTG AAT ACA T, #V2THS\_43452), Rictor (CCC AGG CCA GAC CTC ATG GAT A, # V2THS\_120392) and a negative control (ATC TCG CTT GGG CGA GAG TAA G, # RHS4743; designed and validated by the manufacturer) were obtained from Open Biosystems (Thermo Fisher Scientific, Rockford, IL, USA). All sequences were verified using NCBI Basic Local Alignment Search Tool (BLAST) to confirm specificity (100% match) or non-specificity (at least 3 or more mismatches against any mammalian gene) of the active and non-active sequences, respectively. RNAintro TRIPZ lentiviral shRNAmir starter kit was used to produce the inducible shRNA. Briefly, and according to the manufacturer's instructions, one clone from *E.coli* stocks containing TRIPZ shRNAmir plasmids was grown in 5mL 2xLB (low salt) on a shaker at 37°C for 18hrs. pTRIPZ shRNA DNA was isolated (Qiagen QIAprep Spin Miniprep Kit) and DNA concentration was measured using a NanoDrop® spectrophotometer (ThermoScientific, DE, USA, #ND-001). HEK 293T cells ( $5 \times 10^6$  cells) were seeded in a 100mm plate. Twenty-four hours later, cells were transfected with 37.5µg Trans-lentiviral™ packaging mix, 9µg of pTRIPZ shRNA plasmids and 187.5µL of Arrest-In™ transfection reagent in serum and antibiotic free medium. Medium was replaced with fresh serum and antibiotic-containing medium 4hrs later. Medium containing viruses was harvested 48 and 72hrs after transfection, filtered (0.45µm falcon filters) and concentrated by ultracentrifugation at 23,000 RPM, 4°C for 1.5hrs.

U251MG cells were plated at 40% density and 24hrs later, virus stock (multiplicity of infection of 10 for EGFR and Rictor and 20 for negative control) was added to the cells for 4hrs, then replaced with fresh media and cultured for 48hrs. Ninety-six hours after transfection, cells

were selected for the puromycin resistance gene by adding 50, 15, 22 or 50 $\mu$ g/mL puromycin every three days for negative control, EGFR, Rictor and EGFR/Rictor shRNA transfected cells, respectively. Puromycin was added for the entire time the cells were maintained in culture. The expression of the shRNA plasmid was induced in puromycin selected cells by adding 1 $\mu$ g/mL doxycycline (Sigma) in the culture media.

### **6.2.6 Orthotopic and subcutaneous implantation of shRNA expressing U251MG cell lines**

Negative control shRNA U251MG (U251<sup>Ng2x</sup>), EGFR shRNA U251MG (U251<sup>EGFR</sup>), Rictor shRNA U251MG (U251<sup>Rictor</sup>) and EGFR/Rictor shRNA U251MG (U251<sup>EGFR/Rictor</sup>) cells were implanted ( $7.5 \times 10^4$  cells) into the brain of Rag2M mice (7-10 weeks old females, 8/Gr). A stereotaxic injection frame (Stoelting Company, Wood Dale, IL, USA) was used to inject cells into the right caudate nucleus-putamen (ML -1.5 mm; AP +1mm; DV -3.5mm). Induction of shRNA expression in mice was done 21 days after cell inoculation by dissolving 2mg/mL doxycycline and 5% sucrose in drinking water. Bottles were made black using a black marker pen as doxycycline is light-sensitive, and water was replaced every three days. At the end of the study, animals were imaged using the Maestro fluorescence live animal imaging unit (CRI, Woburn, MA, USA). The animals were anesthetized with isoflurane, and the turbo red fluorescent protein (tRFP) co-expressed with the shRNA sequence in presence of doxycycline was imaged. For the subcutaneous model, cells ( $5 \times 10^6$ ) were implanted subcutaneously (s.c.) into the backs of Rag2M mice (7-10 weeks old females, n=3). S.c. tumour size was measured throughout the study by caliper and tumour weights were extrapolated from the measurements ( $\text{mg} = (\text{tumour width}^2 \times \text{tumour length}) / 2$ ).

### **6.2.7 Marker imaging in orthotopic tumours and quantification**

Forty-nine days after orthotopic tumour cell inoculation, animals were terminated using CO<sub>2</sub> asphyxiation and brains were harvested and cryopreserved in OCT (Sakura Finetek, Torrance, CA, USA) on dry ice and stored at -80°C. OCT preserved brains were cryosectioned

and 10µm sections were collected from Bregma +1.0 location. Sections were fixed with 3.5% paraformaldehyde (Electron Microscopy Sciences, PA, USA) for 15 minutes at room temperature, then blocked with blocking buffer (Odyssey blocking buffer, Rockland, PA, USA) for 1 hour at room temperature, and stained with p(473)AKT (Antibody #4060 from Cell Signaling Technology; rabbit monoclonal; 1:50 dilution), Rictor (Antibody #NB100-1534 from Novus Biologicals; goat polyclonal; 1:250 dilution), EGFR (Antibody #2232 from Cell Signaling Technology; rabbit polyclonal; 1:50 dilution), Ki67 (Invitrogen #18-0191z; 1:100) and Alexa 488 goat anti-rabbit (Molecular Probe #A-11034, Invitrogen; 1:200 in blocking buffer) or Alexa 488 chicken anti-goat (Molecular Probe #A-21467, Invitrogen; 1:200 in blocking buffer) secondary antibodies. Primary antibodies were incubated on sections overnight at 4°C, and secondary antibodies for 1hr at room temperature. Nuclei were stained with Hoechst 33342 (Sigma; 5µg/mL) for 30min at 37°C. Slides were washed with PBS and imaged for Alexa 488 (L5 filter), tRFP (CY3 filter) and Hoechst 33342 (UV filter) using a robotic fluorescence microscope (Leica DM6000B, Leica, ON, Canada). Acquired images were quantified using an in-house segmentation algorithm (MATLAB, The Mathworks, Natick, MA, USA) and a composite colour image of these markers was produced (Surveyor software, Objective Imaging Ltd.). EGFR, Rictor, p(473)-AKT and Ki67 markers are expressed as the number of positive pixels in the tumour area divided by the number of Hoechst (nuclei stain) positive pixels.

### **6.2.8 Statistical analysis**

All statistical data were collected using GraphPad Prism (San Diego, CA, USA). Parametric analysis was done using standard deviation, mean and n, in a multivariate one-way analysis (ANOVA) with Tukey's post-tests. All data are shown as mean +/- SEM.

## 6.3 Results

### 6.3.1 The combined silencing of EGFR and Rictor results in a reduction of cell migration and an increase in cell sensitivity to chemotherapeutic drugs

Rictor, as noted in the introduction, is involved in the activation of the AKT pathway through phosphorylation of the protein at its serine 473 site (p(473)-AKT) [341, 353]. Other proteins also participate in AKT phosphorylation in cancer cell lines, including Integrin-Linked Kinase (ILK) [118, 333, 335]. The level of p(473)-AKT in U251MG cells following siRNA-mediated silencing of Rictor was evaluated and compared with p(473)-AKT levels following silencing of ILK. Transfection of the negative control sequence had no significant impact on the level of proteins that were measured. The representative immunoblots provided in Figure 33 also include the averaged optical density assessments determined from 3 separate experiments (numbers under each band). The values indicated are expressed relative to those obtained from untreated cells (standardized to a value of 1). These data indicate that the selected siRNA sequences designed to silence Rictor or ILK were effective at silencing Rictor and ILK respectively (Figure 33a). Following transfection of siRNA specific to ILK, the protein level of ILK was decreased by 81% ( $p < 0.05$ ). The transfection of the siRNA sequence specific to Rictor reduced Rictor levels by 81% ( $p < 0.001$ ). Under the conditions used here, no reduction in p(473)-AKT were noted when ILK expression was silenced in these cells. However, Rictor silencing resulted in a 66% ( $p < 0.01$ ) reduction in p(473)-Akt expression. Silencing of EGFR in U251MG cells (Figure 33b) could be achieved following transfection of EGFR siRNA (73% reduction in protein levels,  $p < 0.01$ , compared to control cells) and this was associated with a 48% reduction in p(473)-AKT levels ( $p < 0.05$ ); a result that is consistent with previous reports using the U251MG cell line [380] and in GBM clinical samples [381]. As noted in Figure 33c, when the U251MG cells were transfected with Rictor siRNA and EGFR siRNA, the levels of

EGFR and Rictor downregulation were comparable to those observed in cells transfected with the individual siRNA sequences (81% and 75%, respectively;  $p < 0.05$ ). The combination of Rictor and EGFR silencing was associated with a 52% ( $p < 0.05$ ) decrease in p(473)-AKT levels that was comparable to that of cells transfected with the individual siRNAs (52%;  $p < 0.05$ ). Representative fluorescence photomicrographs showing the p(473)AKT staining in cells following Rictor and/or EGFR siRNAs transfection have been provided Figure 33d. These data suggest that significant reductions in p(473)-Akt are achievable when Rictor and EGFR are silenced either alone or in combination. F-actin staining was used to reveal the structure of the cytoplasm in these photomicrographs.

**Figure 33: Co-transfection of siRNA sequences specific to Rictor and EGFR results in downregulation of their respective proteins in the U251MG GBM line and Rictor silencing correlates with decreases in p(473)-AKT levels.**

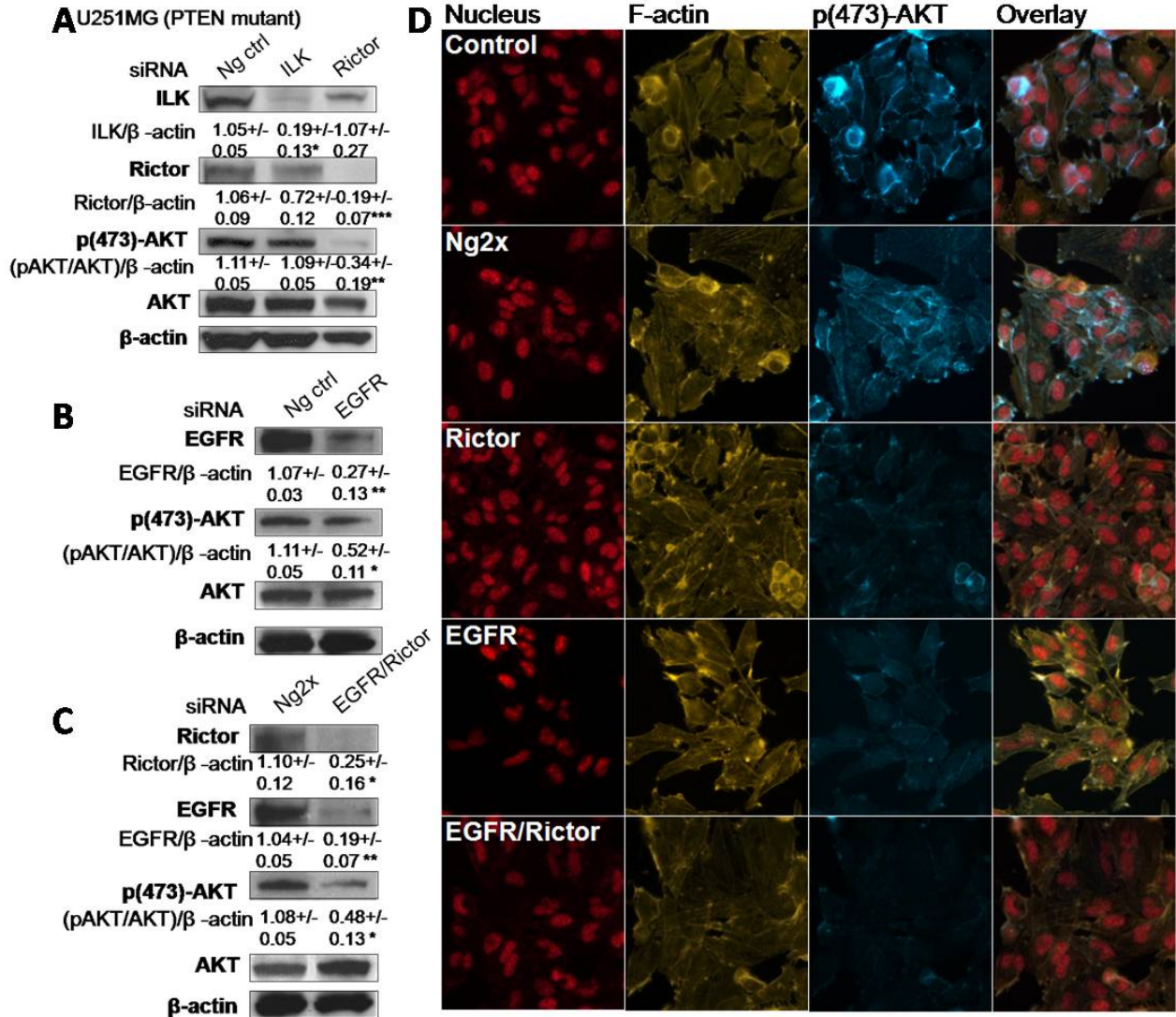


Figure 33: *a*) Representative immunoblots showing ILK, Rictor, p(473)AKT, AKT and  $\beta$ -actin from U251MG cells 96hrs after transfection of siRNA against ILK or Rictor or the negative control sequence (Ng ctrl). *b*) Representative immunoblots showing EGFR, p(473)AKT, AKT and  $\beta$ -actin from U251MG cells 96hrs after transfection of siRNA against EGFR or the negative control sequence (Ng ctrl). *c*) Representative immunoblots showing Rictor, EGFR, p(473)AKT, AKT and  $\beta$ -actin from U251MG cells 96hrs after transfection of the combination of Rictor and EGFR siRNAs or the combination of two negative control sequences (Ng2x). Optical density values shown under each band represent the average obtained from three independent

experiments (+/-SEM) normalized to  $\beta$ -actin, and AKT in the case of p(473)AKT, and expressed as relative to values obtained from untreated cells (=1). **d)** Representative fluorescence photomicrograph (n=3) of U251MG cells showing nuclei (Draq5; red), F-actin (Texas red phalloidin; Yellow), and p(473)-AKT (Alexa 488; blue) 96hrs after transfection of siRNA against Rictor, EGFR, the combination of Rictor and EGFR, and the combination of two negative sequences (Ng2x).

The experiments summarized above for U251MG cells were also completed in U118MG and LN229 cells. The LN229 cell line expresses wild type PTEN, while U251MG and U118MG carry mutant forms of PTEN (caused by inactivating mutations such as a frame shift at codon 241 and an exon/intron 8 splicing defect, respectively [382]). As summarized in Figure 34, Rictor siRNA transfection resulted in an 83% (p<0.05) and 88% (p<0.001) reduction in Rictor protein levels in U118MG and LN229 lines, respectively. The levels of protein suppression seen in both cell lines were similar to what was obtained with the U251MG cell line. Interestingly, Rictor silencing was associated with significant reductions in p(473)-Akt levels only in the PTEN mutant cell lines (U251MG and U118MG cells). Indeed, in U118MG cells, silencing of Rictor resulted in a 68% reduction of p(473)-AKT levels (p<0.001; Figure 34a), almost identical to the 67% reduction in p(473)-Akt levels noted in the U251MG cells. In LN229 cells, a mean suppression of 25% was noted for p(473)AKT but this decrease was not statistically significant when compared to the controls (Figure 34b). Transfection of EGFR siRNAs resulted in a 77% (p<0.01) and 52% (p<0.05) reduction in EGFR protein levels in U118MG and LN229 lines, respectively. No change in p(473)AKT was observed in U118MG and LN229 lines following EGFR siRNA transfection (Figure 34a-b). The results noted for these cells are also consistent with previously reported data obtained from clinical samples [383] and in other GBM cells *in vitro* [384]. When U118MG and LN229 cells were transfected with siRNAs targeting Rictor and EGFR, downregulation of EGFR and Rictor was comparable to that achieved when the siRNA

sequences were used alone (Figure 34). Once again, significant p(473)-AKT suppression was only observed in the PTEN mutant U118MG cell line (49%;  $p < 0.01$ ) and this effect is likely to be a consequence of Rictor silencing.

**Figure 34: Co-transfection of siRNA sequences specific to Rictor and EGFR results in downregulation of their respective proteins in U118MG and LN229 GBM lines and Rictor silencing correlates with decreases in p(473)-AKT levels in U118MG line only.**

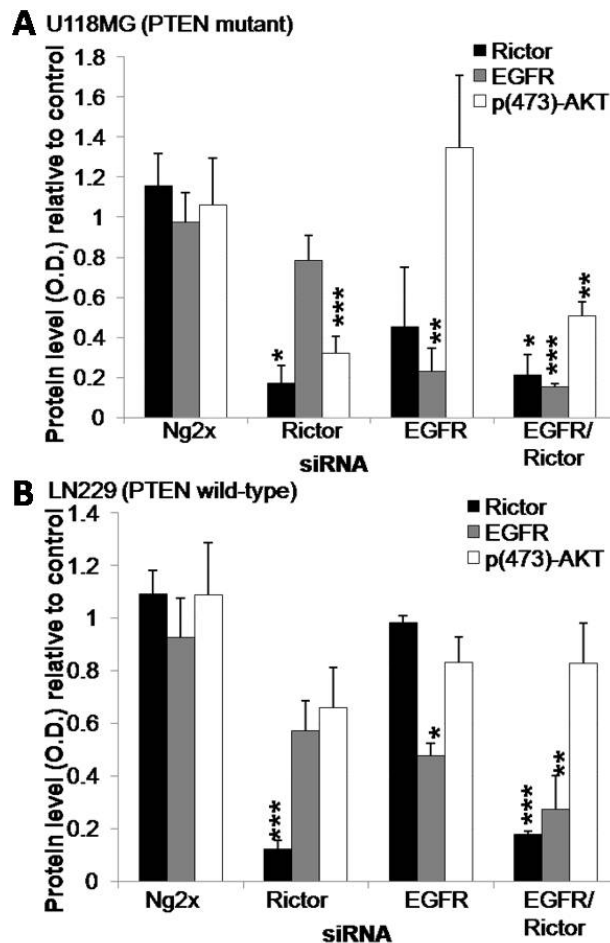


Figure 34: Histograms showing Rictor, p(473)AKT, AKT and  $\beta$ -actin protein levels relative to untreated cells (=1). Optical density values were normalized to the  $\beta$ -actin value, and the AKT value in the case of p(473)AKT, and represent the average obtained from three independent experiments from a) U118MG and b) LN229 cells 96hrs after transfection of siRNA against Rictor, EGFR, the combination of Rictor and EGFR siRNAs or the combination of two negative control sequences (Ng2x). \* $p$ -value  $\leq 0.05$ ; \*\* $p$ -value  $\leq 0.01$ ; \*\*\* $p$ -value  $\leq 0.001$ .

The results described above provided the basis for studies evaluating how Rictor and/or EGFR silencing influence glioma cell migration *in vitro* and exploring whether silencing of these targets influenced cell sensitivity to conventional agents known to exert activity in patients with GBM. It is important to note, however, that EGFR and Rictor silencing, alone or in combination, had little effect on cell viability and proliferation over the course of 96hrs *in vitro*. These data were obtained using the MTT assay described in the Methods. In U251MG and LN229 cells lines transfected with both Rictor and EGFR siRNA, there was a small reduction (<14%) in the number of viable cells measured after a 96hr incubation when compared to negative controls. The combination had no measurable impact on U118MG cell viability. Further, flow cytometric analysis of the sub-G1/G0 fraction at the end of the 96hr time course indicated that the siRNA transfections (Ng control, Ng2x control, Rictor, EGFR or Rictor/EGFR) did not increase the apoptotic or dead cell fraction when compared to untreated controls.

It has already been demonstrated that activation of EGFR and PI3K/AKT pathways promotes GBM cell migration [385]. Rictor is also involved in cell migration through its downstream effector PKC- $\alpha$  [386-390]. For these reasons, it was anticipated that Rictor and/or EGFR silencing might inhibit cell migration. A scratch-wound healing assay was used (as described in the Methods) to study directional cell migration/motility. Changes in the wound width were determined in a blinded fashion 24 hrs after wounding according to criteria described in Methods and illustrated in Figure 35a. It is important to note that data from this assay can be difficult to interpret if the cell populations being studied exhibit different proliferation rates. As noted above, the treated cell populations exhibited similar proliferation rates over 96hrs, so changes in scoring should be reflective of changes in cell migration rates; higher scores (up to 7) represent cells with greater migration capability when compared to cells with lower scores which exhibit reduced migration capability (Figure 35a).

Scratch-wound healing data were collected for three cell lines (U251MG, U118MG and LN229) and these data have been summarized in Figure 35b. When considering the control cells, it is clear that the U118MG cell migration was much lower than that observed in untreated U251MG and LN229 cell lines. Transfection with two negative control sequences (Ng2x) had no effect on cell migration in the three lines when compared to control cells. When the cell lines were transfected with siRNAs targeting Rictor or EGFR alone, no significant changes were observed in wound healing capability (Figure 35b). However, for the cell lines which exhibited the greatest migration capability (U251MG and LN229), silencing of Rictor and EGFR together resulted in significant ( $p < 0.001$ ) reductions in migration. More specifically, control cell populations exhibited a mean score on the scratch assay of 5.4 to 5.7, while cell populations where both Rictor and EGFR were silenced exhibited scores of 3.5 to 4.0 (Figure 35b).

**Figure 35: The combination of EGFR and Rictor silencing results in a reduction in cell migration.**

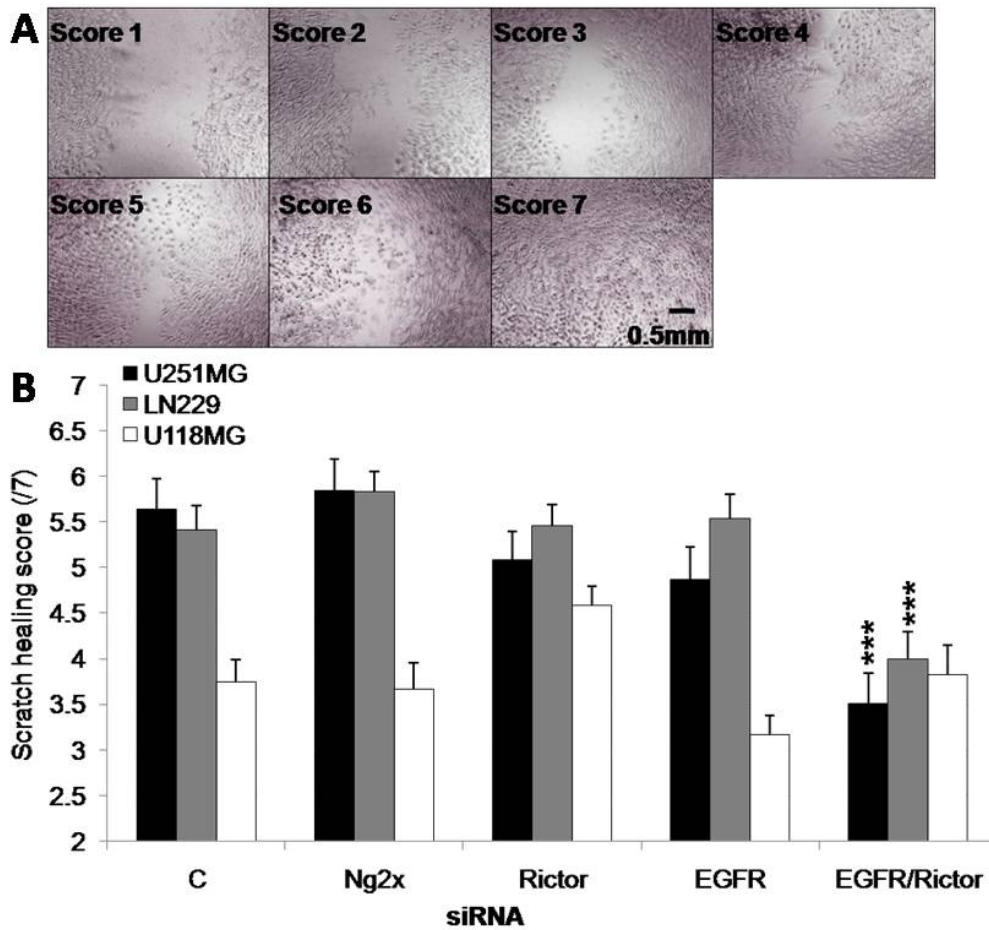


*Figure 35: a) Example of scoring chart for the scratch-wound healing assay. b) Scratch width scoring of U251MG, U118MG and LN229 cells 96hrs after transfection of siRNA against Rictor, EGFR, the combination of Rictor and EGFR or the combination of two negative control sequences (Ng2x), obtained from three independent experiments. \*\*\*p-value  $\leq 0.001$  compared to untreated cells.*

Two of the basic tenets behind this research are: i) target silencing alone will not be sufficient to achieve optimal therapeutic results and ii) targeted therapeutics, such as siRNA sequences, will be used in combination with existing treatments which are known to provide measurable therapeutic benefits to patients. In consideration of these tenets, it is important to establish that target silencing does not reduce tumour cells' sensitivity to conventional treatment

modalities such as chemotherapeutic agents. It is also valuable to assess whether target silencing can increase tumour cells' sensitivity these chemotherapeutic agents. Thus, GBM tumour cell lines transfected with EGFR siRNA, Rictor siRNA, or the combination of both, were exposed *in vitro* to chemotherapeutic drugs commonly used in for treatment of patients with GBM including: irinotecan [35, 36], vincristine [33] and temozolomide [3]. Complete dose response curves for each drug were generated in control cells (i.e. not transfected) using a 72 hour time course. These data were used to determine the drugs' EC<sub>50</sub> i.e. the concentration of drug where cell viability/proliferation was inhibited by 50% when compared to untreated cells (fraction affected or Fa of 0.5). Subsequently, cells transfected with siRNA targeting Rictor and EGFR alone or in combination were exposed (24hrs after cell transfection) to the drugs at their approximate EC<sub>50</sub> (see Figure 36) and cell viability was determined 72hrs later. The results, summarized in Figure 36, are shown as a relative increase or decrease ( $\Delta$ ) in Fa when compared to control cells (non-transfected or Ng2x-transfected cells) that were treated with the same dose. The data suggest that the combination of Rictor and EGFR silencing results in increased drug sensitivity in all examples, with the exception of LN229 and U118MG exposed to irinotecan. In these cases, drug sensitivity in the siRNA transfected cells was not significantly different from that observed in control cell populations. Significant increases in Fa are exemplified by the results obtained with the U251MG cells exposed to 1nM Vincristine (Figure 36a). Silencing of EGFR, Rictor alone or in combination increased the Fa value to 0.26, 0.29 and 0.35 (p<0.001), respectively, compared to the non-transfected control cell population.

**Figure 36: The combination of EGFR and Rictor silencing results in an increase in cell sensitivity to chemotherapeutic drugs.**

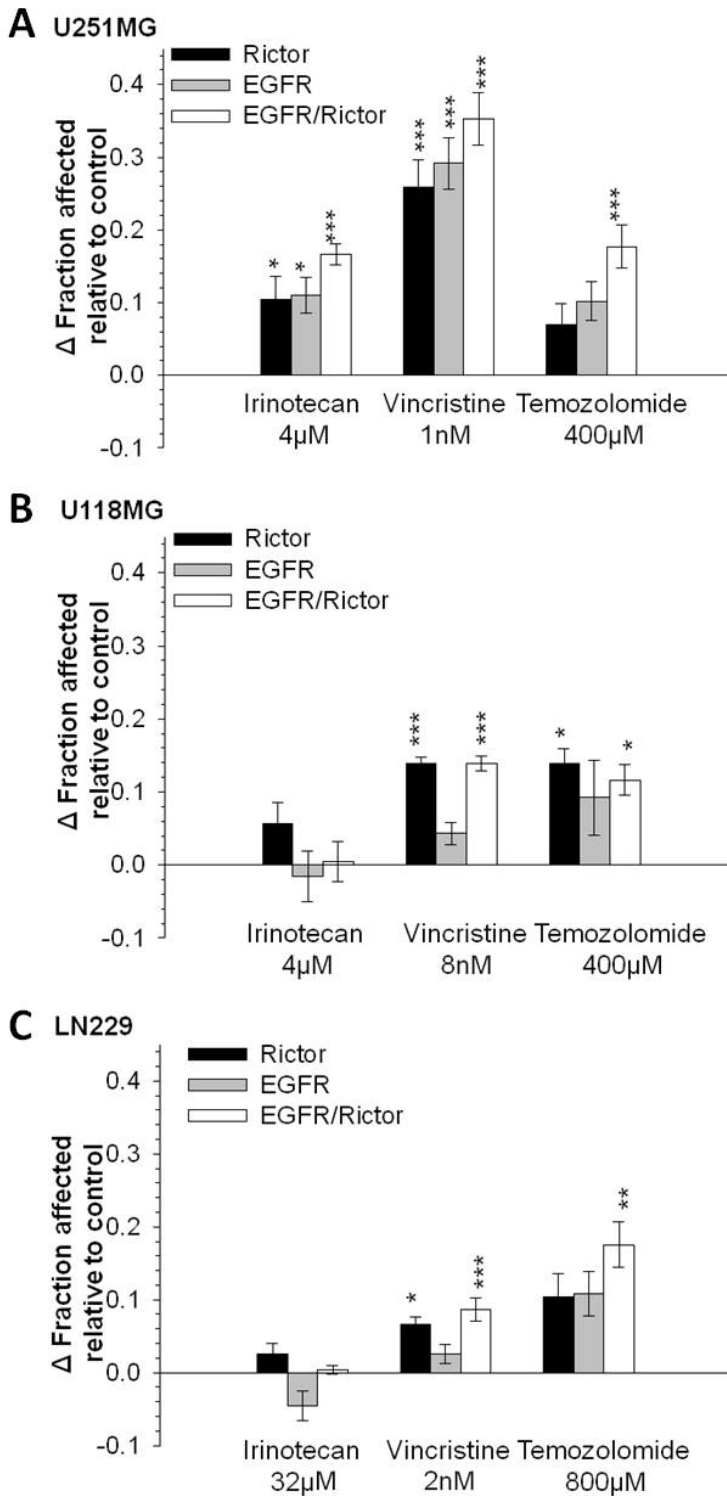


*Figure 36: Changes in fraction affected measured by MTT assay of a) U251MG, b) U118MG and c) LN229 cells 96hrs after transfection of siRNA against Rictor, EGFR or the combination of*

*Rictor and EGFR, and treated with irinotecan, vincristine or temozolomide at EC50 concentrations determined for untreated cells at 72hrs. Transfection of the two negative control sequences did induce an increase in Fa of LN229 exposed to vincristine of 0.13 compared to non-transfected cells and in this case only, changes in Fa are expressed relative to Ng2x-transfected cells. For all other cases, changes in Fa are expressed relative to non-transfected cells. \*p-value  $\leq 0.05$ ; \*\*p-value  $\leq 0.01$ ; \*\*\*p-value  $\leq 0.001$ .*

### **6.3.2 The combined silencing of Rictor and EGFR in an orthotopic model of GBM inhibits tumour growth**

In aggregate the *in vitro* data summarized above suggested that the combined silencing of EGFR and Rictor will decrease cell migration in U251MG and LN229 cells and that dual silencing of these targets did not reduce sensitivity (and in many cases actually increased sensitivity) to selected chemotherapeutic agents. These data were sufficient to justify further studies using an *in vivo* model of GBM. The therapeutic potential of the combined silencing of EGFR and Rictor was assessed *in vivo* in an orthotopic model of GBM generated by intracranial inoculation of shRNA expressing U251MG cells. U251MG cells were transduced using a lentiviral system designed to express shRNA sequences specific to EGFR (U251<sup>EGFR</sup>), Rictor (U251<sup>Rictor</sup>) or both (U251<sup>EGFR/Rictor</sup>). Control cells were produced by transduction with the negative control sequences (U251<sup>Ng2x</sup>) as described in the Methods. The expression system used was inducible in the presence of doxycycline. This facilitated characterization of the transduced cell lines prior to and following induction of shRNA expression. The lentiviral system used was also designed to co-express Turbo Red Fluorescent Protein (tRFP) upon doxycycline induction. tRFP expression was assessed using non-invasive imaging methods or by fluorescent microscopy of thin sections, as a means of confirming shRNA expression.

It was important to determine that lentivirus transduction did not influence the behaviour of the transduced U251MG cells prior to addition of doxycycline. Growth curves of the four

selected cell lines (U251<sup>Rictor</sup>, U251<sup>EGFR</sup>, U251<sup>EGFR/Rictor</sup>, or U251<sup>Ng2x</sup> cells) in the absence of doxycycline are provided in Figure 37a, where increases in cell number were followed over a 96hr time course. The results demonstrate that all four cell lines have identical growth rates *in vitro* when compared to the parental cell line. S.c. inoculation of all four cell lines in Rag2M mice also confirmed that U251<sup>Rictor</sup>, U251<sup>EGFR</sup>, U251<sup>EGFR/Rictor</sup>, or U251<sup>Ng2x</sup> exhibited comparable *in vivo* growth rate. Further, the sensitivity of these cell lines to irinotecan, vincristine and temozolomide was also assessed *in vitro* in the absence of doxycycline. The results, summarized in Figure 37b, indicate that the fraction affected following addition of the indicated drugs was not significantly different in the transduced cells when compared to the parental cells (filled bar), regardless of the drug concentration used.

**Figure 37: Un-induced lentiviral shRNA-transduced cells behave similarly to parental cells.**

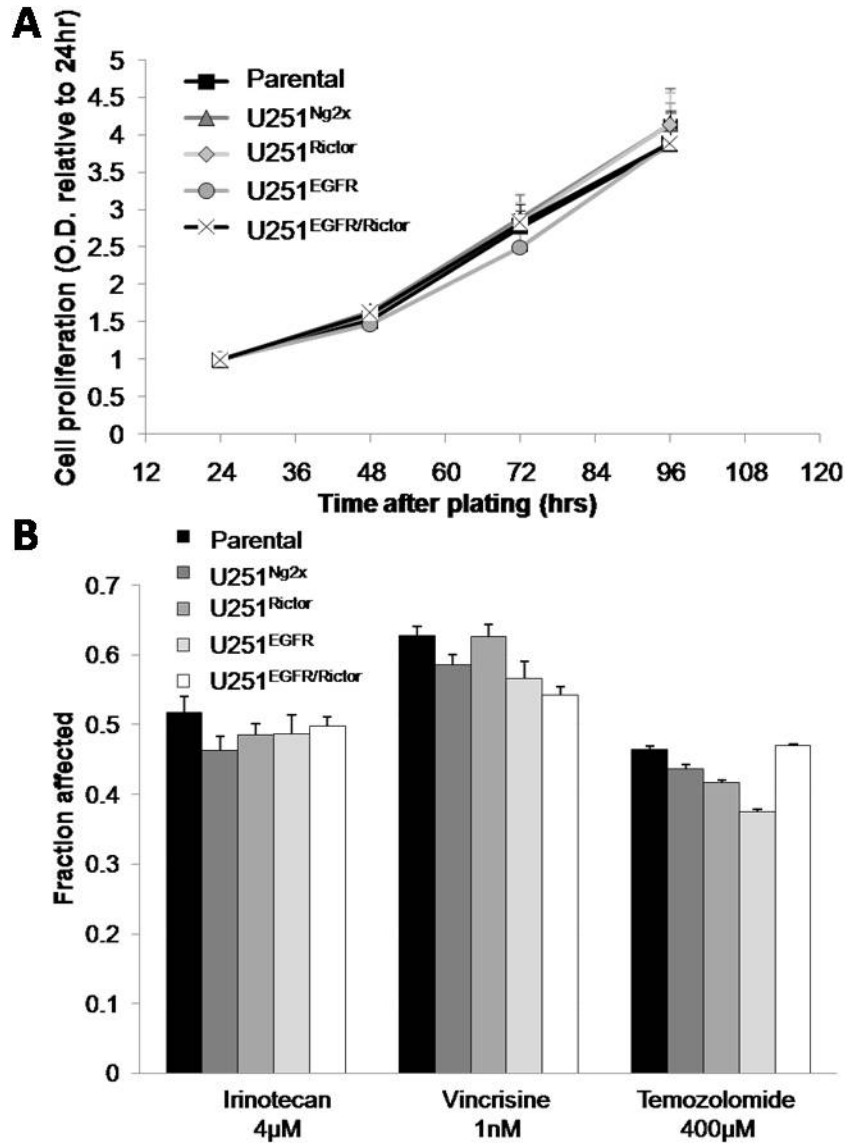


*Figure 37: a) Relative cell proliferation measured by MTT assay (24-96hr time points) of U251<sup>Ng2x</sup>, U251<sup>Rictor</sup>, U251<sup>EGFR</sup> and U251<sup>EGFR/Rictor</sup> in the absence of doxycycline. Optical density values are normalized to values obtained at 24hrs. b) Fraction affected (normalized to untreated cells) measured by MTT assay of U251<sup>Ng2x</sup>, U251<sup>Rictor</sup>, U251<sup>EGFR</sup> and U251<sup>EGFR/Rictor</sup> in the absence of doxycycline and treated with irinotecan, vincristine and temozolomide for 72hrs. All values shown represent the average from three independent experiments.*

To confirm that the shRNA expression caused reductions in EGFR and/or Rictor protein levels following addition of doxycycline, western immunoblot analysis was completed and these

data have been summarized in the representative immunoblot provided in Figure 38. The results (averaged optical density under each band is provided relative to values obtained from untreated controls for 3 independent experiments) show EGFR and Rictor expression in the parental U251MG line as well as U251<sup>Rictor</sup>, U251<sup>EGFR</sup>, U251<sup>EGFR/Rictor</sup>, and U251<sup>Ng2x</sup> cells in the presence (+) or absence (-) of doxycycline. The protein levels of Rictor and EGFR in the U251<sup>Ng2x</sup> cells, in the presence or absence of doxycycline, were not significantly different from the parental cells. In the absence of doxycycline, the levels of Rictor in the U251<sup>Rictor</sup> and U251<sup>EGFR/Rictor</sup> cells were not significantly different from that observed in the parental or the U251<sup>Ng2x</sup> lines. When U251<sup>Rictor</sup> and U251<sup>EGFR/Rictor</sup> cell lines were exposed to doxycycline, the levels of Rictor were reduced by 66% and 57% for U251<sup>Rictor</sup> and U251<sup>EGFR/Rictor</sup>, respectively (p<0.05). In the absence of doxycycline, the levels of EGFR in the U251<sup>EGFR</sup> and U251<sup>EGFR/Rictor</sup> cells were also not significantly different from that observed in the parental or the U251<sup>Ng2x</sup> lines. When the U251<sup>EGFR</sup> and U251<sup>EGFR/Rictor</sup> cells were cultured presence of doxycycline, the levels of EGFR were significantly (p<0.05) reduced (58% and 51%, respectively). Expression of tRFP following doxycycline induction was also confirmed (by fluorescence microscopy) in the U251<sup>Rictor</sup>, U251<sup>EGFR</sup>, U251<sup>EGFR/Rictor</sup>, or U251<sup>Ng2x</sup> cell lines, providing an additional demonstration of the functionality of the inducible system *in vitro*.

**Figure 38: Induction of lentiviral shRNA-transduced cells results in downregulation of the corresponding proteins *in vitro*.**

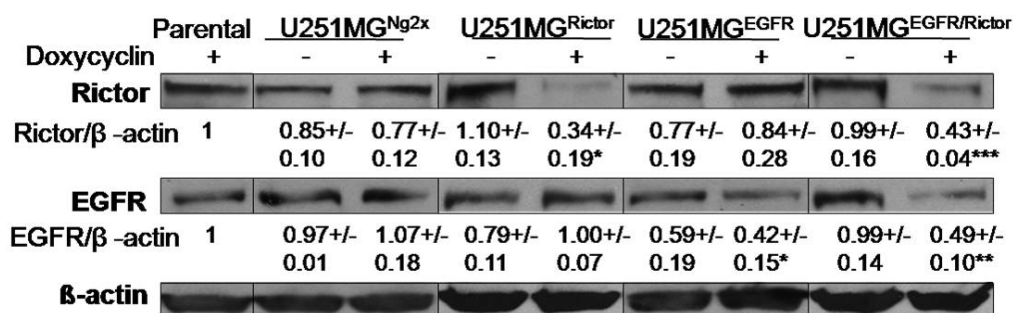


Figure 38: Representative immunoblots showing Rictor, EGFR and  $\beta$ -actin from parental U251MG cells, U251<sup>Ng2x</sup>, U251<sup>Rictor</sup>, U251<sup>EGFR</sup> and U251<sup>EGFR/Rictor</sup> in the absence (-) or presence

(+) of doxycycline. Average of band optical density normalized to  $\beta$ -actin from three independent experiments ( $\pm$ -SEM), and expressed as relative to values obtained from parental cells, is shown under each band. \* $p$ -value  $\leq 0.05$ ; \*\* $p$ -value  $\leq 0.01$ ; \*\*\* $p$ -value  $\leq 0.001$  compared to parental cells.

The effects of EGFR and Rictor downregulation alone or in combination were assessed in GBM models created following orthotopic inoculation of U251<sup>Rictor</sup>, U251<sup>EGFR</sup>, U251<sup>EGFR/Rictor</sup>, or U251MG<sup>Ng2x</sup> cells. Twenty-one days after cell inoculation, mice were given doxycycline *ad libitum* in drinking water as described in the Methods. Four weeks after doxycycline dosing was initiated (49 days after tumour cell inoculation), mice were imaged (Maestro<sup>TM</sup> fluorescence imager) to determine whether tRFP was expressed. Representative images, provided in Figure 39a, show that the expression of tRFP could be detected in animals inoculated with U251<sup>Rictor</sup>, U251<sup>EGFR</sup>, and U251<sup>Ng2x</sup> cells. However, no tRFP was detected in animals inoculated with U251<sup>EGFR/Rictor</sup> cells. All mice were terminated after imaging and their brains were harvested and sectioned as described in the Methods. Figure 39b provides representative images of brain sections isolated from each group. In animals inoculated with U251<sup>Rictor</sup>, U251MG<sup>EGFR</sup>, and U251<sup>Ng2x</sup> cells, tumours were detected and can be seen in Figure 39b by the presence of dense Hoechst-stained nuclei (blue) and tRFP (red) expression. No tumours could be detected in all eight animals inoculated with the U251<sup>EGFR/Rictor</sup> cells. Figure 39c provides representative images of tumour sections isolated from U251<sup>Rictor</sup>, U251<sup>EGFR</sup>, and U251<sup>Ng2x</sup> tumour-bearing animals. These sections were imaged for tRFP (red), EGFR (green), Rictor (yellow) and p(473)-AKT (orange). tRFP expression was confirmed in all three tumour groups. A decrease of 96% ( $p < 0.001$ ) in EGFR staining (normalized to Hoechst nuclei staining) was measured in tumours from animals inoculated with U251<sup>EGFR</sup> cells (Figure 39c and d). Rictor staining (normalized to Hoechst nuclei staining) was decreased by 81% ( $p < 0.01$ ) in tumours from animals inoculated with U251<sup>Rictor</sup> cells. Interestingly, a 65% reduction ( $p < 0.05$ ) in Rictor staining was also

observed in tumours from animals inoculated with U251<sup>EGFR</sup> cells and could be explained by the inhibition of signaling downstream of EGFR, resulting in decreases in Rictor transcription and/or translation levels. Of note, a slight 30% decrease was also observed in EGFR siRNA transfected-U251MG cells *in vitro*, but the effect was not statistically significant (not shown). Finally, a 97-99% reduction ( $p < 0.05$ ) in p(473)-AKT staining (normalized to Hoechst nuclei staining) was measured in tumours from animals inoculated with U251<sup>Rictor</sup> or U251<sup>EGFR</sup> cells.

Tumour size was estimated on the basis of histology data and these data (estimations of pixel number per tumour area of each section) have been summarized in Figure 39e. While the tumours in animals inoculated with U251<sup>Rictor</sup> and U251<sup>EGFR</sup> cells were smaller than those from animals inoculated with U251<sup>Ng2x</sup> cells, these differences were not significant. As noted already, tumour growth was completely inhibited in the animals inoculated with the U251<sup>EGFR/Rictor</sup> cells, an effect confirmed by two additional independent sets ( $n=4-8$ ) of intracranial inoculation with this cell line. The fraction of proliferating tumour cells was also determined in tumours from animals inoculated with U251<sup>Rictor</sup>, U251<sup>EGFR</sup>, and U251<sup>Ng2x</sup> cells by quantification of Ki67 positive staining (normalized to nuclei staining). These data, summarized in Figure 39e, indicate that there were no significant changes in the fraction of proliferating cells when the three groups were compared.

**Figure 39: Induction of orthotopically implanted shRNA-transduced cells results in downregulation of corresponding protein *in vivo* and the combined silencing of Rictor and EGFR results in a complete inhibition of tumour growth.**

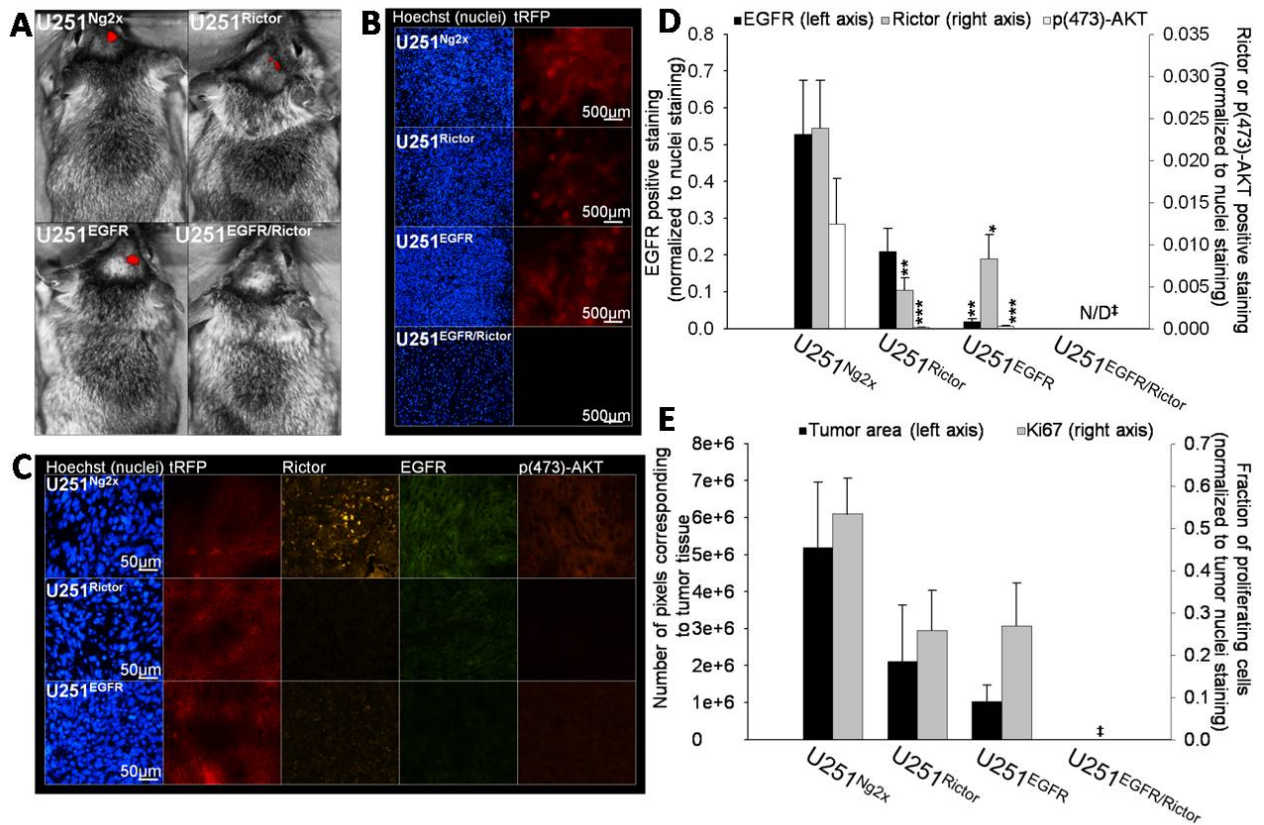


Figure 39: U251<sup>Ng2x</sup>, U251<sup>Rictor</sup>, U251<sup>EGFR</sup> and U251<sup>EGFR/Rictor</sup> cells were implanted into the right caudate nucleus-putamen of Rag2M mice (n=6-8). Induction of shRNA expression in mice was initiated on day 21 by dissolving 2mg/mL doxycycline and 5% sucrose in drinking water. a) On day 49, animals were imaged by Maestro<sup>TM</sup> fluorescence imaging unit for the expression of tRFP co-expressed with the shRNA sequences upon doxycycline-induced expression. Mice were then terminated and brains were harvested, sectioned and stained for nuclei, Rictor, EGFR and p(473)-AKT and imaged for all markers in addition to tRFP by robotic fluorescence microscopy. No tumour was detected in the U251<sup>EGFR/Rictor</sup> group. b) A representative brain section from U251<sup>Ng2x</sup>, U251<sup>Rictor</sup>, U251<sup>EGFR</sup> and U251<sup>EGFR/Rictor</sup> tumour groups is shown: tRFP (red) and Hoechst (blue). c) A representative tumour section from U251<sup>Ng2x</sup>, U251<sup>Rictor</sup> and U251<sup>EGFR</sup> tumour groups is shown: nuclei (blue), tRFP (red), Rictor (yellow), EGFR (green) and p(473)-

*AKT (orange). d) The expression of EGFR (left axis), Rictor (right axis) and p(473)-AKT (right axis) in U251<sup>Ng2x</sup>, U251<sup>Rictor</sup>, U251<sup>EGFR</sup> tumour sections were quantified (positive staining normalized to Hoechst nuclei staining). e) Tumour sizes were estimated by quantification of tumour areas in brain sections from all groups (left axis). The expression of the proliferation marker Ki67 in the tumour (proliferating fraction) was also quantified (right axis). \*p-value ≤ 0.05; \*\*p-value ≤ 0.01; \*\*\*p-value ≤ 0.001 compared to control untreated cells. ‡: No tumour was detected in the U251<sup>EGFR/Rictor</sup> group.*

### **6.3 Discussion**

The importance of mTOR and EGFR signaling in GBM has been reported and discussed extensively. Inhibition of mTOR alone [75, 76] or combined with EGFR targeting (erlotinib and gefitinib) [372, 374] has even been evaluated in GBM patients. These studies were initiated because therapeutic agents against these targets were already validated for use in the clinic and there was a great deal of pre-clinical evidence to support their use in GBM patients. However, results in patients treated with these agents have been disappointing [75, 76, 372, 374]. Recent studies have shed light on the complex protein interactions involving mTOR and this information can help us understand why mTOR inhibitors were not effective in the clinic. Rictor is part of the mTOR rapamycin-insensitive complex (mTORC2) [353], which functions in a manner that is distinct from mTOR rapamycin-sensitive complex (mTORC1). mTORC2 appears to be essential for the activation of AKT and signaling through mTORC2 promotes cell survival and proliferation [341]. In contrast, inhibition of mTORC1 by rapamycin removes the inhibitory signal of S6K1 on the Insulin Receptor Substrate 1 (IRS1), resulting in the activation of the PI3K/mTORC2/AKT pathway [359]. Rapamycin treatment increases p(473)-AKT in approximately 80% of cell lines tested, suggesting that most cancer cell lines will respond to rapamycin-induced mTORC1 inhibition by activating mTORC2 through this S6K1-mediated

feedback loop [359]. These data have led to the suggestion that all non-mTORC2-specific mTOR inhibitors may induce AKT activation while also promoting autophagy [391] and cell survival [364] through mTORC1 inhibition and this, in turn, would affect the therapeutic potential of mTORC2 inhibition. However, little is known about the structure of mTORC2 and how it is regulated by Rictor. Since there are no small molecule inhibitors specific to this complex, the studies described in this report have used RNAi-mediated gene silencing methods to assess the consequences of Rictor and EGFR silencing in models of GBM. This study reports for the first time, to our knowledge, that combined suppression of Rictor and EGFR in *in vitro* and *in vivo* GBM models can provide significant therapeutic benefits.

A shRNA expressing-GBM line was used as an approach towards *in vivo* validation of the therapeutic potential of the combined silencing of EGFR and Rictor in GBM suggested by *in vitro* studies. In brief, comparisons between the effect of Rictor and ILK siRNA-mediated silencing on AKT phosphorylation (p473) completed in PTEN-mutant U251MG cells confirmed the important role of Rictor in modulation of (p473)-AKT. The correlation between Rictor silencing and reductions in (p473)-AKT was also confirmed in the PTEN-mutant line U118MG cells, but could not be demonstrated in the PTEN wild-type LN229 cells. Other consequences associated with siRNA-mediated silencing of Rictor and/or EGFR included a reduction in cell migration (for U251MG and LN229 cells) and an increase in cell sensitivity to irinotecan, vincristine and temozolomide (see Figure 36). Rictor was previously shown to regulate PKC- $\alpha$  and MAPK activity [353, 365, 392-394], and it is possible that the effects observed following Rictor silencing in LN229 were the result of inhibition of these pathways rather than suppression of (p473)-AKT. In the PTEN-negative U118MG, Rictor siRNA alone caused an increase in cell sensitivity to vincristine and temozolomide. The combination of EGFR and Rictor silencing did not provide any additional therapeutic benefits when combined with the selected chemotherapeutics.

An inducible shRNA expression system was chosen as it allows for the *in vitro* analysis of the shRNA transduced lines in absence of shRNA expression in order to confirm that the lentiviral transduction and subsequent cell selection did not alter the characteristics of the cell population. Indeed, assessments of *in vitro* (MTT proliferation assay) and *in vivo* (s.c. inoculation) growth rates and *in vitro* drug sensitivity assays confirmed that the cell lines are comparable to each other and to the parental line in the absence of doxycycline. The utility of this system for validating silencing effects *in vivo* are highlighted by the tRFP expression data shown in Figure 39, which enabled direct confirmation of doxycycline-induced expression of shRNA in each cell line and tumour. Interestingly, while shRNA-mediated silencing of EGFR or Rictor alone had little or no impact on U251MG tumour development following doxycycline induction, three independent studies demonstrated that doxycycline induction in animals inoculated with U251MG cell line expressing shRNAs targeting both Rictor and EGFR resulted in a complete eradication of tumours. This synthetic lethal effect was not expected based on the *in vitro* studies completed with siRNA and is the focus of the discussion below.

The fact that combined silencing of EGFR and Rictor led to tumour eradication may have been anticipated on the basis of previous publications which have demonstrated the involvement of both proteins in tumourigenesis. EGFR signaling involves the PI3K/AKT, STAT3, MAPK and BCL-X<sub>L</sub> pathways regulating apoptosis, proliferation and differentiation [367]. Although the studies summarized here suggested that siRNA-mediated EGFR silencing had no effect on cell proliferation or apoptosis induction, other reports have shown that shRNA-mediated suppression of EGFR (using a non-inducible system) can promote apoptosis, cell cycle arrest and inhibition of cell proliferation *in vitro* [395-398] and can inhibit tumour growth *in vivo* [68, 69]. In this study, induction of EGFR-specific shRNA also caused a reduction in tumour size, albeit the effect was not significant. When considering the Rictor gene silencing data, others have shown that mTORC2/Rictor regulates apoptosis, cell cycle and invasion through

pathways involving AKT, PKC- $\alpha$  and MAPK [353, 365, 392-394], and that suppression of Rictor can reduce cell proliferation and migration *in vitro* [353, 365] and also inhibit tumour growth *in vivo* [365]. Again, the results presented here suggest that significant Rictor silencing (>60%) had no impact on cell proliferation and the effect on cell migration was only noted when both Rictor and EGFR were silenced simultaneously. Further, similar to results with the EGFR-specific shRNA, induction of Rictor silencing *in vivo* did impact tumour growth, but when compared to control cells, this effect was not significant.

In light of these previous reports, our observation showing that suppression of EGFR or Rictor alone did not affect tumour growth *in vivo*, and had little impact on cell proliferation and apoptosis *in vitro*, is intriguing. These results could be explained by the necessity for both targets to be suppressed at a certain threshold level in order to achieve therapeutic benefits. Despite the fact that the level of suppression of both targets was measured to be above 60% *in vitro* and above 80% *in vivo*, the remaining pool of proteins may have been sufficient to maintain survival and growth signals. Alternatively, compensating pathways may have been activated upon Rictor or EGFR suppression to maintain cell survival and proliferation in the conditions and cell lines used in this study. In this context, it is worth noting that the absence of significant therapeutic effects associated with EGFR inhibition in GBM have also been reported previously in pre-clinical [384, 399, 400] as well as in clinical studies [40, 71, 401, 402] using small molecule EGFR inhibitors or siRNA. More specifically, it was reported that the EGFR inhibitor gefitinib or the pan-PI3K inhibitor LY294002 given as monotherapy had no impact on tumour burden in a GBM model, yet when these inhibitors were used in combination, they blocked tumour growth [399]. Synergistic effects between mTOR and EGFR inhibitors in GBM have also been reported elsewhere [400, 403]. Taken together, these studies support the use of EGFR and mTORC2/Rictor pathway suppressors to achieve optimal therapeutic effects that may not be observed by inhibition of either pathway alone. This is exemplified by the synthetic

lethality observed in the studies reported here and induced by the co-suppression of EGFR and Rictor. This finding has not been reported previously and would not have been predicted based on the *in vitro* results summarized in this report.

It is expected that, in the clinic, the pharmacokinetic and toxicity profiles of targeting agents may limit the doses and treatment frequency that can be safely applied, permitting only a partial inhibition of the targets. It is unlikely that the dual targeted therapy validated here using RNAi-mediated gene silencing methods will be applicable to the clinic, unless improved methods for tumour-specific siRNA therapeutic delivery are discovered. Regardless, the *in vitro* data suggest that the combined suppression of EGFR and Rictor increased tumour cell sensitivity to temozolomide, irinotecan and vincristine; drugs which have been proven to prolong the survival time of GBM patients. A treatment including the combined suppression of the targets together with chemotherapy or radiation should then be considered. Most importantly, the *in vivo* data suggest that the dual inhibition of EGFR and Rictor produce significant therapeutic benefits, even in the absence of chemotherapy. Whether the benefits achieved in the clinic will be as significant as those shown here in an orthotopic model of GBM will likely depend on whether the treatment affects the brain tumour initiating cell (BTIC) population. The concept that there is a pool of dormant cancer cells existing within a tumour has emerged over the last few years, and these cells have been described as highly invasive and resistant to chemotherapeutic agents that target actively proliferating cells [11]. It has been proposed that after therapy or surgery, these cells are capable of entering the cell cycle to replenish the tumour cell population [8]. The fact that dual silencing of EGFR and Rictor led to tumour eradication would suggest that such treatment would target BTICs. Obviously, additional studies are needed to address these important questions and will include a comprehensive assessment of tumour phenotype immediately after the beginning of doxycycline induction, as well as an assessment of the fate of the BTIC population (CD133+ cells) in the *in vivo* model used here. In chapter 3, we reported

that IrC<sup>TM</sup> improves the delivery of irinotecan to the brain and increases the drug therapeutic efficacy in GBM [262]. It will be interesting to evaluate whether the dual targeting of EGFR and Rictor in established GBM tumours could lead to improved treatment outcomes when combined with IrC<sup>TM</sup>. The preclinical data generated through this research will be used to support further development of therapeutic approaches using EGFR and Rictor siRNAs or small molecule inhibitors in combination for use in GBM.

#### **6.4 Acknowledgements**

The research described in this original paper was supported by grant funding from the Canadian Institutes of Health Research (CIHR). Animal studies were conducted with the support of the excellent staff within the Animal Resource Centre at the BC Cancer Agency's Research Centre in Vancouver.

## Chapter 7: Discussion and conclusions

### 7.1 Summary

In chapter 2, it was demonstrated that IrC<sup>TM</sup>, Caelyx<sup>®</sup> and liposomal vincristine are effective against GBM grown subcutaneously or orthotopically. The tumour burden in treated animals was significantly smaller compared to control, indicating that the liposomal drugs used in this study are potent against GBM. Analysis of the vascular morphology also indicated that treatments affected the tumour vasculature to various degrees. Overall, IrC<sup>TM</sup> impacted the vasculature to a greater extent than the other formulations, and generated tumours with blood vessels that were morphologically more mature. IrC<sup>TM</sup> treatment restored the basement membrane architecture and reduced blood vessel diameters of the tumour vasculature of orthotopic tumours, suggesting a restoration of the vessel architecture to a more normal state. IrC<sup>TM</sup> treatment also increased the quantity of vessel staining in the center of tumours, suggesting a more homogenous distribution of blood across the entire tumour. Further, IrC<sup>TM</sup> reduced the  $K_{trans}$  value significantly, and this observation was consistent with the suggestion that treatment resulted in an improvement in vascular function. Taken together, these observations strongly suggested a vascular normalization effect where the blood vessels in tumours from animals treated with IrC<sup>TM</sup> behave more like vessels in the normal brain. The normalization of tumour vessels may create a window where blood flow is improved, leading to an opportunity to improve drug delivery [248]. In the case of GBM, normalization of tumour blood vessels should increase delivery of a drug that is capable of crossing the blood brain barrier, such as temozolomide. Pre-clinical studies to assess the impact of IrC<sup>TM</sup> treatments on the delivery and efficacy of temozolomide are currently underway.

The results presented in chapter 3 indicated that following injection of IrC<sup>TM</sup>, there were significantly higher levels of irinotecan and its active metabolite SN-38 in the mouse plasma

compartment compared with the injection of free drug. Although the mean  $AUC_{0-24hrs}$  for irinotecan in brain tissue was comparable for animals treated with IrC<sup>TM</sup> or free drug, exposure of the brain to SN-38 was far greater in mice given IrC<sup>TM</sup>. The data reported also demonstrated that the plasma L/C ratios (wt:wt) for irinotecan and SN-38 were significantly higher in animals treated with IrC<sup>TM</sup> compared to animals treated with free drug, suggesting that the IrC<sup>TM</sup> formulation was able to maintain the drug in its active form for extended time periods. Most importantly, the survival times of tumour bearing mice was increased significantly when mice were treated with IrC<sup>TM</sup> compared to the free drug at equivalent and equitoxic doses. These data supported the conclusion that carrier-mediated changes in the pharmacokinetic and biodistribution profiles of irinotecan and SN-38 increased their therapeutic activity in an orthotopic model of GBM. Data obtained in this chapter support the use of IrC<sup>TM</sup> for GBM treatment.

In chapter 4, cell populations expressing mCherry or mKate2 were generated and it was demonstrated that these cell lines can be used to establish intracranial tumours that allow for non-invasive imaging. *In vitro* and *in vivo* studies were completed to identify fluorescent cell lines that are phenotypically similar to the parental cell line. It was observed that the amount of fluorescent protein generated, which presumably correlates with the number of gene copies transduced into cells, influenced the growth of selected cell populations. However, it was also shown that this parameter was not the only factor involved. Changes in fluorescence signal intensity measured from the brain of animals inoculated with fluorescent cell lines could be used to follow tumour progression/regression and treatment efficacy. The availability of GBM models that can be used for non-invasive imaging will allow for the design of preclinical studies evaluating drug efficacy where experimental endpoints can be defined on the basis of tumour size estimated by imaging methods. A pre-clinical study is currently ongoing where orthotopic

GBM tumour progression and response to IrC<sup>TM</sup> and/or temozolomide treatment are monitored in live animals using the mKate2-U251MG model.

In chapter 5, the optimization of *in vitro* siRNA delivery technique was performed through comparisons between the use of cationic liposomes (Lipofectamine 2000<sup>TM</sup>) and nucleofection. It was found that the delivery of siRNA was significantly greater when using cationic liposomes. However, higher levels of target downregulation were achieved when using nucleofection methods, despite the fact that siRNA delivery was 12 to 30 fold lower compared to cationic liposome transfection (lipofection). Moreover, maximum levels of suppression occurred at a later time point when the siRNA sequence was delivered using lipofection. This delay may have been due to the time needed for the cationic lipid-associated siRNA to dissociate from the lipid and/or lipid structures following intracellular localization. In this chapter, we explored the effects of cationic lipids at the molecular level and how these effects specifically related to the targeted protein ILK. It was demonstrated that Lipofectamine 2000<sup>TM</sup> can influence p473-AKT and protein levels of mTOR. These effects appear to occur independently of ILK mediated silencing. Interestingly, our results suggested that ILK silencing was not associated with reductions in phosphorylation of AKT at Serine 473. It was suggested that this lack of effect may be the result of activation of one or more compensating pathways that eventually result in activation of AKT. Based on previously published literature [341], it was speculated that mTOR/Rictor may be involved in re-phosphorylation of AKT following silencing of ILK. Despite the fact that we recognize that lipid carriers will remain the best strategy for *in vivo* delivery as this system is able to prevent siRNA sequence degradation, maintain long circulation lifetimes of siRNA and foster enhanced delivery to the target cell population [56, 313, 314], we have demonstrated that the effects of cationic lipids on the expression or phosphorylation of proteins involved in the AKT pathway may be significant, and these effects should be considered

when designing siRNA lipid carrier systems. Finally, in light of the results from chapter 5, nucleofection methods were used for subsequent assays involving siRNA transfection *in vitro*.

In chapter 6, the therapeutic benefit of the combined suppression of Rictor and EGFR was assessed *in vitro* and in *in vivo* GBM models. The correlation between Rictor silencing and a reduction in (p473)-AKT was first confirmed in two PTEN-mutant cell lines, U251MG and U118MG, but could not be demonstrated in the PTEN wild-type LN229 cell line. The efficacy of siRNA-mediated combined silencing of Rictor and EGFR was then assessed *in vitro*. In U251MG and LN229 cells, combined suppression of EGFR and Rictor led to a reduction in cell migration and an increase in cell sensitivity to the chemotherapeutic drugs. In U118MG cells, Rictor suppression alone caused an increase in cell sensitivity to chemotherapeutic drugs, and the addition of EGFR in combination with Rictor siRNA did not provide any additional benefits in this cell line. shRNA expressing-U251MG cell lines were used to validate the therapeutic potential of the combination of EGFR and Rictor silencing in an orthotopic model of GBM. Interestingly, while the shRNA-mediated silencing of EGFR or Rictor generated tumours of sizes comparable to the negative control shRNA population, three independent sets of inoculations confirmed that the cell line carrying shRNA against EGFR and Rictor had lost its capacity to generate tumours. Although it could not be confirmed *in vivo*, it is reasonable to suggest, based on *in vitro* results, that treatment which includes the combined suppression of EGFR and Rictor together with chemotherapy or radiation should improve treatment outcome in patients. More importantly, the dual suppression of EGFR and Rictor seemingly inhibited tumour formation *in vivo*. This observation implies that such treatment would prevent chemotherapy and/or radiation resistant tumour cells from replenishing the tumour after treatment. Finally, these studies have provided justification for future studies evaluating the efficacy of the combination of siRNA targeting EGFR and Rictor with IrC<sup>TM</sup>-based chemotherapy in established GBM tumour models.

## 7.2 Defining the optimal siRNA delivery system for GBM therapy

The therapeutic potential for the combined use of siRNA against EGFR and Rictor was demonstrated in chapter 6. However, as discussed previously, the clinical application of siRNA is limited by issues related to delivery, especially in the case of brain tumours. In chapter 1 (Table 2), I listed some reports for which successful target downregulation was obtained in orthotopic brain tumour following i.v. injection of free siRNA sequences. However, the need for large amounts of siRNA to be injected systemically in order to achieve downregulation in the brain (in contrast to the liver) is probably the main reason why siRNAs have not yet made their way into clinical trials for brain pathology patients. Indeed, preferential accumulation of siRNAs in the liver and kidney was previously reported following i.v. administration, while very little accumulation was detected in the brain [175-177].

The concept of targeted delivery has been suggested by many to be the solution to the obstacle of siRNA delivery to brain tumours [404, 405]. An efficient targeting strategy should promote specific crossing of the therapeutic material across tumour-associated BBB, passage through cancer cell membranes, and prevention of accumulation in healthy tissue. Antibody-coupled liposomes (immunoliposomes) combine the capacity of LNPs to increase nucleic acid half-life in the blood compartment with specific targeting to tumour sites. One of the first attempts to deliver material to the brain using immunoliposomes was done by coupling the monoclonal antibody OX26 specific against the transferrin receptor [406] to DSPE-PEG liposomes. The transferrin receptor is present at the surface of normal brain capillary endothelial cells and is upregulated in brain tumour tissue [407]. Following i.v. injection of OX26 coupled-DSPE-PEG immunoliposomes encapsulating the chemotherapeutic agent daunomycin, an average of 0.03% of the injected dose of daunomycin was measured in the brain of rats after 60 min, while only 0.008% of injected daunomycin dose was measured following administration of free daunomycin or non-OX26-conjugated daunomycin DSPE-PEG carrier [406]. The use of

mouse transferrin receptor-targeted immunoliposomes has also shown success in the delivery of bigger molecules such as DNA plasmids [408] or siRNAs [409] to brain tumours.

The arginine-glycine-aspartic acid (RGD) motif of fibronectin has also been used to target delivery of siRNAs in a s.c. model of neuroblastoma [410]. RGD binds to integrins that are expressed on activated endothelial cells found in tumour vasculature of many advanced cancers including GBM [411]. *In vivo* studies demonstrated the accumulation of CY5.5-RGD in cells and vessels of orthotopic GBM tumours following i.v. injection [412], supporting its potential use for siRNA targeting to GBM tumours.

Antibodies against GBM micro-environment specific antigens could also be used to target nucleic acid sequences to the tumour tissue. For example, tumour-associated endothelial cells in GBM have higher levels of VEGFR2 than normal endothelial cells [413]. Targeting VEGFR2 receptor could be used to specifically deliver material across the brain tumour-associated BBB. CD44 is a surface receptor overexpressed in GBM tumour cells [304] and could also be used for immunoliposome targeting. Further, targeting markers found at the surface of brain tumour initiating cells (BTIC) (e.g. CD133) [414, 415] could potentially allow specific suppression of defective genes in these cells. BTIC are a sub-population of cells that have the ability to reconstitute the overall tumour cell population and are typically more resistant to chemotherapy and radiation than the rest of the tumour cell population [416]. It is now believed that treatment resistance and eventual relapse results in part from a failure to eliminate BTICs [417]. It is important to note that CD133 is also expressed in normal stem cells [418] and use of this marker as a target could negatively impact healthy CD133+ cells. Therefore, it appears necessary to combine several targeting strategies to achieve both efficacy and specificity. For example, use of immunoliposomes specific to human insulin receptor and mouse transferrin receptor was more effective at delivering nucleic acid molecules to brain tumours cells than a carrier specific to mouse transferrin receptor only in a human xenograft murine

model [419]. This dual receptor targeting strategy was used to deliver ASOs or shRNA plasmids to orthotopic brain tumours [68, 69] and resulted in 88-100% increase in animals' lifespan when compared to untreated animals. Thus, a treatment aimed at targeting BTIC could include a proportion of transferrin and insulin targeting immunoliposomes that would also incorporate antibodies against the CD133 marker. Such system could increase the likelihood that all targeted CD133+ cells are part of the tumour tissue.

The complex and heterogenous nature of brain tumours seems to require multivalency of delivery systems in order to achieve highly specific and efficient siRNA delivery. Targeted delivery systems will also have to be versatile, allowing the encapsulation of diverse combinations of siRNA (e.g. against EGFR and Rictor) selected based on the patient's tumour genetic profile. Once a system for efficient siRNA delivery to GBM tumours has been optimized, it could be administered subsequently to tumour vascular normalization therapy using agents such as IrC<sup>TM</sup> which, as demonstrated in chapter 2, can increase the tumour vascular functionality as well as the area covered by the vascular network (Figure 9d).

### **7.3 The consequences of vascular normalization are dependent on tumour dynamics**

As presented in Chapter 2, liposomal formulations of irinotecan (IrC<sup>TM</sup>), doxorubicin (Caelyx®) and vincristine induce normalization of the tumour vasculature. The model chosen to demonstrate this effect was the highly angiogenic and aggressive GBM cell line U251MG. To examine the effect of IrC<sup>TM</sup> on tumour micro-environment in relation to tumour dynamics (i.e. growth rate, vasculature functionality, etc.), we also evaluated the effect of IrC<sup>TM</sup> on the vasculature of tumours generated by the PTEN negative U118MG GBM line. U118MG is a much slower growing cell line than U251MG, and its *in vitro* doubling time is 45% greater ( $p < 0.0001$ ) than that of U251MG (Figure 40). *In vivo*, the size of orthotopic tumours (tumour area measured by pixel count; see chapter 2 for method) generated by U118MG was 4.4 fold

( $p < 0.05$ ) smaller ( $67,161 \pm 5,198$  pixels; see Figure 41a) than tumours generated with U251MG ( $295,959 \pm 47,477$  pixels; see Figure 9b) 42 days after tumour inoculation. Moreover, the fraction of endothelial cells/viable tumour area was 67% smaller ( $p < 0.05$ ) in U118MG tumours ( $0.017 \pm 0.002$  positive pixels/unit area; Figure 41b) than in U251MG tumours ( $0.074 \pm 0.009$  positive pixels/unit area; see Figure 9c), suggesting that U118MG tumour model is much less aggressive and angiogenic than the U251MG model. These data justify the use of the U118MG model to evaluate the effect of IrC<sup>TM</sup> in comparison to data obtained with the U251MG (chapter 2) in the context of tumour dynamics.

**Figure 40:** *In vitro* cell proliferation rate of GBM cell lines U251MG, U118MG and LN229

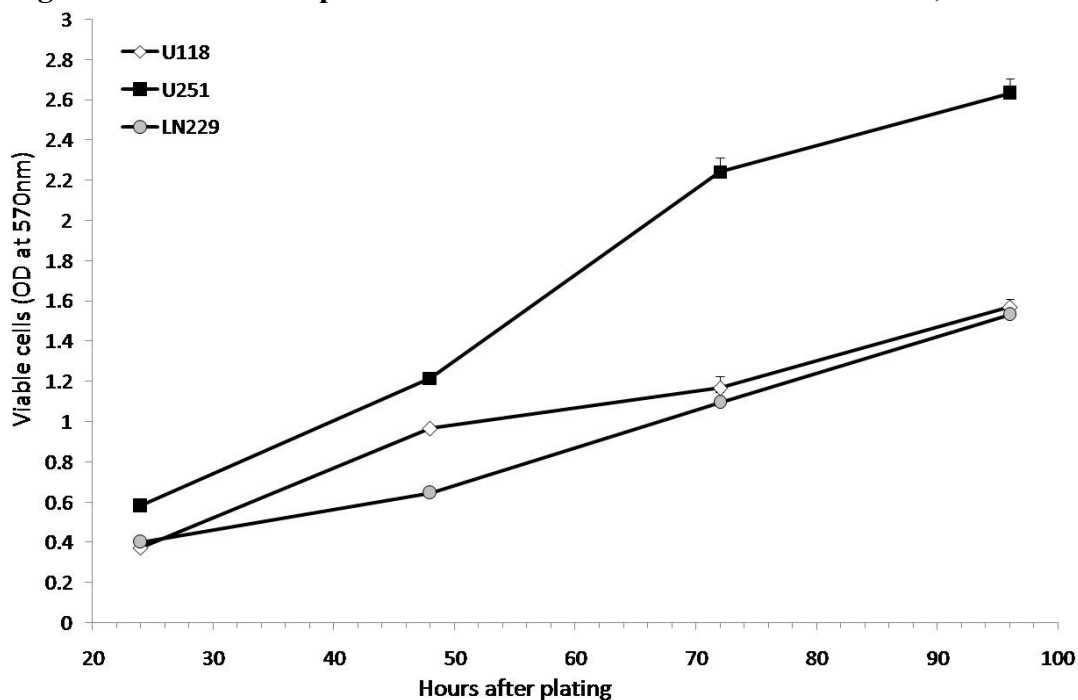


Figure 40: Cells were plated in 96 well plates and MTT reagent was added at 1.25 mg/mL 24-96hrs after. After 3hrs of incubation, MTT containing medium was replaced by DMSO, and plates were read at 570nm using a spectrophotometer. U118MG and LN229 have an *in vitro* doubling time of  $35.3 \pm 3.9$ hrs and  $38.9 \pm 1.3$ hrs respectively, and U251MG is a faster growing line with a doubling time of  $20.9 \pm 1.2$ hrs.

On day 42 after tumour inoculation, U118MG orthotopic tumour bearing Rag2M were treated with 25mg/kg IrC<sup>TM</sup> (Q7d x3). At the end of the study, brains were harvested, sectioned and stained using the same methods described in chapter 2. Surprisingly, IrC<sup>TM</sup> treatment had no impact on tumour size (Figure 41a). The effect of IrC<sup>TM</sup> on the tumour vasculature was also assessed based on the methods described in chapter 2, and values obtained were also not significantly different from untreated tumours (Figure 41 a to c). However, even if these data were not statistically different between treated and untreated tumours, their analysis can still provide valuable information that can be used in the design of future studies using the U118MG model. Although not statistically significant, IrC<sup>TM</sup> treatment increased the fraction of proliferating cells (Ki67/viable unit area) by 4-fold (p=0.10) and the nuclear density by 2.4-fold (p=0.14; Figure 41a). Moreover, IrC<sup>TM</sup> induced changes on the tumour vasculature that were apparently in contrast to what was reported using the U251MG model in chapter 2. IrC<sup>TM</sup> treatment increased the fraction of endothelial cells (per viable unit area) of 1.4-fold (p=0.19) in the tumour, increased the delivery of the perfusion marker Hoechst 33342 (per viable unit area) by 3.1-fold (p=0.19) and increased the fraction of Hoechst-positive endothelial cells (per viable unit area) by 4.6-fold (p=0.21), the latter being an indication of increased presence of perfused functional vessels (Figure 41b). Finally, analysis of the morphology of tumour vessels using the normalization determinants described in chapter 2 revealed that treatment did not induce the same kind of normalization that was described in chapter 2 (Figure 41c).

**Figure 41: Analysis of the effect of Irinophore C<sup>TM</sup> on the tumour micro-environment of U118MG GBM orthotopic model**

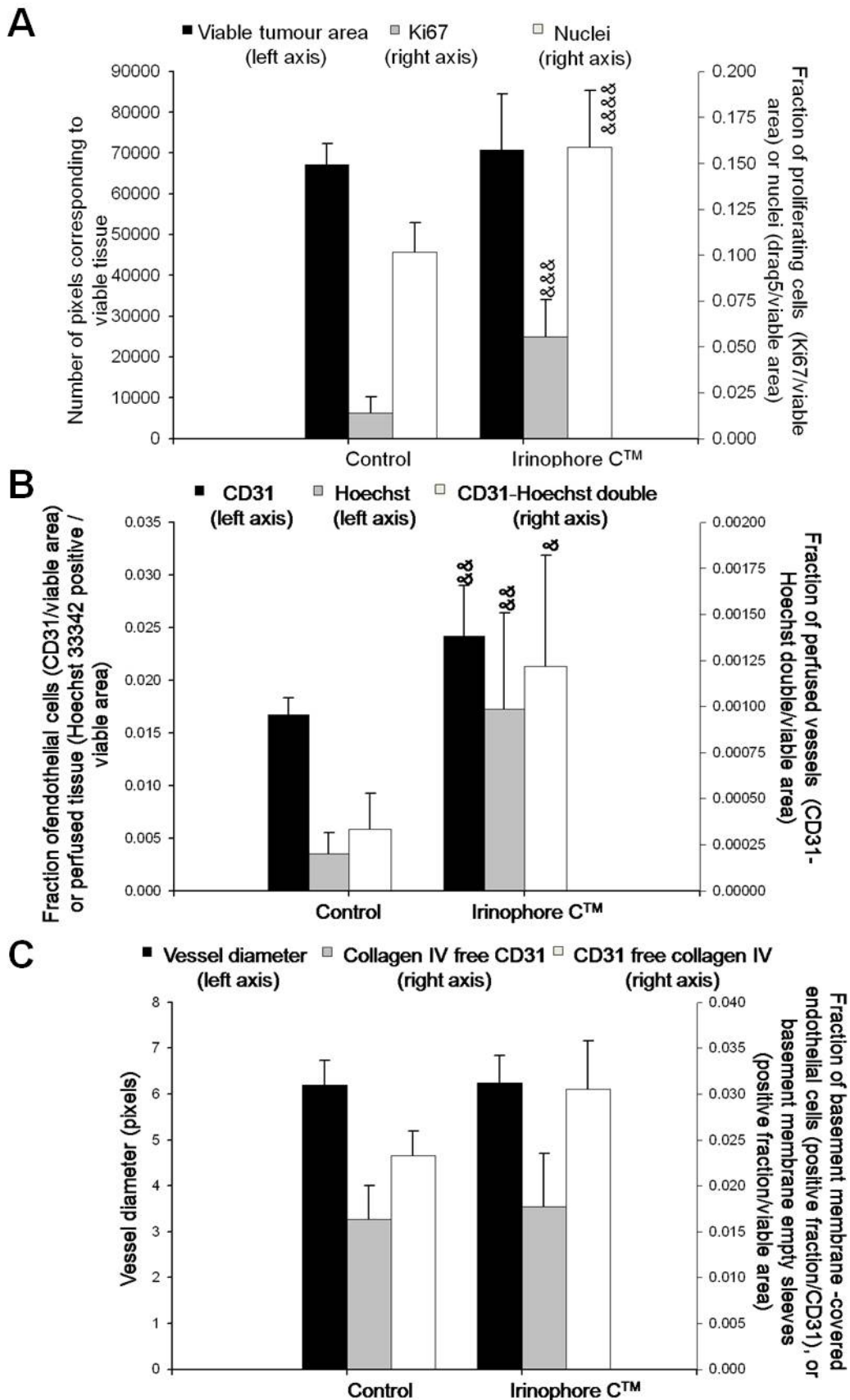


Figure 41: U118MG orthotopic tumour-bearing Rag2M mice were treated i.v. with IrC<sup>TM</sup> at 25mg/kg Q7x3. One week after the last treatment, brains were harvested, sectioned, stained and imaged as described in chapter 2. Twenty minutes prior to termination, Hoechst 33342 was injected i.v. and used as a marker of vessel function. a) Tumour areas were quantified in number of pixels, and used as a measure of treatment induced reduction of the tumour mass (■, left axis). Tumour cell proliferation (Ki67/viable unit area; ■, right axis) and nuclear density (Draq5/viable unit area; □, right axis) were quantified. b) Endothelial cell density (CD31/viable unit area, ■, left axis), Hoechst staining (Hoechst/viable unit area, ■, left axis) and Hoechst and CD31 co-staining (/viable unit area; □, right axis) were quantified. c) Vessel diameter (■, left axis), basement membrane-free endothelial cells (/viable unit area; ■, right axis) and endothelial cells-free basement membrane; □, right axis) were quantified. &p-value=0.21; &&p-value=0.19; &&&p-value=0.14; &&&&p-value=0.10.

These results, at first puzzling, could be explained by the dynamics of this tumour model. It is probable that the slow-growing nature of this cell line reduced the tumour sensitivity to the drug. Moreover, a dramatic difference in Hoechst delivery between the two untreated tumour models (0.0035±0.002 for U118MG; Figure 41b vs 0.39±0.08 pixels/viable unit area for U251MG; Figure 9c; p<0.001) suggests that the vasculature in U118MG model is more organized and less leaky than what was observed in the U251MG, and this could certainly contribute to a reduction in drug delivered to the tumour. In order to circumvent these obstacles, a higher dose could be used.

The fact that IrC<sup>TM</sup> induced a slight increase in endothelial cell fraction, Hoechst delivery, perfused vessel fraction and proliferating tumour cells suggests that the dose used did impact the tumour micro-environment. It is possible that IrC<sup>TM</sup> initially reduced the tumour burden and pruned the non-functional vessel population, leaving behind smaller tumours with a more functional and abundant vasculature, which could explain the increase in endothelial cell

fraction, Hoechst delivery and perfused vessel fraction. This, in turn, would have led to better nutrient delivery promoting an increase in tumour cell proliferation and allowing the treated tumours to grow to a size comparable to untreated tumours. Interestingly, a transient increase in proliferation induced by IrC<sup>TM</sup> was also reported in the U251MG model in chapter 3. This increased proliferation was observed 20 days after the end of treatment only but not 35 days after the end of treatment. For the present study, brain tumour harvest was done 7 days after the last treatment, and the information obtained is only representative of a single time point. Studies analyzing how vascular function is changed over the course of a treatment will be needed to help understand the effect of IrC<sup>TM</sup> on the tumour vasculature and micro-environment over time.

The results of this study suggest that if the capacity of IrC<sup>TM</sup> to alter the tumour vasculature is to be useful in the clinic, it will be important to use imaging technologies [251, 272] to assess changes in tumour micro-environment and vasculature before, during and after treatment in patients. This will allow for adjustments in the treatment dose and scheduling to reach a balance between normalization of the vasculature that would increase the delivery of a second drug and normalization of the vasculature that would promote an increase in tumour growth. Studies using other GBM models with different tumour dynamics (growth rate, vasculature functionality, etc.) are needed to help better define the impact of IrC<sup>TM</sup>-induced vascular normalization on tumour micro-environment. Moreover, assessing changes in  $K_{trans}$  in these models will provide an indication of the correlation between the degree of vascular normalization in response to IrC<sup>TM</sup> treatment using the methods described in chapter 2 and the clinically validated  $K_{trans}$  measurement of blood flow/vascular permeability.

## **7.4 Development of mKate2-expressing U118MG GBM line for non-invasive imaging**

Chapter 3 described the development of mKate2 and mCherry expressing U251MG lines for non-invasive imaging. A U118MG GBM line expressing mKate2 was also developed during this process using the same FACS-based sorting of the different populations of cells based on fluorescence intensity. mKate2-U118MG (medium) proliferation rate and sensitivity to irinotecan *in vitro*, as well as an orthotopic tumour growth rate, were compared to that of the parental line and the results confirmed that the transfected cell line remained unchanged by the transfection process (Figure 42). A small study using U118MG cells demonstrated that the knowledge acquired in the development of mKate2-U251MG cell lines (Chapter 4) can be used to expedite the production of additional cell lines for fluorescence imaging. This aspect will be of great interest in the upcoming research era where pre-clinical studies assessing the efficacy of targeted therapy agents will be conducted using orthotopic inoculation of tumour cells from patient samples to acquire information that will guide individual treatment decisions.

**Figure 42: Comparisons of *in vitro* cell proliferation rate, *in vitro* drug sensitivity, and *in vivo* tumour growth rate between parental and mKate2-expressing U118MG lines**

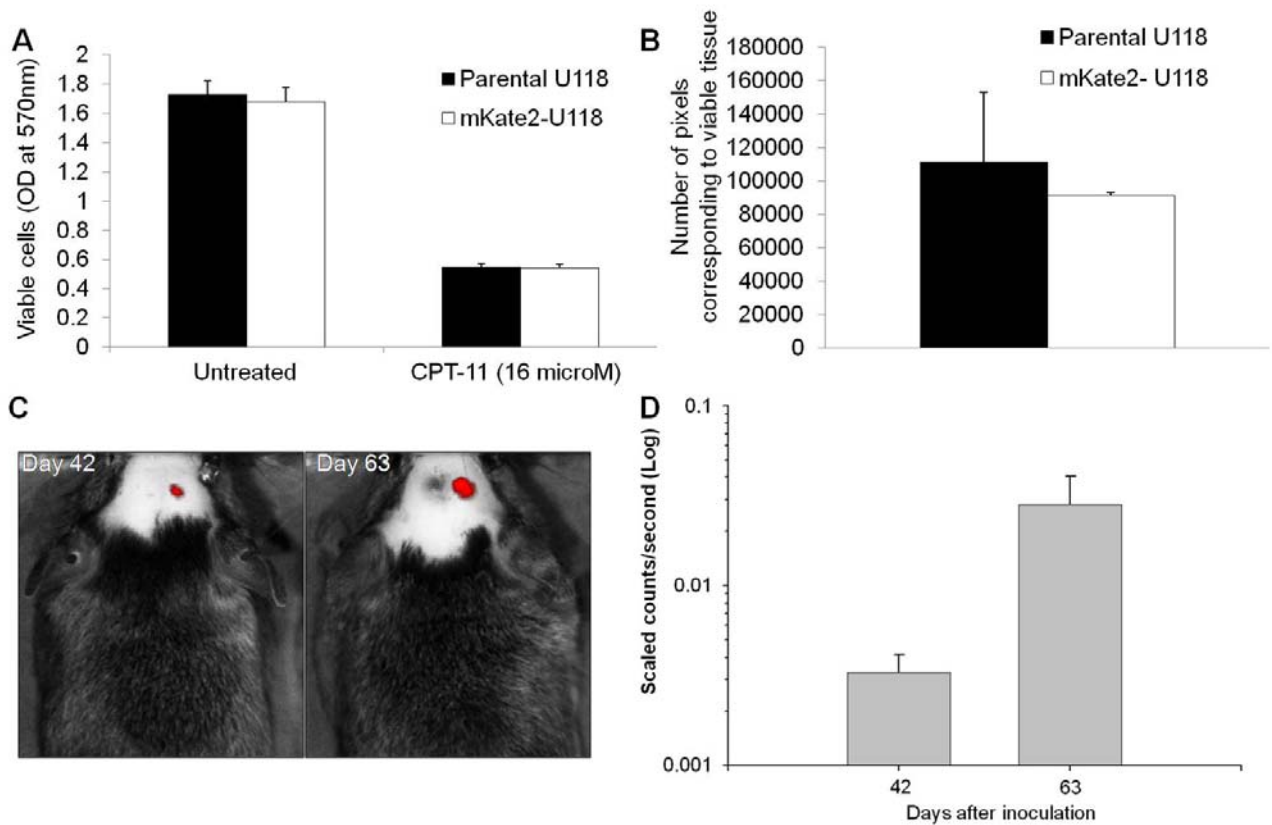


*Figure 42: The a) in vitro proliferation rate 96hrs after plating of untreated mkate2-expressing U118MG cells, or treated with irinotecan (16 $\mu$ M) and b) untreated orthotopic tumour size (tumour area expressed in pixel count) 42 days after tumour cell inoculation. The fluorescence signal emitted from the animal brains was c) captured and d) measured (scaled counts/second) on day 42 and 63 after inoculation.*

## 7.5 Conclusion

It is widely recognized that there is a tremendous potential in the use of targeted agents to treat GBM and, importantly, to become the therapeutic modality of choice when developing target-specific personalized treatment options. I believe that there are three main areas in need of investigation that could lead to improved treatment outcome in GBM: (i) Use of targeted agents in combination with conventional treatment options: the capacity of SMIs or siRNAs to enhance

the activity of chemotherapeutic agents or radiation should be tested in established GBM orthotopic models and in clinical studies. (ii) Use of targeted agents customized therapy: the anti-tumour efficacy of SMIs or siRNAs should be tested using GBM tumours arising from orthotopic inoculation of patient tumour samples for which a list of genetic defects (e.g. EGFR amplification, PTEN mutation) is available. (iii) Use of delivery systems to circumvent the obstacles of delivery to brain tumours and improve efficacy of targeted agents and chemotherapeutics: antibody-coupled carriers should be designed to improve delivery to the tumour, and the ligand specificity of such a carrier should be made based on immunohistopathology analysis of each individual tumour.

Another important issue would be to determine how many treatment agents must be included in order to achieve GBM cure. While most combination clinical trials will typically test 2 or 3 agents, it may be necessary to consider using 5 or even 10 different compounds that will block or eradicate all tumourigenic phenotypes of a cancer. Obviously, the design complexity of these trials may be a limiting factor. However, pre-clinical approaches where animals are inoculated orthotopically with tumor cells from patient samples could provide an avenue for testing several combination therapy options in a model that is more representative of the clinical reality than conventional models using commercially available cell lines. Moreover, non-invasive imaging will facilitate the use of such models by providing immediate information on treatment response. The research reported in this thesis has provided a springboard for these types of studies and will certainly contribute to the future of research aimed at defining more effective treatment options for patients affected by GBM.

## Bibliography

- [1] CBTRUS, Statistical Report: Primary Brain and Central Nervous System Tumors Diagnosed in the United States in 2004-2006. In: Central Brain Tumor Registry of the United States, Hinsdale, IL. (2010) Accessed in February 2011, Available from: [www.cbtrus.org](http://www.cbtrus.org)
- [2] CCS, Statistics for brain cancer. In: Canadian Cancer Society (2010) Accessed in February 2011, Available from: [www.cancer.ca](http://www.cancer.ca).
- [3] Clarke J, Butowski N and Chang S, Recent advances in therapy for glioblastoma. *Arch Neurol* (2010) 67, 279-283.
- [4] Stupp R, Hegi ME, Mason WP, van den Bent MJ, Taphoorn MJ, Janzer RC, Ludwin SK, Allgeier A, Fisher B, Belanger K, Hau P, Brandes AA, Gijtenbeek J, Marosi C, Vecht CJ, Mokhtari K, Wesseling P, Villa S, Eisenhauer E, Gorlia T, Weller M, Lacombe D, Cairncross JG and Mirimanoff RO, Effects of radiotherapy with concomitant and adjuvant temozolomide versus radiotherapy alone on survival in glioblastoma in a randomised phase III study: 5-year analysis of the EORTC-NCIC trial. *Lancet Oncol* (2009) 10, 459-66.
- [5] Blasberg RG, Kobayashi T, Horowitz M, Rice JM, Groothuis D, Molnar P and Fenstermacher JD, Regional blood-to-tissue transport in ethylnitrosourea-induced brain tumors. *Ann Neurol* (1983) 14, 202-15.
- [6] Pardridge WM, Blood-brain barrier delivery. *Drug Discov Today* (2007) 12, 54-61.
- [7] Groothuis DR, Fischer JM, Pasternak JF, Blasberg RG, Vick NA and Bigner DD, Regional measurements of blood-to-tissue transport in experimental RG-2 rat gliomas. *Cancer Res* (1983) 43, 3368-3373.
- [8] Liu JM, Mao BY, Hong S, Liu YH and Wang XJ, The postoperative brain tumour stem cell (BTSC) niche and cancer recurrence. *Adv Ther* (2008) 25, 389-98.
- [9] Frosina G, DNA repair and resistance of gliomas to chemotherapy and radiotherapy. *Mol Cancer Res* (2009) 7, 989-99.
- [10] Lu C and Shervington A, Chemoresistance in gliomas. *Mol Cell Biochem* (2008) 312, 71-80.
- [11] Sanchez-Martin M, Brain tumour stem cells: implications for cancer therapy and regenerative medicine. *Curr Stem Cell Res Ther* (2008) 3, 197-207.
- [12] Chandana SR, Movva S, Arora M and Singh T, Primary brain tumors in adults. *Am Fam Physician* (2008) 77, 1423-30.
- [13] Brada M, Collins VP, Dorward NL and Thomas DGT, Tumours of the brain and spinal cord in adults. *Oxford Textbook of Oncology* (2001) 2, 2707-2753.
- [14] Stupp R, Mason WP, van den Bent MJ, Weller M, Fisher B, Taphoorn MJ, Belanger K, Brandes AA, Marosi C, Bogdahn U, Curschmann J, Janzer RC, Ludwin SK, Gorlia T, Allgeier A, Lacombe D, Cairncross JG, Eisenhauer E and Mirimanoff RO, Radiotherapy plus concomitant and adjuvant temozolomide for glioblastoma. *N Engl J Med* (2005) 352, 987-96.
- [15] Cormack DH, Section 14: Nervous Tissue and the Nervous System. *Ham's Histology* (1987)
- [16] Prados M, Histology of Primary Tumors of the Central Nervous System. *American Cancer Society Atlas of Clinical Oncology: Brain Cancer* (2002) 1, 29-103.
- [17] Kim YH, Nobusawa S, Mittelbronn M, Paulus W, Brokinkel B, Keyvani K, Sure U, Wrede K, Nakazato Y, Tanaka Y, Vital A, Mariani L, Stawski R, Watanabe T, De Girolami U, Kleihues P and Ohgaki H, Molecular classification of low-grade diffuse gliomas. *Am J Pathol* (2010) 177, 2708-14.
- [18] Gray H, Chapter 22: Cerebral Hemisphere & Chapter 23: Basal Ganglia. *Gray's Anatomy: The anatomical basis of Clinical Practice* (2005) 1, 387-430.

- [19] Wikimedia, Glioblastoma macro. In: Wikimedia Commons (2007) Accessed in September 2010, Available at: commons.wikimedia.org.
- [20] Stevens A, Lowe JS and Young B, A colour atlas and text. Wheater's basic histopathology (2002) 1, 65-85.
- [21] Newlands ES, Stevens MF, Wedge SR, Wheelhouse RT and Brock C, Temozolomide: a review of its discovery, chemical properties, pre-clinical development and clinical trials. *Cancer Treat Rev* (1997) 23, 35-61.
- [22] Jacinto FV and Esteller M, MGMT hypermethylation: a prognostic foe, a predictive friend. *DNA Repair (Amst)* (2007) 6, 1155-60.
- [23] Hegi ME, Diserens AC, Gorlia T, Hamou MF, de Tribolet N, Weller M, Kros JM, Hainfellner JA, Mason W, Mariani L, Bromberg JE, Hau P, Mirimanoff RO, Cairncross JG, Janzer RC and Stupp R, MGMT gene silencing and benefit from temozolomide in glioblastoma. *N Engl J Med* (2005) 352, 997-1003.
- [24] Sadones J, Michotte A, Veld P, Chaskis C, Sciort R, Menten J, Joossens EJ, Strauven T, D'Hondt LA, Sartenaer D, Califice SF, Bierau K, Svensson C, De Greve J and Neyns B, MGMT promoter hypermethylation correlates with a survival benefit from temozolomide in patients with recurrent anaplastic astrocytoma but not glioblastoma. *Eur J Cancer* (2009) 45, 146-53.
- [25] Yu J, Zhang H, Gu J, Lin S, Li J, Lu W, Wang Y and Zhu J, Methylation profiles of thirty four promoter-CpG islands and concordant methylation behaviours of sixteen genes that may contribute to carcinogenesis of astrocytoma. *BMC Cancer* (2004) 4, 65.
- [26] Lorente A, Mueller W, Urdangarin E, Lazcoz P, von Deimling A and Castresana JS, Detection of methylation in promoter sequences by melting curve analysis-based semiquantitative real time PCR. *BMC Cancer* (2008) 8, 61.
- [27] Stupp R, Hegi ME, van den Bent MJ, Mason WP, Weller M, Mirimanoff RO and Cairncross JG, Changing paradigms--an update on the multidisciplinary management of malignant glioma. *Oncologist* (2006) 11, 165-80.
- [28] Walker MD, Alexander E, Jr., Hunt WE, MacCarty CS, Mahaley MS, Jr., Mealey J, Jr., Norrell HA, Owens G, Ransohoff J, Wilson CB, Gehan EA and Strike TA, Evaluation of BCNU and/or radiotherapy in the treatment of anaplastic gliomas. A cooperative clinical trial. *J Neurosurg* (1978) 49, 333-43.
- [29] Walker MD, Green SB, Byar DP, Alexander E, Jr., Batzdorf U, Brooks WH, Hunt WE, MacCarty CS, Mahaley MS, Jr., Mealey J, Jr., Owens G, Ransohoff J, 2nd, Robertson JT, Shapiro WR, Smith KR, Jr., Wilson CB and Strike TA, Randomized comparisons of radiotherapy and nitrosoureas for the treatment of malignant glioma after surgery. *N Engl J Med* (1980) 303, 1323-9.
- [30] Brandes AA, Tosoni A, Amista P, Nicolardi L, Grosso D, Berti F and Ermani M, How effective is BCNU in recurrent glioblastoma in the modern era? A phase II trial. *Neurology* (2004) 63, 1281-4.
- [31] Lin SH and Kleinberg LR, Carmustine wafers: localized delivery of chemotherapeutic agents in CNS malignancies. *Expert Rev Anticancer Ther* (2008) 8, 343-59.
- [32] Adamson C, Kanu OO, Mehta AI, Di C, Lin N, Mattox AK and Bigner DD, Glioblastoma multiforme: a review of where we have been and where we are going. *Expert Opin Investig Drugs* (2009) 18, 1061-83.
- [33] Kappelle AC, Postma TJ, Taphoorn MJ, Groeneveld GJ, van den Bent MJ, van Groenigen CJ, Zonnenberg BA, Sneeuw KC and Heimans JJ, PCV chemotherapy for recurrent glioblastoma multiforme. *Neurology* (2001) 56, 118-20.
- [34] Friedman HS, Prados MD, Wen PY, Mikkelsen T, Schiff D, Abrey LE, Yung WK, Paleologos N, Nicholas MK, Jensen R, Vredenburgh J, Huang J, Zheng M and Cloughesy T,

- Bevacizumab alone and in combination with irinotecan in recurrent glioblastoma. *J Clin Oncol* (2009) 27, 4733-40.
- [35] Brandes AA, Tosoni A, Basso U, Reni M, Valduga F, Monfardini S, Amista P, Nicolardi L, Sotti G and Ermani M, Second-line chemotherapy with irinotecan plus carmustine in glioblastoma recurrent or progressive after first-line temozolomide chemotherapy: a phase II study of the Gruppo Italiano Cooperativo di Neuro-Oncologia (GICNO). *J Clin Oncol* (2004) 22, 4779-4786.
- [36] Turner CD, Gururangan S, Eastwood J, Bottom K, Watral M, Beason R, McLendon RE, Friedman AH, Tourt-Uhlig S, Miller LL and Friedman HS, Phase II study of irinotecan (CPT-11) in children with high-risk malignant brain tumors: the Duke experience. *Neuro Oncol* (2002) 4, 102-108.
- [37] Vredenburgh JJ, Desjardins A, Reardon DA and Friedman HS, Experience with irinotecan for the treatment of malignant glioma. *Neuro Oncol* (2009) 11, 80-91.
- [38] NCCN, National Comprehensive Cancer Network Clinical Practice Guidelines in Oncology. In: Anaplastic Glioma/Glioblastoma (2011) Accessed in February 2011, Available from: [www.nccn.org](http://www.nccn.org).
- [39] Kreisl TN, Kim L, Moore K, Duic P, Royce C, Stroud I, Garren N, Mackey M, Butman JA, Camphausen K, Park J, Albert PS and Fine HA, Phase II trial of single-agent bevacizumab followed by bevacizumab plus irinotecan at tumor progression in recurrent glioblastoma. *J Clin Oncol* (2009) 27, 740-5.
- [40] Rich JN, Reardon DA, Peery T, Dowell JM, Quinn JA, Penne KL, Wikstrand CJ, Van Duyn LB, Dancey JE, McLendon RE, Kao JC, Stenzel TT, Ahmed Rasheed BK, Tourt-Uhlig SE, Herndon JE, 2nd, Vredenburgh JJ, Sampson JH, Friedman AH, Bigner DD and Friedman HS, Phase II trial of gefitinib in recurrent glioblastoma. *J Clin Oncol* (2004) 22, 133-42.
- [41] Raizer JJ, Abrey LE, Lassman AB, Chang SM, Lamborn KR, Kuhn JG, Yung WK, Gilbert MR, Aldape KA, Wen PY, Fine HA, Mehta M, Deangelis LM, Lieberman F, Cloughesy TF, Robins HI, Dancey J and Prados MD, A phase II trial of erlotinib in patients with recurrent malignant gliomas and nonprogressive glioblastoma multiforme postirradiation therapy. *Neuro Oncol* (2010) 12, 95-103.
- [42] Razis E, Selvaridis P, Labropoulos S, Norris JL, Zhu MJ, Song DD, Kalebic T, Torrens M, Kalogera-Fountzila A, Karkavelas G, Karanastasi S, Fletcher JA and Fountzilas G, Phase II study of neoadjuvant imatinib in glioblastoma: evaluation of clinical and molecular effects of the treatment. *Clin Cancer Res* (2009) 15, 6258-66.
- [43] Wen PY, Yung WK, Lamborn KR, Dahia PL, Wang Y, Peng B, Abrey LE, Raizer J, Cloughesy TF, Fink K, Gilbert M, Chang S, Junck L, Schiff D, Lieberman F, Fine HA, Mehta M, Robins HI, DeAngelis LM, Groves MD, Puduvalli VK, Levin V, Conrad C, Maher EA, Aldape K, Hayes M, Letvak L, Egorin MJ, Capdeville R, Kaplan R, et al., Phase I/II study of imatinib mesylate for recurrent malignant gliomas: North American Brain Tumor Consortium Study 99-08. *Clin Cancer Res* (2006) 12, 4899-907.
- [44] Fawcett DW, Section 11: The nervous tissue. *A textbook of histology* (1994) 1, 336-339.
- [45] Wolburg H, Noell S, Mack A, Wolburg-Buchholz K and Fallier-Becker P, Brain endothelial cells and the glio-vascular complex. *Cell Tissue Res* (2009) 335, 75-96.
- [46] Engerhard HH, Groothuis DG and Coons SW, Chapter 11: The Blood-Brain barrier: Structure, Function, and Response to Neoplasia & Chapter 20: Anatomy and Growth Patterns of Diffuse Gliomas. *The Gliomas* (1999) 1, 115-121.
- [47] Banks WA, Characteristics of compounds that cross the blood-brain barrier. *BMC Neurol* (2009) 9 Suppl 1, S3.
- [48] Begley DJ, ABC transporters and the blood-brain barrier. *Curr Pharm Des* (2004) 10, 1295-312.

- [49] Begley DJ, Delivery of therapeutic agents to the central nervous system: the problems and the possibilities. *Pharmacol Ther* (2004) 104, 29-45.
- [50] Deane BR and Lantos PL, The vasculature of experimental brain tumours. Part 1. A sequential light and electron microscope study of angiogenesis. *J Neurol Sci* (1981) 49, 55-66.
- [51] Rojiani AM and Dorovini-Zis K, Glomeruloid vascular structures in glioblastoma multiforme: an immunohistochemical and ultrastructural study. *J Neurosurg* (1996) 85, 1078-84.
- [52] Krakstad C and Chekenya M, Survival signalling and apoptosis resistance in glioblastomas: opportunities for targeted therapeutics. *Mol Cancer* (2010) 9, 135.
- [53] Vogelstein B and Kinzler KW, The multistep nature of cancer. *Trends Genet* (1993) 9, 138-41.
- [54] Hanahan D and Weinberg RA, The hallmarks of cancer. *Cell* (2000) 100, 57-70.
- [55] Hanahan D and Weinberg RA, Hallmarks of cancer: the next generation. *Cell* (2011) 144, 646-74.
- [56] Verreault M, Webb MS, Ramsay EC and Bally MB, Gene silencing in the development of personalized cancer treatment: the targets, the agents and the delivery systems. *Curr Gene Ther* (2006) 6, 505-33.
- [57] Tamm I, Dorken B and Hartmann G, Antisense therapy in oncology: new hope for an old idea? *Lancet* (2001) 358, 489-97.
- [58] Da Ros T, Spalluto G, Prato M, Saison-Behmoaras T, Boutorine A and Cacciari B, Oligonucleotides and oligonucleotide conjugates: a new approach for cancer treatment. *Curr Med Chem* (2005) 12, 71-88.
- [59] Bennett CF and Swayze EE, RNA targeting therapeutics: molecular mechanisms of antisense oligonucleotides as a therapeutic platform. *Annual review of pharmacology and toxicology* (2010) 50, 259-93.
- [60] Khan A, Benboubetra M, Sayyed PZ, Ng KW, Fox S, Beck G, Benter IF and Akhtar S, Sustained polymeric delivery of gene silencing antisense ODNs, siRNA, DNazymes and ribozymes: in vitro and in vivo studies. *J Drug Target* (2004) 12, 393-404.
- [61] Fire A, Albertson D, Harrison SW and Moerman DG, Production of antisense RNA leads to effective and specific inhibition of gene expression in *C. elegans* muscle. *Development* (1991) 113, 503-14.
- [62] Bernstein E, Denli AM and Hannon GJ, The rest is silence. *RNA* (2001) 7, 1509-21.
- [63] Shuey DJ, McCallus DE and Giordano T, RNAi: gene-silencing in therapeutic intervention. *Drug Discov Today* (2002) 7, 1040-6.
- [64] Ohgaki H, Dessen P, Jourde B, Horstmann S, Nishikawa T, Di Patre PL, Burkhard C, Schuler D, Probst-Hensch NM, Maiorka PC, Baeza N, Pisani P, Yonekawa Y, Yasargil MG, Lutolf UM and Kleihues P, Genetic pathways to glioblastoma: a population-based study. *Cancer Res* (2004) 64, 6892-9.
- [65] Nicholas MK, Lukas RV, Jafri NF, Faoro L and Salgia R, Epidermal growth factor receptor - mediated signal transduction in the development and therapy of gliomas. *Clin Cancer Res* (2006) 12, 7261-70.
- [66] Ekstrand AJ, James CD, Cavenee WK, Seliger B, Pettersson RF and Collins VP, Genes for epidermal growth factor receptor, transforming growth factor alpha, and epidermal growth factor and their expression in human gliomas in vivo. *Cancer Res* (1991) 51, 2164-72.
- [67] Idbaih A, Ducray F, Sierra Del Rio M, Hoang-Xuan K and Delattre JY, Therapeutic application of noncytotoxic molecular targeted therapy in gliomas: growth factor receptors and angiogenesis inhibitors. *Oncologist* (2008) 13, 978-92.
- [68] Zhang Y, Zhu C and Pardridge WM, Antisense gene therapy of brain cancer with an artificial virus gene delivery system. *Mol Ther* (2002) 6, 67-72.

- [69] Zhang Y, Zhang YF, Bryant J, Charles A, Boado RJ and Pardridge WM, Intravenous RNA interference gene therapy targeting the human epidermal growth factor receptor prolongs survival in intracranial brain cancer. *Clin Cancer Res* (2004) 10, 3667-77.
- [70] Prados MD, Chang SM, Butowski N, DeBoer R, Parvataneni R, Carliner H, Kabuubi P, Ayers-Ringler J, Rabbitt J, Page M, Fedoroff A, Sneed PK, Berger MS, McDermott MW, Parsa AT, Vandenberg S, James CD, Lamborn KR, Stokoe D and Haas-Kogan DA, Phase II study of erlotinib plus temozolomide during and after radiation therapy in patients with newly diagnosed glioblastoma multiforme or gliosarcoma. *J Clin Oncol* (2009) 27, 579-84.
- [71] Franceschi E, Cavallo G, Lonardi S, Magrini E, Tosoni A, Grosso D, Scopece L, Blatt V, Urbini B, Pession A, Tallini G, Crino L and Brandes AA, Gefitinib in patients with progressive high-grade gliomas: a multicentre phase II study by Gruppo Italiano Cooperativo di Neuro-Oncologia (GICNO). *Br J Cancer* (2007) 96, 1047-51.
- [72] Ermoian RP, Furniss CS, Lamborn KR, Basila D, Berger MS, Gottschalk AR, Nicholas MK, Stokoe D and Haas-Kogan DA, Dysregulation of PTEN and protein kinase B is associated with glioma histology and patient survival. *Clin Cancer Res* (2002) 8, 1100-6.
- [73] Haas-Kogan D, Shalev N, Wong M, Mills G, Yount G and Stokoe D, Protein kinase B (PKB/Akt) activity is elevated in glioblastoma cells due to mutation of the tumor suppressor PTEN/MMAC. *Curr Biol* (1998) 8, 1195-8.
- [74] Manning BD and Cantley LC, United at last: the tuberous sclerosis complex gene products connect the phosphoinositide 3-kinase/Akt pathway to mammalian target of rapamycin (mTOR) signalling. *Biochem Soc Trans* (2003) 31, 573-8.
- [75] Galanis E, Buckner JC, Maurer MJ, Kreisberg JI, Ballman K, Boni J, Peralba JM, Jenkins RB, Dakhil SR, Morton RF, Jaeckle KA, Scheithauer BW, Dancey J, Hidalgo M and Walsh DJ, Phase II trial of temsirolimus (CCI-779) in recurrent glioblastoma multiforme: a North Central Cancer Treatment Group Study. *J Clin Oncol* (2005) 23, 5294-304.
- [76] Chang SM, Wen P, Cloughesy T, Greenberg H, Schiff D, Conrad C, Fink K, Robins HI, De Angelis L, Raizer J, Hess K, Aldape K, Lamborn KR, Kuhn J, Dancey J and Prados MD, Phase II study of CCI-779 in patients with recurrent glioblastoma multiforme. *Invest New Drugs* (2005) 23, 357-61.
- [77] George J, Banik NL and Ray SK, Combination of taxol and Bcl-2 siRNA induces apoptosis in human glioblastoma cells and inhibits invasion, angiogenesis, and tumor growth. *J Cell Mol Med* (2008)
- [78] Jain RK, di Tomaso E, Duda DG, Loeffler JS, Sorensen AG and Batchelor TT, Angiogenesis in brain tumours. *Nat Rev Neurosci* (2007) 8, 610-22.
- [79] Norden AD, Drappatz J and Wen PY, Antiangiogenic therapies for high-grade glioma. *Nat Rev Neurol* (2009) 5, 610-20.
- [80] Blasberg RG, Kobayashi T, Horowitz M, Rice JM, Groothuis D, Molnar P and Fenstermacher JD, Regional blood flow in ethylnitrosourea-induced brain tumors. *Ann Neurol* (1983) 14, 189-201.
- [81] Groothuis DR, Pasternak JF, Fischer JM, Blasberg RG, Bigner DD and Vick NA, Regional measurements of blood flow in experimental RG-2 rat gliomas. *Cancer Res* (1983) 43, 3362-7.
- [82] Lai A, Tran A, Nghiemphu PL, Pope WB, Solis OE, Selch M, Filka E, Yong WH, Mischel PS, Liao LM, Phuphanich S, Black K, Peak S, Green RM, Spier CE, Kolevska T, Polikoff J, Fehrenbacher L, Elashoff R and Cloughesy T, Phase II study of bevacizumab plus temozolomide during and after radiation therapy for patients with newly diagnosed glioblastoma multiforme. *J Clin Oncol* (2011) 29, 142-8.
- [83] Lai A, Filka E, McGibbon B, Nghiemphu PL, Graham C, Yong WH, Mischel P, Liao LM, Bergsneider M, Pope W, Selch M and Cloughesy T, Phase II pilot study of bevacizumab in combination with temozolomide and regional radiation therapy for up-front treatment of patients

- with newly diagnosed glioblastoma multiforme: interim analysis of safety and tolerability. *Int J Radiat Oncol Biol Phys* (2008) 71, 1372-80.
- [84] Desgrosellier JS and Cheresh DA, Integrins in cancer: biological implications and therapeutic opportunities. *Nat Rev Cancer* (2010) 10, 9-22.
- [85] Stupp R, Hegi ME, Neyns B, Goldbrunner R, Schlegel U, Clement PM, Grabenbauer GG, Ochsenein AF, Simon M, Dietrich PY, Pietsch T, Hicking C, Tonn JC, Diserens AC, Pica A, Hermisson M, Krueger S, Picard M and Weller M, Phase I/IIa study of cilengitide and temozolomide with concomitant radiotherapy followed by cilengitide and temozolomide maintenance therapy in patients with newly diagnosed glioblastoma. *J Clin Oncol* (2010) 28, 2712-8.
- [86] Carter A, Integrins as target: first phase III trial launches, but questions remain. *J Natl Cancer Inst* (2010) 102, 675-7.
- [87] Nakada M, Okada Y and Yamashita J, The role of matrix metalloproteinases in glioma invasion. *Front Biosci* (2003) 8, e261-9.
- [88] Lakka SS, Gondi CS, Dinh DH, Olivero WC, Gujrati M, Rao VH, Sioka C and Rao JS, Specific interference of urokinase-type plasminogen activator receptor and matrix metalloproteinase-9 gene expression induced by double-stranded RNA results in decreased invasion, tumor growth, and angiogenesis in gliomas. *J Biol Chem* (2005) 280, 21882-92.
- [89] Chu QS, Forouzes B, Syed S, Mita M, Schwartz G, Cooper J, Curtright J and Rowinsky EK, A phase II and pharmacological study of the matrix metalloproteinase inhibitor (MMPI) COL-3 in patients with advanced soft tissue sarcomas. *Invest New Drugs* (2007) 25, 359-67.
- [90] Brinker BT, Krown SE, Lee JY, Cesarman E, Chadburn A, Kaplan LD, Henry DH and Von Roenn JH, Phase 1/2 trial of BMS-275291 in patients with human immunodeficiency virus-related Kaposi sarcoma: a multicenter trial of the AIDS Malignancy Consortium. *Cancer* (2008) 112, 1083-8.
- [91] Holt SE and Shay JW, Role of telomerase in cellular proliferation and cancer. *J Cell Physiol* (1999) 180, 10-8.
- [92] Le S, Zhu JJ, Anthony DC, Greider CW and Black PM, Telomerase activity in human gliomas. *Neurosurgery* (1998) 42, 1120-5.
- [93] Wager M, Menei P, Guilhot J, Levillain P, Michalak S, Bataille B, Blanc JL, Lapierre F, Rigoard P, Milin S, Duthe F, Bonneau D, Larsen CJ and Karayan-Tapon L, Prognostic molecular markers with no impact on decision-making: the paradox of gliomas based on a prospective study. *Br J Cancer* (2008) 98, 1830-8.
- [94] George J, Banik NL and Ray SK, Combination of hTERT knockdown and IFN-gamma treatment inhibited angiogenesis and tumor progression in glioblastoma. *Clin Cancer Res* (2009) 15, 7186-95.
- [95] Mukai S, Kondo Y, Koga S, Komata T, Barna BP and Kondo S, 2-5A antisense telomerase RNA therapy for intracranial malignant gliomas. *Cancer Res* (2000) 60, 4461-7.
- [96] Grossman SA, Alavi JB, Supko JG, Carson KA, Priet R, Dorr FA, Grundy JS and Holmlund JT, Efficacy and toxicity of the antisense oligonucleotide aprinocarsen directed against protein kinase C-alpha delivered as a 21-day continuous intravenous infusion in patients with recurrent high-grade astrocytomas. *Neuro Oncol* (2005) 7, 32-40.
- [97] Kreisl TN, Kotliarova S, Butman JA, Albert PS, Kim L, Musib L, Thornton D and Fine HA, A phase I/II trial of enzastaurin in patients with recurrent high-grade gliomas. *Neuro Oncol* (2010) 12, 181-9.
- [98] Wick W, Puduvalli VK, Chamberlain MC, van den Bent MJ, Carpentier AF, Cher LM, Mason W, Weller M, Hong S, Musib L, Liepa AM, Thornton DE and Fine HA, Phase III study of enzastaurin compared with lomustine in the treatment of recurrent intracranial glioblastoma. *J Clin Oncol* (2010) 28, 1168-74.

- [99] Gondi CS, Lakka SS, Dinh DH, Olivero WC, Gujrati M and Rao JS, Intraperitoneal injection of a hairpin RNA-expressing plasmid targeting urokinase-type plasminogen activator (uPA) receptor and uPA retards angiogenesis and inhibits intracranial tumor growth in nude mice. *Clin Cancer Res* (2007) 13, 4051-60.
- [100] Laterra JJ, Grossman SA, Carson KA, Lesser GJ, Hochberg FH and Gilbert MR, Suramin and radiotherapy in newly diagnosed glioblastoma: phase 2 NABTT CNS Consortium study. *Neuro Oncol* (2004) 6, 15-20.
- [101] Lustig R, Mikkelsen T, Lesser G, Grossman S, Ye X, Desideri S, Fisher J and Wright J, Phase II preradiation R115777 (tipifarnib) in newly diagnosed GBM with residual enhancing disease. *Neuro Oncol* (2008) 10, 1004-9.
- [102] Cloughesy TF, Wen PY, Robins HI, Chang SM, Groves MD, Fink KL, Junck L, Schiff D, Abrey L, Gilbert MR, Lieberman F, Kuhn J, DeAngelis LM, Mehta M, Raizer JJ, Yung WK, Aldape K, Wright J, Lamborn KR and Prados MD, Phase II trial of tipifarnib in patients with recurrent malignant glioma either receiving or not receiving enzyme-inducing antiepileptic drugs: a North American Brain Tumor Consortium Study. *J Clin Oncol* (2006) 24, 3651-6.
- [103] Galanis E, Jaeckle KA, Maurer MJ, Reid JM, Ames MM, Hardwick JS, Reilly JF, Loboda A, Nebozhyn M, Fantin VR, Richon VM, Scheithauer B, Giannini C, Flynn PJ, Moore DF, Jr., Zwiebel J and Buckner JC, Phase II trial of vorinostat in recurrent glioblastoma multiforme: a north central cancer treatment group study. *J Clin Oncol* (2009) 27, 2052-8.
- [104] Marx GM, Pavlakis N, McCowatt S, Boyle FM, Levi JA, Bell DR, Cook R, Biggs M, Little N and Wheeler HR, Phase II study of thalidomide in the treatment of recurrent glioblastoma multiforme. *J Neurooncol* (2001) 54, 31-8.
- [105] Fine HA, Wen PY, Maher EA, Viscosi E, Batchelor T, Lakhani N, Figg WD, Purow BW and Borkowf CB, Phase II trial of thalidomide and carmustine for patients with recurrent high-grade gliomas. *J Clin Oncol* (2003) 21, 2299-304.
- [106] Fadul CE, Kingman LS, Meyer LP, Cole BF, Eskey CJ, Rhodes CH, Roberts DW, Newton HB and Pipas JM, A phase II study of thalidomide and irinotecan for treatment of glioblastoma multiforme. *J Neurooncol* (2008) 90, 229-35.
- [107] Grzelinski M, Urban-Klein B, Martens T, Lamszus K, Bakowsky U, Hobel S, Czubyko F and Aigner A, RNA interference-mediated gene silencing of pleiotrophin through polyethylenimine-complexed small interfering RNAs in vivo exerts antitumoral effects in glioblastoma xenografts. *Hum Gene Ther* (2006) 17, 751-66.
- [108] Gondi CS, Lakka SS, Dinh DH, Olivero WC, Gujrati M and Rao JS, RNAi-mediated inhibition of cathepsin B and uPAR leads to decreased cell invasion, angiogenesis and tumor growth in gliomas. *Oncogene* (2004) 23, 8486-96.
- [109] Hashizume R, Ozawa T, Gryaznov SM, Bollen AW, Lamborn KR, Frey WH, 2nd and Deen DF, New therapeutic approach for brain tumors: Intranasal delivery of telomerase inhibitor GRN163. *Neuro Oncol* (2008) 10, 112-20.
- [110] Wyszko E, Rolle K, Nowak S, Zukiel R, Nowak M, Piestrzeniewicz R, Gawronska I, Barciszewska MZ and Barciszewski J, A multivariate analysis of patients with brain tumors treated with ATN-RNA. *Acta Pol Pharm* (2008) 65, 677-84.
- [111] Zukiel R, Nowak S, Wyszko E, Rolle K, Gawronska I, Barciszewska MZ and Barciszewski J, Suppression of human brain tumor with interference RNA specific for tenascin-C. *Cancer Biol Ther* (2006) 5, 1002-7.
- [112] Edwards LA, Verreault M, Thiessen B, Dragowska WH, Hu Y, Yeung JH, Dedhar S and Bally MB, Combined inhibition of the phosphatidylinositol 3-kinase/Akt and Ras/mitogen-activated protein kinase pathways results in synergistic effects in glioblastoma cells. *Mol Cancer Ther* (2006) 5, 645-54.

- [113] Sauter G, Maeda T, Waldman FM, Davis RL and Feuerstein BG, Patterns of epidermal growth factor receptor amplification in malignant gliomas. *Am J Pathol* (1996) 148, 1047-53.
- [114] Favata MF, Horiuchi KY, Manos EJ, Daulerio AJ, Stradley DA, Feeser WS, Van Dyk DE, Pitts WJ, Earl RA, Hobbs F, Copeland RA, Magolda RL, Scherle PA and Trzaskos JM, Identification of a novel inhibitor of mitogen-activated protein kinase kinase. *J Biol Chem* (1998) 273, 18623-32.
- [115] DeSilva DR, Jones EA, Favata MF, Jaffee BD, Magolda RL, Trzaskos JM and Scherle PA, Inhibition of mitogen-activated protein kinase kinase blocks T cell proliferation but does not induce or prevent anergy. *J Immunol* (1998) 160, 4175-81.
- [116] Lackey K, Cory M, Davis R, Frye SV, Harris PA, Hunter RN, Jung DK, McDonald OB, McNutt RW, Peel MR, Rutkowske RD, Veal JM and Wood ER, The discovery of potent cRaf1 kinase inhibitors. *Bioorg Med Chem Lett* (2000) 10, 223-6.
- [117] Persad S, Attwell S, Gray V, Delcommenne M, Troussard A, Sanghera J and Dedhar S, Inhibition of integrin-linked kinase (ILK) suppresses activation of protein kinase B/Akt and induces cell cycle arrest and apoptosis of PTEN-mutant prostate cancer cells. *Proc Natl Acad Sci U S A* (2000) 97, 3207-12.
- [118] Delcommenne M, Tan C, Gray V, Rue L, Woodgett J and Dedhar S, Phosphoinositide-3-OH kinase-dependent regulation of glycogen synthase kinase 3 and protein kinase B/AKT by the integrin-linked kinase. *Proc Natl Acad Sci U S A* (1998) 95, 11211-6.
- [119] Knobbe CB, Merlo A and Reifenberger G, Pten signaling in gliomas. *Neuro Oncol* (2002) 4, 196-211.
- [120] Schmidt EE, Ichimura K, Goike HM, Moshref A, Liu L and Collins VP, Mutational profile of the PTEN gene in primary human astrocytic tumors and cultivated xenografts. *J Neuropathol Exp Neurol* (1999) 58, 1170-83.
- [121] Rasheed BK, Stenzel TT, McLendon RE, Parsons R, Friedman AH, Friedman HS, Bigner DD and Bigner SH, PTEN gene mutations are seen in high-grade but not in low-grade gliomas. *Cancer Res* (1997) 57, 4187-90.
- [122] Rajasekhar VK, Viale A, Socci ND, Wiedmann M, Hu X and Holland EC, Oncogenic Ras and Akt signaling contribute to glioblastoma formation by differential recruitment of existing mRNAs to polysomes. *Mol Cell* (2003) 12, 889-901.
- [123] Bumcrot D, Manoharan M, Koteliansky V and Sah DW, RNAi therapeutics: a potential new class of pharmaceutical drugs. *Nat Chem Biol* (2006) 2, 711-9.
- [124] Helene C, Control of oncogene expression by antisense nucleic acids. *Eur J Cancer* (1994) 30A, 1721-6.
- [125] Paterson BM, Roberts BE and Kuff EL, Structural gene identification and mapping by DNA-mRNA hybrid-arrested cell-free translation. *Proc Natl Acad Sci U S A* (1977) 74, 4370-4.
- [126] Gewirtz AM, Oligonucleotide therapeutics: a step forward. *J Clin Oncol* (2000) 18, 1809-11.
- [127] Whitesell L, Rosolen A and Neckers LM, In vivo modulation of N-myc expression by continuous perfusion with an antisense oligonucleotide. *Antisense Res Dev* (1991) 1, 343-50.
- [128] Bayever E, Iversen PL, Bishop MR, Sharp JG, Tewary HK, Arneson MA, Pirruccello SJ, Ruddon RW, Kessinger A, Zon G and et al., Systemic administration of a phosphorothioate oligonucleotide with a sequence complementary to p53 for acute myelogenous leukemia and myelodysplastic syndrome: initial results of a phase I trial. *Antisense Res Dev* (1993) 3, 383-90.
- [129] Stein CA and Krieg AM, Problems in interpretation of data derived from in vitro and in vivo use of antisense oligodeoxynucleotides. *Antisense Res Dev* (1994) 4, 67-9.
- [130] Jason TL, Koropatnick J and Berg RW, Toxicology of antisense therapeutics. *Toxicol Appl Pharmacol* (2004) 201, 66-83.

- [131] Krieg AM, Yi AK, Matson S, Waldschmidt TJ, Bishop GA, Teasdale R, Koretzky GA and Klinman DM, CpG motifs in bacterial DNA trigger direct B-cell activation. *Nature* (1995) 374, 546-9.
- [132] Boye SM, Pradhan AA, Grant RJ and Clarke PB, Evidence for sequence-dependent and reversible nonspecific effects of PS-capped antisense treatment after intracerebral administration. *Antisense Nucleic Acid Drug Dev* (2002) 12, 95-102.
- [133] Galderisi U, Di Bernardo G, Melone MA, Galano G, Cascino A, Giordano A and Cipollaro M, Antisense inhibitory effect: a comparison between 3'-partial and full phosphorothioate antisense oligonucleotides. *J Cell Biochem* (1999) 74, 31-7.
- [134] Mui B, Raney SG, Semple SC and Hope MJ, Immune stimulation by a CpG-containing oligodeoxynucleotide is enhanced when encapsulated and delivered in lipid particles. *J Pharmacol Exp Ther* (2001) 298, 1185-92.
- [135] Sfondrini L, Besusso D, Rumio C, Rodolfo M, Menard S and Balsari A, Prevention of spontaneous mammary adenocarcinoma in HER-2/neu transgenic mice by foreign DNA. *FASEB J* (2002) 16, 1749-54.
- [136] Webb MS and Zon G, Preclinical and clinical experience of antisense therapy for solid tumors. *Curr Opin Mol Ther* (1999) 1, 458-63.
- [137] Cerutti H, RNA interference: traveling in the cell and gaining functions? *Trends Genet* (2003) 19, 39-46.
- [138] Hede K, Blocking cancer with RNA interference moves toward the clinic. *J Natl Cancer Inst* (2005) 97, 626-8.
- [139] Karagiannis TC and El-Osta A, RNA interference and potential therapeutic applications of short interfering RNAs. *Cancer Gene Ther* (2005) 12, 787-95.
- [140] He S, Zhang D, Cheng F, Gong F and Guo Y, Applications of RNA interference in cancer therapeutics as a powerful tool for suppressing gene expression. *Mol Biol Rep* (2009) 36, 2153-63.
- [141] Behlke MA, Chemical modification of siRNAs for in vivo use. *Oligonucleotides* (2008) 18, 305-19.
- [142] Huang C, Li M, Chen C and Yao Q, Small interfering RNA therapy in cancer: mechanism, potential targets, and clinical applications. *Expert Opin Ther Targets* (2008) 12, 637-45.
- [143] Persengiev SP, Zhu X and Green MR, Nonspecific, concentration-dependent stimulation and repression of mammalian gene expression by small interfering RNAs (siRNAs). *RNA* (2004) 10, 12-8.
- [144] Sledz CA, Holko M, de Veer MJ, Silverman RH and Williams BR, Activation of the interferon system by short-interfering RNAs. *Nat Cell Biol* (2003) 5, 834-9.
- [145] Sioud M, Does the understanding of immune activation by RNA predict the design of safe siRNAs? *Front Biosci* (2008) 13, 4379-92.
- [146] Judge AD, Sood V, Shaw JR, Fang D, McClintock K and MacLachlan I, Sequence-dependent stimulation of the mammalian innate immune response by synthetic siRNA. *Nat Biotechnol* (2005) 23, 457-62.
- [147] Heidel JD, Hu S, Liu XF, Triche TJ and Davis ME, Lack of interferon response in animals to naked siRNAs. *Nat Biotechnol* (2004) 22, 1579-82.
- [148] Jackson AL, Bartz SR, Schelter J, Kobayashi SV, Burchard J, Mao M, Li B, Cavet G and Linsley PS, Expression profiling reveals off-target gene regulation by RNAi. *Nat Biotechnol* (2003) 21, 635-7.
- [149] Lin X, Ruan X, Anderson MG, McDowell JA, Kroeger PE, Fesik SW and Shen Y, siRNA-mediated off-target gene silencing triggered by a 7 nt complementation. *Nucleic Acids Res* (2005) 33, 4527-35.

- [150] Jackson AL, Burchard J, Leake D, Reynolds A, Schelter J, Guo J, Johnson JM, Lim L, Karpilow J, Nichols K, Marshall W, Khvorova A and Linsley PS, Position-specific chemical modification of siRNAs reduces "off-target" transcript silencing. *RNA* (2006) 12, 1197-205.
- [151] Thakker DR, Natt F, Husken D, van der Putten H, Maier R, Hoyer D and Cryan JF, siRNA-mediated knockdown of the serotonin transporter in the adult mouse brain. *Mol Psychiatry* (2005) 10, 782-9, 714.
- [152] Boiardi A, Bartolomei M, Silvani A, Eoli M, Salmaggi A, Lamperti E, Milanese I, Botturi A, Rocca P, Bodei L, Broggi G and Paganelli G, Intratumoral delivery of mitoxantrone in association with 90-Y radioimmunotherapy (RIT) in recurrent glioblastoma. *J Neurooncol* (2005) 72, 125-31.
- [153] Patchell RA, Regine WF, Ashton P, Tibbs PA, Wilson D, Shappley D and Young B, A phase I trial of continuously infused intratumoral bleomycin for the treatment of recurrent glioblastoma multiforme. *J Neurooncol* (2002) 60, 37-42.
- [154] Pas J, Wyszko E, Rolle K, Rychlewski L, Nowak S, Zukiel R and Barciszewski J, Analysis of structure and function of tenascin-C. *Int J Biochem Cell Biol* (2006) 38, 1594-602.
- [155] Lidar Z, Mardor Y, Jonas T, Pfeffer R, Faibel M, Nass D, Hadani M and Ram Z, Convection-enhanced delivery of paclitaxel for the treatment of recurrent malignant glioma: a phase I/II clinical study. *J Neurosurg* (2004) 100, 472-9.
- [156] Kunwar S, Prados MD, Chang SM, Berger MS, Lang FF, Piepmeyer JM, Sampson JH, Ram Z, Gutin PH, Gibbons RD, Aldape KD, Croteau DJ, Sherman JW and Puri RK, Direct intracerebral delivery of cintredekin besudotox (IL13-PE38QQR) in recurrent malignant glioma: a report by the Cintredekin Besudotox Intraparenchymal Study Group. *J Clin Oncol* (2007) 25, 837-44.
- [157] Querbes W, Ge P, Zhang W, Fan Y, Costigan J, Charisse K, Maier M, Nechev L, Manoharan M, Kotelianski V and Sah DW, Direct CNS delivery of siRNA mediates robust silencing in oligodendrocytes. *Oligonucleotides* (2009) 19, 23-29.
- [158] Brem H, Tamargo RJ, Olivi A, Pinn M, Weingart JD, Wharam M and Epstein JI, Biodegradable polymers for controlled delivery of chemotherapy with and without radiation therapy in the monkey brain. *J Neurosurg* (1994) 80, 283-90.
- [159] Grossman SA, Reinhard C, Colvin OM, Chasin M, Brundrett R, Tamargo RJ and Brem H, The intracerebral distribution of BCNU delivered by surgically implanted biodegradable polymers. *J Neurosurg* (1992) 76, 640-7.
- [160] Brem H, Mahaley MS, Jr., Vick NA, Black KL, Schold SC, Jr., Burger PC, Friedman AH, Ciric IS, Eller TW, Cozzens JW and et al., Interstitial chemotherapy with drug polymer implants for the treatment of recurrent gliomas. *J Neurosurg* (1991) 74, 441-6.
- [161] Gururangan S, Cokgor L, Rich JN, Edwards S, Affronti ML, Quinn JA, Herndon JE, 2nd, Provenzale JM, McLendon RE, Tourt-Uhlig S, Sampson JH, Stafford-Fox V, Zaknoen S, Early M, Friedman AH and Friedman HS, Phase I study of Gliadel wafers plus temozolomide in adults with recurrent supratentorial high-grade gliomas. *Neuro Oncol* (2001) 3, 246-50.
- [162] Thorne RG, Emory CR, Ala TA and Frey WH, 2nd, Quantitative analysis of the olfactory pathway for drug delivery to the brain. *Brain Res* (1995) 692, 278-82.
- [163] Thorne RG, Pronk GJ, Padmanabhan V and Frey WH, 2nd, Delivery of insulin-like growth factor-I to the rat brain and spinal cord along olfactory and trigeminal pathways following intranasal administration. *Neuroscience* (2004) 127, 481-96.
- [164] da Fonseca CO, Linden R, Futuro D, Gattass CR and Quirico-Santos T, Ras pathway activation in gliomas: a strategic target for intranasal administration of perillyl alcohol. *Arch Immunol Ther Exp (Warsz)* (2008) 56, 267-76.
- [165] Wang F, Jiang X and Lu W, Profiles of methotrexate in blood and CSF following intranasal and intravenous administration to rats. *Int J Pharm* (2003) 263, 1-7.

- [166] Sakane T, Yamashita S, Yata N and Sezaki H, Transnasal delivery of 5-fluorouracil to the brain in the rat. *J Drug Target* (1999) 7, 233-40.
- [167] Wang D, Gao Y and Yun L, Study on brain targeting of raltitrexed following intranasal administration in rats. *Cancer Chemother Pharmacol* (2006) 57, 97-104.
- [168] Rubin LL and Staddon JM, The cell biology of the blood-brain barrier. *Annu Rev Neurosci* (1999) 22, 11-28.
- [169] Patel MM, Goyal BR, Bhadada SV, Bhatt JS and Amin AF, Getting into the brain: approaches to enhance brain drug delivery. *CNS Drugs* (2009) 23, 35-58.
- [170] Bellavance MA, Blanchette M and Fortin D, Recent advances in blood-brain barrier disruption as a CNS delivery strategy. *AAPS J* (2008) 10, 166-77.
- [171] Ningaraj NS, Rao M and Black KL, Calcium-dependent potassium channels as a target protein for modulation of the blood-brain tumor barrier. *Drug News Perspect* (2003) 16, 291-8.
- [172] Ningaraj NS, Drug delivery to brain tumours: challenges and progress. *Expert Opin Drug Deliv* (2006) 3, 499-509.
- [173] Bertrand JR, Pottier M, Vekris A, Opolon P, Maksimenko A and Malvy C, Comparison of antisense oligonucleotides and siRNAs in cell culture and in vivo. *Biochem Biophys Res Commun* (2002) 296, 1000-4.
- [174] Filleur S, Courtin A, Ait-Si-Ali S, Guglielmi J, Merle C, Harel-Bellan A, Clezardin P and Cabon F, SiRNA-mediated inhibition of vascular endothelial growth factor severely limits tumor resistance to antiangiogenic thrombospondin-1 and slows tumor vascularization and growth. *Cancer Res* (2003) 63, 3919-22.
- [175] Braasch DA, Paroo Z, Constantinescu A, Ren G, Oz OK, Mason RP and Corey DR, Biodistribution of phosphodiester and phosphorothioate siRNA. *Bioorg Med Chem Lett* (2004) 14, 1139-43.
- [176] Santel A, Aleku M, Keil O, Endruschat J, Esche V, Fisch G, Dames S, Loffler K, Fechtner M, Arnold W, Giese K, Klippel A and Kaufmann J, A novel siRNA-lipoplex technology for RNA interference in the mouse vascular endothelium. *Gene Ther* (2006) 13, 1222-34.
- [177] De Paula D, Bentley MV and Mahato RI, Hydrophobization and bioconjugation for enhanced siRNA delivery and targeting. *RNA* (2007) 13, 431-56.
- [178] Lewis DL, Hagstrom JE, Loomis AG, Wolff JA and Herweijer H, Efficient delivery of siRNA for inhibition of gene expression in postnatal mice. *Nat Genet* (2002) 32, 107-8.
- [179] McCaffrey AP, Meuse L, Pham TT, Conklin DS, Hannon GJ and Kay MA, RNA interference in adult mice. *Nature* (2002) 418, 38-9.
- [180] Song E, Lee SK, Wang J, Ince N, Ouyang N, Min J, Chen J, Shankar P and Lieberman J, RNA interference targeting Fas protects mice from fulminant hepatitis. *Nat Med* (2003) 9, 347-51.
- [181] Lieberman J, Song E, Lee SK and Shankar P, Interfering with disease: opportunities and roadblocks to harnessing RNA interference. *Trends Mol Med* (2003) 9, 397-403.
- [182] Maeda H, Bharate GY and Daruwalla J, Polymeric drugs for efficient tumor-targeted drug delivery based on EPR-effect. *Eur J Pharm Biopharm* (2009) 71, 409-19.
- [183] Storm G and Crommelin DJA, Liposomes: quo vadis? *Pharmaceutical Science & Technology Today* (1998) 1, 19-31.
- [184] Ohvo-Rekila H, Ramstedt B, Leppimaki P and Slotte JP, Cholesterol interactions with phospholipids in membranes. *Prog Lipid Res* (2002) 41, 66-97.
- [185] Park JW, Benz CC and Martin FJ, Future directions of liposome- and immunoliposome-based cancer therapeutics. *Semin Oncol* (2004) 31, 196-205.
- [186] Barenholz Y, Amphipathic weak base loading into preformed liposomes having a transmembrane ammonium ion gradient: from the bench to approved Doxil. *Liposome Technology: Entrapment of drugs and other materials into liposomes* (2007) 2, 1-25.

- [187] Cullis PR, Hope MJ, Bally MB, Madden TD, Mayer LD and Fenske DB, Influence of pH gradients on the transbilayer transport of drugs, lipids, peptides and metal ions into large unilamellar vesicles. *Biochim Biophys Acta* (1997) 1331, 187-211.
- [188] Mayer LD, Bally MB, Loughrey H, Masin D and Cullis PR, Liposomal vincristine preparations which exhibit decreased drug toxicity and increased activity against murine L1210 and P388 tumors. *Cancer Res* (1990) 50, 575-9.
- [189] Ramsay E, Alnajim J, Anantha M, Zastre J, Yan H, Webb M, Waterhouse D and Bally M, A novel liposomal irinotecan formulation with significant anti-tumour activity: use of the divalent cation ionophore A23187 and copper-containing liposomes to improve drug retention. *Eur J Pharm Biopharm* (2008) 68, 607-17.
- [190] Ramsay EC, Anantha M, Zastre J, Meijs M, Zonderhuis J, Strutt D, Webb MS, Waterhouse D and Bally MB, Irinophore C: a liposome formulation of irinotecan with substantially improved therapeutic efficacy against a panel of human xenograft tumors. *Clin Cancer Res* (2008) 14, 1208-17.
- [191] Patankar N, Anantha M, Ramsay E, Waterhouse D and Bally M, The role of the transition metal copper and the ionophore a23187 in the development of irinophore C. *Pharmaceutical research* (2011) 28, 848-57.
- [192] Mayer LD, Masin D, Nayar R, Boman NL and Bally MB, Pharmacology of liposomal vincristine in mice bearing L1210 ascitic and B16/BL6 solid tumours. *Br J Cancer* (1995) 71, 482-8.
- [193] Porter CA and Rifkin RM, Clinical benefits and economic analysis of pegylated liposomal doxorubicin/vincristine/dexamethasone versus doxorubicin/vincristine/dexamethasone in patients with newly diagnosed multiple myeloma. *Clin Lymphoma Myeloma* (2007) 7 S150-5.
- [194] O'Brien ME, Wigler N, Inbar M, Rosso R, Grischke E, Santoro A, Catane R, Kieback DG, Tomczak P, Ackland SP, Orlandi F, Mellars L, Alland L and Tendler C, Reduced cardiotoxicity and comparable efficacy in a phase III trial of pegylated liposomal doxorubicin HCl (CAELYX/Doxil) versus conventional doxorubicin for first-line treatment of metastatic breast cancer. *Ann Oncol* (2004) 15, 440-9.
- [195] Judson I, Radford JA, Harris M, Blay JY, van Hoesel Q, le Cesne A, van Oosterom AT, Clemons MJ, Kamby C, Hermans C, Whittaker J, Donato di Paola E, Verweij J and Nielsen S, Randomised phase II trial of pegylated liposomal doxorubicin (DOXIL/CAELYX) versus doxorubicin in the treatment of advanced or metastatic soft tissue sarcoma: a study by the EORTC Soft Tissue and Bone Sarcoma Group. *Eur J Cancer* (2001) 37, 870-7.
- [196] Hau P, Fabel K, Baumgart U, Rummele P, Grauer O, Bock A, Dietmaier C, Dietmaier W, Dietrich J, Dudel C, Hubner F, Jauch T, Drechsel E, Kleiter I, Wismeth C, Zellner A, Brawanski A, Steinbrecher A, Marienhagen J and Bogdahn U, Pegylated liposomal doxorubicin-efficacy in patients with recurrent high-grade glioma. *Cancer* (2004) 100, 1199-207.
- [197] Fabel K, Dietrich J, Hau P, Wismeth C, Winner B, Przywara S, Steinbrecher A, Ullrich W and Bogdahn U, Long-term stabilization in patients with malignant glioma after treatment with liposomal doxorubicin. *Cancer* (2001) 92, 1936-42.
- [198] Zhou R, Mazurchuk R and Straubinger RM, Antivasculature effects of doxorubicin-containing liposomes in an intracranial rat brain tumor model. *Cancer Res* (2002) 62, 2561-6.
- [199] Krauze MT, Noble CO, Kawaguchi T, Drummond D, Kirpotin DB, Yamashita Y, Kullberg E, Forsayeth J, Park JW and Bankiewicz KS, Convection-enhanced delivery of nanoliposomal CPT-11 (irinotecan) and PEGylated liposomal doxorubicin (Doxil) in rodent intracranial brain tumor xenografts. *Neuro Oncol* (2007) 9, 393-403.
- [200] Noble CO, Krauze MT, Drummond DC, Yamashita Y, Saito R, Berger MS, Kirpotin DB, Bankiewicz KS and Park JW, Novel nanoliposomal CPT-11 infused by convection-enhanced delivery in intracranial tumors: pharmacology and efficacy. *Cancer Res* (2006) 66, 2801-6.

- [201] Messerer CL, Ramsay EC, Waterhouse D, Ng R, Simms EM, Harasym N, Tardi P, Mayer LD and Bally MB, Liposomal irinotecan: formulation development and therapeutic assessment in murine xenograft models of colorectal cancer. *Clin Cancer Res* (2004) 10, 6638-49.
- [202] Hattori Y, Shi L, Ding W, Koga K, Kawano K, Hakoshima M and Maitani Y, Novel irinotecan-loaded liposome using phytic acid with high therapeutic efficacy for colon tumors. *J Control Release* (2009) 136, 30-7.
- [203] Lundstrom K and Boulikas T, Viral and non-viral vectors in gene therapy: technology development and clinical trials. *Technol Cancer Res Treat* (2003) 2, 471-86.
- [204] Cattel L, Ceruti M and Dosio F, From conventional to stealth liposomes: a new Frontier in cancer chemotherapy. *J Chemother* (2004) 16 Suppl 4, 94-7.
- [205] Sioud M and Sorensen DR, Cationic liposome-mediated delivery of siRNAs in adult mice. *Biochem Biophys Res Commun* (2003) 312, 1220-5.
- [206] Sorensen DR, Leirdal M and Sioud M, Gene silencing by systemic delivery of synthetic siRNAs in adult mice. *J Mol Biol* (2003) 327, 761-6.
- [207] Aigner A, Cellular delivery in vivo of siRNA-based therapeutics. *Curr Pharm Des* (2008) 14, 3603-19.
- [208] Shoji Y and Nakashima H, Current status of delivery systems to improve target efficacy of oligonucleotides. *Curr Pharm Des* (2004) 10, 785-96.
- [209] Freimark BD, Blezinger HP, Florack VJ, Nordstrom JL, Long SD, Deshpande DS, Nochumson S and Petrak KL, Cationic lipids enhance cytokine and cell influx levels in the lung following administration of plasmid: cationic lipid complexes. *J Immunol* (1998) 160, 4580-6.
- [210] Li S, Wu SP, Whitmore M, Loeffert EJ, Wang L, Watkins SC, Pitt BR and Huang L, Effect of immune response on gene transfer to the lung via systemic administration of cationic lipidic vectors. *Am J Physiol* (1999) 276, L796-804.
- [211] Scheule RK, St George JA, Bagley RG, Marshall J, Kaplan JM, Akita GY, Wang KX, Lee ER, Harris DJ, Jiang C, Yew NS, Smith AE and Cheng SH, Basis of pulmonary toxicity associated with cationic lipid-mediated gene transfer to the mammalian lung. *Hum Gene Ther* (1997) 8, 689-707.
- [212] Nishikawa M, Takemura S, Takakura Y and Hashida M, Targeted delivery of plasmid DNA to hepatocytes in vivo: optimization of the pharmacokinetics of plasmid DNA/galactosylated poly(L-lysine) complexes by controlling their physicochemical properties. *J Pharmacol Exp Ther* (1998) 287, 408-15.
- [213] Ogris M, Brunner S, Schuller S, Kircheis R and Wagner E, PEGylated DNA/transferrin-PEI complexes: reduced interaction with blood components, extended circulation in blood and potential for systemic gene delivery. *Gene Ther* (1999) 6, 595-605.
- [214] Allen C, Dos Santos N, Gallagher R, Chiu GN, Shu Y, Li WM, Johnstone SA, Janoff AS, Mayer LD, Webb MS and Bally MB, Controlling the physical behavior and biological performance of liposome formulations through use of surface grafted poly(ethylene glycol). *Biosci Rep* (2002) 22, 225-50.
- [215] Morrissey DV, Lockridge JA, Shaw L, Blanchard K, Jensen K, Breen W, Hartsough K, Machemer L, Radka S, Jadhav V, Vaish N, Zinnen S, Vargeese C, Bowman K, Shaffer CS, Jeffs LB, Judge A, MacLachlan I and Polisky B, Potent and persistent in vivo anti-HBV activity of chemically modified siRNAs. *Nature biotechnology* (2005) 23, 1002-7.
- [216] Heyes J, Palmer L, Bremner K and MacLachlan I, Cationic lipid saturation influences intracellular delivery of encapsulated nucleic acids. *Journal of controlled release* (2005) 107, 276-87.
- [217] Ambegia E, Ansell S, Cullis P, Heyes J, Palmer L and MacLachlan I, Stabilized plasmid-lipid particles containing PEG-diacylglycerols exhibit extended circulation lifetimes and tumor selective gene expression. *Biochimica et biophysica acta* (2005) 1669, 155-63.

- [218] Judge AD, Robbins M, Tavakoli I, Levi J, Hu L, Fronda A, Ambegia E, McClintock K and MacLachlan I, Confirming the RNAi-mediated mechanism of action of siRNA-based cancer therapeutics in mice. *The Journal of clinical investigation* (2009) 119, 661-73.
- [219] Zimmermann TS, Lee AC, Akinc A, Bramlage B, Bumcrot D, Fedoruk MN, Harborth J, Heyes JA, Jeffs LB, John M, Judge AD, Lam K, McClintock K, Nechev LV, Palmer LR, Racie T, Rohl I, Seiffert S, Shanmugam S, Sood V, Soutschek J, Toudjarska I, Wheat AJ, Yaworski E, Zedalis W, Koteliensky V, Manoharan M, Vornlocher HP and MacLachlan I, RNAi-mediated gene silencing in non-human primates. *Nature* (2006) 441, 111-4.
- [220] Semple SC, Akinc A, Chen J, Sandhu AP, Mui BL, Cho CK, Sah DW, Stebbing D, Crosley EJ, Yaworski E, Hafez IM, Dorkin JR, Qin J, Lam K, Rajeev KG, Wong KF, Jeffs LB, Nechev L, Eisenhardt ML, Jayaraman M, Kazem M, Maier MA, Srinivasulu M, Weinstein MJ, Chen Q, Alvarez R, Barros SA, De S, Klimuk SK, Borland T, et al., Rational design of cationic lipids for siRNA delivery. *Nature biotechnology* (2010) 28, 172-6.
- [221] Vajkoczy P, Schilling L, Ullrich A, Schmiedek P and Menger MD, Characterization of angiogenesis and microcirculation of high-grade glioma: an intravital multifluorescence microscopic approach in the athymic nude mouse. *J Cereb Blood Flow Metab* (1998) 18, 510-20.
- [222] Baish JW, Gazit Y, Berk DA, Nozue M, Baxter LT and Jain RK, Role of tumor vascular architecture in nutrient and drug delivery: an invasion percolation-based network model. *Microvasc Res* (1996) 51, 327-46.
- [223] Yuan F, Salehi HA, Boucher Y, Vasthare US, Tuma RF and Jain RK, Vascular permeability and microcirculation of gliomas and mammary carcinomas transplanted in rat and mouse cranial windows. *Cancer Res* (1994) 54, 4564-8.
- [224] Vajkoczy P and Menger MD, Vascular microenvironment in gliomas. *J Neurooncol* (2000) 50, 99-108.
- [225] Baker JH, Lam J, Kyle AH, Sy J, Oliver T, Co SJ, Dragowska WH, Ramsay E, Anantha M, Ruth TJ, Adam MJ, Yung A, Kozlowski P, Minchinton AI, Ng SS, Bally MB and Yapp DT, Irinophore C, a novel nanoformulation of irinotecan, alters tumor vascular function and enhances the distribution of 5-fluorouracil and doxorubicin. *Clin Cancer Res* (2008) 14, 7260-71.
- [226] Baffert F, Le T, Sennino B, Thurston G, Kuo CJ, Hu-Lowe D and McDonald DM, Cellular changes in normal blood capillaries undergoing regression after inhibition of VEGF signaling. *Am J Physiol Heart Circ Physiol* (2006) 290, H547-59.
- [227] Jain RK, Normalizing tumor vasculature with anti-angiogenic therapy: a new paradigm for combination therapy. *Nat Med* (2001) 7, 987-9.
- [228] Mabeta P and Pepper MS, A comparative study on the anti-angiogenic effects of DNA-damaging and cytoskeletal-disrupting agents. *Angiogenesis* (2009) 12, 81-90.
- [229] Chen Q, Tong S, Dewhirst MW and Yuan F, Targeting tumor microvessels using doxorubicin encapsulated in a novel thermosensitive liposome. *Mol Cancer Ther* (2004) 3, 1311-7.
- [230] Arnold RD, Mager DE, Slack JE and Straubinger RM, Effect of repetitive administration of Doxorubicin-containing liposomes on plasma pharmacokinetics and drug biodistribution in a rat brain tumor model. *Clin Cancer Res* (2005) 11, 8856-65.
- [231] Tomayko MM and Reynolds CP, Determination of subcutaneous tumor size in athymic (nude) mice. *Cancer Chemother Pharmacol* (1989) 24, 148-54.
- [232] Lyng H, Dahle GA, Kaalhus O, Skretting A and Rofstad EK, Measurement of perfusion rate in human melanoma xenografts by contrast-enhanced magnetic resonance imaging. *Magn Reson Med* (1998) 40, 89-98.
- [233] Tofts PS, Brix G, Buckley DL, Evelhoch JL, Henderson E, Knopp MV, Larsson HB, Lee TY, Mayr NA, Parker GJ, Port RE, Taylor J and Weisskoff RM, Estimating kinetic parameters

- from dynamic contrast-enhanced T(1)-weighted MRI of a diffusable tracer: standardized quantities and symbols. *J Magn Reson Imaging* (1999) 10, 223-32.
- [234] Low J, Huang S, Blosser W, Dowless M, Burch J, Neubauer B and Stancato L, High-content imaging characterization of cell cycle therapeutics through in vitro and in vivo subpopulation analysis. *Mol Cancer Ther* (2008) 7, 2455-63.
- [235] Stravopodis DJ, Karkoulis PK, Konstantakou EG, Melachroinou S, Lampidonis AD, Anastasiou D, Kachrilas S, Messini-Nikolaki N, Papassideri IS, Aravantinos G, Margaritis LH and Voutsinas GE, Grade-dependent effects on cell cycle progression and apoptosis in response to doxorubicin in human bladder cancer cell lines. *Int J Oncol* (2009) 34, 137-60.
- [236] Foroodi F, Duivenvoorden WC and Singh G, Interactions of doxycycline with chemotherapeutic agents in human breast adenocarcinoma MDA-MB-231 cells. *Anticancer Drugs* (2009) 20, 115-22.
- [237] Saleh EM, El-Awady RA, Abdel Alim MA and Abdel Wahab AH, Altered expression of proliferation-inducing and proliferation-inhibiting genes might contribute to acquired doxorubicin resistance in breast cancer cells. *Cell Biochem Biophys* (2009) 55, 95-105.
- [238] Landberg G, Tan EM and Roos G, Flow cytometric multiparameter analysis of proliferating cell nuclear antigen/cyclin and Ki-67 antigen: a new view of the cell cycle. *Exp Cell Res* (1990) 187, 111-8.
- [239] Bernsen HJ, Rijken PF, Hagemeyer NE and van der Kogel AJ, A quantitative analysis of vascularization and perfusion of human glioma xenografts at different implantation sites. *Microvasc Res* (1999) 57, 244-57.
- [240] Bernsen HJ, Rijken PF, Peters H, Raleigh JA, Jeuken JW, Wesseling P and van der Kogel AJ, Hypoxia in a human intracerebral glioma model. *J Neurosurg* (2000) 93, 449-54.
- [241] Kamoun WS, Ley CD, Farrar CT, Duyverman AM, Lahdenranta J, Lacorre DA, Batchelor TT, di Tomaso E, Duda DG, Munn LL, Fukumura D, Sorensen AG and Jain RK, Edema control by cediranib, a vascular endothelial growth factor receptor-targeted kinase inhibitor, prolongs survival despite persistent brain tumor growth in mice. *J Clin Oncol* (2009) 27, 2542-52.
- [242] Winkler F, Kozin SV, Tong RT, Chae SS, Booth MF, Garkavtsev I, Xu L, Hicklin DJ, Fukumura D, di Tomaso E, Munn LL and Jain RK, Kinetics of vascular normalization by VEGFR2 blockade governs brain tumor response to radiation: role of oxygenation, angiopoietin-1, and matrix metalloproteinases. *Cancer Cell* (2004) 6, 553-63.
- [243] Baluk P, Hashizume H and McDonald DM, Cellular abnormalities of blood vessels as targets in cancer. *Curr Opin Genet Dev* (2005) 15, 102-11.
- [244] Yang Z, Suzuki R, Daniels SB, Brunquell CB, Sala CJ and Nishiyama A, NG2 glial cells provide a favorable substrate for growing axons. *J Neurosci* (2006) 26, 3829-39.
- [245] Bocci G, Falcone A, Fioravanti A, Orlandi P, Di Paolo A, Fanelli G, Viacava P, Naccarato AG, Kerbel RS, Danesi R, Del Tacca M and Allegrini G, Antiangiogenic and anticolorrectal cancer effects of metronomic irinotecan chemotherapy alone and in combination with semaxinib. *Br J Cancer* (2008) 98, 1619-29.
- [246] Bocci G, Nicolaou KC and Kerbel RS, Protracted low-dose effects on human endothelial cell proliferation and survival in vitro reveal a selective antiangiogenic window for various chemotherapeutic drugs. *Cancer Res* (2002) 62, 6938-43.
- [247] O'Connor JP, Jackson A, Parker GJ and Jayson GC, DCE-MRI biomarkers in the clinical evaluation of antiangiogenic and vascular disrupting agents. *Br J Cancer* (2007) 96, 189-95.
- [248] Jain RK, Normalization of tumor vasculature: an emerging concept in antiangiogenic therapy. *Science* (2005) 307, 58-62.
- [249] Le Serve AW and Hellmann K, Vascular changes in tumours after treatment with ICRF 159. *Br J Pharmacol* (1971) 43, 457P-458P.

- [250] Vajkoczy P and Menger MD, Vascular microenvironment in gliomas. *Cancer Treat Res* (2004) 117, 249-62.
- [251] Sorensen AG, Batchelor TT, Zhang WT, Chen PJ, Yeo P, Wang M, Jennings D, Wen PY, Lahdenranta J, Ancukiewicz M, di Tomaso E, Duda DG and Jain RK, A "vascular normalization index" as potential mechanistic biomarker to predict survival after a single dose of cediranib in recurrent glioblastoma patients. *Cancer Res* (2009) 69, 5296-300.
- [252] Ma J, Li S, Reed K, Guo P and Gallo JM, Pharmacodynamic-mediated effects of the angiogenesis inhibitor SU5416 on the tumor disposition of temozolomide in subcutaneous and intracerebral glioma xenograft models. *J Pharmacol Exp Ther* (2003) 305, 833-9.
- [253] Shapiro AB, Corder AB and Ling V, P-glycoprotein-mediated Hoechst 33342 transport out of the lipid bilayer. *Eur J Biochem* (1997) 250, 115-21.
- [254] Hanahan D, Bergers G and Bergsland E, Less is more, regularly: metronomic dosing of cytotoxic drugs can target tumor angiogenesis in mice. *J Clin Invest* (2000) 105, 1045-7.
- [255] Browder T, Butterfield CE, Kraling BM, Shi B, Marshall B, O'Reilly MS and Folkman J, Antiangiogenic scheduling of chemotherapy improves efficacy against experimental drug-resistant cancer. *Cancer Res* (2000) 60, 1878-86.
- [256] Cham KK, Baker JH, Takhar KS, Flexman JA, Wong MQ, Owen DA, Yung A, Kozlowski P, Reinsberg SA, Chu EM, Chang CW, Buczkowski AK, Chung SW, Scudamore CH, Minchinton AI, Yapp DT and Ng SS, Metronomic gemcitabine suppresses tumour growth, improves perfusion, and reduces hypoxia in human pancreatic ductal adenocarcinoma. *Br J Cancer* (2010) 103, 52-60.
- [257] Vacca A, Ribatti D, Iurlaro M, Merchionne F, Nico B, Ria R and Dammacco F, Docetaxel versus paclitaxel for antiangiogenesis. *J Hematother Stem Cell Res* (2002) 11, 103-18.
- [258] Slatter JG, Su P, Sams JP, Schaaf LJ and Wienkers LC, Bioactivation of the anticancer agent CPT-11 to SN-38 by human hepatic microsomal carboxylesterases and the in vitro assessment of potential drug interactions. *Drug Metab Dispos* (1997) 25, 1157-64.
- [259] Lavelle F, Bissery MC, Andre S, Roquet F and Riou JF, Preclinical evaluation of CPT-11 and its active metabolite SN-38. *Semin Oncol* (1996) 23, 11-20.
- [260] Duyndam MC, van Berkel MP, Dorsman JC, Rockx DA, Pinedo HM and Boven E, Cisplatin and doxorubicin repress Vascular Endothelial Growth Factor expression and differentially down-regulate Hypoxia-inducible Factor I activity in human ovarian cancer cells. *Biochem Pharmacol* (2007) 74, 191-201.
- [261] Asai A, Shibui S, Barker M, Vanderlaan M, Gray JW and Hoshino T, Cell kinetics of rat 9L brain tumors determined by double labeling with iodo- and bromodeoxyuridine. *J Neurosurg* (1990) 73, 254-8.
- [262] Verreault M, Strutt D, Masin D, Anantha M, Waterhouse D, Yapp DT and Bally MB, Irinophore C<sup>TM</sup>, a lipid-based nanoparticulate formulation of irinotecan, is more effective than free irinotecan when used to treat an orthotopic glioblastoma model. In revision for *Journal of Controlled Release* (2011).
- [263] Wang F, Zhou F, Kruh GD and Gallo JM, Influence of blood-brain barrier efflux pumps on the distribution of vincristine in brain and brain tumors. *Neuro Oncol* (2010) 12, 1043-9.
- [264] Cloughesy T, FDA accelerated approval benefits glioblastoma. *Lancet Oncol* (2010) 11, 1120.
- [265] Quinn JA, Jiang SX, Reardon DA, Desjardins A, Vredenburgh JJ, Friedman AH, Sampson JH, McLendon RE, Herndon JE, 2nd and Friedman HS, Phase II trial of temozolomide (TMZ) plus irinotecan (CPT-11) in adults with newly diagnosed glioblastoma multiforme before radiotherapy. *J Neurooncol* (2009) 95, 393-400.
- [266] Tobin P, Rivory L and Clarke S, Inhibition of acetylcholinesterase in patients receiving irinotecan (camptothecin-11). *Clin Pharmacol Ther* (2004) 76, 505-6; author reply 507-8.

- [267] Mayer LD, Hope MJ and Cullis PR, Vesicles of variable sizes produced by a rapid extrusion procedure. *Biochim Biophys Acta* (1986) 858, 161-8.
- [268] Bally MB, Mayer LD, Hope MJ and Nayar R, Chapter 3: Pharmacodynamics of liposomal drug carriers: methodological considerations. *Liposome Technology* (1993) Volume III, 2nd edition,
- [269] Blaney SM, Takimoto C, Murry DJ, Kuttesch N, McCully C, Cole DE, Godwin K and Balis FM, Plasma and cerebrospinal fluid pharmacokinetics of 9-aminocamptothecin (9-AC), irinotecan (CPT-11), and SN-38 in nonhuman primates. *Cancer Chemother Pharmacol* (1998) 41, 464-8.
- [270] Zamboni WC, Houghton PJ, Thompson J, Cheshire PJ, Hanna SK, Richmond LB, Lou X and Stewart CF, Altered irinotecan and SN-38 disposition after intravenous and oral administration of irinotecan in mice bearing human neuroblastoma xenografts. *Clin Cancer Res* (1998) 4, 455-62.
- [271] Verreault M, Strutt D, Masin D, Anantha M, Yung A, Kozlowski P, Waterhouse D, Bally MB and Yapp DT, Vascular normalization in orthotopic glioblastoma following intravenous treatment with lipid-based nanoparticulate formulations of irinotecan (Irinophore CTM), doxorubicin (Caelyx®) or vincristine. *BMC Cancer* (2011) Apr 8, 124.
- [272] Fukumura D and Jain RK, Imaging angiogenesis and the microenvironment. *APMIS* (2008) 116, 695-715.
- [273] Zhou Q and Gallo JM, Differential effect of sunitinib on the distribution of temozolomide in an orthotopic glioma model. *Neuro Oncol* (2009) 11, 301-10.
- [274] Bergers G and Hanahan D, Modes of resistance to anti-angiogenic therapy. *Nat Rev Cancer* (2008) 8, 592-603.
- [275] Tailor TD, Hanna G, Yarmolenko PS, Dreher MR, Betof AS, Nixon AB, Spasojevic I and Dewhirst MW, Effect of pazopanib on tumor microenvironment and liposome delivery. *Mol Cancer Ther* (2010) 9, 1798-808.
- [276] Rivory LP, Chatelut E, Canal P, Mathieu-Boue A and Robert J, Kinetics of the *in vivo* interconversion of the carboxylate and lactone forms of irinotecan (CPT-11) and of its metabolite SN-38 in patients. *Cancer Res* (1994) 54, 6330-3.
- [277] Burke TG and Mi Z, The structural basis of camptothecin interactions with human serum albumin: impact on drug stability. *J Med Chem* (1994) 37, 40-6.
- [278] Wallin A, Svanvik J, Holmlund B, Ferreud L and Sun XF, Anticancer effect of SN-38 on colon cancer cell lines with different metastatic potential. *Oncol Rep* (2008) 19, 1493-8.
- [279] te Poele RH and Joel SP, Schedule-dependent cytotoxicity of SN-38 in p53 wild-type and mutant colon adenocarcinoma cell lines. *Br J Cancer* (1999) 81, 1285-93.
- [280] O'Neill K, Lyons SK, Gallagher WM, Curran KM and Byrne AT, Bioluminescent imaging: a critical tool in pre-clinical oncology research. *J Pathol* (2010) 220, 317-327.
- [281] Hauck ES, Zou S, Scarfo K, Nantz MH and Hecker JG, Whole animal *in vivo* imaging after transient, nonviral gene delivery to the rat central nervous system. *Mol Ther* (2008) 16, 1857-1864.
- [282] Bryant MJ, Chuah TL, Luff J, Lavin MF and Walker DG, A novel rat model for glioblastoma multiforme using a bioluminescent F98 cell line. *J Clin Neurosci* (2008) 15, 545-551.
- [283] Pike L, Petravic J and Wang S, Bioluminescence imaging after HSV amplicon vector delivery into brain. *J Gene Med* (2006) 8, 804-813.
- [284] Evans SM, Judy KD, Dunphy I, Jenkins WT, Hwang WT, Nelson PT, Lustig RA, Jenkins K, Magarelli DP, Hahn SM, Collins RA, Grady MS and Koch CJ, Hypoxia is important in the biology and aggression of human glial brain tumors. *Clin Cancer Res* (2004) 10, 8177-8184.

- [285] Sun A, Hou L, Prugpichailers T, Dunkel J, Kalani MA, Chen X, Kalani MY and Tse V, Firefly luciferase-based dynamic bioluminescence imaging: a noninvasive technique to assess tumor angiogenesis. *Neurosurgery* (2010) 66, 751-757.
- [286] Zhao D, Richer E, Antich PP and Mason RP, Antivasular effects of combretastatin A4 phosphate in breast cancer xenograft assessed using dynamic bioluminescence imaging and confirmed by MRI. *FASEB J* (2008) 22, 2445-2451.
- [287] Deliolanis NC, Kasmieh R, Wurdinger T, Tannous BA, Shah K and Ntziachristos V, Performance of the red-shifted fluorescent proteins in deep-tissue molecular imaging applications. *J Biomed Opt* (2008) 13, 044008.
- [288] Hoffman RM, The multiple uses of fluorescent proteins to visualize cancer *in vivo*. *Nat Rev Cancer* (2005) 5, 796-806.
- [289] Shcherbo D, Murphy CS, Ermakova GV, Solovieva EA, Chepurnykh TV, Shcheglov AS, Verkhusha VV, Pletnev VZ, Hazelwood KL, Roche PM, Lukyanov S, Zaraisky AG, Davidson MW and Chudakov DM, Far-red fluorescent tags for protein imaging in living tissues. *Biochem J* (2009) 418, 567-574.
- [290] Mansfield JR, Distinguished photons: a review of *in vivo* spectral fluorescence imaging in small animals. *Curr Pharm Biotechnol* (2010) 11, 628-638.
- [291] Zhou L and El-Deiry WS, Multispectral fluorescence imaging. *J Nucl Med* (2009) 50, 1563-1566.
- [292] Shu X, Shaner NC, Yarbrough CA, Tsien RY and Remington SJ, Novel chromophores and buried charges control color in mFruits. *Biochemistry* (2006) 45, 9639-9647.
- [293] Lois C, Hong EJ, Pease S, Brown EJ and Baltimore D, Germline transmission and tissue-specific expression of transgenes delivered by lentiviral vectors. *Science* (2002) 295, 868-872.
- [294] Fink D, Wohrer, S., Pfeffer, M., Tombe, T., Ong, C.J., Sorensen, P.H.B., Ubiquitous expression of the monomeric red fluorescent protein mCherry in transgenic mice. *Genesis* (2010) 48, 723-729.
- [295] Zufferey R, Nagy D, Mandel RJ, Naldini L and Trono D, Multiply attenuated lentiviral vector achieves efficient gene delivery *in vivo*. *Nat Biotechnol* (1997) 15, 871-875.
- [296] Oliveras-Ferraros C, Vazquez-Martin A, Martin-Castillo B, Cufi S, Del Barco S, Lopez-Bonet E, Brunet J and Menendez JA, Dynamic emergence of the mesenchymal CD44(pos)CD24(neg/low) phenotype in *HER2*-gene amplified breast cancer cells with *de novo* resistance to trastuzumab (Herceptin). *Biochem Biophys Res Commun* (2010) 397, 27-33.
- [297] Lopes MBS, Frankfurter A, Zientek GM and Herman MM, The presence of neuron-associated microtubule proteins in the human U-251 MG cell line: A comparative immunoblot and immunohistochemical study. *Molecular and Chemical Neuropathology* (1998) 1, 273-287.
- [298] Heppner GH, Tumor heterogeneity. *Cancer Res* (1984) 44, 2259-2265.
- [299] Virtanen I, Lehtonen E, Narvanen O, Leivo I and Lehto VP, Population heterogeneity in the surface expression of *Ulex europaeus* I-lectin (UEA I)-binding sites in cultured malignant and transformed cells. *Exp Cell Res* (1985) 161, 53-62.
- [300] Langley RR and Fidler IJ, Tumor cell-organ microenvironment interactions in the pathogenesis of cancer metastasis. *Endocr Rev* (2007) 28, 297-321.
- [301] Germano I, Swiss V and Casaccia P, Primary brain tumors, neural stem cell, and brain tumor cancer cells: Where is the link? *Neuropharmacology* (2010) 58, 903-910.
- [302] Qiang L, Yang Y, Ma YJ, Chen FH, Zhang LB, Liu W, Qi Q, Lu N, Tao L, Wang XT, You QD and Guo QL, Isolation and characterization of cancer stem like cells in human glioblastoma cell lines. *Cancer Lett* (2009) 279, 13-21.
- [303] Liu HS, Jan MS, Chou CK, Chen PH and Ke NJ, Is green fluorescent protein toxic to the living cells? *Biochem Biophys Res Commun* (1999) 260, 712-717.

- [304] Axelsen JB, Lotem J, Sachs L and Domany E, Genes overexpressed in different human solid cancers exhibit different tissue-specific expression profiles. *Proc Natl Acad Sci USA* (2007) 104, 13122-13127.
- [305] Xu Y, Stamenkovic I and Yu Q, CD44 attenuates activation of the hippo signaling pathway and is a prime therapeutic target for glioblastoma. *Cancer Res* (2010) 70, 2455-2464.
- [306] Wei KC, Huang CY, Chen PY, Feng LY, Wu TW, Chen SM, Tsai HC, Lu YJ, Tsang NM, Tseng CK, Pai PC and Shin JW, Evaluation of the prognostic value of CD44 in glioblastoma multiforme. *Anticancer Res* (2010) 30, 253-259.
- [307] Uchida N, Buck DW, He D, Reitsma MJ, Masek M, Phan TV, Tsukamoto AS, Gage FH and Weissman IL, Direct isolation of human central nervous system stem cells. *Proc Natl Acad Sci USA* (2000) 97, 14720-14725.
- [308] Murayama A, Matsuzaki Y, Kawaguchi A, Shimazaki T and Okano H, Flow cytometric analysis of neural stem cells in the developing and adult mouse brain. *J Neurosci Res* (2002) 69, 837-847.
- [309] Escors D and Breckpot K, Lentiviral vectors in gene therapy: their current status and future potential. *Arch Immunol Ther Exp (Warsz)* (2010) 58, 107-119.
- [310] Sumimoto H and Kawakami Y, Lentiviral vector-mediated RNAi and its use for cancer research. *Future Oncol* (2007) 3, 655-664.
- [311] Sathornsumetee S and Rich JN, New treatment strategies for malignant gliomas. *Expert Rev Anticancer Ther* (2006) 6, 1087-104.
- [312] Heyes J, Palmer L, Bremner K and MacLachlan I, Cationic lipid saturation influences intracellular delivery of encapsulated nucleic acids. *Journal of Controlled Release* (2005) 107, 276-287.
- [313] Pardridge WM, Intravenous, non-viral RNAi gene therapy of brain cancer. *Expert Opin Biol Ther* (2004) 4, 1103-13.
- [314] Sioud M, On the delivery of small interfering RNAs into mammalian cells. *Expert Opin Drug Deliv* (2005) 2, 639-51.
- [315] Taniguchi K, Yamamoto Y, Itakura K, Miichi H and Hayashi S, Assessment of ocular irritability of liposome preparations. *J Pharmacobiodyn* (1988) 11, 607-11.
- [316] Chonn A, Cullis PR and Devine DV, The role of surface charge in the activation of the classical and alternative pathways of complement by liposomes. *J Immunol* (1991) 146, 4234-41.
- [317] Eliyahu H, Serivel N, Domb AJ and Barenholz Y, Lipoplex-induced hemagglutination: potential involvement in intravenous gene delivery. *Gene Ther* (2002) 9, 850-8.
- [318] Panzner EA and Jansons VK, Control of in vitro cytotoxicity of positively charged liposomes. *J Cancer Res Clin Oncol* (1979) 95, 29-37.
- [319] Lappalainen K, Jaaskelainen I, Syrjanen K, Urtti A and Syrjanen S, Comparison of cell proliferation and toxicity assays using two cationic liposomes. *Pharm Res* (1994) 11, 1127-31.
- [320] Filion MC and Phillips NC, Toxicity and immunomodulatory activity of liposomal vectors formulated with cationic lipids toward immune effector cells. *Biochim Biophys Acta* (1997) 1329, 345-56.
- [321] Dass CR, Biochemical and biophysical characteristics of lipoplexes pertinent to solid tumour gene therapy. *Int J Pharm* (2002) 241, 1-25.
- [322] Lv H, Zhang S, Wang B, Cui S and Yan J, Toxicity of cationic lipids and cationic polymers in gene delivery. *J Control Release* (2006) 114, 100-9.
- [323] Webb MS, Johnstone S, Morris TJ, Kennedy A, Gallagher R, Harasym N, Harasym T, Shew CR, Tardi P, Dragowska WH, Mayer LD and Bally MB, In vitro and in vivo characterization of a combination chemotherapy formulation consisting of vinorelbine and phosphatidylserine. *Eur J Pharm Biopharm* (2007) 65, 289-99.

- [324] Szulc ZM, Bielawski J, Gracz H, Gustilo M, Mayroo N, Hannun YA, Obeid LM and Bielawska A, Tailoring structure-function and targeting properties of ceramides by site-specific cationization. *Bioorg Med Chem* (2006) 14, 7083-104.
- [325] Shtilbans V, Wu M and Burstein DE, Current overview of the role of Akt in cancer studies via applied immunohistochemistry. *Annals of Diagnostic Pathology* (2008) 12, 153-160.
- [326] Cavenee WK, Accumulation of genetic defects during astrocytoma progression. *Cancer* (1992) 70, 1788-93.
- [327] Furnari FB, Huang HJ and Cavenee WK, Genetics and malignant progression of human brain tumours. *Cancer Surv* (1995) 25, 233-75.
- [328] Holland EC, Celestino J, Dai C, Schaefer L, Sawaya RE and Fuller GN, Combined activation of Ras and Akt in neural progenitors induces glioblastoma formation in mice. *Nat Genet* (2000) 25, 55-7.
- [329] Kucab JE, Lee C, Chen CS, Zhu J, Gilks CB, Cheang M, Huntsman D, Yorida E, Emerman J, Pollak M and Dunn SE, Celecoxib analogues disrupt Akt signaling, which is commonly activated in primary breast tumours. *Breast Cancer Res* (2005) 7, R796-807.
- [330] Scheid MP, Marignani PA and Woodgett JR, Multiple phosphoinositide 3-kinase-dependent steps in activation of protein kinase B. *Mol Cell Biol* (2002) 22, 6247-60.
- [331] Troussard AA, Mawji NM, Ong C, Mui A, St -Arnaud R and Dedhar S, Conditional knock-out of integrin-linked kinase demonstrates an essential role in protein kinase B/Akt activation. *J Biol Chem* (2003) 278, 22374-8.
- [332] Tan C, Cruet-Hennequart S, Troussard A, Fazli L, Costello P, Sutton K, Wheeler J, Gleave M, Sanghera J and Dedhar S, Regulation of tumor angiogenesis by integrin-linked kinase (ILK). *Cancer Cell* (2004) 5, 79-90.
- [333] Edwards LA, Thiessen B, Dragowska WH, Daynard T, Bally MB and Dedhar S, Inhibition of ILK in PTEN-mutant human glioblastomas inhibits PKB/Akt activation, induces apoptosis, and delays tumor growth. *Oncogene* (2005) 24, 3596-605.
- [334] Yau CY, Wheeler JJ, Sutton KL and Hedley DW, Inhibition of integrin-linked kinase by a selective small molecule inhibitor, QLT0254, inhibits the PI3K/PKB/mTOR, Stat3, and FKHR pathways and tumor growth, and enhances gemcitabine-induced apoptosis in human orthotopic primary pancreatic cancer xenografts. *Cancer Res* (2005) 65, 1497-504.
- [335] Troussard AA, McDonald PC, Wederell ED, Mawji NM, Filipenko NR, Gelmon KA, Kucab JE, Dunn SE, Emerman JT, Bally MB and Dedhar S, Preferential dependence of breast cancer cells versus normal cells on integrin-linked kinase for protein kinase B/Akt activation and cell survival. *Cancer Res* (2006) 66, 393-403.
- [336] McDonald PC, Oloumi A, Mills J, Dobрева I, Maidan M, Gray V, Wederell ED, Bally MB, Foster LJ and Dedhar S, Rictor and Integrin-Linked Kinase Interact and Regulate AKT Phosphorylation and Cancer Cell Survival. *Cancer Research* (2008) 68, 1618-1624.
- [337] Hannigan GE, Leung-Hagesteijn C, Fitz-Gibbon L, Coppolino MG, Radeva G, Filmus J, Bell JC and Dedhar S, Regulation of cell adhesion and anchorage-dependent growth by a new beta 1-integrin-linked protein kinase. *Nature* (1996) 379, 91-6.
- [338] D'Abaco GM and Kaye AH, Integrin-linked kinase: a potential therapeutic target for the treatment of glioma. *Journal of clinical neuroscience : official journal of the Neurosurgical Society of Australasia* (2008) 15, 1079-84.
- [339] Reddig PJ and Juliano RL, Clinging to life: cell to matrix adhesion and cell survival. *Cancer metastasis reviews* (2005) 24, 425-39.
- [340] Hay N and Sonenberg N, Upstream and downstream of mTOR. *Genes Dev* (2004) 18, 1926-45.
- [341] Sarbassov DD, Guertin DA, Ali SM and Sabatini DM, Phosphorylation and regulation of Akt/PKB by the rictor-mTOR complex. *Science* (2005) 307, 1098-101.

- [342] Hagemann C, Meyer C, Stojic J, Eicker S, Gerngas S, Kuhnel S, Roosen K and Vince GH, High efficiency transfection of glioma cell lines and primary cells for overexpression and RNAi experiments. *J Neurosci Methods* (2006) 156, 194-202.
- [343] Rothmann-Cosic K, Wessendorf, H., Helfrich, J., Thiel, C., Riemen, G., Brosterhus, H., et al Buffer solution for electroporation and a method comprising the use of the same. European Patent Office, Patent # 1390518 (2002)
- [344] Dunne J, Drescher B, Riehle H, Hadwiger P, Young BD, Krauter J and Heidenreich O, The apparent uptake of fluorescently labeled siRNAs by electroporated cells depends on the fluorochrome. *Oligonucleotides* (2003) 13, 375-80.
- [345] Chen WW, Chan DC, Donald C, Lilly MB and Kraft AS, Pim family kinases enhance tumor growth of prostate cancer cells. *Mol Cancer Res* (2005) 3, 443-51.
- [346] Koul D, Shen R, Bergh S, Lu Y, de Groot JF, Liu TJ, Mills GB and Yung WK, Targeting integrin-linked kinase inhibits Akt signaling pathways and decreases tumor progression of human glioblastoma. *Mol Cancer Ther* (2005) 4, 1681-8.
- [347] Omid Y, Barar J and Akhtar S, Toxicogenomics of cationic lipid-based vectors for gene therapy: impact of microarray technology. *Curr Drug Deliv* (2005) 2, 429-41.
- [348] Yan W, Chen W and Huang L, Mechanism of adjuvant activity of cationic liposome: phosphorylation of a MAP kinase, ERK and induction of chemokines. *Molecular Immunology* (2007) 44, 3672-3681.
- [349] Heidenreich O, Krauter J, Riehle H, Hadwiger P, John M, Heil G, Vornlocher HP and Nordheim A, AML1/MTG8 oncogene suppression by small interfering RNAs supports myeloid differentiation of t(8;21)-positive leukemic cells. *Blood* (2003) 101, 3157-63.
- [350] Zabner J, Fasbender AJ, Moninger T, Poellinger KA and Welsh MJ, Cellular and molecular barriers to gene transfer by a cationic lipid. *J Biol Chem* (1995) 270, 18997-9007.
- [351] Simoes S, Filipe A, Faneca H, Mano M, Penacho N, Duzgunes N and de Lima MP, Cationic liposomes for gene delivery. *Expert Opin Drug Deliv* (2005) 2, 237-54.
- [352] Friend DS, Papahadjopoulos D and Debs RJ, Endocytosis and intracellular processing accompanying transfection mediated by cationic liposomes. *Biochim Biophys Acta* (1996) 1278, 41-50.
- [353] Sarbassov DD, Ali SM, Kim DH, Guertin DA, Latek RR, Erdjument-Bromage H, Tempst P and Sabatini DM, Rictor, a novel binding partner of mTOR, defines a rapamycin-insensitive and raptor-independent pathway that regulates the cytoskeleton. *Curr Biol* (2004) 14, 1296-302.
- [354] Huang TT, Sarkaria SM, Cloughesy TF and Mischel PS, Targeted therapy for malignant glioma patients: lessons learned and the road ahead. *Neurotherapeutics* (2009) 6, 500-12.
- [355] Koul D, PTEN signaling pathways in glioblastoma. *Cancer Biol Ther* (2008) 7, 1321-5.
- [356] Li XY, Zhang LQ, Zhang XG, Li X, Ren YB, Ma XY, Li XG and Wang LX, Association between AKT/mTOR signalling pathway and malignancy grade of human gliomas. *J Neurooncol* (2010) Epub.
- [357] Molina JR, Hayashi Y, Stephens C and Georgescu MM, Invasive glioblastoma cells acquire stemness and increased Akt activation. *Neoplasia* (2010) 12, 453-63.
- [358] Carnero A, The PKB/AKT pathway in cancer. *Curr Pharm Des* (2010) 16, 34-44.
- [359] Sabatini DM, mTOR and cancer: insights into a complex relationship. *Nat Rev Cancer* (2006) 6, 729-34.
- [360] Albert L, Karsy M, Murali R and Jhanwar-Uniyal M, Inhibition of mTOR Activates the MAPK Pathway in Glioblastoma Multiforme. *Cancer Genomics Proteomics* (2009) 6, 255-61.
- [361] Gulati N, Karsy M, Albert L, Murali R and Jhanwar-Uniyal M, Involvement of mTORC1 and mTORC2 in regulation of glioblastoma multiforme growth and motility. *Int J Oncol* (2009) 35, 731-40.

- [362] Sun SY, Rosenberg LM, Wang X, Zhou Z, Yue P, Fu H and Khuri FR, Activation of Akt and eIF4E survival pathways by rapamycin-mediated mammalian target of rapamycin inhibition. *Cancer Res* (2005) 65, 7052-8.
- [363] O'Reilly KE, Rojo F, She QB, Solit D, Mills GB, Smith D, Lane H, Hofmann F, Hicklin DJ, Ludwig DL, Baselga J and Rosen N, mTOR inhibition induces upstream receptor tyrosine kinase signaling and activates Akt. *Cancer Res* (2006) 66, 1500-8.
- [364] Sparks CA and Guertin DA, Targeting mTOR: prospects for mTOR complex 2 inhibitors in cancer therapy. *Oncogene* (2010) 29, 3733-44.
- [365] Masri J, Bernath A, Martin J, Jo OD, Vartanian R, Funk A and Gera J, mTORC2 activity is elevated in gliomas and promotes growth and cell motility via overexpression of rictor. *Cancer Res* (2007) 67, 11712-20.
- [366] Nakamura JL, The epidermal growth factor receptor in malignant gliomas: pathogenesis and therapeutic implications. *Expert Opin Ther Targets* (2007) 11, 463-72.
- [367] Huang PH, Xu AM and White FM, Oncogenic EGFR signaling networks in glioma. *Sci Signal* (2009) 2, re6.
- [368] Hatanpaa KJ, Burma S, Zhao D and Habib AA, Epidermal growth factor receptor in glioma: signal transduction, neuropathology, imaging, and radioresistance. *Neoplasia* (2010) 12, 675-84.
- [369] Moscatello DK, Holgado-Madruga M, Emler DR, Montgomery RB and Wong AJ, Constitutive activation of phosphatidylinositol 3-kinase by a naturally occurring mutant epidermal growth factor receptor. *J Biol Chem* (1998) 273, 200-6.
- [370] Huang HS, Nagane M, Klingbeil CK, Lin H, Nishikawa R, Ji XD, Huang CM, Gill GN, Wiley HS and Cavenee WK, The enhanced tumorigenic activity of a mutant epidermal growth factor receptor common in human cancers is mediated by threshold levels of constitutive tyrosine phosphorylation and unattenuated signaling. *J Biol Chem* (1997) 272, 2927-35.
- [371] Boado RJ, RNA interference and nonviral targeted gene therapy of experimental brain cancer. *NeuroRx* (2005) 2, 139-50.
- [372] Kreisl TN, Lassman AB, Mischel PS, Rosen N, Scher HI, Teruya-Feldstein J, Shaffer D, Lis E and Abrey LE, A pilot study of everolimus and gefitinib in the treatment of recurrent glioblastoma (GBM). *J Neurooncol* (2009) 92, 99-105.
- [373] Yung WK, Vredenburgh JJ, Cloughesy TF, Nghiemphu P, Klencke B, Gilbert MR, Reardon DA and Prados MD, Safety and efficacy of erlotinib in first-relapse glioblastoma: a phase II open-label study. *Neuro Oncol* (2010) 12, 1061-70.
- [374] Reardon DA, Desjardins A, Vredenburgh JJ, Gururangan S, Friedman AH, Herndon JE, 2nd, Marcello J, Norfleet JA, McLendon RE, Sampson JH and Friedman HS, Phase 2 trial of erlotinib plus sirolimus in adults with recurrent glioblastoma. *J Neurooncol* (2009) 96, 219-30.
- [375] Ramnarain DB, Park S, Lee DY, Hatanpaa KJ, Scoggin SO, Otu H, Libermann TA, Raisanen JM, Ashfaq R, Wong ET, Wu J, Elliott R and Habib AA, Differential gene expression analysis reveals generation of an autocrine loop by a mutant epidermal growth factor receptor in glioma cells. *Cancer Res* (2006) 66, 867-74.
- [376] Wang S, Guo P, Wang X, Zhou Q and Gallo JM, Preclinical pharmacokinetic/pharmacodynamic models of gefitinib and the design of equivalent dosing regimens in EGFR wild-type and mutant tumor models. *Mol Cancer Ther* (2008) 7, 407-17.
- [377] Allen C, Vongpunsawad S, Nakamura T, James CD, Schroeder M, Cattaneo R, Giannini C, Krempski J, Peng KW, Goble JM, Uhm JH, Russell SJ and Galanis E, Retargeted oncolytic measles strains entering via the EGFRvIII receptor maintain significant antitumor activity against gliomas with increased tumor specificity. *Cancer Res* (2006) 66, 11840-50.
- [378] Grill J, Van Beusechem VW, Van Der Valk P, Dirven CM, Leonhart A, Pherai DS, Haisma HJ, Pinedo HM, Curiel DT and Gerritsen WR, Combined targeting of adenoviruses to

- integrins and epidermal growth factor receptors increases gene transfer into primary glioma cells and spheroids. *Clin Cancer Res* (2001) 7, 641-50.
- [379] Verreault M and Bally MB, siRNA-mediated integrin-linked kinase suppression: nonspecific effects of siRNA/cationic liposome complexes trigger changes in the expression of phosphorylated-AKT and mTOR independently of ILK silencing. *Oligonucleotides* (2009) 19, 129-40.
- [380] Kapoor GS, Christie A and O'Rourke DM, EGFR inhibition in glioblastoma cells induces G2/M arrest and is independent of p53. *Cancer Biol Ther* (2007) 6, 571-9.
- [381] Guo D, Prins RM, Dang J, Kuga D, Iwanami A, Soto H, Lin KY, Huang TT, Akhavan D, Hock MB, Zhu S, Kofman AA, Bensinger SJ, Yong WH, Vinters HV, Horvath S, Watson AD, Kuhn JG, Robins HI, Mehta MP, Wen PY, DeAngelis LM, Prados MD, Mellinghoff IK, Cloughesy TF and Mischel PS, EGFR signaling through an Akt-SREBP-1-dependent, rapamycin-resistant pathway sensitizes glioblastomas to antilipogenic therapy. *Sci Signal* (2009) 2, ra82.
- [382] Ishii N, Maier D, Merlo A, Tada M, Sawamura Y, Diserens AC and Van Meir EG, Frequent co-alterations of TP53, p16/CDKN2A, p14ARF, PTEN tumor suppressor genes in human glioma cell lines. *Brain Pathol* (1999) 9, 469-79.
- [383] Choe G, Horvath S, Cloughesy TF, Crosby K, Seligson D, Palotie A, Inge L, Smith BL, Sawyers CL and Mischel PS, Analysis of the phosphatidylinositol 3'-kinase signaling pathway in glioblastoma patients in vivo. *Cancer Res* (2003) 63, 2742-6.
- [384] Vollmann A, Vornlocher HP, Stempf T, Brockhoff G, Apfel R and Bogdahn U, Effective silencing of EGFR with RNAi demonstrates non-EGFR dependent proliferation of glioma cells. *Int J Oncol* (2006) 28, 1531-42.
- [385] Lefranc F, Brotchi J and Kiss R, Possible future issues in the treatment of glioblastomas: special emphasis on cell migration and the resistance of migrating glioblastoma cells to apoptosis. *J Clin Oncol* (2005) 23, 2411-22.
- [386] Ikenoue T, Inoki K, Yang Q, Zhou X and Guan KL, Essential function of TORC2 in PKC and Akt turn motif phosphorylation, maturation and signalling. *EMBO J* (2008) 27, 1919-31.
- [387] Facchinetti V, Ouyang W, Wei H, Soto N, Lazorchak A, Gould C, Lowry C, Newton AC, Mao Y, Miao RQ, Sessa WC, Qin J, Zhang P, Su B and Jacinto E, The mammalian target of rapamycin complex 2 controls folding and stability of Akt and protein kinase C. *EMBO J* (2008) 27, 1932-43.
- [388] Guertin DA, Stevens DM, Thoreen CC, Burds AA, Kalaany NY, Moffat J, Brown M, Fitzgerald KJ and Sabatini DM, Ablation in mice of the mTORC components raptor, rictor, or mLST8 reveals that mTORC2 is required for signaling to Akt-FOXO and PKCalpha, but not S6K1. *Dev Cell* (2006) 11, 859-71.
- [389] Cho KK, Mikkelsen T, Lee YJ, Jiang F, Chopp M and Rosenblum ML, The role of protein kinase Calpha in U-87 glioma invasion. *Int J Dev Neurosci* (1999) 17, 447-61.
- [390] Guo H, Gu F, Li W, Zhang B, Niu R, Fu L, Zhang N and Ma Y, Reduction of protein kinase C zeta inhibits migration and invasion of human glioblastoma cells. *J Neurochem* (2009) 109, 203-13.
- [391] White E and DiPaola RS, The double-edged sword of autophagy modulation in cancer. *Clin Cancer Res* (2009) 15, 5308-16.
- [392] Das G, Shiras A, Shanmuganandam K and Shastry P, Rictor regulates MMP-9 activity and invasion through Raf-1-MEK-ERK signaling pathway in glioma cells. *Mol Carcinog* (2010) Epub.
- [393] Nakashima S, Protein kinase C alpha (PKC alpha): regulation and biological function. *J Biochem* (2002) 132, 669-75.

- [394] Reddy KB, Nabha SM and Atanaskova N, Role of MAP kinase in tumor progression and invasion. *Cancer Metastasis Rev* (2003) 22, 395-403.
- [395] Fan QW and Weiss WA, RNA interference against a glioma-derived allele of EGFR induces blockade at G2M. *Oncogene* (2005) 24, 829-37.
- [396] Kang CS, Zhang ZY, Jia ZF, Wang GX, Qiu MZ, Zhou HX, Yu SZ, Chang J, Jiang H and Pu PY, Suppression of EGFR expression by antisense or small interference RNA inhibits U251 glioma cell growth in vitro and in vivo. *Cancer Gene Ther* (2006) 13, 530-8.
- [397] Tian XX, Lam PY, Chen J, Pang JC, To SS, Di-Tomaso E and Ng HK, Antisense epidermal growth factor receptor RNA transfection in human malignant glioma cells leads to inhibition of proliferation and induction of differentiation. *Neuropathol Appl Neurobiol* (1998) 24, 389-96.
- [398] Saydam O, Glauser DL, Heid I, Turkeri G, Hilbe M, Jacobs AH, Ackermann M and Fraefel C, Herpes simplex virus 1 amplicon vector-mediated siRNA targeting epidermal growth factor receptor inhibits growth of human glioma cells in vivo. *Mol Ther* (2005) 12, 803-12.
- [399] Fan QW, Specht KM, Zhang C, Goldenberg DD, Shokat KM and Weiss WA, Combinatorial efficacy achieved through two-point blockade within a signaling pathway—a chemical genetic approach. *Cancer Res* (2003) 63, 8930-8.
- [400] Wang MY, Lu KV, Zhu S, Dia EQ, Vivanco I, Shackelford GM, Cavenee WK, Mellinghoff IK, Cloughesy TF, Sawyers CL and Mischel PS, Mammalian target of rapamycin inhibition promotes response to epidermal growth factor receptor kinase inhibitors in PTEN-deficient and PTEN-intact glioblastoma cells. *Cancer Res* (2006) 66, 7864-9.
- [401] de Groot JF, Gilbert MR, Aldape K, Hess KR, Hanna TA, Ictech S, Groves MD, Conrad C, Colman H, Puduvalli VK, Levin V and Yung WK, Phase II study of carboplatin and erlotinib (Tarceva, OSI-774) in patients with recurrent glioblastoma. *J Neurooncol* (2008) 90, 89-97.
- [402] Fan QW and Weiss WA, Targeting the RTK-PI3K-mTOR axis in malignant glioma: overcoming resistance. *Curr Top Microbiol Immunol* (2010) 347, 279-96.
- [403] Rao RD, Mladek AC, Lamont JD, Goble JM, Erlichman C, James CD and Sarkaria JN, Disruption of parallel and converging signaling pathways contributes to the synergistic antitumor effects of simultaneous mTOR and EGFR inhibition in GBM cells. *Neoplasia* (2005) 7, 921-9.
- [404] Prakash S, Malhotra M and Rengaswamy V, Nonviral siRNA delivery for gene silencing in neurodegenerative diseases. *Methods Mol Biol* (2010) 623, 211-29.
- [405] Lichota J, Skjorringe T, Thomsen LB and Moos T, Macromolecular drug transport into the brain using targeted therapy. *J Neurochem* (2009) 113, 1-13.
- [406] Huwyler J, Wu D and Pardridge WM, Brain drug delivery of small molecules using immunoliposomes. *Proc Natl Acad Sci U S A* (1996) 93, 14164-9.
- [407] Recht L, Torres CO, Smith TW, Raso V and Griffin TW, Transferrin receptor in normal and neoplastic brain tissue: implications for brain-tumor immunotherapy. *J Neurosurg* (1990) 72, 941-5.
- [408] Shi N, Zhang Y, Zhu C, Boado RJ and Pardridge WM, Brain-specific expression of an exogenous gene after i.v. administration. *Proc Natl Acad Sci U S A* (2001) 98, 12754-9.
- [409] Pirolo KF, Zon G, Rait A, Zhou Q, Yu W, Hogrefe R and Chang EH, Tumor-targeting nanoimmunoliposome complex for short interfering RNA delivery. *Hum Gene Ther* (2006) 17, 117-24.
- [410] Schiffelers RM, Ansari A, Xu J, Zhou Q, Tang Q, Storm G, Molema G, Lu PY, Scaria PV and Woodle MC, Cancer siRNA therapy by tumor selective delivery with ligand-targeted sterically stabilized nanoparticle. *Nucleic Acids Res* (2004) 32, e149.
- [411] Gladson CL and Cheresch DA, Glioblastoma expression of vitronectin and the alpha v beta 3 integrin. Adhesion mechanism for transformed glial cells. *J Clin Invest* (1991) 88, 1924-32.

- [412] Hsu AR, Hou LC, Veeravagu A, Greve JM, Vogel H, Tse V and Chen X, In vivo near-infrared fluorescence imaging of integrin  $\alpha v\beta 3$  in an orthotopic glioblastoma model. *Mol Imaging Biol* (2006) 8, 315-23.
- [413] Charalambous C, Chen TC and Hofman FM, Characteristics of tumor-associated endothelial cells derived from glioblastoma multiforme. *Neurosurg Focus* (2006) 20, E22.
- [414] Altaner C, Glioblastoma and stem cells. *Neoplasma* (2008) 55, 369-74.
- [415] Guo W, Lasky JL, 3rd and Wu H, Cancer stem cells. *Pediatr Res* (2006) 59, 59R-64R.
- [416] Hadjipanayis CG and Van Meir EG, Tumor initiating cells in malignant gliomas: biology and implications for therapy. *J Mol Med* (2009) 87, 363-74.
- [417] Xie Z and Chin LS, Molecular and cell biology of brain tumor stem cells: lessons from neural progenitor/stem cells. *Neurosurg Focus* (2008) 24, E25.
- [418] Tarnok A, Ulrich H and Bocsi J, Phenotypes of stem cells from diverse origin. *Cytometry A* (2009) 77, 6-10.
- [419] Zhang Y, Boado RJ and Pardridge WM, Marked enhancement in gene expression by targeting the human insulin receptor. *J Gene Med* (2003) 5, 157-63.